September 2010

INVESTIGATING THE PATHOGENESIS AND THERAPY OF FRIEDREICH ATAXIA

A thesis submitted for the degree of Doctor of Philosophy by

Chiranjeevi Sandi

Division of Biosciences
School of Health Sciences and Social Care

Brunel UNIVERSITY WEST LONDON

Declaration

I hereby declare that the research presented in this thesis is my own work, except where otherwise specified, and has not been submitted for any other degree.

Chiranjeevi Sandi

Abstract

Friedreich ataxia (FRDA) is an inherited autosomal recessive neurodegenerative disorder caused by a GAA trinucleotide repeat expansion mutation within the first intron of the *FXN* gene. Normal individuals have 5 to 30 GAA repeats, whereas affected individuals have from approximately 70 to more than 1,000 GAA triplets. In addition to progressive neurological disability, FRDA is associated with cardiomyopathy and an increased risk of diabetes mellitus. Currently there is no effective therapy for FRDA and this is perhaps due to the lack of an effective system to test potential drugs. Therefore, the main aim of this thesis is to develop a novel cell culture system, to aid in rapid drug screening for FRDA.

Firstly, I have demonstrated the establishment of novel cell culture systems, including primary fibroblasts, neural stem cells (NSC) and splenocytes, from FRDA YAC transgenic mouse models (YG8 and YG22). Then, I have shown the differentiation of NSCs into neurons, oligodendrocytes and astrocytes. The presence of these cells was confirmed by using cell specific immunofluorescence assays. I have also shown that both YG8 and YG22 rescue mice have less tolerance to hydrogen peroxide induced oxidative stress than WT mice, as similarly seen in FRDA patient fibroblasts.

Recent findings indicate that FRDA is associated with heterochromatin-mediated silencing of the *FXN* gene accompanied by histone changes, flanking the GAA repeats. This suggested potential therapeutic use of compounds which can reduce the methylation and increase the acetylation of histone proteins. Therefore, using human and mouse primary fibroblast cell lines I have investigated the efficacy and tolerability of various DNA demethylating agents, GAA interacting compounds and class III histone deacetylase (HDAC) inhibitors. Although DNA demethylating agents showed increased *FXN* expression, no

correlation between the level of DNA methylation and *FXN* expression was identified. Nevertheless, the use of GAA interacting compounds, particularly DB221, and the HDAC inhibitor, nicotinamide, have shown encouraging results, provoking us to use such compounds in future long-term *in vivo* studies.

In addition, I have also investigated the long-term efficacy of two benzamide-type HDAC inhibitors, RGFA 136 and RGFP 109, on the FRDA YAC transgenic mice. No overt toxicity was identified with either drug, indicating a safe administration of these compounds. Both compounds produced improved functional analysis together with significantly reduced DRG neurodegeneration. However, neither of these compounds was shown to significantly increase the *FXN* mRNA expression. Nevertheless, elevated levels of frataxin protein in the brain tissues were obtained with RGFP 109, suggesting that RGFP 109 is capable of crossing the blood-brain barrier. I have also found increased levels of global acetylated H3 and H4 histone proteins in brain tissues, along with significant increase in aconitase enzyme activity, particularly with RGFP 109 treatments. Overall, these results support future clinical trial development with such compounds.

Acknowledgements

Foremost, I would like to express my deep and sincere gratitude to my supervisor, Dr. Mark Pook for accepting me as his student. His immense knowledge, patience, motivation, enthusiasm and logical way of thinking have been of great value for me. His understanding, encouragement and personal guidance have provided a good basis for my thesis.

I must also thank Dr. Sahar Al-Mahdawi for various helpful discussions, guidance and encouragement with her positive thinking throughout my PhD. A very big "thank you" must go to all past and present members of the 'Hereditary ataxia group' especially Dr. Ricardo Mouro Pinto and Vahid Ezzatizadeh for ever being nice colleagues.

I must also thank my second supervisor Dr. David Tree for his useful discussions and Dr. Satyan Chintawar (Brussels, Belgium) for teaching me the establishment of neural stem cells.

It is my pleasant honour to thank Muscular Dystrophy Association (MDA) for providing financial support. I would also like to acknowledge Repligen Corporation and Dr. David Boykin for kindly providing the HDAC inhibitors RGFA 136 and RGFP 109, and DB221, respectively.

I would also like to express special thanks to Dr. Sahar Al-Mahdawi for performing methylscreen, aconitase and western blot analysis, Dr. Ricardo Mouro Pinto for his critical advice on statistical analysis, Dr. Chris Parris, Dr. Joanna Bridger and Dr. Ian Kill for their helpful suggestions with the immunoflourescence assay and Lorraine Lawrence (Imperial College London) for assistance with histology.

I am grateful to Steve Pash, Julie Walker and Sue Toogood for their invaluable assistance in successful maintenance of animal husbandry.

Finally, I would like to thank my family members and friends, specially my brother and mom, Sridhar Reddy and Laxmi, and my wife, Madhavi Sandi, who have always been very encouraging and enthusiastic about my work.

Last but not least, I would also like to say a ‘big thank you’ to both of my daughters, Sanjana and Meghana, for being peaceful during my thesis writing.

Table of contents

List of figures

List of tables

List of abbreviations

µl	microlitre
106	*N*1-(2-aminophenyl)-*N*7-*p*-tolylheptanediamide (4b derivative)
4b	*N*1-(2-aminophenyl)-*N*7-phenylheptanediamide (BML-210 derivative)
5-aza-CdR	5-aza-2'-deoxycytidine
ACK	ammonium chloride potassium (K)
AMV RT	avian myeloblastosis virus reverse transcriptase
A-T	ataxia-telangiectasia
ATP	adenosine triphosphate
BAC	bacterial artificial chromosome
BCA	bicinchoninic acid
BME	beta-mercaptoethanol
BML-210	*N*1-(2-aminophenyl)-*N*8-phenyloctanediamide (SAHA derivative)
BPB	bromophenol blue
BSA	bovine serum albumin
cAMP	cyclic adenosine monophosphate
ChIP	chromatin immunoprecipitation
CNS	central nervous system
CoQ	coenzyme Q
CTCF	CCCTC-binding factor
DAPI	4', 6-diamidino-2-phenylindole
DEPC	diethyl pyrocarbonate
DMEM	Dulbecco's modified Eagle's medium
DMSO	dimethyl sulfoxide
DNA	deoxyribonucleic acid
dNTP	deoxynucleotide triphosphate
DRG	dorsal root ganglion
DTT	dithiothreitol
EBSS	Earl's balanced salt solution
EDTA	ethylene diamine-tetra acetic acid

EPO	erythropoietin
EtOH	ethanol
FBS	fetal bovine serum
FCS	fetal calf serum
FDA	food and drug administration
FISH	fluorescent in situ hybridization
FRDA	Friedreich ataxia
Gal-c	Galactocerebroside C
GAPDH	glyceraldehyde-3-phosphate dehydrogenase
GFAP	glial fibrillary acidic protein
GFP	green fluorescent protein
iPS	induced pluripotent stem cells
H&E	haematoxylin and eosin
HAT	histone acetyltransferase
HD	Huntington disease
HMTases	histone methyltransferases
i.p.	intraperitoneally
IMS	industrial methylated spirit
kb	kilo base
Kg	kilogram
LMW	low molecular weight
MAP-2	microtubule associated protein 2
MEF	mouse embryonic fibroblasts
mg	milligram
ml	millilitre
MRC	mitochondrial respiratory chain
mRNA	messenger RNA
NADP	nicotinamide adenine dinucleotide phosphate
NMR	nucleic magnetic resonance
NSC	neural stem cells
NSE	neuron-specific enolase

OD	optical density
ODN	oligodeoxyribonucleotides
p.c	post coitum
PAGE	polyacrylamide gel electrophoresis
PBMCs	Peripheral blood mononuclear cells
PBS	phosphate-buffered saline
PCR	polymerase chain reaction
PD	Parkinson disease
pen-strep	penicillin and streptomycin
PG	pen-strep and glucose
PNS	peripheral nervous system
Q-PCR	quantitative real-time PCR
QRT-PCR	quantitative real-time RT-PCR
RBC	red blood cells
rhEGF	recombinant human epidermal growth factor
rhFGF-b	recombinant human fibroblast growth factor-basic
rhu-EPO	recombinant human erythropoietin
RNA	ribonucleic acid
rpm	revolutions per minute
RPMI	Roswell Park Memorial Institute
RT-PCR	reverse transcriptase PCR
SAHA	suberoylanilide hydroxamic acid
SDS	sodium dodecyl sulphate
SEM	standard error of the mean
SP-PCR	small-pool PCR
SSC	sodium citrate
TBE	Tris-borate-EDTA
TE	Tris EDTA
TEMED	tetramethylethylenediamine
TNR	trinucleotide repeat
Tris	tris(hydroxymethyl)aminomethane

TRS	trinucleotide/triplet repeats sequence
TSA	trichostatin A
U	units
UTR	untranslated region
UV	ultra violet
VPA	valproic acid
WT	wild-type
YAC	yeast artificial chromosome

Chapter 1 - Friedreich ataxia: Introduction

Friedreich ataxia (FRDA, OMIM #229300) is an autosomal recessive trinucleotide repeat neurodegenerative disorder for which there is currently no effective therapy. It is the commonest inherited ataxia, with an incidence of approximately 1 in 50,000 (reviewed inSchulz *et al.* 2009). However, the carrier frequency varies depending on the ethnic group from 1 in 60 to 1 in 120 (Cossee *et al.* 1999). FRDA is predominantly caused by homozygous expanded GAA repeats in the first intron of the *FXN* gene (Campuzano *et al.* 1996). Normal individuals have 5 to 30 GAA repeat sequences, whereas affected individuals have from 70 to a maximum of 1600 repeats, but most commonly 600-900 repeats (Pandolfo 2002). The effect of the GAA expansion mutation is to reduce greatly the expression of frataxin (Campuzano *et al.* 1997), a mitochondrial protein involved in iron-sulphur cluster biosynthesis (Gerber *et al.* 2003). Frataxin insufficiency leads to oxidative stress, mitochondrial iron accumulation and resultant cell death, with the primary sites of pathology being the large sensory neurons of the dorsal root ganglia (DRG) and the dentate nucleus of the cerebellum (Koeppen *et al.* 2007; Koeppen *et al.* 2009).

Generally the first symptoms appear at childhood but age of onset may vary from childhood to adult (Pandolfo 2002). The main symptoms include loss of coordination (known as ataxia), muscle weakness, scoliosis, and sensory loss. There is also some pathological involvement of non-neuronal tissues, with cardiomyopathy as a common secondary effect and risk of diabetes also found in 10% of FRDA patients (Schulz *et al.* 2009). Within 20 years after the first appearance of symptoms, affected individuals are confined to a wheelchair and most commonly die in early adulthood from the associated heart disease (Delatycki *et al.* 2000). Therefore, there is a high unmet clinical need to develop a therapy for this devastating disorder.

1.1 - *Frataxin* gene: structure, function and expression

The gene, which is responsible for the production of frataxin protein and plays a crucial role in FRDA, is the '*FXN*' gene, previously known as X25. The *FXN* gene was mapped to chromosome 9 in 1988 (Chamberlain *et al.* 1988) and is localized in the proximal long arm at position 9q13 (Figure 1.1).

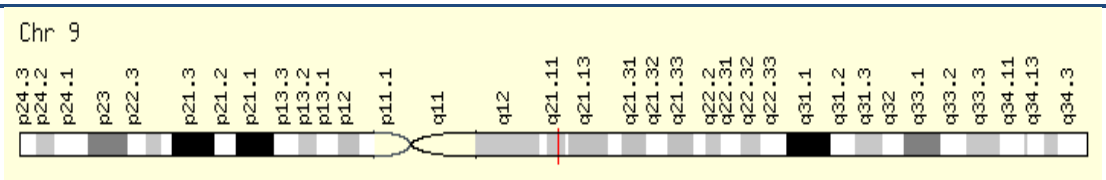

Figure 1.1 - Schematic representation of human chromosome 9. The red mark indicates the location of frataxin gene (Ensembl 2006).

The *FXN* gene structure was resolved by obtaining intronic sequences flanking the identified exons, by inverse polymerase chain reaction (PCR) and by the direct sequencing of cosmids (Campuzano *et al.* 1996). The *FXN* gene spans 95 kb of genomic DNA and contains seven exons, 1-5a, 5b and 6 (Figure 1.2) (Campuzano *et al.* 1996). Generally the first five exons, 1 to 5a, transcribe and produce the major transcript encoding a 210 amino acid mitochondrial protein called frataxin (Campuzano *et al.* 1996). Rarely, by alternative splicing, exon 5b can be transcribed and here a predicted 171 amino acid protein arises. Exon 6 is non-coding (Campuzano *et al.* 1996).

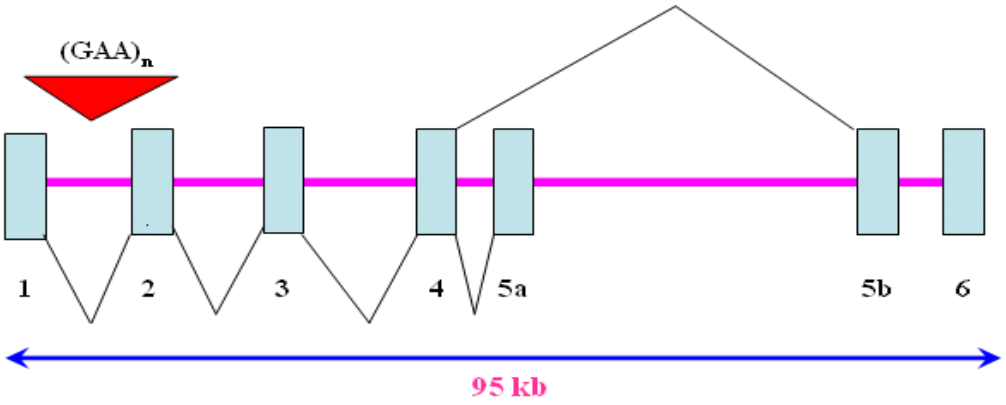

Figure 1.2 - Schematic representation of exons and splicing pattern of the *FXN* gene. The GAA repeat in intron 1 is indicated (▼). This diagram was adapted from (Cossee *et al.* 1997b).

Since there is no *in vivo* evidence for an effect on RNA processing in FRDA, it is believed that the disease results directly from reduced *FXN* mRNA levels followed by reduced amounts of frataxin protein (Cossee *et al.* 1997a; Bidichandani *et al.* 1998; Ohshima *et al.* 1998). However, it has been recently reported that the GAA repeats affect the pre-mRNA splicing in a position-dependent and repeat length-dependent manner in a hybrid minigene construct inserted with 15 or 100 GAA repeats (Baralle *et al.* 2008). In contrast, Punga and Buhler (2010) demonstrated that *FXN* mRNA levels were inversely correlated with repeat length in FRDA lymphoblastoid cell lines showing more consistent reduction of *FXN* mRNA in cell lines with larger GAA repeats. Importantly, the authors also reported that no alternatively spliced *FXN* transcripts were observed in any FRDA cell lines, suggesting that long GAA repeat tracts at the *FXN* gene locus are unlikely to affect pre-mRNA splicing but perhaps affect either mRNA half-life or transcription of the *FXN* gene (Punga and Buhler 2010).

The *FXN* gene is expressed in all cells, but at varying levels in different tissues and during development (Campuzano *et al.* 1996; Koutnikova *et al.* 1997). *FXN* mRNA is expressed predominantly in tissues with a high metabolic rate, including kidney, liver, heart and brown fat. However, highest levels of *FXN* were identified in the spinal cord and somewhat lower levels in cerebellum. Frataxin expression is generally higher in mitochondria-rich cells, such as cardiomyocytes and neurons (Koutnikova *et al.* 1997). The *FXN* mRNA levels in FRDA patients vary in between 13% and 30% compared to unaffected individuals (Campuzano *et al.* 1996; Pianese *et al.* 2004). Along with FRDA, other diseases have also been reported to be caused by the expansion of various trinucleotide repeats in the non-coding region of the gene(s) (Table 1.1).

Table 1.1 - Diseases caused by expansion of non-coding trinucleotide repeats (adopted from Cummings and Zoghbi 2000).

Disease	Gene/Locus	Protein	Location
Fragile X-syndrome	FRAXA/Xq27.3	FMRP	5'-UTR
Fragile XE-syndrome	FRAXE/Xq28	FMR-2 protein	Promoter
Myotonic Dystrophy	DMPK /19q13	DMPK	3'-UTR
Spinocerebellar ataxia type 8	SCA8 /13q21	None	3'-terminal exon
Spinocerebellar ataxia type 12	SCA12/5q31-33	PP2A-PR55β	5'-UTR

As mentioned earlier, the common mutation that causes FRDA is the hyperexpansion of the GAA repeats in the first intron of the *FXN* gene. Ninety six percent of FRDA patients are homozygous for GAA expansions (Campuzano *et al.* 1996), and the remaining 4% are compound heterozygous for an expanded allele and a point mutation within the coding sequence of the gene (Christodoulou *et al.* 2001). So far, no patients have been identified that carry point mutations in both copies of the frataxin gene.

Normal individuals contain less than 30 GAA repeats, whereas disease-causing expanded GAA repeats (>1000 triplets) arise from hyperexpansion of a premutation (30-65 triplets) (Cossee *et al.* 1997b; Montermini *et al.* 1997b). Late onset patients of FRDA can be divided into three sub groups; firstly, late onset FRDA (LOFA), posses fewer than 500 GAA repeats (Durr *et al.* 1996; Filla *et al.* 1996). Secondly, very late onset FRDA, which contains fewer than 300 GAA repeats and have at least one expanded allele (Bidichandani *et al.* 2000; Berciano *et al.* 2002), and thirdly, acadians, who are different from the other types of FRDA and show a late onset with a mean age of 27 years, accompanied by wheelchair confinement (Montermini *et al.* 1997a).

1.1.1 - Origin of the GAA repeat expansion

There is no clear explanation of how the GAA repeats are expanding in the FRDA patients. To obtain clues about the origin of the GAA repeat expansions, Pandolfo *et al.* (1998) investigated the GAA repeats in normal chromosomes and they found that GAA repeats were distributed in two ways; small normal (83%, 6-10 triplets), and large normal (17%, 12-36 triplets) groups. This finding suggested that polymerase 'stuttering' may take place that leads to size heterogeneity within small normal and large normal groups. Furthermore, the authors also speculated that the jump from the small normal to the large normal group was probably a rare or singular event, as also suggested by linkage disequilibrium results revealing the association of different marker haplotypes to small normal and large normal alleles (Cossee *et al.* 1997b; Montermini *et al.* 1997a). Eventually, in consistency with myotonic dystrophy (Imbert *et al.* 1993), large number alleles containing uninterrupted triplet of more than 34 GAA repeats, so called risk alleles, have indeed been observed to undergo hyperexpansion to hundreds of GAA triplets in one generation, and this leads to FRDA pathology with expanded GAA repeats (Cossee *et al.* 1997b; Montermini *et al.* 1997a; Pandolfo 1998).

1.1.2 - GAA repeat instability

The FRDA-associated expanded alleles show both intergenerational and somatic (mitotic) instability.

Intergenerational instability

Like other trinucleotide repeat disorders, the GAA repeat that underlies FRDA is unstable when it is transmitted from parent to offspring, showing both expansions and contractions (Campuzano *et al.* 1996; Durr *et al.* 1996; Montermini *et al.* 1997b). However, the intergenerational GAA instability showed a sex bias as both expansions and contractions were found during maternal transmission, while predominantly contractions were identified during paternal transmission (Monros *et al.* 1997; Pianese *et al.* 1997).

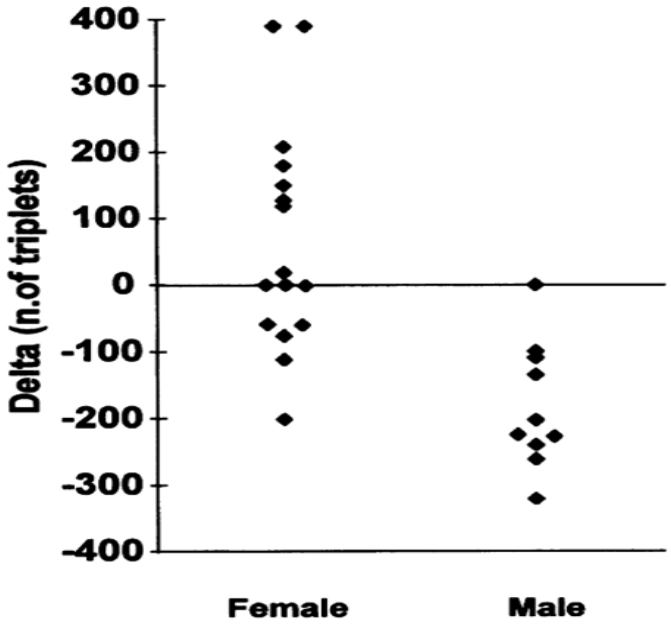

Figure 1.3 - Analysis of Intergenerational repeat length variation in parental gender. Contraction/expansion ratio differed according parental gender ($p<0.004$) (Pianese *et al.* 1997)

Somatic instability

Small pool PCR (SP-PCR) analysis of DNA from tissues of an 18-week foetus, homozygous for the expanded allele, has revealed that there are remarkably low levels of somatic instability (4.2%) in all tissues tested compared to tissues from a 24 year old adult (30.6%) (Figure 1.4) (De Biase *et al.* 2007b). These findings indicate that somatic instability in FRDA is age-dependent and maybe perhaps DNA replication has a potential role.

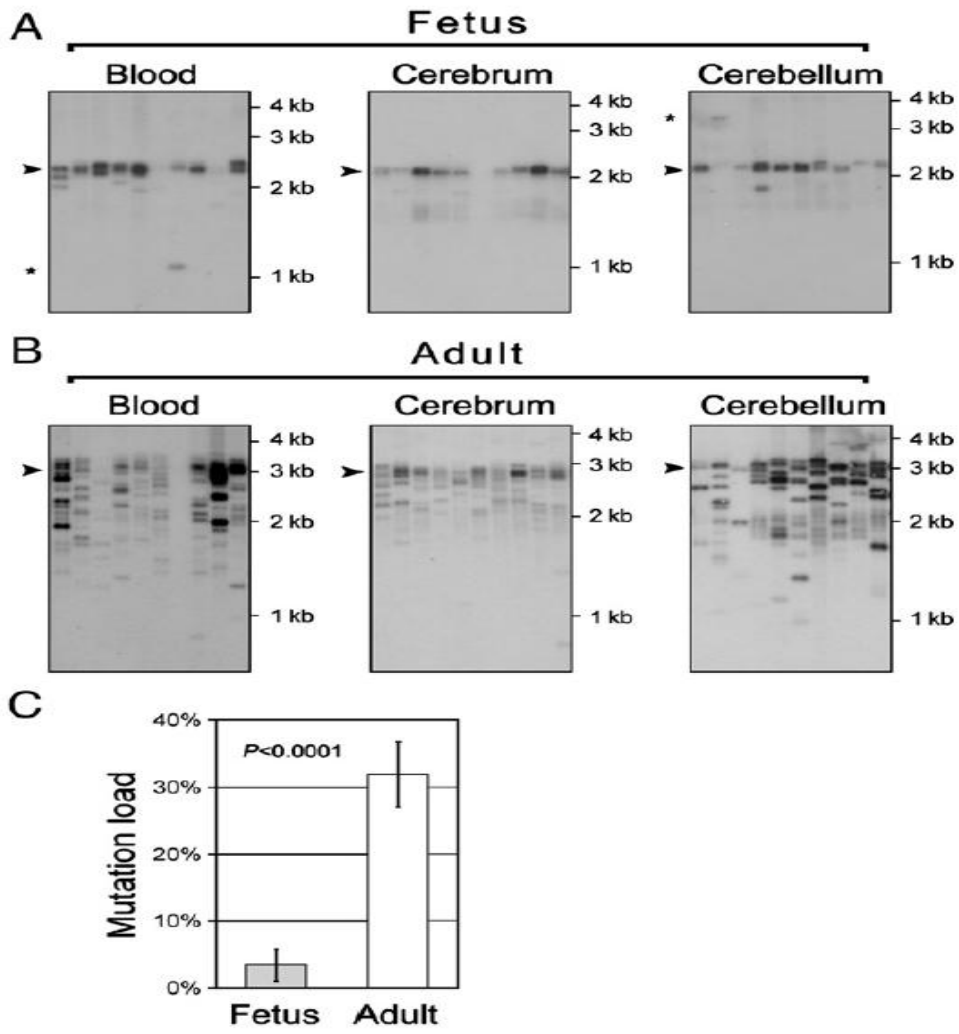

Figure 1.4 - Small pool PCR analysis of somatic instability in foetus and adult tissues. Southern blot showing limited somatic instability in representative tissues of A) foetus, and B) adult, each of whom is homozygous for expanded alleles. C) Cumulative average mutation load of fetal and adult tissues. Error bars depict ±2 SEM (De Biase *et al.* 2007b).

Subsequently, the mutation load was also investigated in blood samples from multiple patients and carriers and showed significantly (p=0.0001) increased mutation load with age, ranging from 7.5% at 18-weeks gestation to 78.7% at 49 years of age. It has been hypothesized that in FRDA somatic instability occurs after early embryonic development (De Biase *et al.* 2007b).

Recently, SP-PCR analysis on multiple tissues obtained from six autopsies of FRDA patients revealed that somatic instability was exhibited in a tissue specific manner (Figure 1.5A) (De Biase *et al.* 2007a). In addition, a significantly greater frequency of expansions was detected in DRG in an age-dependent manner showing small expansions in early age and large expansions at a later stage (Figure 1.5B) (De Biase *et al.* 2007a). The increased levels of somatic instability in post-mitotic tissues indicate that erroneous DNA replication alone is unlikely to be the mechanism and the other factors must be at play.

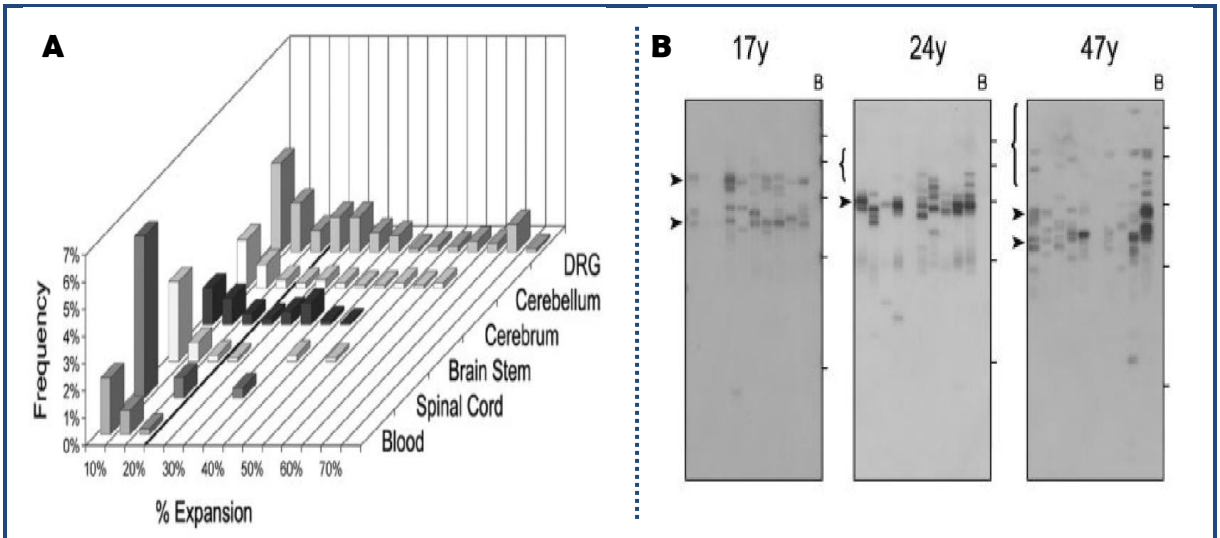

Figure 1.5 - High prevalence of large expansions in DRG as identified by SP-PCR in foetus and adult tissues. A) Frequency distribution (plotted on the y-axis) of expansion seen in various tissues derived from a FRDA patient, and B) increasing levels of large expansions in DRG samples derived from the patients aged 17, 24, and 47 years. Each lane contains "small pools" of 10-15 individual *FXN* molecules (De Biase *et al.* 2007a).

1.1.3 - Pathological GAA repeat expansions and abnormal structures

It has been suggested that development of FRDA is caused by an expanded GAA repeat in intron 1 of the *FXN* gene. Severely reduced levels of *FXN* mRNA and protein have been demonstrated in FRDA patients' tissue samples and cultured cells (Campuzano *et al.* 1997). Inhibition of the *FXN* gene is characterized at the transcriptional level and not at the post transcriptional RNA processing level (Delatycki *et al.* 2000). The expanded GAA·TTC repeat sequence associated with FRDA adopts non-B DNA structures, such as triplex and sticky DNA structures (Mariappan *et al.* 1999; Sakamoto *et al.* 1999; Sakamoto *et al.* 2001).

A DNA triplex is formed upon binding of a pyrimidine (Y) or a purine (R) single-stranded DNA to the major groove of a double helix, forming Hoogsten or reverse-Hoogsten hydrogen bonds between the purine strand and the duplex (Jain *et al.* 2002). Triplexes in general may take the form R·R·Y or Y·R·Y, depending on whether the third strand is purine-rich or pyrimidine-rich (Figure 1.6a) (Grabczyk and Usdin 2000). Eventually, these structures can be formed as intermolecular structures or as folded intramolecular structures (Frank-Kamenetskii and Mirkin 1995; Grabczyk and Usdin 2000; Mirkin 2007). However, the exact molecular mechanism by which the GAA·TTC expansion reduces the *FXN* mRNA levels is still unknown. Furthermore, models based on several different triplex variants have been suggested to explain the effects of GAA·TTC tract expansion as a possible block to transcription elongation in *FXN* (Sakamoto *et al.* 1999; Jain *et al.* 2002; Krasilnikova and Mirkin 2004).

Sticky DNA structures are the expanded state of triplex DNA and are more stable than triplex structures. Son *et al.* (2006) have described that sticky DNA structures were formed by the association of two long GAA·TTC repeat sequences and this was a novel and unprecedented feature of the repeat (Figure 1.6b) (Son *et al.* 2006).

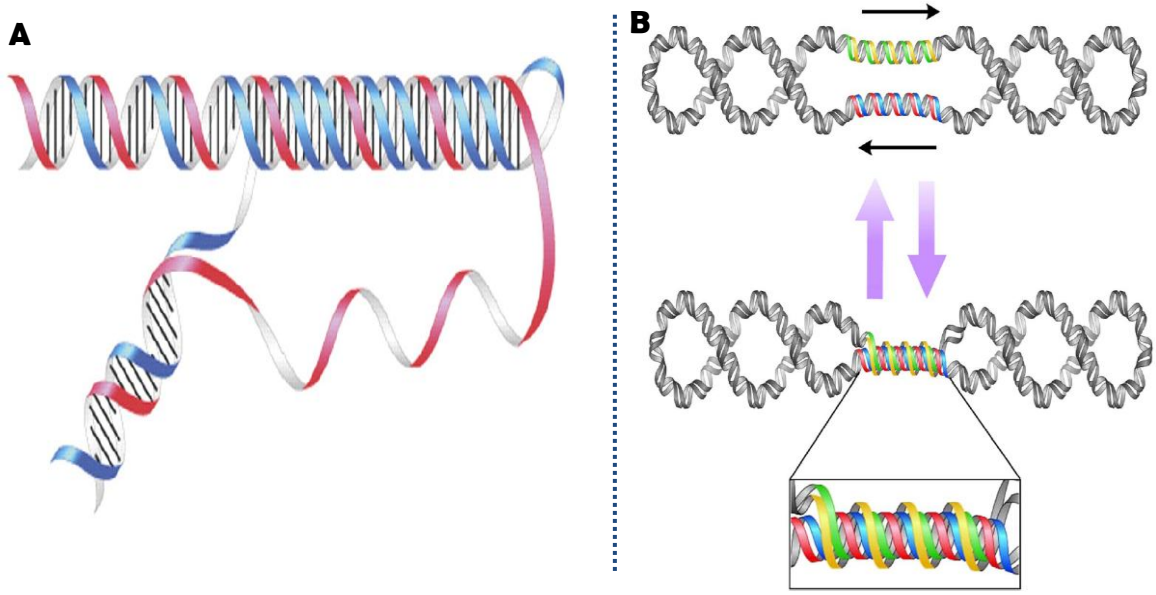

Figure 1.6 - Model of intramolecular DNA triplex and sticky DNA structures. A) Diagram showing DNA triplex structure formed by the expansion of GAA·TTC triplet repeats (Wells 2008), B) Model diagram showing the sticky DNA in a closed circular plasmid. The green and yellow strands represent one GAA•TTC duplex and the red and blue strands represent the other duplex (Son *et al.* 2006).

1.1.4 - Epigenetic changes in FRDA

In contrast to the earlier mentioned abnormal structure hypothesis, Saveliev *et al.* (2003) showed that when expanded GAA repeats were introduced into the mouse genome, position-effect variegation (PEV) of an adjacent reporter gene was induced. PEV is the hallmark of heterochromatin-mediated gene silencing and is thought to be caused by variable spreading of heterochromatin, which renders the gene inaccessible to the transcriptional machinery (Dillon and Festenstein 2002). Therefore, one can speculate that in FRDA where *FXN* deficiency is associated with expanded GAA repeats, there may be abnormal chromatin organization. PEV occurs when a gene is located abnormally close to regions of heterochromatin, and silent heterochromatin is characterized by the presence of certain types of histone modifications. These are indicated by the absence of acetylated histones and the presence of methylated histones, histone deacetylases (HDACs), DNA methyltransferases, chromodomain proteins and polycomb group proteins (Elgin and Grewal 2003).

It has been shown that when heterochromatin protein 1 (HP1), a key constituent of heterochromatin (Eissenberg *et al.* 1992; Elgin 1996), is over expressed, it acts as a powerful modifier of mammalian PEV, leading to increased GAA repeat-associated reporter gene silencing in transgenic mice (Festenstein *et al.* 1999; Saveliev *et al.* 2003). Furthermore, recent studies have indicated that FRDA may be caused by heterochromatin formation Inhibiting *FXN* transcription factors, thereby leading to gene silencing (Figure 1.7) (Saveliev *et al.* 2003; Festenstein 2006). This hypothesis was further strengthened by the finding of a differential DNA methylation profile accompanied by histone acetylation and methylation changes in FRDA (Herman *et al.* 2006; Greene *et al.* 2007; Al-Mahdawi *et al.* 2008).

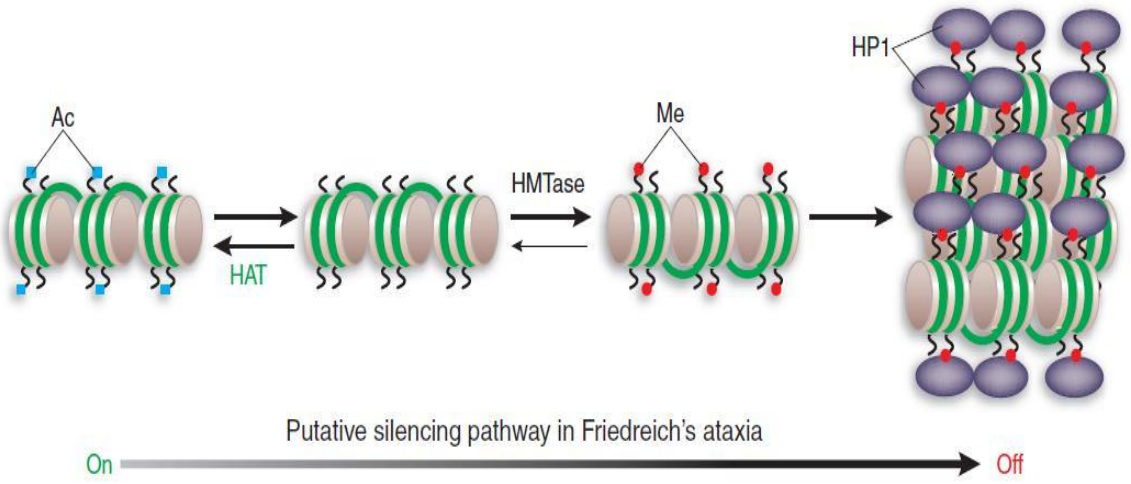

Figure 1.7 - Putative heterochromatin-mediated silencing pathway in FRDA. The chromatin organization of an active *FXN* gene is shown on the far left. Protruding from the nucleosomes are acetylated histone tails (Ac, acetyl). The presence of GAA repeats might nucleate heterochromatin formation, pushing the pathway to the right through several stages. An early step in this process may be the deacetylation of the lysines on histones, which would provide a substrate for histone methyltransferases (HMTases). Methylation of the histone H3 tail (on Lys9) would provide a binding site for HP1, consistent with a histone code for silencing. If the nucleosomes were sufficiently close (possibly because of the repetitive nature of the DNA), then HP1 dimers might stabilize a condensed higher-order heterochromatin structure that prohibits access of the transcriptional machinery to the *FXN* locus (Festenstein 2006).

For the consideration of future FRDA therapy, it is first essential to understand the mechanism of GAA-induced inhibition of *FXN* gene transcription. Therefore, Al-Mahdawi and colleagues (2008) have investigated the DNA methylation changes of *FXN* flanking GAA regions in FRDA patients' brain, heart and cerebellum tissues. This investigation revealed a shift in the FRDA DNA methylation profile, with upstream CpG sites comparatively hypermethylated and downstream CpG sites becoming consistently hypomethylated. In addition, differential DNA methylation at three specific CpG sites within the *FXN* promoter and one CpG site within exon 1 were also identified (Al-Mahdawi *et al.* 2008).

In FRDA patients, comparable histone modifications were also observed such as reduced H3 and H4 acetylation, and increased H3K9 trimethylation at the upstream and downstream regions of the expanded GAA repeat tract compared to normal individuals (Herman *et al.* 2006; Al-Mahdawi *et al.* 2008).

Although several epigenetic changes have been identified in FRDA (Table 1.2), it is still unclear of which histone modification is directly involved in *FXN* silencing. However, it has been shown that the promoter region of FRDA patients is associated with reduced levels of acetylated H3K5, H3K14, H4K5 and H4K16 (Herman *et al.* 2006; Al-Mahdawi *et al.* 2008; Kumari and Usdin 2010) indicating a less permissive region for transcription. In particular, acetylated H4K16 is thought to play an important role in maintaining an open chromatin configuration (Shogren-Knaak *et al.* 2006). In addition, lymphoblasts derived from FRDA patients have shown reduced levels of H3K4me3 and H4K36me3, two important histone modifications associated with transcription initiation and elongation respectively, compared with normal lymphoblasts (Kumari and Usdin 2010). These findings have suggested that *FXN* silencing in FRDA alleles may be as a consequence of transcription initiation and elongation problems due to abnormal histone modifications. Therefore, considering these histone changes in future studies may perhaps give rise to more potential FRDA therapies.

Table 1.2 - Epigenetic changes as seen in FRDA patients, cell lines or mouse models.

Chromatin Change	Location	Patients/Cell type/animal model	Reference(s)
DNA methylation ↑	*FXN* promoter	Lymphoblasts, FRDA patients, FRDA YAC transgenic mice, primary fibroblasts	(Herman *et al.* 2006; Greene *et al.* 2007; Al-Mahdawi *et al.* 2008)
	GAA upstream	FRDA patients and FRDA YAC transgenic mice	(Al-Mahdawi *et al.* 2008)
H3K9me2/3↑	*FXN* promoter	FRDA patients, FRDA YAC transgenic mice, Primary fibroblasts	(Al-Mahdawi *et al.* 2008; De Biase *et al.* 2009)
	GAA upstream	Lymphoblasts, FRDA YAC transgenic mice, KIKI mice (H3K9me3)	(Herman *et al.* 2006; Al-Mahdawi *et al.* 2008; Rai *et al.* 2008; Punga and Buhler 2010)
	GAA downstream	FRDA patients, FRDA YAC transgenic mice, Lymphoblasts	(Al-Mahdawi *et al.* 2008; Punga and Buhler 2010)
H3K4me2↓	*FXN* promoter, GAA up and downstream	Lymphoblasts	(Kumari *et al.* 2010)
H3K4me3↓	*FXN* exon 1, GAA up and downstream	Lymphoblasts	(Kumari *et al.* 2010)
H3K27me3 and HP1α/δ↑	*FXN* 5'UTR	Primary fibroblasts	(De Biase *et al.* 2009)
H3K36me3↓	GAA downstream, *FXN* exon 2	Lymphoblasts	(Kumari *et al.* 2010)
H3K9ac↓	*FXN* promoter	FRDA patient brain tissue, Lymphoblasts	(Al-Mahdawi *et al.* 2008; Kumari *et al.* 2010)
	GAA upstream	FRDA patients, FRDA YAC transgenic mice, Lymphoblasts cells, KIKI mice	Al-Mahdawi, 2008 #2911}(Herman *et al.* 2006; Rai *et al.* 2008; Kumari *et al.* 2010)
	GAA downstream	FRDA patients, FRDA YAC transgenic mice, Lymphoblasts	(Herman *et al.* 2006; Al-Mahdawi *et al.* 2008; Kumari *et al.* 2010)
H3K14ac↓	*FXN* promoter	FRDA patients	(Al-Mahdawi *et al.* 2008)
	GAA upstream	KIKI mice, Lymphoblasts	(Herman *et al.* 2006; Kumari *et al.* 2010)
	GAA downstream	FRDA YAC transgenic mice, Lymphoblasts	(Kumari *et al.* 2010)
H4K5ac↓	*FXN* promoter	Lymphoblasts	(Kumari *et al.* 2010)
	GAA upstream	Lymphoblasts, KIKI mice	(Herman *et al.* 2006; Rai *et al.* 2008; Kumari *et al.* 2010)
	GAA downstream	FRDA patients, FRDA YAC transgenic mice, Lymphocytes	(Herman *et al.* 2006; Al-Mahdawi *et al.* 2008; Kumari *et al.* 2010)
H4K8ac↓	GAA upstream	Lymphoblasts, FRDA patients, KIKI mice	(Herman *et al.* 2006; Al-Mahdawi *et al.* 2008; Rai *et al.* 2008; Kumari *et al.* 2010)
	GAA downstream	Lymphoblasts, FRDA patients	(Herman *et al.* 2006; Kumari *et al.* 2010)
H4K12ac↓	*FXN* promoter	Lymphoblasts	(Herman *et al.* 2006)
	GAA up and downstream	Lymphoblasts, FRDA patients, FRDA YAC transgenic mice	(Herman *et al.* 2006; Al-Mahdawi *et al.* 2008)
H4K16ac↓	*FXN* promoter	Lymphoblasts	(Rai *et al.* 2008; Kumari *et al.* 2010)
	GAA up and downstream	Lymphoblasts, FRDA patients, FRDA YAC transgenic mice, KIKI mice	(Herman *et al.* 2006; Al-Mahdawi *et al.* 2008; Rai *et al.* 2008; Kumari *et al.* 2010)

Abbreviations/symbols: ↓- reduced, ↑-increased, H-histone, K-lysine, me2-dimethylation, me3-trimethylation, ac-acetylation, HP-heterochromatin protein

1.2 - Frataxin protein: structure

To date, crystal structures of yeast, human and bacterial (CyaY) frataxin orthlogues have been reported and they were shown to be structurally similar (Cho *et al.* 2000; Dhe-Paganon *et al.* 2000; Musco *et al.* 2000; Nair *et al.* 2004). Frataxin does not resemble any other protein of known function. Mature frataxin is a compact, globular protein containing an N-terminal α-helix; seven β strands and a C-terminal end (Figure 1.8) (Dhe-Paganon *et al.* 2000; Musco *et al.* 2000). Strands β1– β5 form a flat anti-parallel β sheet that interacts with the two helices, α1 and α2. The axes of the two helices are nearly parallel to each other, and both are parallel to the plane of the large β sheet. The C terminus of β5 and strands β6 and β7 forms a second, smaller β sheet. This smaller sheet projects from the N terminus of α2 along its long axis. The connections between all elements of secondary structures are short and well ordered, which contributes to the compact appearance of frataxin (Dhe-Paganon *et al.* 2000).

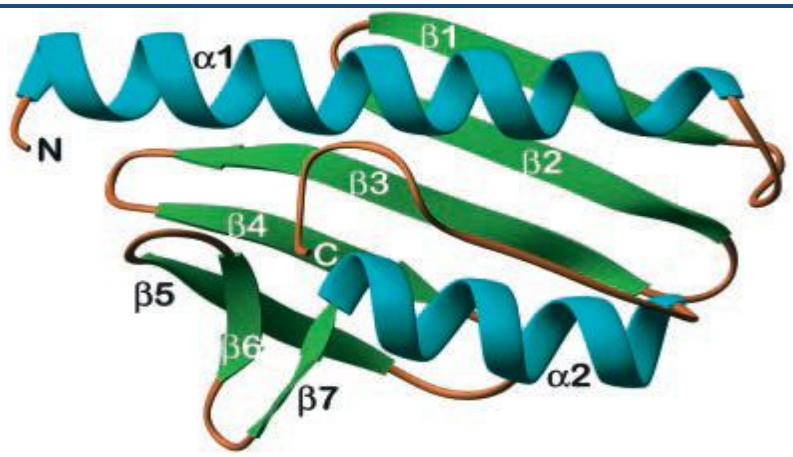

Figure 1.8 - Structure of frataxin protein. Ribbon diagram showing the fold of frataxin, a compact αβ sandwich, with helices coloured *turquoise* and β strands in *green*. (Dhe-Paganon *et al.* 2000).

1.2.1 - Localization and maturation of frataxin protein

Frataxin is a conserved protein found ubiquitously in prokaryotes and eukaryotes and it is required for the cellular regulation of iron homeostasis. Frataxin homologues are expressed in the cytoplasm as larger precursors, which are proteolytically removed by the mitochondrial processing peptidase (MPP) enzyme upon entry into the mitochondria to yield mature frataxin protein (Koutnikova *et al.* 1998; Gordon *et al.* 1999). Selective deletion of yeast frataxin homologue, Yfh1p, has shown reduced mitochondrial respiration (Wilson and Roof 1997), loss of mtDNA (Koutnikova *et al.* 1997) and accumulation of iron in the mitochondria (Babcock *et al.* 1997). Frataxin is predominantly localized to the mitochondrial cristae and is a free soluble protein within the mitochondrial matrix (Campuzano *et al.* 1997). However, recently extramitochondria localization of frataxin has also been demonstrated in Caco-2 cells (Acquaviva *et al.* 2005), lymphocytes, HeLa and HEK293 cells (Condo *et al.* 2006; Condo *et al.* 2010)

The mature form of frataxin was initially reported to be 56-210 amino acids (m56-*FXN*). However, two independent reports have challenged these studies describing two different forms encoded by amino acids 78-210 (m_{78}-*FXN*) (Condo *et al.* 2007; Yoon *et al.* 2007) and 81-210 (m_{81}-*FXN*) (Figure 1.9) (Schmucker *et al.* 2008). Boehm *et al.* (2010) have recently shown that frataxin protein levels vary up to three fold between normal individuals (<26 GAA repeats). Interestingly, the protein levels in these individuals are independent of age and GAA repeat size.

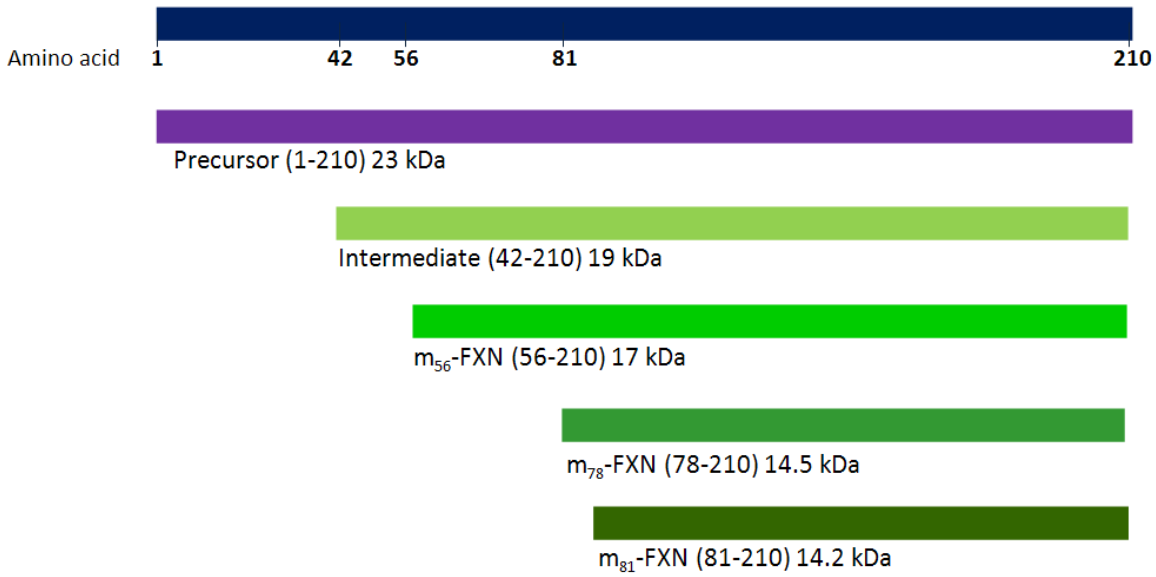

Figure 1.9 - Schematic representation of different forms of frataxin protein. The precursor of frataxin (encoded by amino acids 1–210) is targeted to the mitochondria and undergoes a two-step maturation process. The intermediate (i-*FXN*) and the three described mature forms beginning at the amino acids 56 (m56-*FXN*), 78 (m78-*FXN*) or 81 (m_{81}-*FXN*) are represented. This picture was adopted from Schmucker *et al.*(2008).

1.2.2 - Molecular functions of frataxin

Although the exact function of *FXN* is still unknown, complete deficiency of *FXN* in mice leads to early embryonic lethality (Cossee *et al.* 2000), indicating that *FXN* is essential for early development. In eukaryotes, frataxin is necessary for normal mitochondrial function (Koutnikova *et al.* 1997; Pianese *et al.* 1997). Studies in human, yeast and mouse models of FRDA have provided further insights into FRDA pathogenesis. These studies have suggested that frataxin may be involved in mitochondrial iron homeostasis (Bradley *et al.* 2000; Lodi *et al.* 2001b), synthesis of Fe-S cluster proteins (Koutnikova *et al.* 1997; Cavadini *et al.* 2000; Puccio *et al.* 2001) and protection from oxidative stress (Schulz *et al.* 2000; Wilson 2003).

Frataxin and iron homeostasis

The investigation of the yeast frataxin homologue gene 1 (*Yfh1*) demonstrated that the frataxin protein was involved in iron efflux from mitochondria (Radisky *et al.* 1999). Furthermore, accumulation of iron was consistently observed in autopsy of heart muscle (Bradley *et al.* 2000) and the dentate nucleus (Waldvogel *et al.* 1999; Koeppen *et al.* 2007) of FRDA patients. In addition, small but significant intra-mitochondrial iron accumulation has also been reported in FRDA patients (Schapira *et al.* 1990). However, total mitochondrial iron levels were not increased (Puccio and Koenig 2000; Wong *et al.* 2000). In addition, mitochondrial iron accumulation and changes in Fe-S dependent enzyme activity, in a conditional mouse model of FRDA occur considerably later than the onset of pathology (Puccio *et al.* 2001), indicating that this cannot be the causative pathological mechanism.

In contrast, by using the bacterial frataxin orthologue (CyaY), Adinolfi *et al.* (2009) proposed that frataxin is not merely an iron chaperon, but it works as a molecular regulator able to inhibit, depending on the extent to which it is iron saturated, the formation of 2Fe-2S clusters (Figure 1.10). However, more investigation is needed to confirm the details of the molecular mechanism underlying the Fe-S cluster biosynthesis inhibition exerted by CyaY.

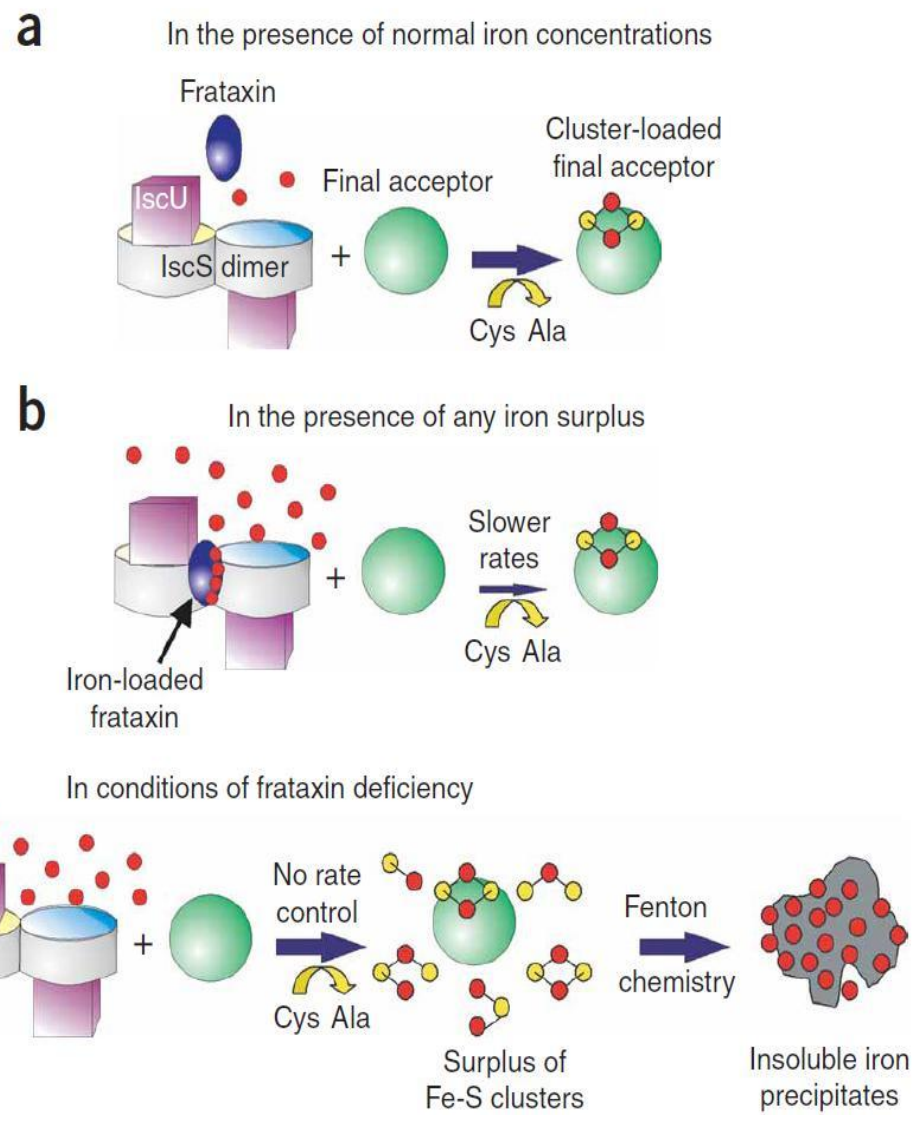

Figure 1.10 - Schematic representation of the molecular mechanism of frataxin in the cell during **a)** normal iron concentrations, **b)** excess of iron concentrations, and **c)** absent/insufficient of frataxin conditions (Adinolfi *et al.* 2009).

Frataxin and oxidative stress

Regardless of the mechanism of mitochondrial iron accumulation, which is probably a secondary consequence in FRDA, it is likely that it contributes to the production of reactive oxygen species (ROS) leaking from the respiratory chain, leading to the formation of free radicals through Fenton chemistry (Lenaz *et al.* 2002; Lodi *et al.* 2002; Voncken *et al.* 2004). In support to this hypothesis, evidence of increased oxidative stress and damage in FRDA patients includes raised 8 hydroxy 2' deoxyguanosine (8OH2'dG) levels in urine (Schulz *et al.* 2000) and raised plasma malondialdehyde (MDA) levels (Emond *et al.* 2000; Bradley *et al.* 2004). In addition, reduced aconitase activity and mitochondrial electron transport complexes I-III were also demonstrated in endomyocardial biopsies of FRDA patients (Rotig *et al.* 1997). Recent evidence has revealed an impaired response of antioxidant enzymes in cell lines and model organisms (Wong *et al.* 1999; Chantrel-Groussard *et al.* 2001; Seznec *et al.* 2005; Calmels *et al.* 2009).

Interestingly, a recent study has demonstrated increased levels of nuclear and mitochondrial DNA damage in peripheral blood samples from FRDA patients (Haugen *et al.* 2010). However, whether the increase in DNA damage is a consequence of an impaired antioxidant defence or directly linked to an ISC deficit remains to be determined, as several damaged proteins are ISC proteins (reviwed in Schmucker and Puccio 2010).

1.3 - Therapeutic approaches

Since the identification of the disease gene causing FRDA in 1996, important progress in the comprehension of frataxin function has been made. To date several agents have been found to increase frataxin expression in cellular and mouse models of FRDA and some of these compounds are already in different stages of clinical trial (Figure 1.11). However, the mode of action for most of these compounds in up-regulating *FXN* expression is still unclear.

1.3.1 - Iron chelators

Recent discoveries on the potential function of frataxin suggested that intracellular iron imbalance resulting in oxidative stress is involved in pathogenesis of FRDA. Therefore, it has been considered that iron chelation therapy may be able to ameliorate disease by protecting mitochondria from the adverse effects of iron over load. In a first instance iron chelator, desferrioxamine (DFO) which is already in the clinical trial for rheumatoid arthritis (Voest *et al.* 1994), was used as a potential therapy for FRDA. Wong et al. (1999), demonstrated that DFO significantly rescues human fibroblast cells from induced oxidative stress by hydrogen peroxide. However, due to the lack of ability to target mitochondrial iron pools (Richardson 2003), DFO may cause severe generalized iron deficiency. Furthermore, reduced frataxin mRNA and protein levels were identified in fibroblasts from individuals with FRDA and normal individuals treated with DFO (Li *et al.* 2008). Therefore, care should be taken when using iron chelators as therapeutic agents since they could displace rather than protect against iron mediated toxicity.

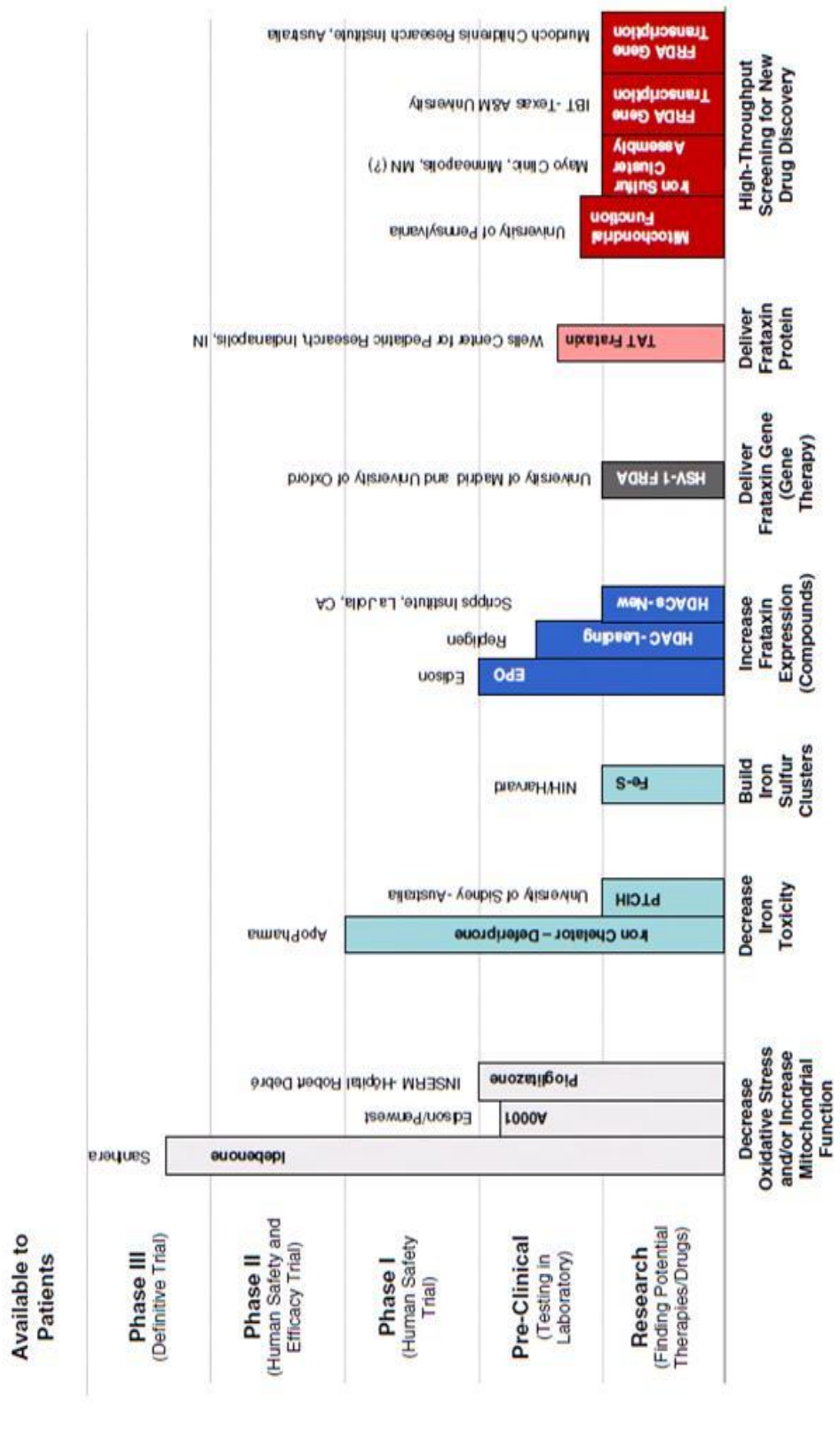

Figure 1.11 - Schematic representation of the FRDA clinical pipeline, which is an illustration of potential therapies being developed. On the horizontal axis, each leading drug candidate is represented by its own bar and is grouped by its mechanism of action. Each mechanism of action targets one of the known causes of FRDA. The milestones for drug development are listed on the vertical axis (adopted from *http://www.curefa.org/pipeline.html*).

In the next approach, a mitochondrial-specific iron chelator, 2-pyridylcarboxaldehyde isonicotinoyl hydrazone (PCIH), was used in an *in vivo* study and produced more promising results (Richardson *et al.* 2001; Richardson 2003). However, due to the lack of efficacy, this clinical trial was terminated. More recently, a small phase I/II clinical trial of individuals affected with FRDA has been carried out using the orally-available iron chelator, deferiprone (Boddaert *et al.* 2007). Encouraging results have now prompted the use of deferiprone in larger phase II clinical trial, which is ongoing. However, recently it has been reported that treatment of FRDA patients' fibroblasts with deferiprone showed reduced aconitase enzyme activity (Goncalves *et al.* 2008), indicating that iron-chelation is beneficial only at some particular step of the disease.

1.3.2 - Antioxidant therapy

Coenzyme Q10 and vitamin E

The involvement of mitochondrial respiratory chain dysfunction and oxidative stress in the pathogenesis of FRDA suggests that the course of the disease may be modified by treatment with antioxidant agents. Initial clinical trials utilizing a combination of coenzyme Q_{10} and vitamin E over a period of three months resulted in improved ATP production in heart and skeletal muscle of individuals with FRDA (Lodi *et al.* 2001a). Another long-term follow-up study over a period of 47 months with 10 FRDA patients showed sustained improvement in bioenergetics and improved cardiac function (Hart *et al.* 2005). However, due to the absence of a placebo group in this clinical trial these results must be interpreted with caution and/or the results will be evaluated with additional controlled trials. Recently, it

has been reported that FRDA patients showed decreased serum CoQ_{10} and vitamin E levels (Cooper *et al.* 2008), which may contribute to the clinical progression of the disease.

Idebenone

Idebenone, a short-chain benzoquinone structurally related to coenzyme Q_{10}, has been investigated in patients with FRDA. Early clinical trials with idebenone treatment at doses of 5mg/kg/day showed a reduction of the left ventricular mass and wall thickness (Rustin *et al.* 1999; Hausse *et al.* 2002; Mariotti *et al.* 2003; Hart *et al.* 2005). However, no neurological effect was determined with idebenone (Rustin *et al.* 1999). In addition, Ribai *et al.* (2007) investigated the efficacy of idebenone in a large cohort of 61 patients and found a marked reduction of left-ventricular mass, which was accomplished by worsening, rather than improvement, of ejection fraction. Furthermore, idebenone treatment has also resulted in decreased levels of urinary 8-hydroxy-2'-deoxyguanosine, which is a peripheral marker of oxidative DNA damage (Schulz *et al.* 2000). However, it has been confirmed that high doses (45mg/kg/day) of idebenone were generally well tolerated and associated with slight improvement in neurological function and activities of daily living (ADL) in individuals with FRDA (Di Prospero *et al.* 2007a; Di Prospero *et al.* 2007b). This finding indicating that a higher dose of idebenone may be necessary to have a beneficial neurological function.

Mito Q and Mito Vit E

Recent evidence has revealed that the limited effectiveness of idebenone and vitamin E as antioxidant therapies for FRDA is due to the distribution of these compounds through extracellular and intracellular compartments, with only a small proportion accumulating in mitochondria (Jauslin *et al.* 2003). Thus, targeting these molecules to mitochondria may improve their effectiveness. Therefore, in an effort to improve the efficiency and delivery of idebenone and vitamin E, two mitochondria-targeted antioxidants, Mito Q and Mito Vit E, were developed by covalently coupling with lipophilic cations (Murphy 1997; Smith *et al.* 1999; Murphy and Smith 2000; Kelso *et al.* 2001). Jauslin *et al.* (2003), showed that Mito Q successfully protected the cells 800 times more than idebenone, from endogenous oxidative stress. However, Mito Vit E failed to protect the cells more than Mito Q, but was still 20 times more effective than idebenone. Interestingly, an *in vivo* study demonstrated the accumulation of Mito Q in the heart and brain of mice, indicating its capacity to cross the blood brain barrier (Smith *et al.* 2003). In conclusion, these data suggested that mitochondria-targeted antioxidants may be therapeutically more effective than untargeted antioxidants, particularly as they are rapidly taken up by the brain.

1.3.3 - Gene based approaches

The current therapeutic strategies for FRDA mainly act to slow down the consequences of frataxin deficiency. Drugs that are able to increase the amount of frataxin would represent excellent candidates for a rational approach. Recently, several drugs have been assessed for their ability to increase the amount of cellular frataxin, including; histone deacetylase (HDAC) inhibitors, peroxisome proliferator-activated receptor (PPAR)-agonists and recombinant human erythropoietin (rhu-EPO).

HDAC inhibitors

Recent studies indicated that expanded GAA repeats have been shown to induce heterochromatin mediated silencing of *FXN* gene in a manner reminiscent to PEV gene silencing (Saveliev *et al.* 2003). Since acetylation and deacetylation of histone proteins are involved in transcriptional regulation, it has been suggested that HDAC inhibitors may revert silent heterochromatin to an active chromatin and restore the normal function of genes that are silenced in these diseases (Langley *et al.* 2005). The use of HDAC inhibitors as an effective therapy for FRDA has been very well explored in recent years. Treatment of HDAC inhibitors produced significant increase of frataxin mRNA and protein expression, and elevated levels of histone acetylation in *in vitro* (Herman *et al.* 2006) and *in vivo* (Rai *et al.* 2008; Rai *et al.* 2010) model systems. However, HDAC inhibitor therapeutic approaches still require long term *in vivo* studies. Therefore, we have investigated for the first time the long term efficacy of HDAC inhibitors in FRDA therapy and this will be discussed in more detail in chapter 5.

Peroxisome proliferator-activated receptor (PPAR)-agonists

The peroxisome proliferator-activated receptors (PPAR α, β/δ and γ) are members of nuclear receptor family, and recently emerged as transcription factors that regulate diverse aspects of metabolism (Theocharis *et al.* 2004). PPAR-γ agonists, such as rosiglitazone and piogliotazone have already shown their potential use in diabetes mellitus (Richter *et al.* 2007), other neurodegenerative disorders including Alzheimer's disease, Parkinson's disease, multiple sclerosis, and amylotrophic lateral sclerosis (ALS) (Heneka and Landreth 2007). In FRDA, Marmolino *et al.* (2009) showed that the commercially available PPAR-γ agonist, azelaoyl PAF (APAF), produced statistically significant increases in frataxin mRNA and protein levels in fibroblasts and SKNBE cells from FRDA patients up to 2-fold. The first clinical trial is currently underway with pioglitazone.

Recombinant human erythropoietin (rhu-EPO)

Recently, erythropoietin (EPO) has received considerable attention because of the unexpected finding that it also has broad neuroprotective and cardioprotective capabilities (Bogoyevitch 2004; Li *et al.* 2004). Additionally, considerable increase in *FXN* mRNA expression was achieved in FRDA lymphocytes, cardiomyocytes and neuronal cells following treatment with rhu-EPO (Sturm *et al.* 2005). Subsequently, rhu-EPO also showed significant increase in *FXN* expression levels in FRDA patients in a 2-month "proof-of-concept" study (Boesch *et al.* 2007). Furthermore, a first clinical trial with rhu-EPO over a period of 6 months showed stable and significant increase of frataxin expression (Boesch *et al.* 2008), suggesting that rhu-EPO is a good candidate for FRDA therapy. However, in a recent study Acquaviva *et al.* (2008) reported that rhu-EPO was able to increase the frataxin protein without increasing

mRNA at any of the times and doses tested, suggesting that the regulatory effects of rhu-EPO on the frataxin protein are at the post-translational level.

Gene therapy

Although some of the above treatments improved the course of FRDA, they did not affect frataxin expression, so more specific and effective therapies are still needed. Therefore, the development of gene therapy would appear a valuable alternative to treat the neurological disorders in addressing the cause rather than the consequences of FRDA. As a first attempt, Fleming *et al.* (2005) reported the functional recovery of frataxin by delivering human frataxin cDNA by adeno-associated viral (AAV) and lentiviral (LV) vectors in human primary fibroblasts. In another experiment, selective deletion of frataxin in the brain stem of loxP(frda) mice resulted in deficit in the rotarod assay which was recovered by delivering human frataxin cDNA using HSV-1 amplicon vector (Lim *et al.* 2007). Recently, Gomez-Sebastian *et al.* (2007) demonstrated the successful construction and delivery of high capacity herpes simplex virus type 1 (HSV-1) amplicon vectors expressing the entire 80 kb FRDA genomic locus. Following vector transduction, increased frataxin expression and reduced oxidative stress was identified in FRDA fibroblasts (Gomez-Sebastian *et al.* 2007). However, a significant amount of research is still required before gene therapy may be practicable for clinical trials.

1.4 - Development of model systems for FRDA

Model systems of human cells and/or non-human organisms can provide insights into FRDA disease pathology. The high evolutionary conservation of frataxin across the species has enabled the development of disease models in various organisms, from the unicellular eukaryote *Saccharomyces cerevisiae* to the multicellular mouse model. Depending on the frataxin expression levels, various models of FRDA have shown that different, and even opposite, phenotypes can be observed. Therefore, enhanced studies will be needed for the better understanding of the pathophysiological functions of frataxin (reviewed in Puccio 2009).

1.4.1 - Human cell models

In order to generate a cellular model of a neural lineage, human neuronal precursor NT2 (N-tera2) cells were transfected with frataxin-specific interfering RNA (RNAi). The resultant cell line showed approximately 70% reduction in *FXN* mRNA and corresponding reduced levels of frataxin protein were found compared with a scrambled RNAi treated cell line (Tan *et al.* 2003). Sarsero and colleagues (2003) have generated another cell model with a BAC genomic reporter construct consisting of an in-frame fusion between the human *FXN* gene and EGFP under the control of *FXN* promoter (Sarsero *et al.* 2003). However, due to the absence of expanded GAA repeats (the construct has 6 GAA repeats) this model only allows the identification of molecules which act on the WT promoter but not on GAA repeats. Grant *et al*. (2006) have generated an additional GFP reporter cell line by combining part of the first intron of *FXN*, containing either 15 or 148 GAA•TTC repeats, to the coding sequence of

EGFP (Grant *et al.* 2006). Subsequent analysis of GFP expression levels by fluorescence assay and western blotting demonstrated reduced levels of GFP expression in the $[GAA•TTC]_{148}$ cell line compared with the $[GAA•TTC]_{15}$ cell line (Grant *et al.* 2006), suggesting that these cell lines are appropriate models to study the GAA•TTC-mediated silencing effect of *FXN* gene.

Later, Calmels *et al* (2009) have reported the establishment of first cellular models based on the frataxin missense mutation. These new cell models have shown all the biochemical phenotypes associated with FRDA. In addition, it has been recently reported the establishment of induced pluripotent stem (iPS) cells from FRDA patient fibroblasts (Ku *et al.* 2010) and found *MSH2* dependent expansion of GAA repeats. Therefore, one can speculate that such model systems are more accessible resource to study repeat instability mechanism as well as for differentiation of iPS into other cell types affected in this disease.

1.4.2 - *Drosophila* model

A *Drosophila* model of FRDA was generated by selective suppression of *Drosophila* frataxin homologue (*dfh*) by a UAS-GAL4 transgene based RNA-interference (RNAi) technique (Anderson *et al.* 2005). Following suppression of *dfh* gene, distinct phenotypes were observed, such as giant long-lived larvae and conditional short-lived adults. Additionally, deficiency of DFH protein results in diminished activities of numerous haem and Fe-S containing enzymes, loss of iron homeostasis and increased susceptibility to iron toxicity (Anderson *et al.* 2005). In a next attempt, to assess both the role of frataxin and oxidative stress in FRDA, Llorens and colleagues (2007) generated another *Drosophila* line by reducing the *dfh* levels by 30% compared to the controls thus overcoming the pre-adult

lethality observed in the previous model. This model has shown remarkably shortened life span and reduced climbing ability in adulthood. However, no differences in the activity of SDH and aconitase activity between control and *dfh*-RNAi flies were observed (Llorens *et al.* 2007). Recently, this model also showed an increase in fatty acids catalyzing enhancement of lipid peroxidation levels in glial cells, elevating the intracellular toxic potential (Navarro *et al.* 2010), suggesting a strong involvement of glial cells and lipid peroxidation in the generation of FRDA like symptoms.

1.4.3 - *Caenorhabditis elegans (C. elegans)* model

To date several *C. elegans* models with knockdown of the *C. elegans FXN* homolog *frh-1* have been published, but with conflicting findings. Intriguingly, the inactivation of several mitochondrial genes by RNAi prolonged the life span of *C. elegans* (Feng *et al.* 2001; Dillin *et al.* 2002; Lee *et al.* 2003; Rea and Johnson 2003). Similar effects were identified by Ventura et al. (2005), where knockdown of the *frh-1* gene extends the life span of *C. elegans* despite small body size, reduced fertility and altered oxidative response. In contrast, Vazquez-Manrique and colleagues (2006) reported that selective suppression of *frh-1* gene by RNAi technology resulted in a consistent pleiotropic phenotype (slow growth, lethargic behaviour, egg laying defects, reduced brood size and altered defecation) associated with sensitivity to oxidative stress. However, it has been confirmed that the extended lifespan in *C. elegans* following suppression of *frh-1* gene was due to the partial knockdown of the gene, and increased (not complete) inhibition of *frh-1* gene has been shown to reduce lifespan (Rea *et al.* 2007).

1.4.4 - *Saccharomyces cerevisiae* (yeast) model

Many studies in frataxin function arise from experiments performed with yeast, as frataxin and the yeast homologue *YFH1* are orthologues. Yeast cells lacking *Yfh1* have shown decreased cellular respiration, alterations in iron homeostasis and that leads to accumulation of iron (Babcock *et al.* 1997; Foury and Cazzalini 1997). It has been reported that mitochondrial DNA was lost when the *ΔYfh1* cells were grown in iron rich media (Foury 1999). In contrast, accumulation of zinc protoporophyrin (instead of haem) was accumulated in the *ΔYfh1* mutant strains during the development. Microarray analysis of gene expression in *ΔYfh1* mutant strains have shown enhanced expression of genes that are under the control of the iron-sensing transcription factors AFT1/AFT2, including genes involved in iron uptake (Foury and Talibi 2001). Depending on the strain background, the severity of these phenotypes differs quite substantially, thus rendering conclusions on the function of frataxin rather difficult (Muhlenhoff *et al.* 2002).

1.4.5 - Mouse models

Mouse models of FRDA will provide valuable insights into the cascade of events associated with frataxin function, particularly in the early disease states, which can rarely be studied in the humans.

1.4.5.1 - Knockout mouse models

In order to investigate the function of frataxin and the mechanism of the disease, a mouse model was generated by homologous inactivation of *Fxn* gene (Cossee *et al.* 2000). However, this led to embryonic lethality, demonstrating an important function for frataxin during mouse development. Therefore, in parallel, through a conditional gene targeting approach, two lines of conditional knockout mouse models were generated (Puccio *et al.* 2001). These two lines were produced by using a *loxP*-flanked allele and Cre-lines that are driven by the neuron-specific enolase (NSE) and muscle creatine kinase (MCK) promoters, which exhibited heart and striated muscle, and neuron-restricted deletion of frataxin, respectively (Puccio *et al.* 2001). These mice displayed cardiac hypertrophy, large sensory neuron dysfunction, respiratory chain dysfunction, and time dependent intramitochondrial iron accumulation. However, the dorsal columns of the spinal cord, the primary sites of FRDA pathology, were not affected in these mice.

To obtain specific and progressive neurological models for FRDA, Simon and colleagues (2004) have generated inducible knockout mouse models using two transgenic lines expressing the tamoxifen-dependent recombinase (Cre-ER^{T}) under the mouse Prion protein (Prp) promoter. These mouse models have developed prominent features resembling FRDA such as neurodegeneration in DRG, slowly progressive mixed cerebellar

and sensory ataxia associated with posterior columns of the spinal cord and absence of motor involvement.

Subsequently, the involvement of frataxin in diabetes was also investigated in the knockout mice (Ristow *et al.* 2003), where selective suppression of *frataxin* in pancreatic β cells led to a reduction of insulin-secretory capacity, resulting in overt diabetes mellitus in older animals.

1.4.5.2 - Knockin mouse models

Although conditional knockout mouse models are excellent tools for studying disease pathophysiology and for evaluating some therapeutic approaches, they do not precisely mimic the human disease. Therefore, a new approach, the knockin strategy, was developed and resulted in producing knockin mouse models.

In a first attempt to produce the knockin mouse model for FRDA, Miranda *et al*. (2002) introduced 230 GAA repeats into the mouse *frataxin* gene by homologous recombination. Knockin mice were crossed with *Frda* knockout mice to obtain double heterozygous mice ($GAA^{-/230GAA}$) expressing 25-36% of WT frataxin levels. In humans, these levels were typically associated with mild pathology of FRDA. In contrast, although a clear microarray gene expression was determined (Coppola *et al.* 2006), the knockin mice failed to develop FRDA associated pathology such as motor deficits, iron overload or meiotic/mitotic instability of GAA repeats (Miranda *et al.* 2002). Therefore, one can suggest that longer repeats might be essential to produce a good model of FRDA mouse model.

1.4.5.3 - FRDA YAC transgenic mouse models

The FRDA YAC transgenic mouse model, perhaps the best model for FRDA, has been established by the generation of transgenic mice containing the human FRDA gene on a 370 kb YAC clone (Pook *et al.* 2001).

Generation of FRDA YAC transgenic mice

In an effort to overcome the embryonic lethality of homozygous *Fxn* knockout mice and to study the behaviour of human frataxin in a mouse cellular environment, a human wild type FRDA YAC (Figure 1.12) transgenic mouse line was generated (Pook *et al.* 2001) and crossbred with heterozygous *Fxn* exon 4 deletion knockout mice ($Fxn^{+/-}$) (Cossee *et al.* 2000). The resultant homozygous *Frda* knockout *FXN* transgenic mice (FXN^{+}, $Fxn^{-/-}$) were phenotypically normal, with lethality rescued by expression of functional YAC-derived human frataxin (Pook *et al.* 2001). These results demonstrated that the re-introduction of human frataxin onto a mouse null background was an effective method that paved the way for further FRDA mouse models and frataxin functional studies.

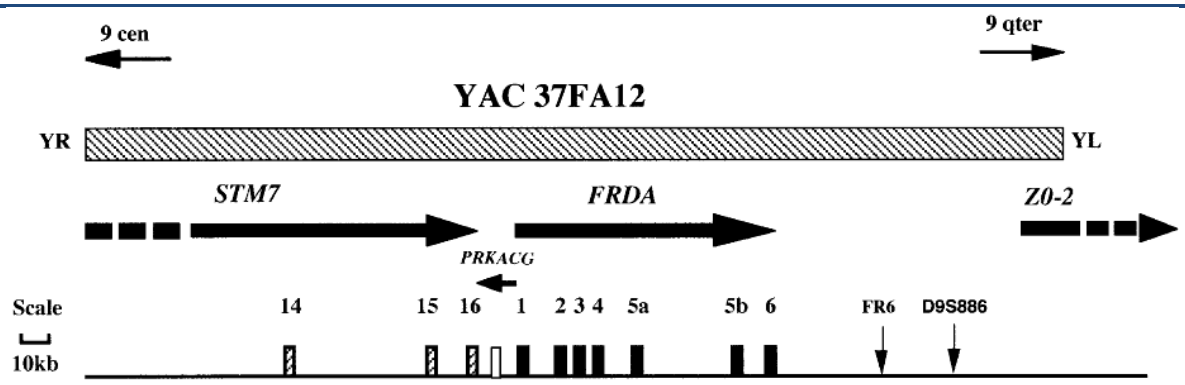

Figure 1.12 - The position of YAC 37FA12 with respect to the FRDA locus at 9q13. The position of YAC 37FA12 with respect to the FRDA locus at 9q13. Genes are represented as *solid arrows*, which indicate the direction of transcription, and the *broken lines* represent incomplete gene sequence. Individual exons are numbered and are shown below the relevant gene. STS markers used in the analysis are shown as downward pointing arrows (Pook *et al.* 2001).

Generation of GAA containing FRDA YAC transgenic mice

Subsequently, by using a yeast pop-in/pop-out homologous recombination strategy (Cemal *et al.* 1999), two lines of human FRDA YAC transgenic mice, YG8 and YG22, containing GAA repeat expansions derived from FRDA patient DNA were generated (Figure 1.13) (Al-Mahdawi *et al.* 2004). Additionally, both lines were shown to contain transgene sequences spanning the whole 370 kb human YAC clone. The two founder mice, YG8 and YG22, differed in their GAA content as YG8 contained two copies of GAA repeats with 190 and 90 repeats (GAA_{190+90}), whereas YG22 was shown to have only one copy of 190 GAA repeats (GAA_{190}) (Table 1.3) (Al-Mahdawi *et al.* 2004). Interestingly, both mice have shown intergenerational and age dependant somatic instability as seen in FRDA patients.

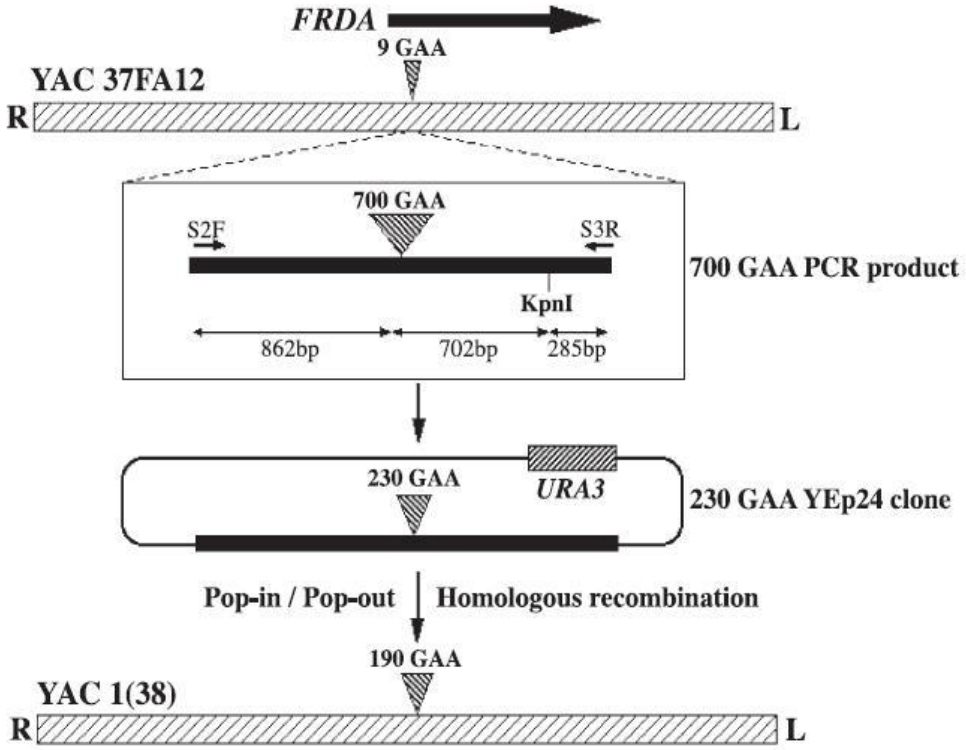

Figure 1.13 - GAA repeat modification of YAC 37FA12. The position and orientation of the normal FRDA gene (9 GAA repeats) within the human YAC clone 37FA12 are indicated by the arrow. L and R indicate left and right arms of the YAC. A 700-GAA PCR product was amplified from FRDA patient DNA using primers S2F and S3R. The PCR product was first cloned into pCR2.1 and then into YEp24, which contains a selectable URA3 gene, with resultant contraction to 230 GAA repeats. Pop-in/pop-out homologous recombination between Yep24 and YAC 37FA12 FRDA sequences produced the 190-GAA repeat YAC clone 1(38), which was subsequently used to generate transgenic mice (Al-Mahdawi *et al.* 2004).

Table 1.3 - Analysis of FRDA YAC transgenic mouse lines

Transgenic line	YAC transgene integrity	*FXN* copy number	Founder GAA repeat length(s)	Range of GAA repeats in offspring
YG8	Complete	2	190 + 90	<9 to 223
YG22	Complete	1	190	<9 to 235

Intergenerational instability in FRDA YAC transgenic mice

Intergenerational instability of the GAA repeat expansions was assessed in both YG8 and YG22 FRDA YAC transgenic mouse lines during transmission from transgenic parents to offspring. The results demonstrated that both lines have intergenerational contractions and expansions (Figure 1.14) (Al-Mahdawi *et al.* 2004). However, a trend towards a significant ($p<0.05$) excess of expansions upon paternal transmission was observed in the YG8 line. In contrast, no significant overall bias in the YG22 line was seen, but a bias toward contractions was seen upon maternal transmission ($p<0.001$) (Al-Mahdawi *et al.* 2004). However, large GAA expansions similar to those described in FRDA patients (Montermini *et al.* 1997a; Delatycki *et al.* 1998) have not yet been detected in this mouse model.

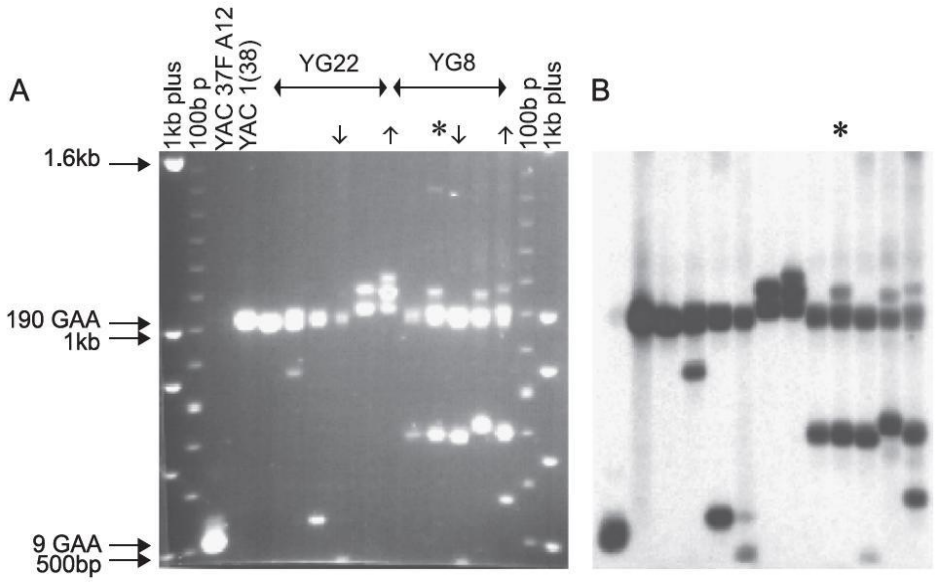

Figure 1.14 - Intergenerational instability in FRDA YAC transgenic mice.**(A)** Ethidium bromide-stained agarose gel and **(B)** Southern blot autoradiograph of GAA PCR products from representative YG22 (190 repeats) and YG8 (90 + 190 repeats) transgenic mice showing expansions (↑)and contractions (↓) down to fewer than 9 repeats (both lines). An example of a discrete PCR product potentially corresponding to 340 repeats that failed to hybridize with a GAA probe is indicated by an asterisk (Al-Mahdawi *et al.* 2004).

Somatic instability in FRDA YAC *transgenic mice*

To date, little is known about the somatic instability displayed by the expanded GAA trinucleotide repeat sequence in FRDA. Therefore, a variety of tissues from YG8 mice and YG22 mice (2-12 months of age) were assessed for possible somatic instability (Al-Mahdawi *et al.* 2004) as seen in FRDA patients (De Biase *et al.* 2007b). Interestingly, no somatic instability was detected at the early age of the mice, but remarkable changes in somatic instability were detected in tissues from older mice of both lines (Figure 1.15) (Al-Mahdawi *et al.* 2004), suggesting that somatic instability is age dependent as observed in FRDA patients (De Biase *et al.* 2007b).

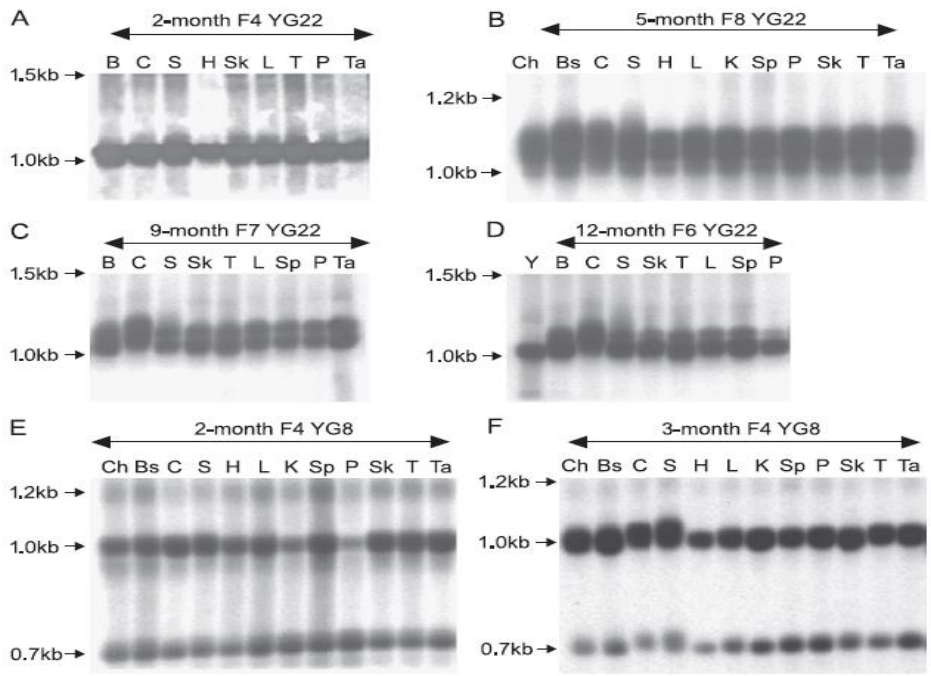

Figure 1.15 - Somatic instability in FRDA YAC transgenic mice. Autoradiographs of Southern-blotted GAA PCR products from somatic tissues of representative transgenic mice. (A) 2-month F4 YG22, (B) 5-month F8 YG22, (C) 9-month F7 YG22, (D) 12-month F6 YG22, (E) 2-month F4 YG8, and (F) 3-month F4 YG8. B, whole brain; Ch, cerebral hemisphere; Bs, brain stem; C, cerebellum; S, spinal cord; H, heart; L, liver; K, kidney; Sp, spleen; P, pancreas; Sk, skeletal muscle; T, testis; Ta, tail (Al-Mahdawi *et al.* 2004).

In contrast to the situation with intergenerational instability, noticeable similarities were observed between the FRDA patients and FRDA YAC transgenic mice when it comes to somatic instability of the GAA repeat as both YG8 and YG22 showed prominent GAA expansion changes in CNS tissues, particularly in the cerebellum (Al-Mahdawi *et al.* 2004). Recently, by using small-pool PCR (SP-PCR), a sensitive assay that utilizes low levels of genomic DNA (typically 6-600pg), somatic instability of the $(GAA)_{190}$ tract was analysed in multiple tissues from 12-month old mice derived from both transgenic lines (Clark *et al.* 2007). Although, both expansions and contractions were observed in most tissues, the $(GAA)_{190}$ sequence was most unstable in the cerebellum and DRG suggesting that somatic instability is tissue specific.

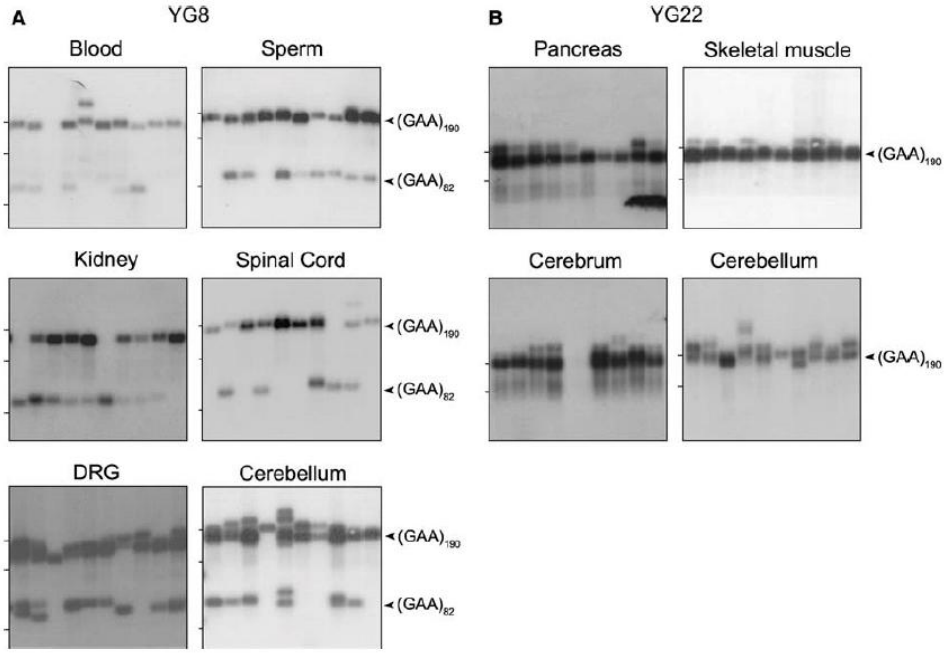

Figure 1.16 - Small-pool PCR analysis showing somatic instability of the GAA triplet-repeat sequence in multiple tissues from YG8 (**a**) and YG22 (**b**) transgenic mice. The locations of the constitutional $(GAA)_{190}$ and $(GAA)_{82}$ alleles, as determined by conventional PCR, are indicated by *arrowheads* (Clark *et al.* 2007).

In summary, both YG8 and YG22 lines show progressive and tissue specific GAA repeat instability specifically in regions of the nervous system that show a primary pathology in FRDA patients, when neither was observed with the 230-GAA repeat knockin mouse model (Miranda *et al.* 2002). Therefore, such a mouse model serves as a useful resource to delineate the mechanism(s) of somatic instability seen in FRDA patients, and to test potential interventional strategies.

Human GAA expansion-containing FRDA YAC transgene rescue FRDA knockout mice

To determine the viability of each GAA *FXN* transgene, both YG22 or YG8 mice (FXN^{+}, $Fxn^{+/+}$) were crossbred with heterozygous *Fxn* knockout mice (Al-Mahdawi *et al.* 2006). The FXN^{+}, $Fxn^{+/-}$ offsprings from these crosses were further bred with $Fxn^{+/-}$ mice to generate FXN^{+}, $Fxn^{-/-}$ "rescues". Correct Mendelian ratios of rescue mice to overall offspring number were obtained from both YG22 and YG8 crosses, indicating that functional frataxin were obtained from both GAA repeat-containing transgenes (Al-Mahdawi *et al.* 2006).

Decreased levels of frataxin mRNA and protein

It has been confirmed that the YG8 and YG22 rescue mice show reduced levels of human *FXN* mRNA in all tissues and decreased levels of human frataxin protein in some tissues, compared to Y47, a normal-sized GAA containing FRDA YAC transgenic mice (Al-Mahdawi *et al.* 2006; Al-Mahdawi *et al.* 2008). However, when compared with mouse endogenous frataxin (WT) all transgenic mice have produced more pronounced increases in *FXN* mRNA levels. Currently, there is no explanation for this phenomenon; however, it could be possibly due to several factors. Firstly, it could be over-expression of the human *FXN* gene

in a mouse background. Although YG8 mice have displayed increased levels of *FXN* mRNA compared with WT control mice, this may not fully translate into functional frataxin protein (Figure 1.17), hence an FRDA like phenotype is observed in such mice.

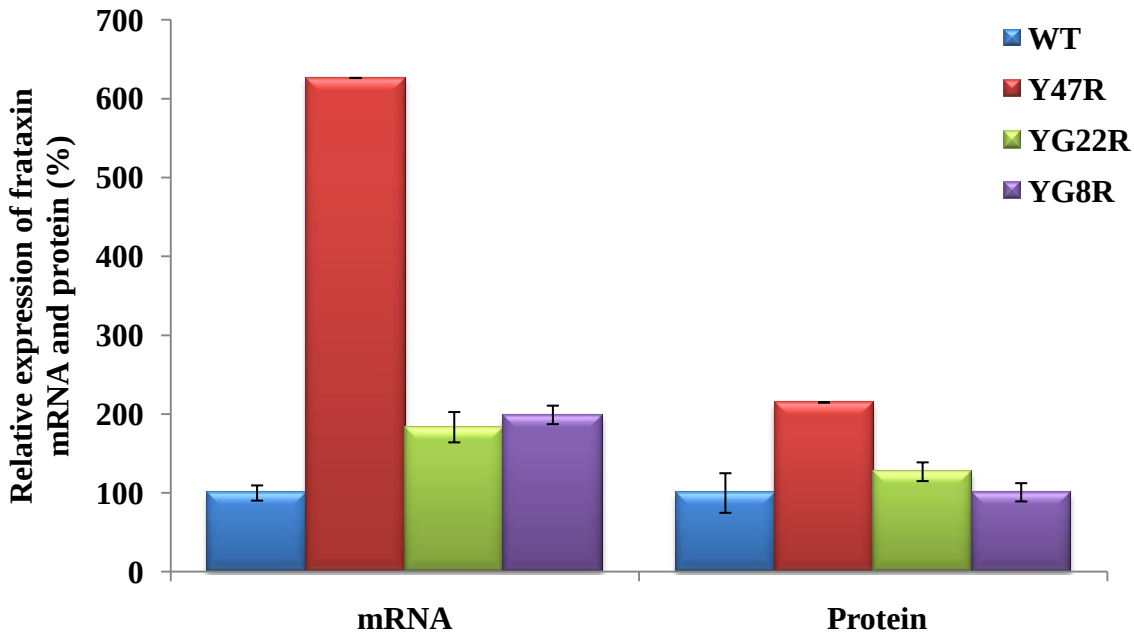

Figure 1.17 - Relative expression of frataxin mRNA and protein. Comparison of frataxin mRNA and protein levels in brain tissues isolated from WT, Y47R (9 GAA), YG22R (190 GAA) and YG8R (190+90 GAA). Data are normalized to the mean *FXN* mRNA and protein level found in the WT control samples taken as 100%.

Oxidative stress in FRDA YAC transgenic mice

To detect the potential oxidative stress in both transgenic mice lines (YG8 and YG22), the levels of oxidized proteins and malondialdehyde (MDA; a marker of lipoperoxides) were quantified in cerebrum, cerebellum, heart, and skeletal muscle tissues, compared with WT controls. Interestingly, oxidized proteins were increased in all tissues, most prominently in cerebrum and cerebellum, from both YG8 and YG22 rescue mice (Figure 1.18) (Al-Mahdawi *et al.* 2006).

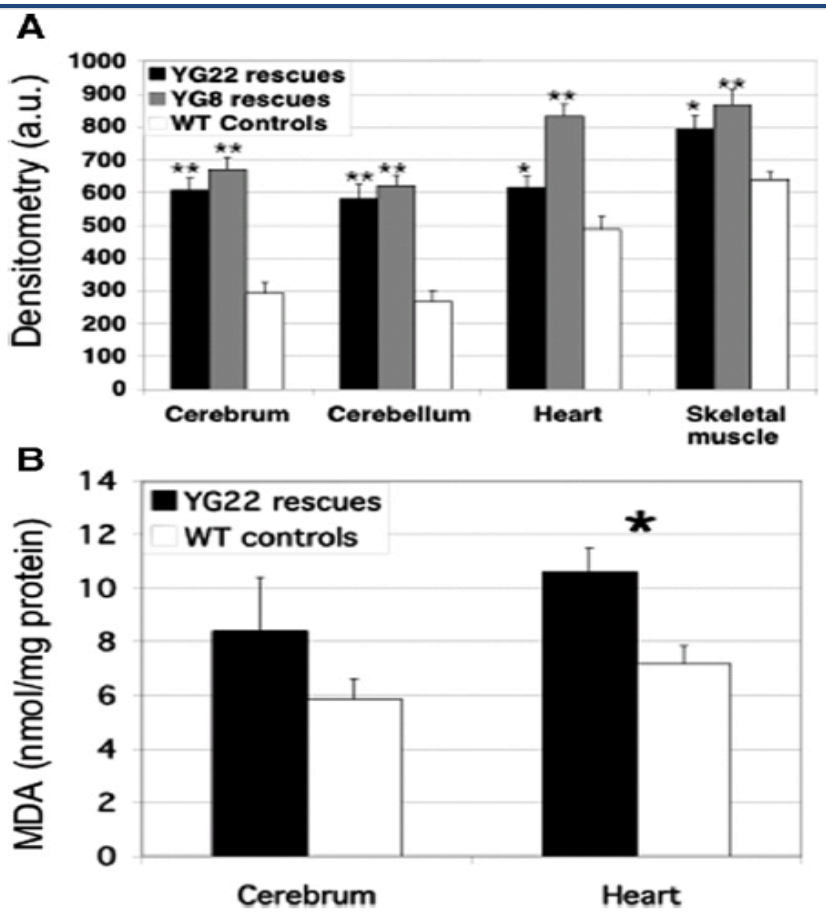

Figure 1.18 - Oxidative stress in FRDA YAC transgenic mice **(A)** Oxyblot analysis detects protein oxidation in cerebrum, cerebellum, heart, and skeletal muscle tissues of 6- to 9-month old YG22 and YG8 rescue mice, compared with WT controls. Error bars indicate SEM. *p<0.05, **p<0.01. **(B)** TBARS analysis shows levels of MDA (nmol/mg of protein) as a marker of lipoperoxidation in YG22 cerebrum and heart tissue compared with WT controls (n=6). Error bars indicate SEM. *p<0.05 (Al-Mahdawi *et al.* 2006).

Neurobehavioral deficits in FRDA YAC transgenic mice

Subsequently, the neurobehavioral deficits were investigated in YG8 and YG22 mice and the coordination ability of these two mice were impaired from the age of 3 months as determined by reduced performance on an accelerating rotarod treadmill apparatus compared with WT littermate controls ($p<0.01$) (Al-Mahdawi *et al.* 2006). Muscle strength, assessed by forelimb grip strength test, was decreased in YG22 rescues from 9 months of age ($p<0.01$), but no significant changes were detected in YG8 rescue mice. Locomotor activity, assessed by examining the unrestricted movement of mice in an open field, was decreased in both lines. The YG22 rescues showed a decreased trend in locomotor activity from 6 months of age, but no statistically significant difference was seen until one year of age $p<0.05$). On the other hand, YG8 rescue mice showed a significant decrease in locomotor activity from 6 months of age ($p<0.05$) (Al-Mahdawi *et al.* 2006).

Histological pathology in FRDA YAC transgenic mice

Sections of brain, spinal cord and DRG of YG8 and YG22 mice were analysed to detect possible neuronal histopathology. Although, no histological abnormalities were identified in the brain and spinal cord, giant vacuoles were identified in the large sensory neuronal cell bodies of the DRG in both YG8 and YG22 rescue mice, but not in WT controls (Figure 1.19A) (Al-Mahdawi *et al.* 2006). In addition, Perl's staining identified iron deposition within the heart, but only from the oldest (14-18 months) YG22 rescue mice studied (Figure 1.19B) (Al-Mahdawi *et al.* 2006), confirming the later onset aspect of this pathology as previously described for cardiac frataxin conditional knockout mouse models (Puccio *et al.* 2001). Furthermore, electron microscopy of DRG from FRDA YAC GAA mice identified deposition of lipofuscin, chromatolysis, swelling of neuronal bodies and demyelination of axons (Al-Mahdawi *et al.* 2006).

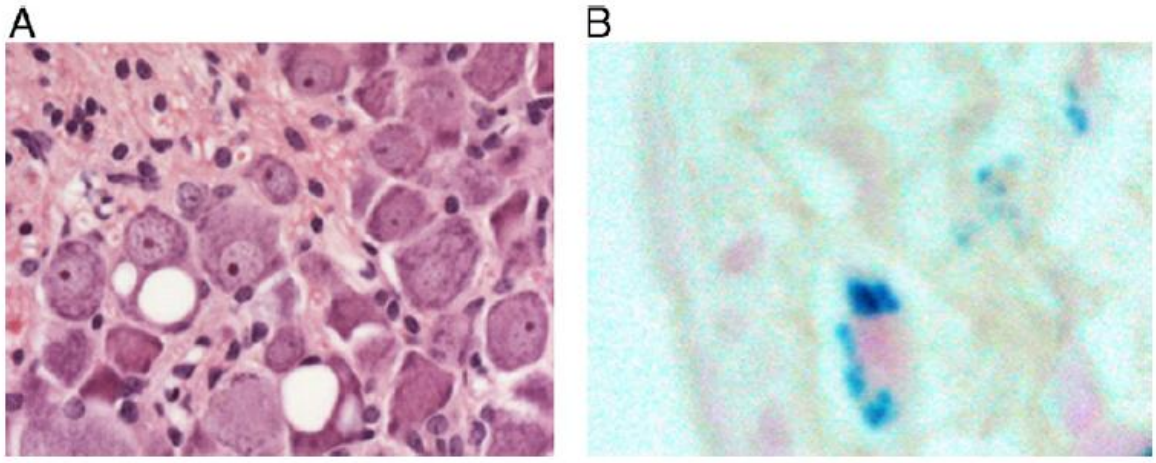

Figure 1.19 - Neuronal and cardiac histopathology. (**A**) H&E-stained section of lumbar DRG from a representative YG22 rescue mouse over 1 year of age, showing two neurons containing large vacuoles. Original magnification 400×. (**B**) Perl's staining of a heart section from a representative YG22 rescue mouse over 1 year of age, showing characteristic blue staining indicating iron deposition. Original magnification 600× (Al-Mahdawi *et al.* 2006).

Epigenetic changes in FRDA YAC transgenic mice

Having determined the epigenetic profile around the human *FXN* gene (Herman *et al.* 2006; Al-Mahdawi *et al.* 2008), epigenetic changes in FRDA YAC transgene mice have been investigated in the brain and heart tissues isolated from YG8 and YG22 mice compared to Y47 mice (Al-Mahdawi *et al.* 2008). Epigenetic changes, such as differential DNA methylation and histone modifications, have been identified in both the FRDA YAC transgenic mice (Al-Mahdawi *et al.* 2008), similar to those observed in FRDA patients.

DNA methylation profile in FRDA YAC transgenic mice

Investigation of the DNA methylation profile in FRDA YAC transgenic mice has revealed a shift in DNA methylation, as the upstream GAA region is consistently hypermethylated and downstream GAA region is consistently hypomethylated (Figure 1.20) (Al-Mahdawi *et al.* 2008).

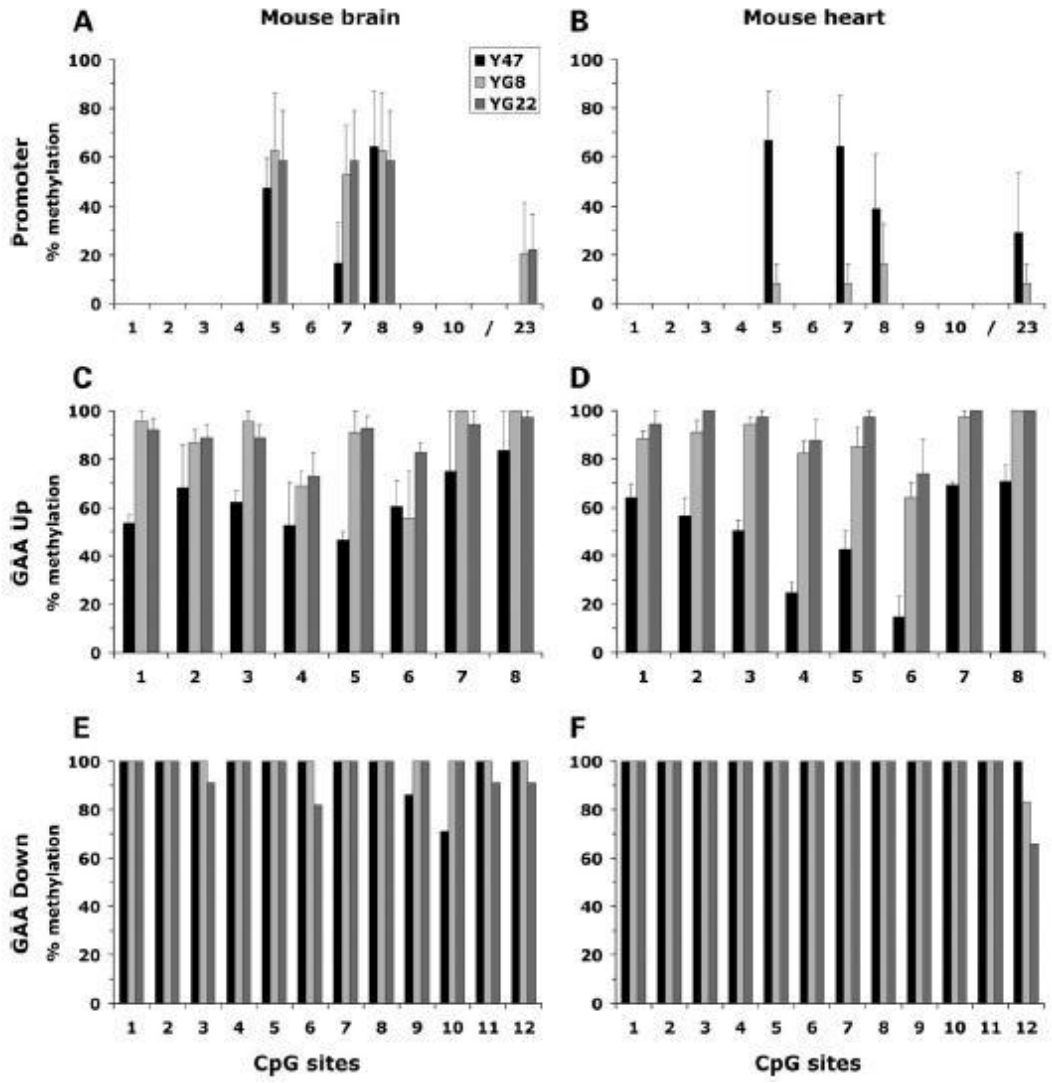

Figure 1.20 - DNA methylation analysis of the FRDA YAC transgenic promoter (**A** and **B**), upstream GAA (**C** and **D**) and downstream GAA (**E** and **F**) regions of Y47 (black columns), YG8 (light grey columns) and YG22 (dark grey columns) transgenic mouse brain and heart tissues (Al-Mahdawi *et al.* 2008).

Histone modification in FRDA YAC transgenic mice

Subsequently, histone modifications were also investigated in FRDA YAC transgenic mice at exactly the same three regions of the *FXN* gene that had previously been analysed in human tissue (Al-Mahdawi *et al.* 2008). This analysis showed overall GAA repeat-induced decreases in histone H3K9 acetylation and increases in H3K9 methylation for both YG8 and YG22 transgenic mice (Figure 1.21) (Al-Mahdawi *et al.* 2008) as previously identified in human FRDA tissue. However, the level of deacetylation in the transgenic mouse brain tissue was not as great as that seen in the human brain tissue, possibly as a consequence of the smaller transgenic GAA repeat expansion sizes compared with FRDA patients.

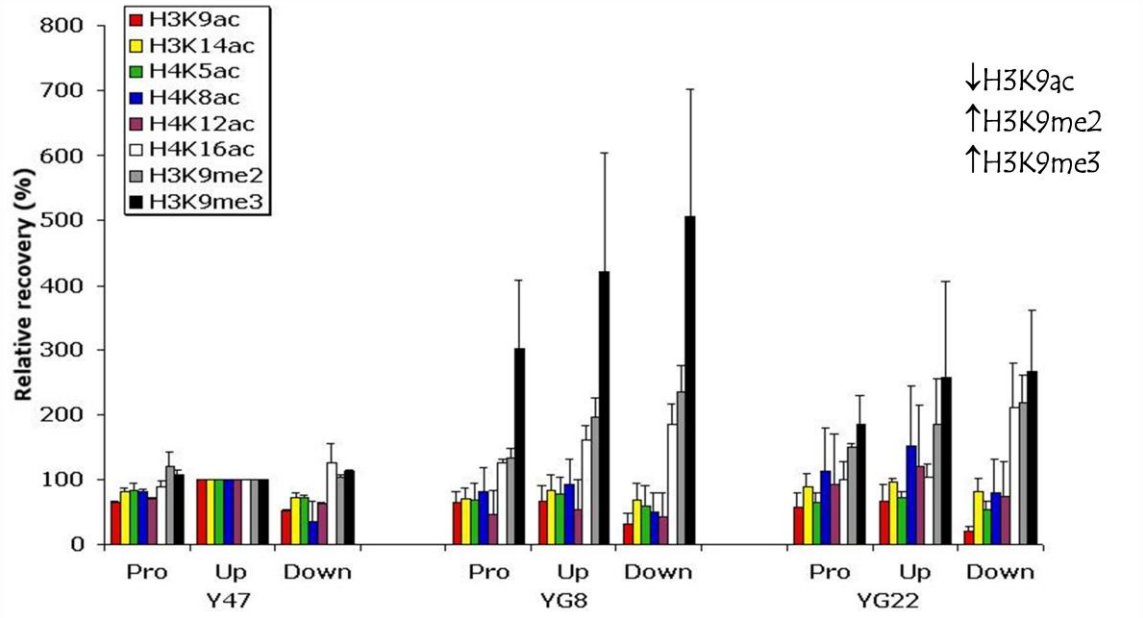

Figure 1.21 - Analysis of histone modifications in transgenic mouse brain tissue.ChIP quantitative PCR results for the transgenic *FXN* promoter/exon1 (Pro), upstream GAA (Up) and downstream GAA (Down) amplified regions are represented as the relative amount of immunoprecipitated DNA compared with input DNA, having taken negligible -Ab control values into account. *FXN* values were normalized with mouse *GAPDH* and all values have been adjusted so that all of the upstream GAA values from the non-GAA transgenic mouse tissues (Y47) are 100%. In each case two individual ChIP samples were analysed in triplicate from each of two mice per group. The means and SEMs of these values are shown (Al-Mahdawi *et al.* 2008).

1.4.5.4 - *FXN* BAC transgenic mouse model

Recently, similar to the FRDA YAC transgenic mouse model strategy, Sarsero et al. (2004) have generated a *FXN* bacterial artificial chromosome (BAC) transgenic mouse model by inserting a 188 kb BAC clone (pBAC265) containing exon 1-5b of the normal human FRDA locus. The human FRDA orthologue successfully rescued the embryonic lethality of the *Fxn* knockout mice (Sarsero *et al.* 2004). This *FXN* BAC transgene displays extensive tissue-specific differential expression in relation to the endogenous locus, implying the existence of tissue-specific transcriptional mechanisms regulating *FXN* expression (Sarsero *et al.* 2004). Subsequently, a *FXN* BAC transgenic mouse model has also been generated by inserting large GAA expansion mutation (>500 GAA repeats), but this mouse, which retains a marker gene sequence, failed to exhibit any FRDA-like phenotype (Sarsero personal communication).

In conclusion, there are many types of FRDA mouse models: knock-outs, knock-ins and YAC or BAC transgenics. In principle, the knock-ins, YAC transgenics and BAC transgenics are all suitable models to investigate epigenetics in FRDA. However, the currently available knock-ins and BAC transgenics retain disruptive marker gene sequences, whereas the YAC transgenics do not contain any such artificial sequences. Therefore, the YAC transgenics, which have shown comparable epigenetic changes and GAA instability as seen in FRDA patients, are regarded as the best model to study epigenetics in FRDA. This mouse model is considered a valuable resource in the study of FRDA pathology and/or therapeutic strategies aimed at interacting and modifying the GAA repeat expansion itself.

1.5 - Aims of the study

FRDA is a progressive neurodegenerative disorder and currently there is no effective therapy available that can stop the progression of this disease. To understand the pathological consequences and to find a potential therapy for FRDA, *in vitro* and/or *in vivo* model systems are considered to be essential. Therefore, the main aim of this research project was to establish a model cell culture system that would help drug screening for FRDA. Chapter 3 of this thesis describes the establishment of novel cell culture systems, including FRDA mouse primary fibroblasts and neural stem cells for *in vitro* therapeutic testing of FRDA.

Recently, it has also been reported that FRDA is associated with increased DNA methylation and decreased acetylation of histones flanking the GAA repeat (Herman *et al.* 2006; Greene *et al.* 2007; Al-Mahdawi *et al.* 2008). Therefore, in efforts to reduce the DNA methylation and increase the histone acetylation, I have investigated the use of DNA demethylating agents and HDAC inhibitors in the cell culture systems, as described in chapter 4. In addition, I also studied the efficacy of some GAA interacting compounds as potential therapeutics.

Finally, recently described HDAC inhibitors, RGFA 136 and RGFP 109, have been reported to show increased frataxin mRNA and protein, along with increased levels of acetylated histone H3 and H4 levels, in a short-term preliminary study (Rai *et al.* 2010). Therefore, in chapter 5 I describe the efficacy and tolerability of such compounds in long-term studies using the YG8 FRDA YAC transgenic mouse model.

Chapter 2 - Materials and methods

2.1 - Solutions/reagents

DMEM medium

- 1x DMEM medium, 10% FCS, 2% pen-strep (5000U/ml penicillin and 5000mg/ml of streptomycin, Fisher Scientific).

NSC medium (complete medium)

- 1x NSC basal medium, 10% NSC proliferation supplements, 20ng/ml recombinant human epidermal growth factor (rhEGF), 10ng/ml recombinant fibroblast growth factor-basic (rhFGF-b), 2µg/ml heparin and 1% pen-strep (all from Stem Cell Technologies).

NSC differentiation medium

- 1x NSC basal medium, 10% NSC differentiation supplements (Stem Cell Technologies) and 1% pen-strep

DMEM/F12 medium

- 1x DMEM and F12 in 1:1 ratio, 10% FCS and 2% pen-strep (GIBCO)

Neurobasal/B27 medium

- 1x Neurobasal medium, 2% B27 supplements and 1% pen-step

RPMI 1640

- 1x RPMI 1640 medium, 2mM glutamine, 15% FCS and 2% pen-step

ACK lysis buffer

- NH_4Cl - 8.29 g/L; $KHCO_3$ - 1g/L; disodium EDTA•$2H_2O$ - 0.0372 g/L in Cell Culture Grade Water

Immunoflourescence assay

- 4% paraformaldehyde saline (pH 7.4): 4% w/v paraformaldehyde, 30mM NaOH in PBS (or) 50% acetone + 50% methanol
- Permeabilization buffer: 0.5% Triton X-100 in 1x PBS
- Blocking buffer: 0.2% skimmed dry milk, 0.1% Triton X-100 in 1x PBS
- Washing buffer: 0.1% Triton X-100 in 1x PBS

Histological analysis

- Heparinised saline: 2u/ml heparin in PBS
- 4% paraformaldehyde saline (pH 7.4): 4% w/v paraformaldehyde, 30mM NaOH in PBS
- Hillman & Lee's EDTA: 150mM EDTA, 10% formalin
- Acid alcohol: 1% HCl in 70% IMS

General solutions

- Tail digestion buffer: 100mM Tris-HCl (pH 8), 5mM EDTA, 200mM NaCl, 0.2% SDS
- TE buffer: 10mM Tris-HCl (pH 7.5), 1mM EDTA
- Orange G loading dye (6x): 0.35% Orange G dye, 30% sucrose
- 1x TBE: 90mM Tris, 90mM Boric acid, 2mM EDTA
- 1x TAE: 40mM Tris, 20mM Acetic acid, 1mM EDTA
- Tris/glycerol homogenization buffer: 100mM Tris-HCl (pH 9.0), 15% glycerol filter sterilized via 0.2µm pore

Western blot analysis

- Running buffer: 25mM Tris, 190mM glycine, 3.5mM SDS
- Sample buffer: 80mM Tris-HCl (pH 6.8), 12.5% glycerol, 10% SDS, 0.5% BPB, 1% BME
- Transfer buffer: 25mM Tris, 190mM glycine, 10% methanol
- PBS/T: 0.2% Tween-20 in PBS
- 5% milk PBS/T: 5% w/v milk, 0.2% Tween-20 in PBS

2.2 - Primers for genotyping and quantification of *FXN*

Various primers were used for genotyping the FRDA YAC transgenic mouse model and for the quantification of the *FXN* gene (Table 2.1 and Table 2.2). Primer sequences were obtained either from previous studies (as indicated) or newly designed by using primer 3 software (Rozen and Skaletsky 2000) and all primers were purchased from Sigma-Aldrich.

Table 2.1 - Primers used for genotyping FRDA YAC transgenic mice

Primer Name	Sequence (5' - 3')	Product length
GAA repeat (Campuzano *et al.* 1996)		
GAA - F	GGGATTGGTTGCCAGTGCTTAAAAGTTAG	457 bp + $(GAA)_n$
GAA - R	GATCTAAGGACCATCATGGCCACACTTGCC	
FXN knockout (Cossee *et al.* 2000)		
WJ5	CTGTTTACCATGGCTGAGATCTC	
WN39 (WT specific)	CCAAGGATATAACAGACACCATT	520 bp
WC76 (KO specific)	CGCCTCCCCTACCCGGTAGAATTC	245 bp
Msh2 knockout (Toft *et al.* 1999)		
Msh2-P1	CGGCCTTGAGCTAAGTCTATTATAAGG	
Msh2-P2 (KO specific)	GGTGGGATTAGATAATGCCTGCTCT	194 bp
Msh2-P3 (WT specific)	CCAAGATGACTGGTCGTACATAAG	164 bp
Msh3 Knockout (de Wind *et al.* 1995)		
Msh3-P1 (WT specific)	CAGGAAGAGGTCACTGGGAAATGG	130 bp
Msh3-P2 (KO specific)	GGTGGGATTAGATAATGCCTGCTCT	250 bp
Msh3-P3	GCTGAGAATACTTAGTCTCTGGCA	
Msh6 knockout (de Wind *et al.* 1995)		
Msh6-P1 (WT specific)	CAAGTCCTAGGATTAGAGGTCTGG	220 bp
Msh6-P2 (KO specific)	CCGGTGGATGTGGAATGTGTGCG	253 bp
Msh6-P3	CCATGCAAATCAGACTCGATACAA	
Pms2 knockout (designed by Mark Pook)		
Pms2-P1	ACAGTTACATTCGGTGACAG	
Pms2-P2 (KO specific)	TTTACGGAGCCCTGGCGC	189 bp
Pms2-P3 (WT specific)	ACTAATTCCCCTACGGTTTAG	385 bp

Atm knockout (Liao *et al.* 1999)		
Atm - F	GACTTCTGTCAGATGTTGCTGCC	
Atm - B (WT specific)	CGAATTTGCAGAAGTTGCTGAG	162 bp
Atm - Neo (KO specific)	GGGTGGGATTAGATAAATGCCTG	441 bp

Table 2.2 - List of primers used for quantification of *FXN* expression

Primer name	**Sequence (5' - 3')**	**Product length**
FXN expression (Human Specific) (Al-Mahdawi *et al.* 2008)		
*FXN*RT-F	CAGAGGAAACGCTGGACTCT	172 bp
*FXN*RT-R	AGCCAGATTTGCTTGTTTGGC	
FXN expression (Human and Mouse)		
FRT I-F	TTGAAGACCTTGCAGACAAG	121 bp
RRT II-R	AGCCAGATTTGCTTGTTTGG	
Gapdh (Human) (Al-Mahdawi *et al.* 2008)		
Gapdh-h-F	GAAGGTGAAGGTCGGAGT	226 bp
Gapdh-h-R	GAAGATGGTGATGGGATTTC	
Gapdh (Mouse) (Al-Mahdawi *et al.* 2008)		
Gapdh-m-F	ACCCAGAAGACTGTGGATGG	81 bp
Gapdh-m-R	GGATGCAGGGATGATGTTCT	
RER1 (Mouse)		
RER1-F	CCACCTAAACCTTTTCATTGCG	159 bp
RER1-R	TTTGTAGCTGCGTGCCAAAAT	

2.3 - General techniques

Dilutions or stock solutions were prepared in deionised water (18.2 MΩ) unless otherwise specified. The only exceptions were RNA experiments where RNAse-free DEPC-treated sterile water was used. Centrifugation of samples was performed in different equipment according to sample size and temperature requirements. Centrifugation of small samples (≤ 1.5ml) at room temperature was performed using a standard bench top micro-centrifuge (16K, BioRad) and at 4°C using a refrigerated micro-centrifuge (5415R, Eppendorf). The larger volumes (≤ 50ml) were centrifuged in a Centaur 2 centrifuge (Sanyo/MSE) and 96 well plates were centrifuged at room temperature using a Legend T centrifuge (Sorvall).

Incubations at lower temperatures (37-60°C) were performed in water baths (Grant); while for higher temperatures a heating block (DB-2A, Techne) was used. The pH of solutions was determined using a pH meter (Delta 340, Mettler) and pH adjustments were made by adding either concentrated HCl or NaOH. DNA containing solutions were stored at 4°C for short time in the fridge and in the cold room for long term. RNA samples were snap frozen and stored at -80°C. All mouse tissues were stored at -80°C. Antibodies were stored either at 4°C or -20°C according to the manufacturer's recommendations, if necessary in the dark.

2.3.1 - Agarose gel electrophoresis

Agarose gel electrophoresis was used to separate the DNA fragments according to their size. Agarose gels were prepared in a range of 1% to 3% with agarose (UltraPure electrophoresis grade, Invitrogen) for the separation, in 1x TBE/TAE. The agarose was first boiled in a standard microwave and allowed to cool. Then, ethidium bromide was added to the gel in a final concentration of 0.5µg/ml and the gel was poured in to a casting tray with the required well comb. The small gels (50ml) were run in mini gel tanks (Flowgen Biosciences), while midi gels were used for the large volumes (>150ml). After adding 6X Orange G loading dye to a final concentration of 1x, the products were loaded into the gels and were run for a period of 30min at 60V. The gels were visualized and documented by a UV transilluminator imaging system (Alpha Innotech).

2.3.2 - DNA extraction - ethanol method

This method was used to extract the genomic DNA quickly (where there was no need of great quality) for routine genotyping of mice or cell culture. Tail samples/cell pellet were collected in Eppendorf tubes and 400µl of tail digestion buffer and 10µl of proteinase K (50mg/ml) was added followed by a brief vortex and incubated at 55°C overnight. After the incubation, samples were vortexed and centrifuged at 14K rpm for 15min and the supernatant was carefully transferred into a new eppendorf tube by avoiding transferring any cell/hair/bone debris. Then 1ml of absolute alcohol was added and the samples were mixed by inverting the tube several times. Samples were incubated at -80°C for 10min followed by centrifugation at 14K rpm for 30min at 4°C. The ethanol was drained off and the

pellet washed with 1ml of 70% ethanol. The samples were again centrifuged at 14K rpm for 20min at 4°C and then ethanol was carefully drained off and the DNA pellet was air dried by inverting the Eppendorf tube on paper towels for a period of ~10min. The DNA pellet was resuspended in 50-100µl of TE buffer and stored at 4°C.

2.3.3 - DNA extraction – Phenol/Chloroform method

Genomic DNA extraction by the phenol/chloroform method was used for samples where greater quality was necessary. Digestion of samples by proteinase K was performed as described in section 2.3.2. After digestion, samples were vortexed and 400µl of phenol (equilibrated with Tris-HCl pH 8.0) was added. Samples were mixed well by vortexing twice for 15 sec and centrifuged at 14K rpm for 5min at 4°C. Then, 380µl of the supernatant was removed to a fresh Eppendorf and 380µl of chloroform/isoamyl alcohol (24:1, v/v) was added. Samples were vortexed briefly and centrifuged again at 14K rpm for 5min at 4°C. Afterwards, 350µl of the resulting supernatant was removed to a fresh Eppendorf and 35µl of 3M Na-acetate (pH 5.2) was added. 700µl of absolute ethanol was then added and ethanol precipitation carried out as previously described (section 2.3.2).

2.3.4 - Extraction of total RNA - Trizol® method (Invitrogen)

Total RNA was extracted from the drug-treated cells and mouse tissues using the Trizol® method following supplier guidelines. About 10^6 cells or 30-40mg tissue were used to extract the RNA. The cell pellet was first washed once with PBS and collected by centrifugation at 1.5K rpm for 5min. The cell pellet was loosened by flicking the tube gently and resuspended in 1ml of Trizol®. Mouse tissues were similarly homogenized in 1ml of Trizol® by Eppendorf homogenizing rod. Samples were then incubated for 10min at room temperature. 0.2ml of chloroform per 1ml of Trizol® was added followed by vigorous shaking of samples for 15sec and incubated for further 15min at room temperature. Samples were phase separated by centrifugation at 14k rpm for 15min at 4°C. The upper aqueous phase (~0.5ml) was then transferred to a fresh labelled eppendorf tube and RNA was precipitated by adding 0.5ml of isopropyl alcohol. Samples were incubated for 10min at room temperature and centrifuged at 14k for 15min at 4°C. The supernatant was carefully removed and the RNA pellet was washed once with 1ml of 75% ethanol (made with DEPC-water) and centrifuged again at 7.5k rpm for 5min at 4°C. The supernatant was removed carefully and the RNA pellet was briefly dried for a period of 5-10min and resuspended in 10-20µl of DEPC-water. RNA samples were stored at -80°C, until required to use.

2.3.5 - Complementary DNA (cDNA) synthesis

Complementary DNA (cDNA) was synthesized by using cloned AMV first-strand cDNA synthesis kit (Invitrogen). On ice, 2µl of RNA was added to 10µl of primer component mastermix (7µl of DEPC-water, 2µl of 10mM dNTP mix and 1µl of Oligo $(dT)_{20}$ primer). RNA and primer were denatured by keeping the samples at 65°C for 5min and immediately placing the samples on ice. Then the following reagents were added in order: 4µl of 5X cDNA synthesis buffer, 1µl of DEPC-water, 1µl of 0.1M DTT, 1µl of RNase OUT™ (40U/µl) and 1µl of cloned AMV RT (15 units/µl). The 20µl reaction mixture was gently mixed by flicking the tube and briefly centrifuged to bring all the contents to the bottom. The reaction mixture was incubated at 55°C for 60min. The reverse transcriptase reaction was terminated by keeping the samples at 85°C for 5min. The cDNA samples were used immediately or stored at -20°C.

2.3.6 - Determination of RNA/DNA quantity and purity

RNA/DNA concentration and purity was determined by using NanoDrop™ 2000c spectrophotometer (NanoDrop, Thermo Scientific). The absorption (A) of ultra violet light (UV-light) was measured at 260nm and the quality was determined by using $A_{260/280}$ ratio.

2.3.7 - Poly-D-lysine coating of plates/coverslips

Poly-D-lysine coated plates/coverslips were used for the immunofluorescence assay for neural stem cells to improve the cell attachment capacity to the surface. A stock solution of poly-D-lysine (50µg/ml, Sigma) was prepared with tissue culture grade distilled water. Enough poly-D-lysine was added to the culture flask to cover the surface and the flask was incubated at room temperature overnight. Coverslips were coated by soaking in poly-D-lysine. After incubation, the solution was aspirated and culture plates/coverslips were washed once with sterile tissue culture grade distilled water. Plates were allowed to air dry for 2-3 hours and stored at 4^{o}C.

2.4 - Genotyping and breeding pattern of mice

The animal husbandry was maintained in controlled temperature and light/dark cycles. New born mice were weaned approximately 3 weeks of age and were processed for genotyping. The ears were clipped for identification and the tip of the tail (<5mm) was collected by local anaesthesia with ethyl chloride BP (Cryogesic, Acorus Therapeutics Ltd) for DNA isolation and genotyping. The DNA from newborn mice was used for different types of genotyping, including estimation of GAA repeat size and knockout genotypes for *Fxn, Msh2, Msh3, Msh6, Pms2* and *Atm*.

All PCRs were performed in 1x *Taq* mastermix (Qiagen) with primers (Table 2.1), primer concentrations (Table 2.3) and conditions specified (Table 2.4) in a final volume of 25µl, using appropriate volumes of forward and reverse primers and 1µl of sample DNA. For each PCR experiment a control with known genotype was used as a reference. In addition, a sample containing dH_20 in place of DNA was also prepared as a contamination control.

Table 2.3 - Concentrations of primers used in genotyping PCRs

Primer	Concentration per reaction
GAA PCR (repeat estimation)	
GAA - F	12.5pmol
GAA - R	12.5pmol
Fxn Knockout	
WJ5	20pmol
WN39	20pmol
WC76	3.5pmol

Primer	Concentration per reaction
Msh2/Msh3/Msh6/Atm knockout	
Primer 1	12.5pmol
Primer 2	12.5pmol
Primer 3	12.5pmol
Pms2 knockout	
Primer 1	30pmol
Primer 2	20pmol
Primer 3	10pmol

Table 2.4 - Cycling conditions for various genotyping PCRs

GAA	*Fxn*	*Msh2/3/6*	*Pms2*	*Atm*
94°C 2min	94°C 2min	94°C 1min	94°C 1min	94°C 1min
10x 94°C 10s, 60°C 30s, 68°C 45s	40x 94°C 20s, 54°C 20s, 72°C 20s	30x 94°C 30s, 60°C 30s, 72°C 1min	30x 94°C 20s, 49°C 20s, 72°C 20s	30x 94°C 30s, 60°C 30s, 72°C 1min
20x 94°C 10s, 58°C 30s, 68°C 1min*	72°C 6min	72°C 10min	72°C 10min	72°C 10min
68°C 6min				

* - time increased 20s per cycle

PCR reactions were performed in 0.25ml tubes (Fisher Scientific) using a thermo cycler (PTC-225, MJ Research) and the results were obtained by separating the products in 1-2% agarose mini gels with 1% TBE buffer along with a 1kb^{+} DNA ladder (Invitrogen). For the estimation of GAA repeat size, samples which proved positively for the presence of the FRDA

YAC transgene were run in a 20cm long gels with 1.5% agarose and 1x TBE gels overnight along with 100bp and $1kb^{+}$ DNA ladders.

The breeding pattern of mice for drug treatment was designed to produce litters with a maximum number of FRDA rescue or WT mice. Rescue mice were achieved by a cross between homozygous *FXN* rescue ($FXN^{+/+}$, $Fxn^{-/-}$) with a *frataxin* heterozygous mouse ($Fxn^{+/-}$) and the WT mice were generated by a cross between two C57BL6/J WT mice. Resultant newborn mice were genotyped as previously described and grouped by gender and age with a maximum of 5 mice per cage.

Expand long range PCR

Long range PCR is used to efficiently amplify large genomic DNA fragments from 5kb to 25kb in length and this was done by using Expand Long Range PCR System kit from Roche Applied Science (USA, cat no 4829034001). The PCR mastermix was prepared in a final volume of 49µl using appropriate volumes of forward and reverse primers and 1µl of sample DNA (Table 2.5). For each PCR experiment a positive control was used as a reference. In addition, a sample containing dH_20 in place of DNA was also prepared as a contamination control.

Table 2.5 - Expand long range PCR mastermix concentrations

Components	Final concentration
5x buffer (12.5mM $MgCl_2$)	1x
dNTPs	500µM
DMSO	10%
Expand *Taq* polymerase	3.5U
Forward primer	0.5µM
Reverse primer	0.5µM

2.5 - Functional studies during drug treatment

Weight and functional measurements were taken at the start and repeated every month during drug treatment. Three different types of functional data were collected in each drug trail: locomotor activity, rotarod analysis and open-field activity.

Locomotor activity analysis

Locomotor activity was assessed by placing the mice in a 3X5 gridded (33cm X 55cm) perspex box. The number of gridded squares entered by each mouse over a period of 30 seconds was recorded, and the experiment was repeated four times for each mouse. A minimum of 200 seconds rest time was given in between each run.

Rotarod analysis

Rotarod analysis of mice was performed using a Ugo-Basille 7650 accelerating rotarod treadmill apparatus (Figure 2.1) and used to assess motor co-ordination and balance. The rotarod apparatus consists of a rotating drum with a grooved surface for gripping with the speed of the rotation gradually increasing from 4 to 40 rpm. The mice were placed on the rotating rod and up to 5 mice were assessed per run. The time taken for each mouse to fall from the rod was recorded over a maximum period of 400 seconds. Four runs were performed and a minimum of 200 seconds rest time was given in between each run.

Figure 2.1 – Rotarod apparatus with mice

Open field activity monitor (Beam breaker)

Open field activity was monitored by using a MED-OFA-510 activity chamber (MED Associates Inc) with SOF-811 software. This windows application was specifically written and it allows flexible configuration of experiments and repeated data analysis. Each chamber measures 27.3cm X 27.3cm with three 16-beam I/R arrays (Figure 2.1) and two chambers were connected to the computer. Each chamber takes only one mouse per run, which was measured over a period of 2 min. Four runs were performed for each mouse and an average of four runs was taken for the calculations. The software counts the standard measures including ambulatory counts, distance, time and episodes; stereotypic counts and time; vertical counts and time; resting time; jump counts and time; average velocity. The data was directly exported to an excel spread sheet for statistical analysis.

Figure 2.2 – Open field activity monitor chambers

2.6 - Sample collection of mice post drug treatment

At the completion of each drug treatment the mice were appropriately culled and all the tissues were collected according to the type of analysis desired.

Preparation of mouse tissue for expression and biochemical analysis

The samples with intended use for *frataxin* expression and/or biochemical studies were collected by culling the mice by cervical dislocation and dissecting immediately. The collected tissues were snap-frozen in liquid nitrogen and stored at -80°C. The following samples were collected: brain (B); brain stem (Bs); cerebellum (C); spinal cord (Sc); heart (H); lung (Lu); liver (L); pancreas (P); kidney (K); spleen (Sp); skeletal muscle (Sk); blood (Bl); tail (Ta); lumbar vertebral column (Vl); thoracic vertebral column (Vt); cervical vertebral column (Vc); testis (T) and sperm (S) from males; and ovaries (O) from females.

Preparation of mouse tissues for histological analysis

For histological analysis, mice were terminally anaesthetized by intraperitoneal injection with 5µl/g pentobarbitone sodium (Pentoject, Ph.Eur. Animal Care Ltd), followed by a preliminary intracardial perfusion with approximately 50ml of heparinised saline. Then, tissue fixation was performed by intracardial perfusion with approximately 100ml of 4% paraformaldehyde in PBS. The fixed mice were dissected immediately and the whole brain, spinal cord, lung, pancreas, liver and heart were collected carefully. The fixed tissues were left in 4% paraformaldehyde for first three days followed by a brief wash with dH_20 and immersion in 70% (v/v) ethanol at 4°C for long term storage.

2.7 - Establishment of primary fibroblasts

Primary fibroblasts cells were derived from selected WT and FRDA mice and were maintained in DMEM culture medium.

2.7.1 - Culture medium of fibroblasts

Preparation

Aliquots of FCS and pen-strep were thawed at 37°C for 2 hours or 4°C overnight. Inside the hood, FCS and pen-strep were added to 500ml of 1x DMEM and mixed well by shaking the bottle gently. The contents were filter sterilized with a 0.22µM pour size filter unit (Nalgene) and stored at 4°C until required to use.

2.7.2 - Culture procedure of fibroblasts

This method was based on Gomes-Pereira and Monckton (2004) and it is recommended for the establishment of cell cultures from large mouse organs like lung, liver, kidney and heart.

Culture requirements

DMEM medium, 1x sterile PBS (Invitrogen), 0.25% trypsin/EDTA (Thermo Scientific), sterile scalpel blades, scissors, forceps, Petri dish, culture flasks, 18G needles, syringe and centrifuge tubes.

Procedure

The DMEM medium and trypsin solutions were prewarmed to 37°C in a water bath. The mouse was dissected on a clean bench and the kidney was collected aseptically in 50ml sterile ice-cold PBS. The kidney was transferred to a laminar-flow hood to avoid contamination and placed on a 10-cm tissue culture dish with 10ml of ice-cold sterile PBS and washed briefly to remove blood cells and fat tissues. The tissue was minced into approx 1-mm^3 cubes and transferred into a sterile 15ml conical tube containing 10ml sterile ice-cold PBS. These tissue pieces were allowed to settle down over a period of 2min and aspirated PBS, washed twice with 10ml sterile PBS. Then 5ml of Trypsin/EDTA solution was added and the culture dish was incubated in a humidified 5% CO_2 incubator at 37^oC for 30min by gently inverting the tube after every 5 min.

The plunger was removed from a 5ml syringe and the pieces of tissue and enzymatic solution were transferred into the syringe. The plunger was placed back in syringe and the contents of the syringe were squirted into a 25-cm^2 tissue culture flask, through a sterile 18-gauge needle. The tissue culture flask was placed in the incubator for an extra 15min. The contents of the flask were transferred into a 15ml conical tube, the pieces of cellular debris were allowed to settle down over a period of 2min and then the supernatant was transferred into a fresh 15ml conical tube for centrifugation at 1.5K rpm for 5 min. The supernatant was removed and the cell pellet was resuspended in 4ml of complete culture medium and plated into one well of a 6-well plate. The primary cultures were incubated at 37^oC in a 5% CO_2 humidified incubator. 5ml of Trypsin/EDTA solution was added to the remaining undigested tissue. This step was repeated until the entire tissue sample was fully

digested or six primary cultures had been independently plated on a 6-well tissue culture plate. The primary fibroblasts were ready in 5-7 days in culture.

2.7.3 - Passage of fibroblasts

Once cells attach to the substratum and spread, they begin to divide, and the cell number increases. Cells progress from sparse to sub-confluent to confluent. Subculture provides the cell with fresh nutrients and space for continuous growth. The simplest way to remove the cells is to digest the attachment molecules, leaving the cells intact and free to float in suspension. The continuous subculture of mouse cell cultures results in spontaneous immortalization and generation of cell lines exhibiting unlimited proliferative capacity.

Culture medium, PBS and Trypsin/EDTA solutions were prewarmed to 37^{o}C in a water bath. The medium was removed by vacuum suction and cells were washed gently with sterile PBS. Adherent fibroblasts were digested with trypsin/EDTA for 5min at 37^{o}C in the CO_2 incubator to bring them into suspension. The trypsin/EDTA solution was neutralized by adding 10ml of DMEM culture medium. Cells were collected by centrifugation at 1.5K rpm for 5min and subcultured in 10ml DMEM culture medium at a 1:5 or 1:10 ratio. The cells were incubated at 37^{o}C, 5% CO_2 with 95% humidity and at every passage, the number of population doublings was determined based on the cell number.

2.7.4 - Cell quantification and viability (Trypan blue exclusion assay)

It is important to know the number of cells in the culture at given stages and whether these cells are viable. The use of haemocytometer and a dye, such as trypan blue, gives a quantitative standard for the viability of the cells. Cells that exclude trypan blue are considered viable, whereas cells that take up the dye are irreversibly dead. To perform this, cells were first digested with trypsin/EDTA and a cell suspension was made with DMEM medium. 100-200µL of cell suspension was taken into a fresh Eppendorf and an equal volume of 0.4% (w/v) trypan blue (Sigma) was added, mixed well by pipetting up and down. Cells were counted by using a haemocytometer and their viability was determined by the following formula:

$$\text{Viability (\%)} = \left(\frac{\text{No of Viable Cells}}{\text{Total no. of cells}} \right) \text{X } 100$$

2.7.5 - Mycoplasma PCR testing

Mycoplasma PCR was carried out using Mycosensor™ PCR Assay Kit (Stratagene). In brief, 100-µl of supernatant was taken carefully from a culture flask into a sterile 1.5ml Eppendorf tube and incubated for 5min at 95^{o}C in a water bath. 10µl of strataclean was added to the tube and mixed well by flicking the tube followed by the centrifugation. Then, 20-50µl of sample was taken from the supernatant (this acted as a template) and placed on ice. Mycoplasma PCR mastermix was prepared by adding the following reagents in order; 33µl dH_20, 5µl 10x PCR buffer (Qiagen), 1µl Q buffer (Qiagen), 2.5µl 10mM dNTP mix, 1µl primer mix, 2µl *Taq* DNA polymerase, 5µl internal control and 5µl test sample.

PCR amplification was performed in 0.25ml tubes using a thermal cycler (PTC-225, MJ Research) and the cycling conditions were as described for "PCR using *Taq* DNA polymerase" in Table 2.6. To visualize the results, 10-15µl of PCR products were separated in 1-2% agarose TBE mini-gels along with a 1kb+ DNA ladder (Invitrogen) at 75V for ~30min.

Table 2.6 - Mycoplasma PCR cycling parameters (Adopted from www.stratagene.com)

Cycle(s)	Temperature	Duration			
		PCR using *Taq* DNA polymerase[a]	PCR using *Taq* DNA polymerase with dUTP/UNG decontamination	PCR using the Brilliant QPCR master mix	PCR using the Brilliant QPCR master mix with dUTP/UNG decontamination
1	37°C	—	10 minutes	—	10 minutes
	94°C	—	10 minutes	10 minutes	10 minutes
35	94°C	30 seconds	30 seconds	30 seconds	30 seconds
	55°C	1 minute	1 minute	1 minute	1 minute
	72°C	1 minute	1 minute	1 minute	1 minute

[a] If using a chemically-based hot start *Taq* DNA polymerase (e.g., SureStart *Taq* DNA polymerase), include a 10-minute preincubation step at 94°C. See the hot start polymerase manufacturer's recommendations for optimal polymerase activation.

2.7.6 - Cryopreservation and regeneration of fibroblasts

Cells were digested with Trypsin/EDTA and their viability was determined by the trypan blue exclusion test. Cells were pelleted by centrifugation at 1.5K rpm for 5 min. and cells were resuspended in 1ml of DMEM culture medium supplemented with 10% (v/v) DMSO, at the desired density. A good standard to freeze is (0.5-1.0) x 10^6 cells/ml. Cells were frozen slowly using a cooling container containing isopropanol to avoid ice crystal formation, which may damage the cells.

In contrast to the slow rate of cooling required to freeze cells, cells should be thawed as rapidly as possible to minimize the risk of cell damaging during ice crystal formation. The vial of cells was removed from the liquid nitrogen tank, quickly thawed by immersing the entire vial in a water bath at 37^{o}C and transferring the cells into a 15-ml conical tube. Then, 10ml of prewarmed culture medium was added to the cells, which were mixed gently by pipetting up and down. Then cells were collected by centrifugation at 1.5K rpm for 5 min. Afterwards, the old freezing medium was discarded and a new DMEM culture medium was added to the flask. Cells were incubated in a CO_2 incubator at 37^{o}C and 90-95% humidity.

2.7.7 - Drug evaluation in primary fibroblasts

Stock solutions of drug compounds were prepared in various solutions and aliquots of the drugs were stored at -80°C until required to use. When the confluence of the cells reached to 60 - 70%, old medium was removed and cells were washed once with PBS. Required concentrations of drug were freshly dissolved in complete culture medium from the stock solution and added to the cells. The cells were incubated for the specified time according to the type of the drug and concentrations used. After the incubation, cells were

washed once with PBS and cells were collected by centrifugation for RNA, DNA and protein extraction.

2.8 - Isolation of primary mouse embryonic fibroblasts (MEFs)

Mouse embryonic fibroblasts (MEFs) were isolated from both WT and FRDA transgenic mice. The pregnant female mouse at day 13 p.c (post coitum) was sacrificed by cervical dislocation. The uterine horns were dissected out carefully, rinsed in 70% (v/v) ethanol and placed in ice cold PBS. Each embryo was separated from its placenta and surrounding membranes. The brain region, dark red organs and as much blood as possible was removed from the embryos, which were washed twice with ice cold PBS. Embryos were then finely minced in minimal amount of PBS with sterile razor blades and transferred to a fresh 15ml centrifuge tube. The minced tissues were allowed to settle down over a period of 2min. The supernatant was removed and 5ml of trypsin/EDTA was added to each embryo followed by incubation with gentle shaking at 37°C for 15min.

After the incubation, the cell suspension was transferred to a 50ml falcon tube and 2 volumes of fresh DMEM medium were added. To remove the undigested pieces of tissues, the cell suspension was allowed to settle down over few minutes and the supernatant was collected in another fresh 50ml falcon tube, followed by centrifugation at 1.5k rpm for 5min. The cell pellet was resuspended in 5ml of prewarmed DMEM medium and plated into one well of a 6-well plate. This step was repeated until the entire tissue sample was fully digested or six primary cultures had been independently plated on a 6-well tissue culture plate. Subculture, cryopreservation and maintenance of MEFs were carried out as normal for fibroblasts (sections 2.7.3-2.7.6).

2.9 - Establishment of neural stem cells (NSCs/neurospheres)

Neural stem cells (NSCs), often referred as neurospheres, were established from the WT and both strains of FRDA mouse model (YG8 and YG22). This method was made available by Satyan Chintawar, Laboratory of Experimental Neurology, Erasme Hospital, Brussels.

2.9.1 - Culture medium of neurospheres

Neurospheres were grown in a selective medium called, Neurocult® NSC proliferation medium and it consists of NSC basal medium, NSC proliferation supplements, recombinant human epidermal growth factor (rhEGF), recombinant human fibroblast growth factor-basic (rhFGF-b), heparin and pen-strep.

1) Stock solutions of growth factors

a) Recombinant human epidermal growth factor (rhEGF)

A stock solution (10µg/ml) of rhEGF (Stem cell technologies) was prepared by adding 0.1mL of sterile 10mM acetic acid containing at least 0.1% bovine serum albumin to initially dissolve the rhEGF powder and then added 19.9ml of NSC basal medium containing NSC proliferation supplements. The stock solution was stored as 1ml aliquots at -20°C until required for use. 2µl of 10µg/ml rhEGF was needed for to every 1ml of NSC medium, to give a final concentration of 20ng/ml of rhEGF.

b) Recombinant human fibroblast growth factor-basic (rhFGF-b)

A stock solution (10µg/ml) of rhFGF-b (Stem cell technologies) was prepared in 1x PBS and 0.1% BSA and stored as 0.5 ml aliquots at -20°C until required for use. 1µl of 10µg/ml

rhEGF was needed for to every 1ml of NSC medium, to give a final concentration of 10ng/ml of rhEGF.

2) Stock solution of heparin

0.2% heparin in PBS was purchased from Stem cell technologies and aliquoted into 0.5ml. The stock solution was stored at 4°C until required for use. 1µl of 0.2% heparin was added to every 1ml of NSC medium, to get a final concentration of 0.0002% (2µg/ml).

3) Stock solution of Pen-strep

A stock solution of pen-strep (5000U/ml penicillin and 5000µg/ml streptomycin) was prepared and stored at -20°C as an aliquot of 5ml in dark until required to use.

2.9.2 - NSC medium preparation

Aliquots of growth factors, heparin, pen-strep and 50ml NSC proliferation supplements were thawed by keeping at 37°C for 2 hours or at 4°C overnight. All the contents were mixed well in 450ml of NSC basal medium. Then, the medium was filter sterilized through 0.22µM pour size filter unit (Thermo Fisher) and aliquoted into 50ml universal tubes and stored at 4°C until required to use.

2.9.3 - Culture of neurospheres

Requirements

Papain solution, Pg Solution, EBSS and NSC medium

1. **Papain solution (10ml)**

NSCs were prepared from the sub-ventricular zone (SVZ) of the brain, and each brain requires at least 10ml of freshly prepared papain solution. Papain solution consists of papain enzyme (Worthington), EDTA (Sigma), cysteine (Sigma) and EBSS (Invitrogen).

Preparation

10mg of papain enzyme was accurately weighed in an Eppendorf and transferred to a 15ml centrifuge tube. The papain enzyme was dissolved in 5ml of EBSS by vortex. In another Eppendorf tube, 2mg of EDTA and 2mg of cysteine was accurately weighed and transferred to a 15ml centrifuge tube. The contents were dissolved in 5ml of EBSS by vortex. Inside the hood (laminar air flow), two solutions of EBSS were mixed well and filter sterilized through a 0.22µM pour size filter attached to a 10ml syringe.

2. **Pen-strep and glucose solution (Pg solution)**

Each brain requires about 200-250ml of Pg solution for transferring the brain and washing and it consists of 1x PBS, 30% glucose and pen-strep.

Preparation

5ml of pen-strep and 10ml of 30% glucose was added to 485ml of 1x PBS and mixed well by shaking the bottle gently. The solution was filter sterilized by a 0.22µM pour size filter and stored in dark at 4°C until required to use.

Culture procedure

Neurospheres were established individually from WT and FRDA (YG8 and YG22) mice. All mice were sacrificed and the brains were collected carefully in Pg solution. The brains were washed once in Pg solution and the SVZ was carefully isolated. The tissues were minced into small pieces with scalpel blades and transferred into a Petri dish containing 10ml of papain solution, followed by incubation at 37°C for 60min on a rocking platform. At the end of the incubation, cells were collected by centrifugation at 1K rpm for 10 min and almost all the supernatant was removed overlaying the cell pellet carefully without using suction. The cell pellet was dissociated by triturating up and down with p1000 Gilson tips several times. Cells were resuspended in 7ml of EBSS followed by centrifugation at 1K rpm for 10min.

After the centrifugation, the supernatant was discarded and the cell pellet was dissociated with p200 Gilson tips by pipetting up and down about 20-30 times. Cells were resuspended in 8ml of EBSS and centrifuged at 500rpm for 15min. The supernatant was discarded cell pellet was gently dissociated with a p200 Gilson tip. Finally, the cell pellet was resuspended in 1ml of complete NSC medium and transferred to a flask containing 7ml of NSC medium. Cells were incubated at 5% CO_2, 95% humidity and 37°C. A schematic representation of the entire procedure is shown in Figure 2.3.

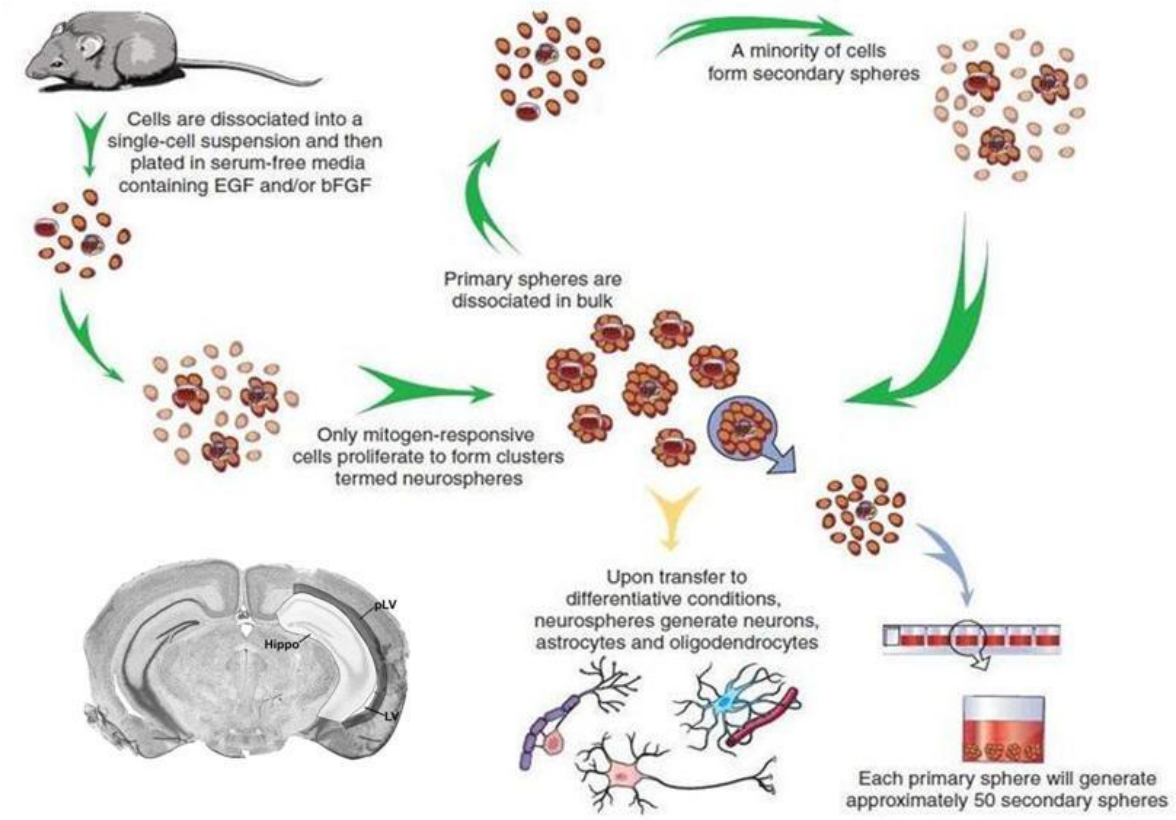

Figure 2.3 - Establishment and maintenance of neural stem cells in culture at different stages (Reynolds and Rietze 2005).

2.9.4 - Passage of Neurospheres

Over time, cells proliferate and form spheroids, called neurospheres, which in general detach from the tissue culture flask and float in suspension. The neurospheres are ready for subculture 6-8 days after plating. If the neurospheres are attached to the culture substrate, tapping the culture flask against the bench top helps to detach the neurospheres. Subculture of neurospheres was accomplished by two different methods:

i. Mechanical dissociation

The medium with suspended neurospheres was removed and placed in an appropriately sized sterile culture tube. Any cells that remained attached to the flask were detached by shooting a stream of medium across the attached cells. The neurospheres were pelleted by centrifugation at 500rpm for 10 minutes. The supernatant was carefully removed leaving behind about 200-300µl. The pellet was dissociated gently by pipetting up and down 20-25 times with a Gilson p200 tip or fire polished Pasteur pipette until a single cell suspension was achieved.

ii. Chemical dissociation

To obtain a higher percentage of viability and total cell expansion, the chemical dissociation method (Figure 2.4) was recommended. The chemical dissociation kit (Stem Cell Technologies) contains solution A, B and C.

Procedure

The cells were collected by centrifugation at 1K rpm as mentioned above. As much supernatant as possible was removed by leaving a minimal volume (less than 50µl) of supernatant above the cell pellet. 0.5ml of solution A was added to the pellet and resuspended by Gilson p1000 tip set at approximately 450µl by pipetting gently up and down 10-15 times. At this point the lab timer was set for 8 minutes and 125µl of solution B was added to the cell suspension. The tube was gently tapped to mix the solution with cell suspension and the lab timer immediately started. At the 3-minute time point, the cell suspension was gently mixed by pipetting up and down 8 times with a Gilson p200 tip volume set at 180µl. This process was repeated at 7- and 8-minute time points. At the 8-minute time point, 40µl of solution C and 350µl of NSC proliferation medium was added to bring the final total volume up to approximately 1ml. The cell suspension was mixed by pipetting up and down and at this point the cell suspension contained only single cells and no aggregates.

The precise volume of the cell suspension was measured and the cell number was counted with a haemocytometer by using a dilution (1/5 or 1/10 dilution) in trypan blue to assess cell density and viability. If a larger volume of cells (>100µl) was needed for the next subculture, a wash step was then necessary to remove the chemical reagents. This was performed by adding 10ml of NSC culture medium to the cell suspension and centrifuging for 5min at 800rpm. The cell pellet was gently resuspended in 1ml of NSC proliferation medium and a further cell count was performed if required. Cells were incubated in a CO_2 incubator for the next passage in NSC proliferation medium.

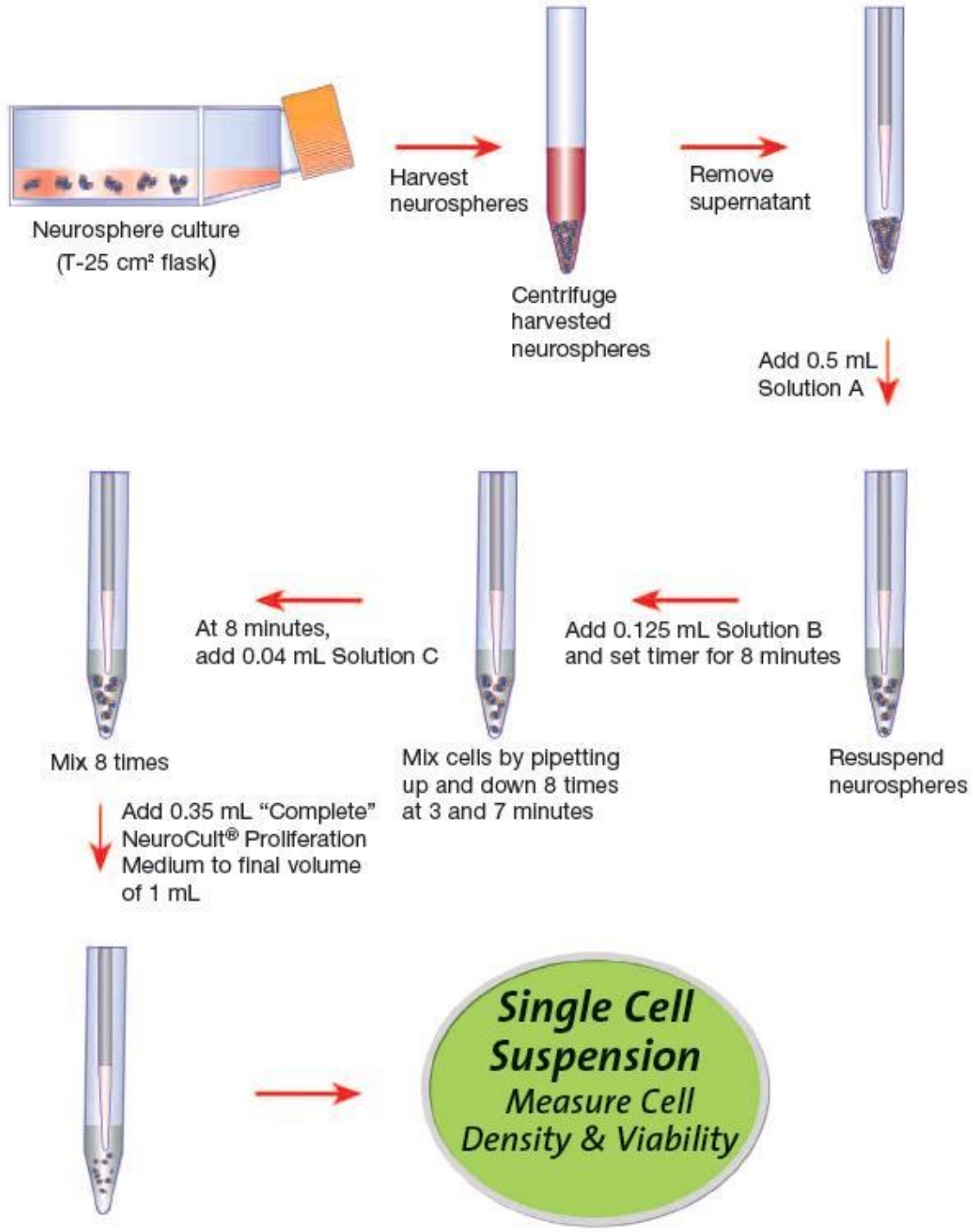

Figure 2.4 - Schematic representation different stages in chemical dissociation method (Stem Cell Technologies 2006).

2.9.5 - Differentiation of NSCs

This method was based on Jana *et al.* (2007) and used for the isolation of purified neurons, oligodendrocytes, astrocytes and microglia from the same mouse brain tissue and neural stem cells (Figure 2.5). It is important to note that microglial cells are only obtained from brain tissues and not from the NSCs.

I. Isolation of primary neurons

Neurospheres were pelleted by centrifugation at 500rpm for 10min and dissociated with p200 Gilson tips. The cell pellet was washed once with PBS and once with neurobasal medium. In the first step, neurons were enriched by allowing the cells to adhere to poly-D-lysine coated flasks for 5min. Non-adherent cells containing astrocytes and oligodendrocytes were removed and used for the isolation of other cells. Adherent cells, mostly neurons, were incubated with DMEM/B27 medium including 10µM of cytosine arabinoside (AraC) for 10 days to prevent proliferation of dividing cells (Jana *et al.* 2007).

II. Isolation of primary microglia (only from brain)

The remaining non-adherent suspensions enriched with mixed glial cells were collected by centrifugation for 10min at 1.5k rpm and then resuspended in DMEM supplemented with 10% heat inactivated FBS. Cells were seeded on poly-D-lysine coated flasks followed by incubation at 37^{o}C with 5% CO_2. The culture medium was replaced in regular intervals of 3 days. On ninth day these mixed glial cultures were placed on a rotary shaker at 240rpm at 37^{o}C for 2 hours to separate the mixed glial cells based on selective cell adhesion properties.

The cell suspension was placed on uncoated culture plates for 30min followed by removal of non-adherent cells by washing (Jana *et al.* 2007).

III. Isolation of primary oligodendrocytes

The oligodendrocytes were obtained after shaking the remaining cell culture for 18 h at 190rpm on eleventh day. To purify oligodendrocytes from astrocytes, the detached cell suspension was plated in non-coated tissue culture dishes for 60 min at 37°C. This step was repeated twice to minimize the contamination. The non-adherent cells were seeded into poly-D-lysine-coated culture plates in NSC medium at 37°C with 5% CO_2 in air (Jana *et al.* 2007).

IV. Isolation of primary astrocytes

The attached cells remaining after removal of oligodendrocytes were primarily astrocytes. These cells were trypsinized and subcultured in complete media at 37°C with 5% CO_2 in air to yield more viable and healthy cells (Jana *et al.* 2007).

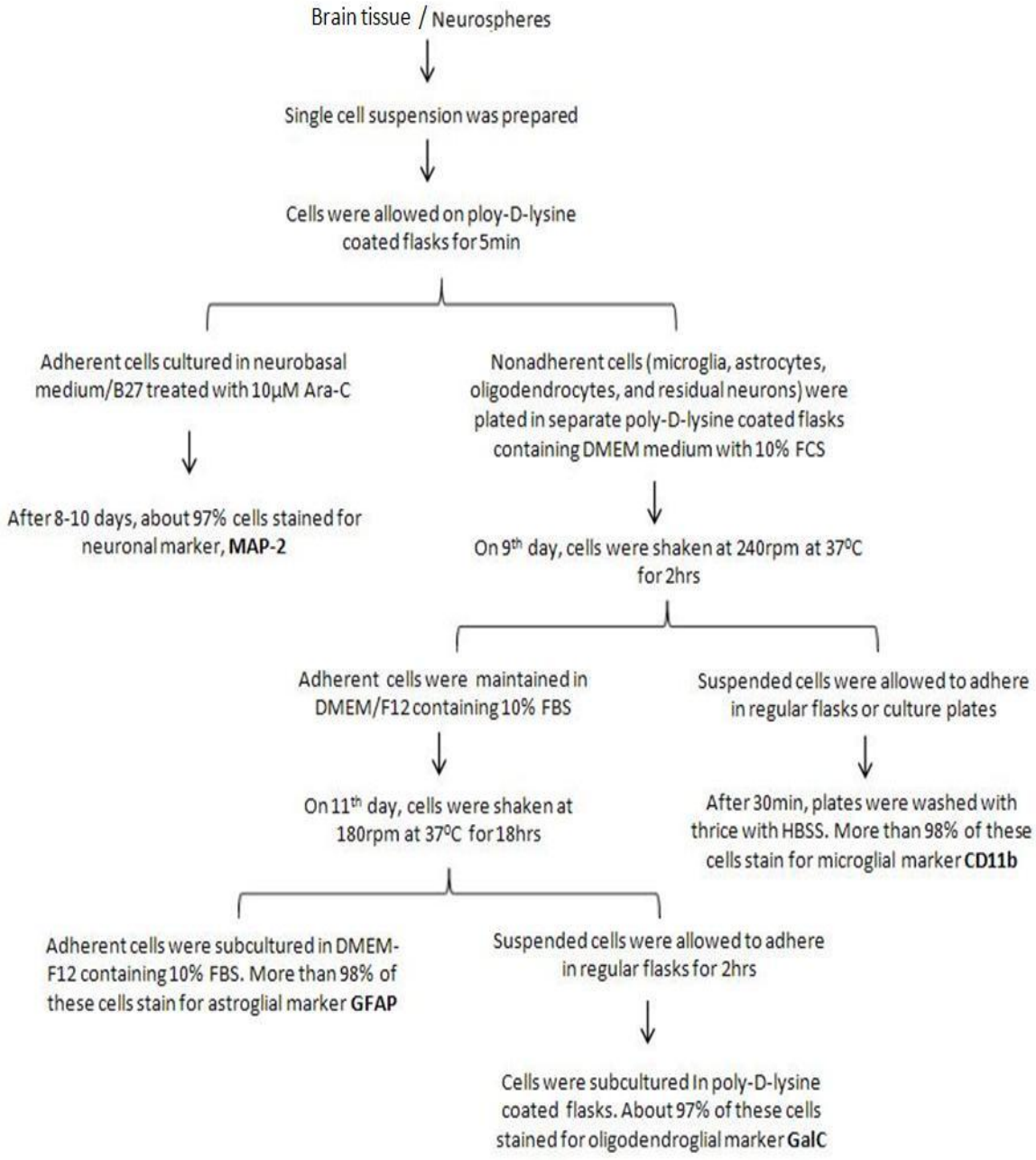

Figure 2.5 - Differentiation of NSCs. Flow chart representing the entire process of isolation method (Jana *et al.* 2007).

2.9.6 - Cryopreservation and regeneration of neurospheres

Neurospheres were stored in serum free cell freezing medium (Sigma). All the neurospheres were pooled together by centrifugation at 500rpm for 10min and almost all the supernatant was removed by vacuum suction (leaving not more than 50µl). The cell pellet was gently dissociated by tapping the tube and cells were resuspended in 1.5ml of serum free freezing medium. The cell suspension was transferred to a new polypropylene cryovial (Nunc), which was then placed in a cooling container at -80^{0}C for 3 hours, followed by transfer to liquid nitrogen. To re-establish the neurospheres, the vial containing neurospheres from the liquid nitrogen was carefully collected and quickly thawed at 37°C. The cells were added to a 15ml centrifuge tube containing 8ml of NSC medium and centrifuged at 500rpm for 10min. The supernatant was removed and cell pellet was gently dissociated with a Gilson p200 tip. The cells were incubated with 10ml NSC medium at 37°C, 95% humidity and 5% CO_2.

2.10 - Isolation of murine fetal neural stem cells

Mouse fetal neural stem cells were derived from selected WT and FRDA mice and were maintained in NSC culture medium.

The pregnant female mouse at day 13.5 p.c (post coitum) was sacrificed by cervical dislocation. The uterine horns were dissected out carefully, rinsed in 70% (v/v) ethanol and placed in ice cold PBS. Each embryo was separated from its placenta and surrounding membranes. The brain region of the embryo was collected carefully and placed in 1ml of NSC medium. The tissue was homogenized with Gilson p1000 tips (set at 500µl) by pipetting up and down about 10-15 times, followed by adding 9ml NSC medium. Homogenized tissue was centrifuged at 1k rpm for 10min at room temperature and almost all the supernatant was removed overlaying the cell pellet carefully without using suction. The cell pellet was dissociated by triturating up and down with Gilson p200 tips and resuspended in 7ml of EBSS, followed by a centrifugation at 1k rpm for 10min.

After the centrifugation, the supernatant was discarded and again the cell pellet was dissociated with Gilson p200 tip. Cells were resuspended in 8ml of EBSS and centrifuged at 500rpm for 15min. The supernatant was discarded and the cell pellet was gently dissociated with Gilson p200 tip. Finally, the cell pellet was resuspended in 8ml of NSC medium and transferred to T25 flask, followed by incubation at 5% CO2, 95% humidity and 37°C.

2.11 - Isolation of murine splenocytes

Splenocytes are white blood cells established from the spleens of WT and FRDA mice for their similarity to human lymphocytes.

To isolate splenocytes, the selected mouse was culled appropriately and wiped with 70% ethanol. The spleen was collected aseptically and placed on ice-cold PBS. Immediately, the spleen was mashed through a 70µM cell strainer using the plunger end of the syringe into a Petri dish containing 5ml of RPMI 1640 medium. The cell strainer was washed with an additional 5ml of medium and then discarded. The suspended cells were transferred to a 15ml centrifuge tube and centrifuged at 1.5k rpm for 5min. The supernatant was discarded and the cell pellet was resuspended with 1ml of ACK lysis buffer (to remove RBC) followed by an incubation of 10min at room temperature. Afterwards, 9ml of RPMI 1640 medium was added and the cells were centrifuged as before. Again, the supernatant was discarded and the cell pellet was resuspended in 3ml of RPMI 1640 medium, followed by removing of any dead cells mass. Cell count and viability was measured by the trypan blue exclusion assay as described before (section 2.7.4). Cells were resuspended at a concentration of $1x10^7$/ ml and incubated at 37°C with 5% CO_2.

2.12 - Western blot analysis

Protein lysates were obtained from frozen brain tissues, and frataxin western blot analysis was carried out as previously described (Pook *et al.* 2001), using an anti-frataxin rabbit polyclonal antibody (Santa Cruz). Histone H3 and H4 acetylation levels were determined by western blot analysis using anti-acetyl-histone H3 (Upstate) and anti-acetyl-histone H4 (Upstate) antibodies, respectively. In all cases, normalization was carried out using an anti-tubulin rabbit polyclonal antibody (Sigma). Densitometry was carried out using UN-SCAN-IT software (Silk Scientific Corporation).

2.13 - Aconitase assay

Aconitase is a Fe-S cluster protein that catalyzes the conversion of citrate to isocitrate. The assay used for this study was based on a combined protocol provided by Cayman Chemical Company (USA, Cat. No. 705502) and Dr. Mark Cooper (Royal Free Hospital, London). It involves coupled enzymatic reactions that convert citrate to isocitrate, which is then converted to α-ketoglutarate in a reaction catalysed by isocitric dehydrogenase (IDH). An increase in the absorbance at 340 nm is measured, which monitors the formation of NADPH. The production of NADPH is proportional to the aconitase activity.

To perform the assay, mouse brain tissues were homogenised on ice in CellLytic MT Mammalian Tissue Lysis/Extraction buffer (SIGMA, C3228) to 10% w/v. Lysates were centrifuged at 800 x g for 10min at 4^{o}C and used immediately.

A substrate reaction premix was made up as follows:

Table 2.7 - Aconitase assay substrate reaction premix

Component	Final Concentration
Tris/HCl (pH 7.4)	50mM
NADP	0.4mM
Na Citrate	5mM
$MgCl_2$	0.6mM
Triton X-100	0.1%
Isocitrate dehydrogenase	1U

200µl of substrate premix was added to each well of a preheated 96 well plate, and reactions were initiated by adding 50µl of a 1 in 10 dilution of homogenised tissue sample. Reactions were incubated at 37^{o}C for 15min in the dark and then the absorbance was measured once every minute at 340 nm for 15 min at 37^{o}C using a spectrophotometer. The aconitase activity was determined from the slope of a graph by plotting the absorbance value over time.

2.14 - MethylScreen assay

DNA methylation analysis was performed using the 'methylscreen' method described by Holemon *et al.* (2007), which uses combined restriction digestion of DNA with methylation sensitive and methylation dependent restriction enzymes, MSRE and MDRE respectively.

Methylscreen was used to analyse the *FXN* CpG site 4 region upstream of the GAA repeat (Al-Mahdawi *et al.* 2008). Specific MSRE, *Aji*I (Fermentas) and MDRE, *Mcr*Bc (*BioLabs*), were used to perform four treatments of each DNA in the assay. All digestion

cocktails contained 1xTANGO™ with BSA (Fermentas). In addition, the *Mcr*Bc digests required the use of 2mM GTP (guanosine-5'-triphosphate).

In a typical experiment, genomic DNA was prepared by phenol/chloroform extraction and 0.5-1µg DNA was restricted in four separate eppendorf tubes as described in Table 2.8 and adjusted the final volume to 100µl by PCR grade water.

Table 2.8 - Preparation of restriction digestion samples for methylscreen assay

Components	Volume	*AjiI*	*McrBc*	Double Digest	Mock
0.5 - 1µg DNA	1µl	✔	✔	✔	✔
AjiI (5U/µl)	2µl	✔		✔	
McrBc (10U/µl)	1µl		✔	✔	
10X TANGO™	10µl	✔	✔	✔	✔
GTP (100mM)	1µl		✔	✔	
50% Glycerol	3µl				✔

Samples are incubated for 16 hours at 37°C. After incubation, enzyme was deactivated by heating to 65°C for 20min followed by placing the samples on ice. Spin the samples briefly and use 5µl to check efficiency of digestion on a 1% agarose gel.

For QRT-PCR, 5µl of above digested sample was used with forward (Fmet 5'-GATCCGTCTGGGCAAAGGCCAG-3') and reverse (Rmet 5'-ATCCCAAAGTTTCTTCAAACACAATG-3') primers designed to amplify across the *FXN* CpG site 4. A 196bp product is expected when no digestion occurs (mock). Full digestion is expected in the double digest samples and hence no PCR product is obtained.

For calculations, mock treated sample C_t values were normalized to 100% and MSRE, MDRE or double digested samples were expressed relative to mock treated sample. The percentage of densely methylated and unmethylated values were calculated by subtracting

MSRE and MDRE digested sample values from the double digested value, respectively. Intermediately methylated values were detected by subtracting the value of densely methylated plus unmethylated value from 100. In all methylscreen assays the mock sample showed a lower Ct value than the digested samples and the highest Ct value was reported in the sample digested with both enzymes (double digest) (Figure 2.6).

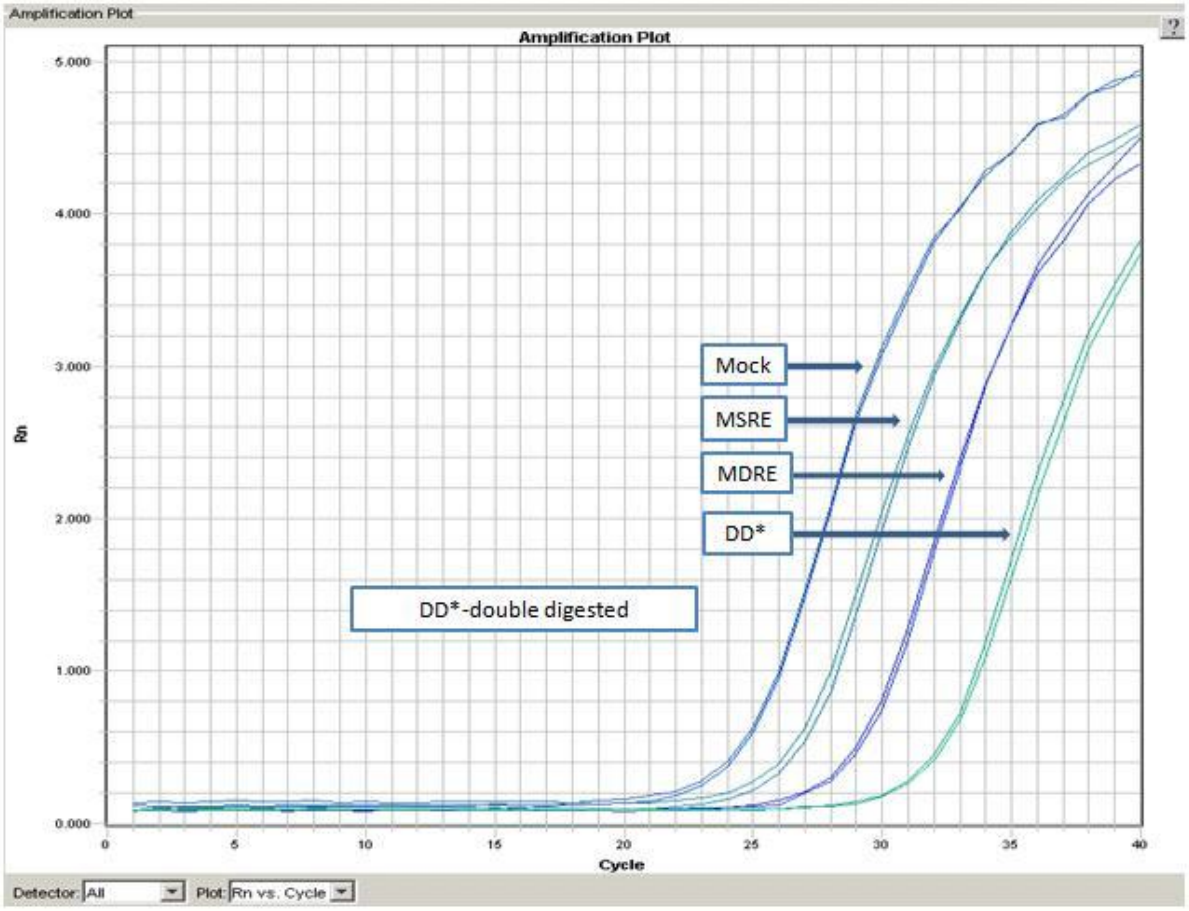

Figure 2.6 - A typical QRT-PCR profile of methylscreen assay. Undigested sample (mock) showed a lower Ct value than the MSRE, MDRE or double digested (DD) sample.

2.15 - Histological analysis of DRG sections

This method was kindly performed by Lorraine Lawrence, Imperial College London.

Preparation of vertebral column paraffin wax blocks

Vertebral column samples were prepared for the histological analysis as described earlier (section 2.6) and placed in a tissue-tek cassette. Decalcification of vertebral column was done by immersing the cassettes in 500ml of Hillman and Lee's EDTA for a minimum of five days. Then the cassettes were washed under running tap water for at least 4 hours followed by immersing the cassettes in increasing concentration of IMS (as described in Table 2.9) using an automated embedding unit (Hypercenter XP, Shandon). Afterwards, the cassettes were immersed in Histo-Clear (Sigma-Aldrich) and molten paraffin wax-based embedding medium (Kendall), followed by the final paraffin wax incubation under vacuum for the time durations specified in Table 2.9. The block was then allowed to cool down in a cold plate.

Preparation and H&E staining of section slides

Using a rotary microtome (AS 325, Shandon) DRG-containing vertebral columns were cut into thin (6µM) slices and briefly suspended on the surface of a 37°C water bath. The sections were then transferred to microscope slides and allowed to dry overnight at 37°C. To remove the excessive wax and staining solutions from the slides, sections were soaked twice (5min each) in Histo-Clear followed by immersion in 100% and 70% IMS giving a brief (2min) rinse with water between each solution. Then the sections were immersed in Haematoxylin Harris (BIOS Europe) for 2min and placed under running tap water until sections turn blue. The colour was then distained by dipping the sections twice in acid alcohol (1% HCl in 70%

IMS) and returned the sections to running tap water until sections went blue again. Afterwards, sections were incubated in 1% Eosin (BIOS, Europe) for 1min and washed once with running tap water. Subsequently, the sections were dehydrated by rinsing in increasing concentration of IMS (70%, 90% and 100%) for 30s each. Finally, the sections were washed 3 times (5min each) in Histo-Clear and coverslips were applied using DPX mountant.

Table 2.9 - Incubation schedule of H&E staining of DRG sections

Solution*	Duration
Hillman & Lee's EDTA	5 days
70% IMS	Overnight
90% IMS	4 hours
100% IMS	1.5 hours
100% IMS	1.5 hours
100% IMS	1 hour
Histo-Clear	Overnight
Histo-Clear	1 hour
Paraffin Wax	1.5 hours
Paraffin Wax	1.5 hours
Paraffin Wax - Vacuum	1 hour

*fresh solutions were used at each incubation step.

The levels of DRG neurodegeneration were determined by counting the number of vacuoles in neuronal cell bodies as a percentage of the total number of DRG cells counted.

2.16 - Immunofluorescence assay

Cells were grown on poly-D-lysine coated coverslips until they reach 70-80% confluence and then the coverslips were transferred to a micro dish with cells facing up using a sterile tweezers. The cells were washed twice with sterile ice-cold PBS and fixed by incubating in 4% paraformaldehyde for 8 min at 4^{o}C. Afterwards, cells were washed 3 times 5 min each with sterile ice-cold PBS and then incubated with permeabilizing buffer for 5 min at room temperature. Again, cells were washed twice with sterile ice-cold PBS and incubated with blocking buffer in a humidified chamber at 4^{o}C overnight.

Next day, cells were washed twice with sterile ice-cold PBS and once with blocking buffer. Cells were incubated with appropriately diluted primary antibody (15-20µl/cover slip) for 2 hours at room temperature in the dark followed by three 5min washes with washing buffer. Then cells were coated with secondary antibody for 2 hours at room temperature in the dark. The washing steps were repeated again two times with washing buffer, as before, and once with sterile distilled water. A drop of mounting medium with DAPI stain was added to a clean and properly labelled microscopic slide. Coverslips were transferred to the slide carefully with sterile tweezers facing with the cells facing downwards on the mounting medium. Excess mounting medium was removed with paper towels and cells were visualized with a fluorescent microscope.

2.17 - Quantitative real-time RT PCR (QRT-PCR)

Quantitative real-time reverse transcriptase PCR (QRT-PCR) was performed using SYBR® green master mix (Applied Biosystems) in a real time PCR machine (ABI Prism 7900HT, Applied Biosystems). QRT-PCR reactions were carried out in 96-well plates (Microamp, Applied Biosystems) in triplicates. A final volume of 25µl mastermix was prepared containing 12.5µl of 2x SYBR® green mastermix, 0.5-1.0µl of 2.5-5pmol of optimized respective forward and reverse primers (see Table 2.2 for primers used), 5µl of (5x diluted) cDNA and distilled water to make the final volume up to 25µl. Samples were minimized to light exposure. Target and endogenous mastermixes were prepared separately and added to the plate with a repetitive electronic pipette (Rainin) followed by adding the cDNA. Then the plate was sealed with real time plate sealers (MicroAmp, Applied Biosystems) and the contents were mixed gently by shaking the plate. The plate was then briefly (1min) centrifuged at 1K rpm to bring all the contents to the bottom of the well.

The cycling conditions varied according to the application and were optimized to amplify the different targets with similar efficiencies. Following each real time PCR reaction a dissociation curve run was performed by increasing the temperatures gradually from 60°C to 95°C. Relative quantification values were determined by $2^{-\Delta\Delta Ct}$ method using SDS 2.1 software (Applied Biosystems).

2.18 - Statistical analysis

Statistical analyses such as descriptive measurements and graphical visualization were done using Microsoft excel 2007 software. Functional measurements of weight, rotarod performance, locomotor activity, average velocity, ambulatory distance and vertical counts were analysed using two way analysis of variance (ANOVA) for repeated measures. All other measurements comparing two sample groups were analysed using student's *t* test to determine if the mean values differed significantly or not. In all cases a statistical significance level of 5% was chosen.

Chapter 3 - Developing a model cell culture system for FRDA

3.1 - Introduction

In order to gain further understanding of the physiological function of frataxin and FRDA pathogenesis, and to develop an effective system for testing potential therapies, a model cell culture system is considered most useful. Although animal models are considered essential to study whole organism aspects of the disease, whenever possible, alternatives should also be used to ensure successful research, upholding the principles of the 3Rs (reduction, replacement and refinement).

Cell culture was first devised at the beginning of this century (Harrison 1907) as a method for studying the behaviour of animal cells free of systematic variations. Cell culture systems are now used extensively in research for wide variety of diseases. Mammalian cell models are important to study the molecular mechanisms of the disease and are powerful tools for large-scale therapeutic screening approaches.

As mentioned earlier, a FRDA YAC transgenic mouse model has been generated that exhibits FRDA-like pathology (Pook *et al.* 2001; Al-Mahdawi *et al.* 2004; Al-Mahdawi *et al.* 2006; Al-Mahdawi *et al.* 2008). The development of a model cell culture system from such animals is of paramount importance to study the *in vivo* trinucleotide dynamics *in vitro*. In addition, this cell culture system can create new avenues to investigate the multiple factors affecting FRDA pathogenesis under controlled conditions. Furthermore, these cells have the advantage of being readily renewable, easily accessible, and relatively inexpensive to maintain. Therefore, we have decided to establish a novel model cell culture system for FRDA in order to hasten therapeutic drug screening and to analyse the repeat dynamics over extensive periods of time.

3.2 - Types of cells

In FRDA it is difficult to obtain the critical affected tissues, such as DRG, heart and cerebellum, from FRDA patients. Therefore, we have performed experiments using various human and mouse cell types. Human primary fibroblasts were obtained from Coriell Cell Repository (USA) and as kind gift from Dr. Ian Kill (Brunel University). Mouse primary fibroblasts, embryonic fibroblasts, splenocytes, neural stem cells (NSCs), and fetal neural stem cells were established in our laboratory from the FRDA YAC transgenic mouse model as described earlier (chapter 2).

3.2.1 - Human primary fibroblasts

Since FRDA patients are relatively rare, most initial experiments were conducted with fibroblasts from three healthy individuals (H.Normal, GM04503 and GM07492) and three FRDA patients (GM04078, GM03816 and GM03665) (Figure 3.1 and Table 3.1). The GAA size in FRDA primary fibroblasts was determined using expand long range PCR system as described (section 2.4).

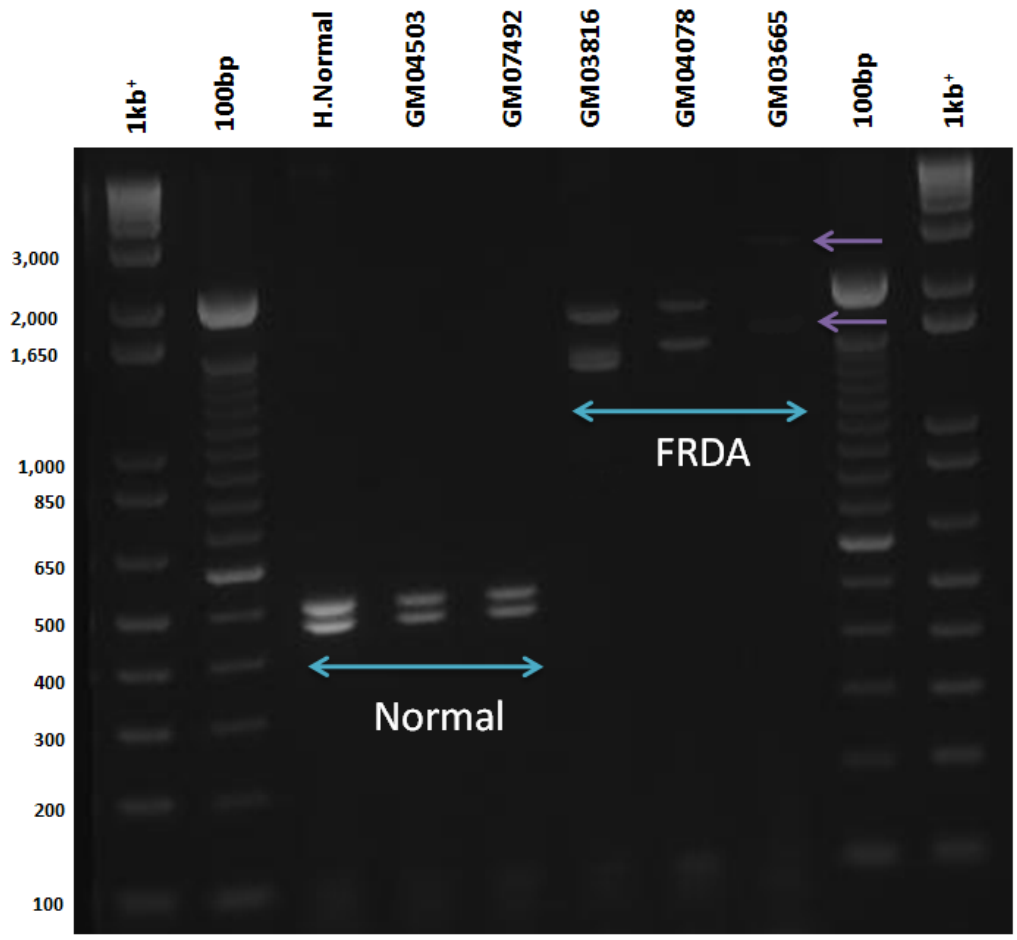

Figure 3.1 - Long-range PCR analysis of GAA repeat length in normal and FRDA patient primary fibroblasts. DNA length markers (1kb plus and 100bp) are shown in bp. Left panel corresponds the GAA length of three normal primary fibroblasts (H.Normal, GM04503 and GM07492) and right panel consists the length of three FRDA patients fibroblasts GAA size (GM03816, GM04078 and GM03665).

Table 3.1 - Details of the human primary fibroblasts

ID	Sex	Age (Yrs)	Number of GAA repeats
H.Normal	Male	27	Normal
GM04503	Female	31	Normal
GM07492	Male	17	Normal
GM03816	Female	36	330/380
GM04078	Male	30	541/420
GM03665	Female	13	445/740

3.2.2 - Mouse adult and embryonic primary fibroblasts

Mouse primary fibroblasts have a number of properties that make them an attractive culture models. They are relatively easy to establish and maintain, they proliferate rapidly and, as a result, large numbers of cells can be produced. Mouse adult primary kidney fibroblasts were established from the wild-type (WT), YG8 and YG22 mice (Figure 3.2), whereas embryonic fibroblasts were developed only from the WT and YG8 mice. For each line of FRDA YAC transgenic mice, fibroblasts were derived from rescue and transgenic mice to compare the frataxin mRNA levels. It is important to understand the genotype of the mice which we used in the subsequent experiments. The transgenic mice have both human and mouse *frataxin* genes, whereas rescue mice possess only the human *frataxin* gene (*FXN*) and WT mice contain only the mouse *frataxin* gene (*Fxn*).

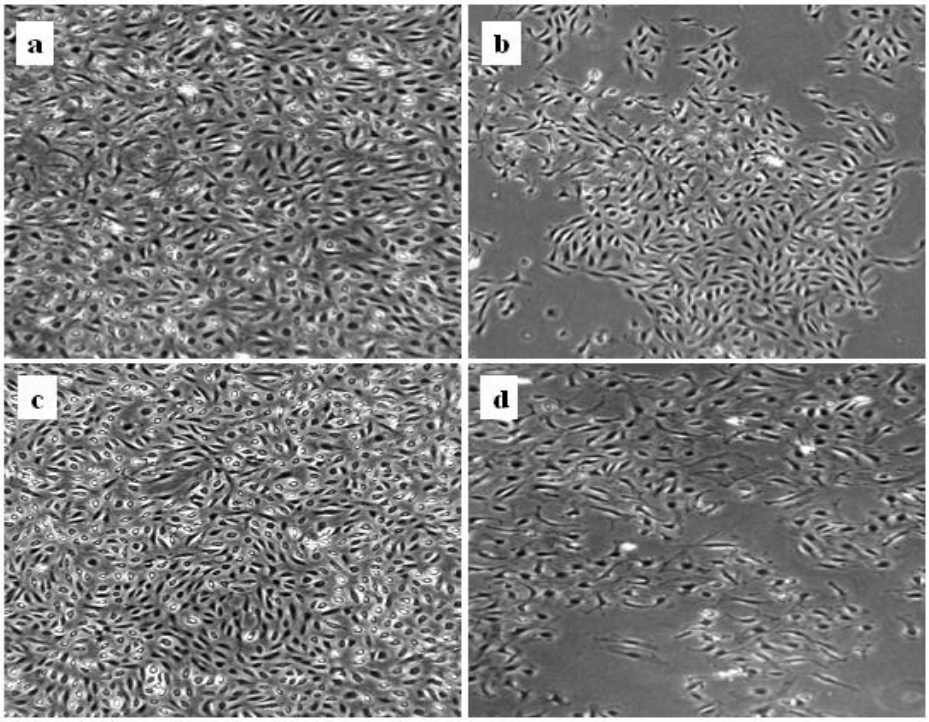

Figure 3.2 - Fibroblast cells of FRDA YAC transgenic mice. The fibroblasts were established from the kidney and after 7 days in incubation, about 90% confluence was seen in YG8 and YG22 transgenic mice (a, c), and 40-50% in YG8 and YG22 rescue mice (b, d).

3.2.3 - Mouse adult and fetal neural stem cells (NSCs)

Neural stem cells (NSCs) are immature cells with extended self-renewal capacity that are able to differentiate into neurons, astrocytes and oligodendrocytes (Abematsu *et al.* 2010). These properties have led to expectations that NSCs might be useful to understand neurological disease mechanism. Most of the neurodegenerative disorders are characterized by a continuous loss of specific populations of neurons. Therefore, possible regenerative interventions include transplanting developing neural stem cells (NSCs) into the host brain or inducing the proliferation of endogenous stem cells by pharmacological manipulations. In fact, use of human embryos faces ethical controversies that hinder the applications of human stem cells, and it is difficult to generate patient or disease-specific stem cells, which are required for their successful implementation. Therefore, alternative methods are currently being developed and such methods include the use of cells from an animal model of disease or induced pluripotent stem cells (iPS) derived from fibroblasts of affected individuals (Abeliovich and Doege 2009).

In order to study the effect of the GAA repeat expansion on *FXN* expression in CNS tissues, we have established adult NSCs from WT, YG8 and YG22 rescue mice, and fetal NSCs were produced from the WT and YG8 rescue mice, as described in section 2.9. Briefly, NSCs were isolated from the sub-ventricular zone of the brain and dissociated mechanically followed by enzymatic digestion of the tissue. Both adult and fetal NSCs were maintained in NSC medium with rhEGF and rhFGF growth factors. After 10-14 days in culture (6-8 days for fetal NSCs), free floating colonies were observed, with each colony containing approximately 200-500 cells (Figure 3.3).

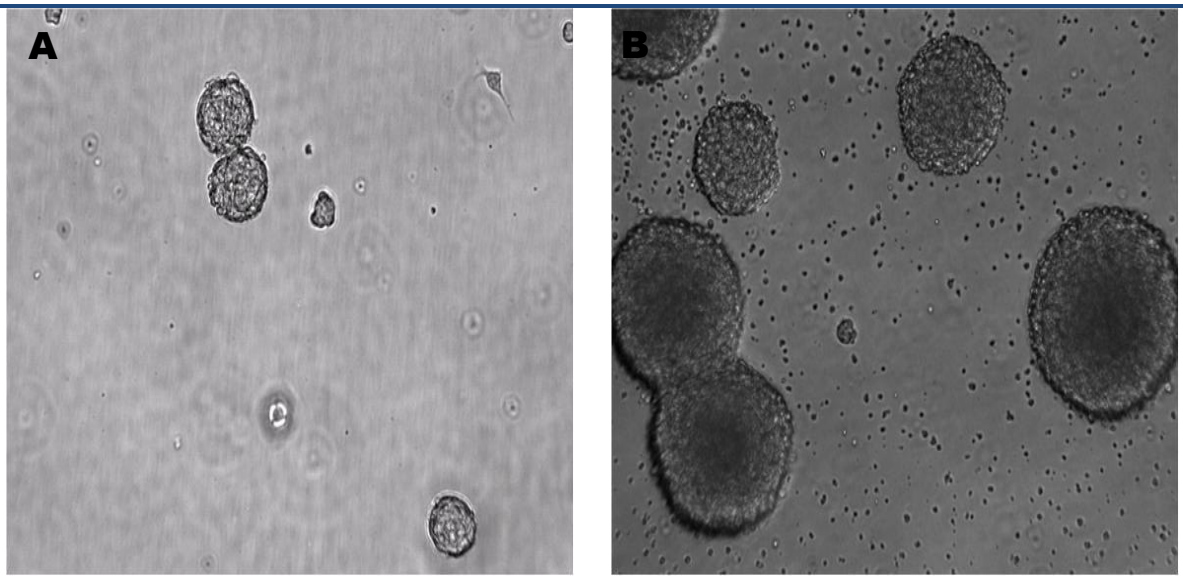

Figure 3.3 - Primary cultures of mouse neural stem cells in culture. **A**) The initial free floating cells were formed after 5-6 days of plating with NSC medium supplemented with rhEGF and rhFGF growth factors, and **B**) after 10-14 days, NSCs were approached their greatest diameter, and look like large spheres with sharp bright outer borders (10X).

3.2.4 - Mouse primary splenocytes

Splenocytes are white blood cells derived from the spleen and used for their similarity to human lymphocytes. Splenocytes consist of a variety of cell populations, such as T and B lymphocytes, dendritic cells and macrophages, which have different immune functions. In order to compare *FXN* expression between the murine splenocytes and human primary lymphocytes, we have established the splenocytes from WT and YG8 rescue mice. Currently no experiments have been performed with these cells, but we have developed the system to compare the level of frataxin mRNA or protein for future experiments.

3.3 - Results

3.3.1 - Quantification of *FXN* mRNA in human primary fibroblasts

In order to verify the *FXN* mRNA levels in human primary fibroblasts of normal and FRDA cells, QRT-PCR measurements were performed as described in section 2.17. Briefly, RNA was extracted from about 1 million cells by the Trizol® method and converted into cDNA, followed by QRT-PCR. In order to account for possible differences in gene expression efficiency or RNA amounts, the Ct values obtained for *FXN* were normalized to *GAPDH* (human) or *Gapdh* (mouse) genes (endogenous control). Each sample was run in triplicate and each experiment was performed at least twice. The mean value of each triplet was used for further calculations using the $2^{-\Delta\Delta Ct}$ method to obtain relative quantification (RQ) values. The relative levels of mRNA expression in FRDA and normal fibroblasts were then calibrated by calculating the means of the RQ values, setting one group arbitrarily as 100%. The passage numbers of all primary fibroblasts were closely matched throughout all mRNA quantification experiments to avoid any possible cell culture variability.

QRT-PCR analysis of human fibroblasts clearly indicated reduced levels of *FXN* expression in all three FRDA fibroblast cell lines, GM04078, GM03816 and GM03665, with 41% ($p<0.01$), 48% ($p<0.01$) and 27% ($p<0.001$), respectively compared to one of the normal fibroblast cell lines, H.Normal (Figure 3.4A). Although, there are slight fluctuations in *FXN* expression within the normal fibroblasts, no significant differences were identified. The mean decreased level of *FXN* in FRDA fibroblasts was confirmed as 40% of normal fibroblast levels ($p<0.001$) (Figure 3.4B), consistent with previously published data (Pianese *et al.* 2004).

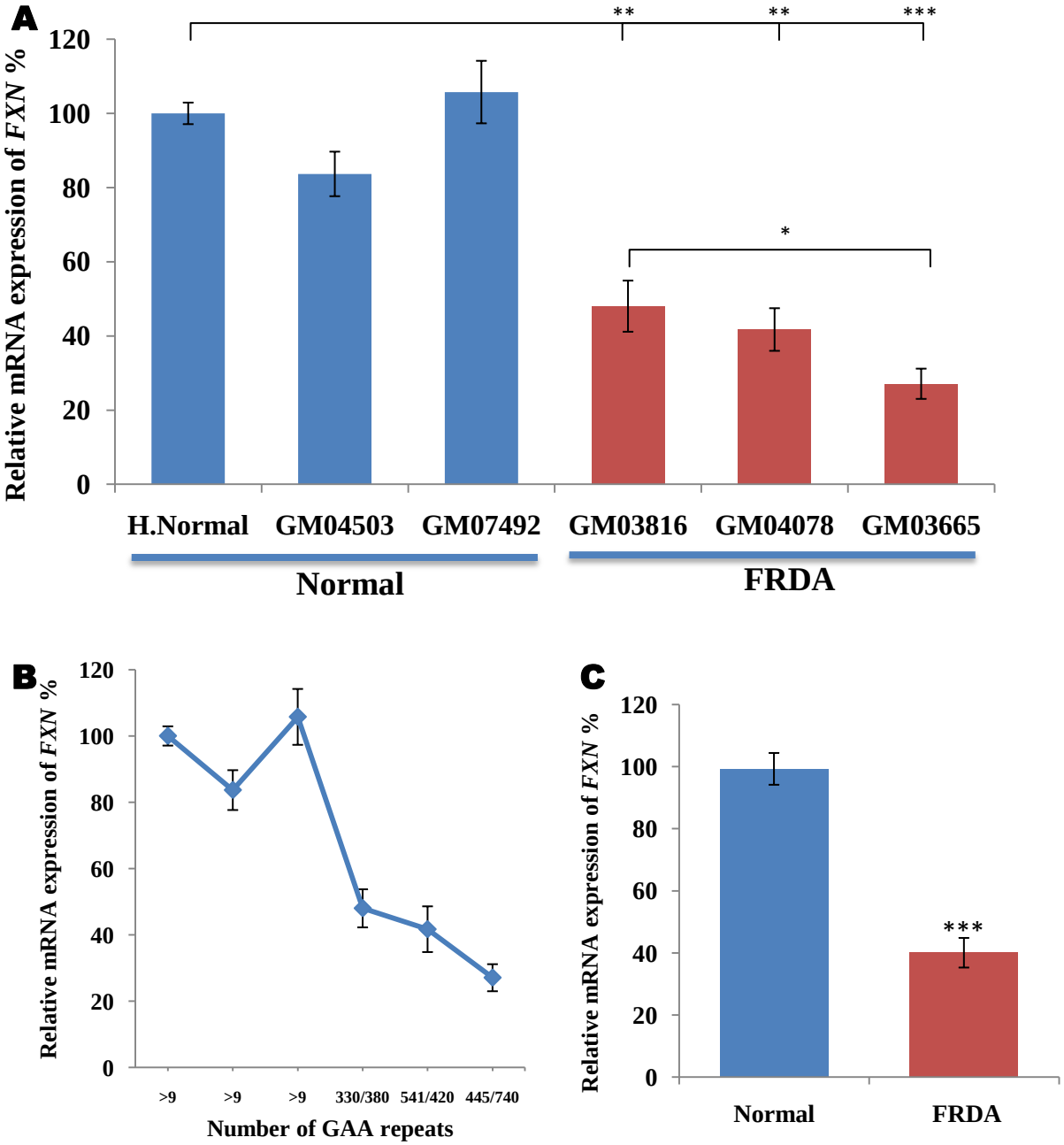

Figure 3.4 - Quantification of *FXN* mRNA in human primary fibroblasts. QRT-PCR measurement of *FXN* mRNA expression in **A-B**) individual fibroblast cell lines, and **C**) average expression between the normal and FRDA primary fibroblasts. *FXN* expression values were first normalized to *GAPDH* and then calibrated to normal fibroblasts expression. Each result is the mean of two independent experiments. The error bars represents the SEM (*p<0.05, ** p<0.01, ***p<0.001).

The comparatively small GAA repeat expansion containing cell line, GM03816 (330/380), shows significantly ($p<0.05$) increased *FXN* expression compared to the large GAA repeat expansion containing cell line (GM03665, GAA repeats 445/740). This finding indicates that *FXN* expression in FRDA fibroblasts depends on the number of GAA repeats. Although there are variations in the number of GAA repeats between GM03816 and GM04078 (541/420) cell lines, no obvious difference in *FXN* expression was identified, suggesting that significant variations in *FXN* levels are achievable only when there is a big difference in number of GAA repeats.

3.3.2 - Quantification of *FXN* mRNA in mouse primary fibroblasts

The *FXN* mRNA expression in mouse adult and embryonic fibroblasts was quantified by QRT-PCR using primers that equally amplified that human and mouse *frataxin* genes and *Gapdh* was used as an endogenous control. The WT values were used as a calibrator to express the YG8 and YG22 mice *FXN* values relatively.

FXN mRNA in adult primary fibroblasts

All fibroblasts derived from the FRDA YAC transgenic lines of mice have shown increased *FXN* expression compared to WT mouse fibroblasts. The YG8 rescue and transgenic mouse cells showed 2.6- and 4.3-fold increases, whereas the YG22 rescue and transgenic mouse cells showed 3.2- and 3.9-fold increases in *FXN* expression compared to WT mouse fibroblasts, respectively (Figure 3.5A). The smaller levels of *FXN* expression in rescue mouse fibroblasts compared with transgenic mouse fibroblasts are likely due to the fact that they only contain a single functioning human *FXN* transgene and no functioning

mouse *Fxn* genes. It is speculated that when the human *FXN* gene transferred into the mouse genome it perhaps became over expressed. However, it has also been reported that YG8 and YG22 rescue mice have greatly decreased mRNA levels compared to the normal GAA-containing Y47 rescue mice *in vivo* (Figure 1.17) (Al-Mahdawi *et al.* 2008). Therefore, even though all *FXN* transgenes appear to show very high levels of mRNA expression in the mouse, this does not necessarily translate into increased levels of functional frataxin, which is why YG8 and YG22 rescue mice show FRDA-like disease.

FXN mRNA in embryonic primary fibroblasts

The quantification of *FXN* expression by QRT-PCR analysis in mouse embryonic fibroblasts (MEFs) has revealed that the YG8 MEFs show a similar pattern of *FXN* expression as adult fibroblasts. The *FXN* expression levels were significantly increased in YG8 rescue MEFs (1.5-fold) and transgenic MEFs (2.3-fold) as compared to WT MEFs (Figure 3.5B), but these increases are less than with the adult fibroblasts. However, an overall increased *FXN* expression was observed in MEFs compared with adult fibroblasts (Figure 3.5c). In particular, the WT MEFs showed significant (2.3-fold, $p<0.01$) increase in *FXN* expression compared to adult WT fibroblasts (Figure 3.5C). This may be due to differential DNA methylation of the *frataxin* and other genes in MEFs compared to adult fibroblasts.

A comparison of *FXN* expression between YG8 rescue and WT fibroblasts shows that there is much less increase of YG8 rescue *FXN* expression in the MEFs (1.5-fold) compared to adult fibroblasts (2.6-fold). Therefore, the two different systems may both have uses in future drug screening experiments. Although we have not yet determined the epigenetic status of these two cell types, such investigations may give additional information.

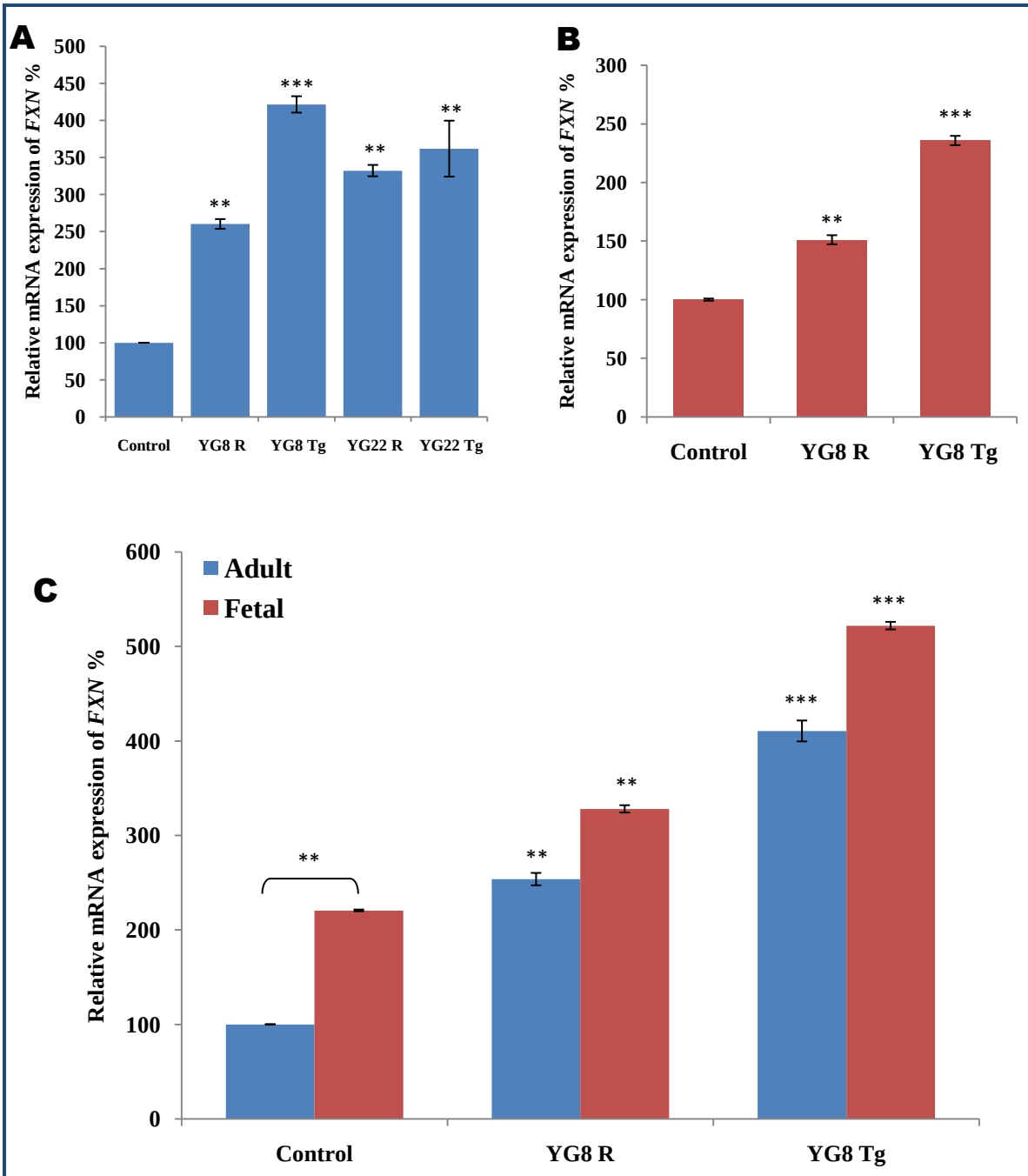

Figure 3.5 - *FXN* mRNA expression levels in mouse primary fibroblasts **A**) Quantification of *FXN* levels as determined by QRT-PCR in WT (control), YG8 and YG22 rescue and transgenic mice. **B**) *FXN* expression levels in MEFs of WT, YG8 rescue and transgenic mice. **C)** Comparison of *FXN* expression levels between adult and embryonic fibroblasts. All quantifications were done in triplicates, and values were expressed relative to *Gapdh*. Error bars represent the SEM. (*p<0.05, ** p<0.01, ***p<0.001).

3.3.3 - Oxidative stress in mouse primary fibroblasts

Biochemical studies of mitochondrial enzymes have revealed that FRDA is the result of oxidative stress and mitochondrial dysfunction. Thus, the endomyocardial biopsies from two unrelated FRDA patients resulted in deficient activity of Fe-S containing enzymes but the enzyme activities were normal in skeletal muscle, lymphocytes, and fibroblasts (Rotig *et al.* 1997). Also, human fibroblasts derived from FRDA patients showed sensitivity to hydrogen peroxide induced oxidative stress (Figure 3.6) (Wong *et al.* 1999). Additionally, the FRDA YAC transgenic mouse model also exhibited oxidative stress (Al-Mahdawi *et al.* 2006).

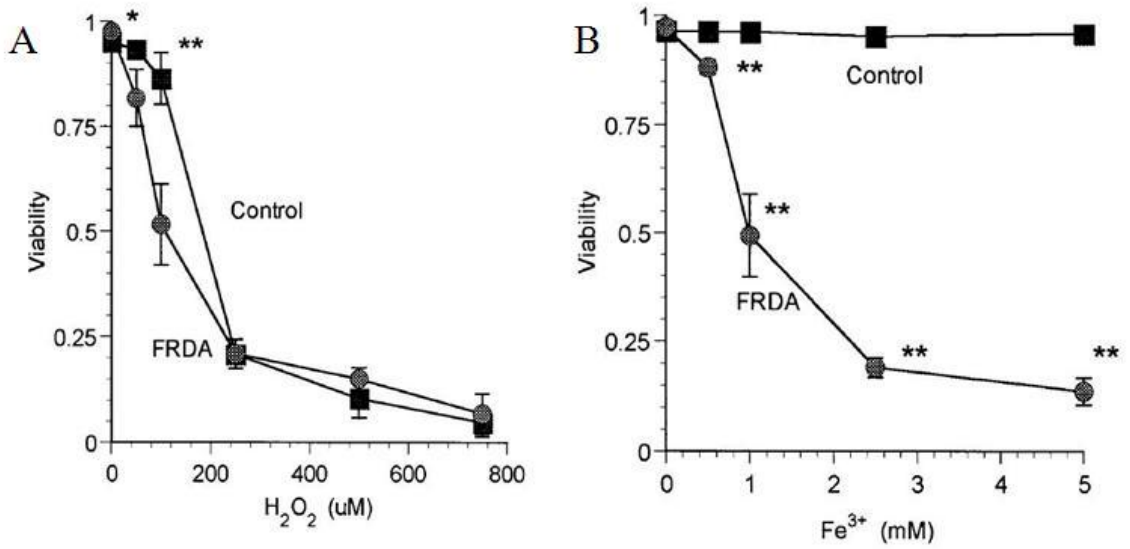

Figure 3.6 - Sensitivity of FRDA fibroblasts to oxidative stress. Treatment of FRDA and normal fibroblasts with A) hydrogen peroxide, and B) Fe^{3+}. Significant levels at each individual dose are represented by asterisks: *p<0.05 and **p<0.005 (Wong *et al.* 1999).

In order to find whether the fibroblasts derived from FRDA YAC transgenic mice show an oxidative stress as described *in vivo* (Al-Mahdawi et al. 2006), we have followed the same method as Wong *et al.* (1999) used to induce the oxidative stress in human fibroblasts. To do this experiment, we used all five types of mouse fibroblasts as mentioned earlier and the mean passage numbers for the WT, YG8 and YG22 mice were 7, 8 and 6, respectively. At first, the fibroblasts were grown in DMEM medium for 48 hours and then cells were treated with hydrogen peroxide continuously for six hours at the final concentrations of 0mM to 0.8mM. At the end of the treatment, cells were washed once with PBS and collected by centrifugation. Cell viability was determined by trypan-blue exclusion assay.

The treatment of mouse primary fibroblasts with hydrogen peroxide resulted in both YG8 and YG22 rescue mouse cells exhibiting hypersensitivity to oxidative stress compared to WT and transgenic mouse cells. At hydrogen peroxide concentrations of 0.15mM, 0.2mM and 0.3mM the viability in rescue mouse cells was significantly reduced to 36%, 29% and 18%, respectively (Figure 3.7). At 0.8mM, the highest concentration tested, all the cells died including the WT fibroblasts. The bias in sensitivity to oxidative stress in rescue mouse cells started at a hydrogen peroxide concentration of 0.15mM, where a significant difference ($p<0.001$) in response to induced oxidative stress was identified between the rescue and WT mouse cells. In contrast, the transgenic mouse cells showed the same pattern of sensitivity to hydrogen peroxide as the WT cells.

Although the WT mouse fibroblasts have shown reduced levels of *FXN* expression as compared to YG8 and YG22 rescue mouse fibroblasts, they tolerated the hydrogen peroxide induced oxidative stress well, suggesting that the human YG8 and YG22 transgenic *frataxin* may not be fully functional. It is also speculated that in the transgenic mouse cells which

have also shown resistance to oxidative stress, the sensitivity to oxidative stress with a single human *FXN* transgene is prevented by the endogenously expressing mouse frataxin gene.

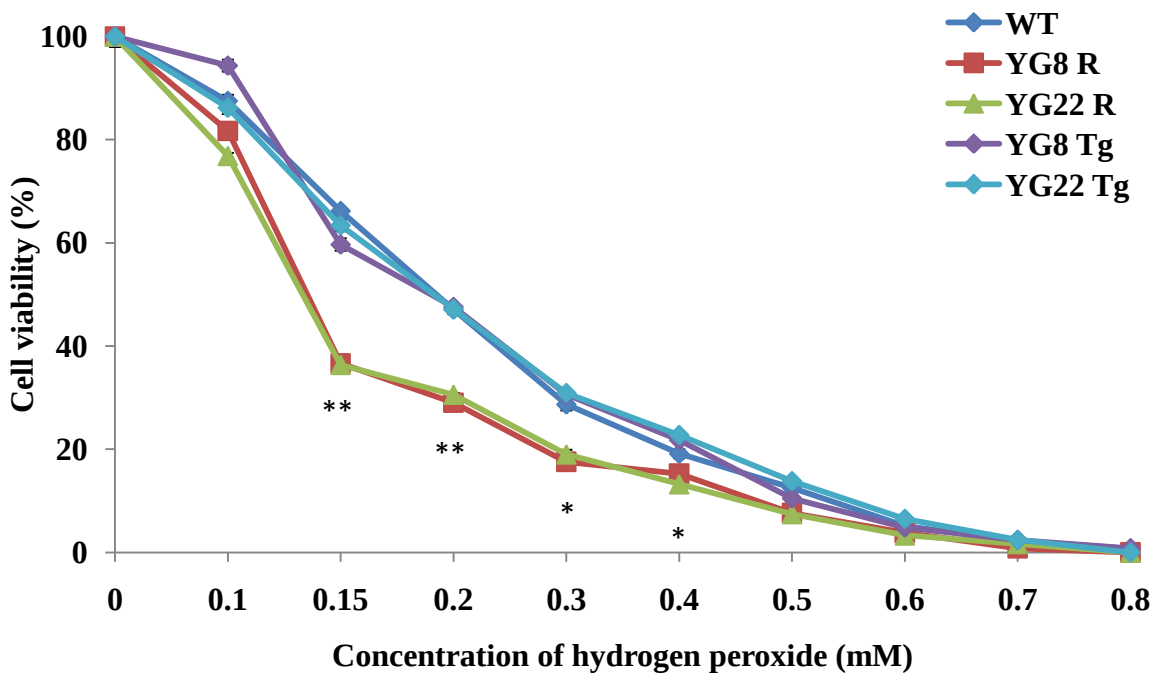

Figure 3.7 - Hydrogen peroxide induced oxidative stress in mouse fibroblasts as compared to WT mouse fibroblasts. Treatment of mouse primary fibroblasts resulted in increased sensitivity in both YG8 and YG22 rescue mice. The transgenic mouse of YG8 and YG22 show relatively less sensitivity to oxidative stress as seen in WT fibroblasts. The errors bars represent SEM (*p<0.05 and **p<0.01).

In summary, the cell lines we have established from the FRDA YAC transgenic mice have displayed an FRDA-associated phenotype of oxidative stress, suggesting that such cells are valuable resources to help in understanding the concealed pathogenesis of this disease. In future, it would also be important to quantify the oxidized proteins and MDA levels following treatment with hydrogen peroxide to support this hypothesis.

3.3.4 - Quantification of *FXN* mRNA in neural stem cells

In order to examine the levels of *FXN* expression in NSCs, we have performed the QRT-PCR analysis using *Gapdh* as an endogenous control. All values were normalized to WT *Fxn* expression and experiments were carried out in triplicate. Interestingly, initial determination of *FXN* expression in YG8 and YG22 NSCs revealed decreased mRNA levels of 49% and 71%, respectively compared to WT mouse cells (Figure 3.8A). Remarkably, when compared to YG8 rescue fibroblasts, the level of *FXN* expression in NSCs was considerably reduced to 30% ($p<0.001$) (Figure 3.8B). Although we do not know the exact explanation of why the NSCs have reduced levels of *FXN* expression compared to fibroblasts, it could be due to several factors. Firstly, it may be due to the expansion of GAA repeats during the establishment of NSCs, as reported previously for the conversion of fibroblasts to iPS cells (Ku *et al.* 2010) or secondly it could be due to the differential epigenetic changes between NSCs and fibroblasts. Therefore, future experiments need to be carried out to unravel any such changes in NSCs. However, the NSCs, in addition to primary fibroblasts, are an excellent model system for future FRDA pathogenesis and therapeutic studies.

Subsequently, the levels of *FXN* mRNA expression in fetal NSCs have also been determined by QRT-PCR and the values were expressed relative to *Gapdh* gene (endogenous control). These findings have revealed 79% reduced levels of *FXN* expression (not significant) in YG8 rescue mice compared to WT mice (Figure 3.8C). We then assessed the *FXN* levels between the adult and fetal NSCs and found that fetal NSCs showed approximately 2.4- and 2-fold increases in *FXN* expression in WT and YG8 rescue mice, respectively as compared to adult WT NSCs (Figure 3.8D). Similar to MEFs, fetal NSCs also showed an overall increased *FXN* expression compared to adult NSCs.

Overall, these results reveal an age-related, neural cell specific decline in *FXN* expression that may be relevant of FRDA pathology. Further, comparison of fetal and adult NSCs may reveal other useful information concerning the nature of FRDA disease progression. Thus, future studies of these two cell types will include comparison of GAA repeat instability, mitochondrial function and oxidative stress.

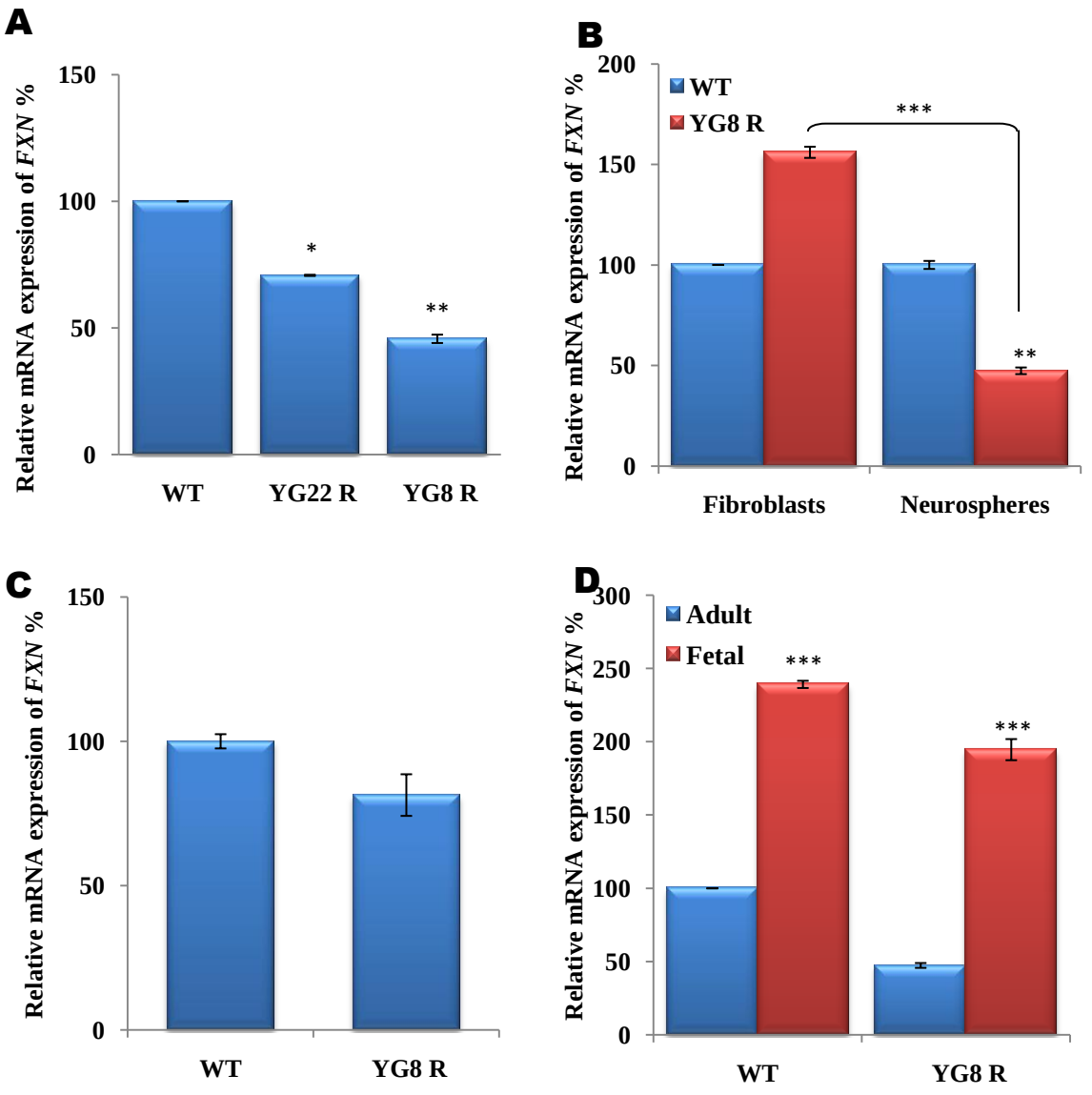

Figure 3.8 - *FXN* mRNA expression levels in mouse neural stem cells **A**) Quantification of *FXN* levels in adult NSCs, **B**) comparison of *FXN* levels between NSCs and fibroblasts of WT and YG8 rescue mice as determined by QRT-PCR. **C**) Quantification of *FXN* levels in fetal NSCs of WT and YG8 rescue mice, and **D**) comparison of *FXN* levels between adult and fetal NSCs. All quantifications were done in triplicates, and values were expressed relative to *Gapdh*. Error bars represent the SEM. (*p<0.05, ** p<0.01, ***p<0.001).

3.3.5 - Differentiation and immunofluorescence assay of NSCs

In order to determine whether the NSCs are capable of differentiating into neural cells, such as neurons, oligodendrocytes and astrocytes, we have induced differentiation as described earlier (section 2.9.5) (Figure 3.9). The differentiation was carried out in two ways, using either intact neurospheres or dissociated neurospheres as a starting cells. After differentiation, the resultant cells were subjected to immunofluorescence assays with cell specific antibodies: beta III-tubulin, Gal-C and GFAP primary antibodies for neurons, oligodendrocytes and astrocytes, respectively (Figure 3.10). For negative controls, a set of culture slides was incubated under similar conditions without the primary antibodies (Figure A.1 - see appendix).

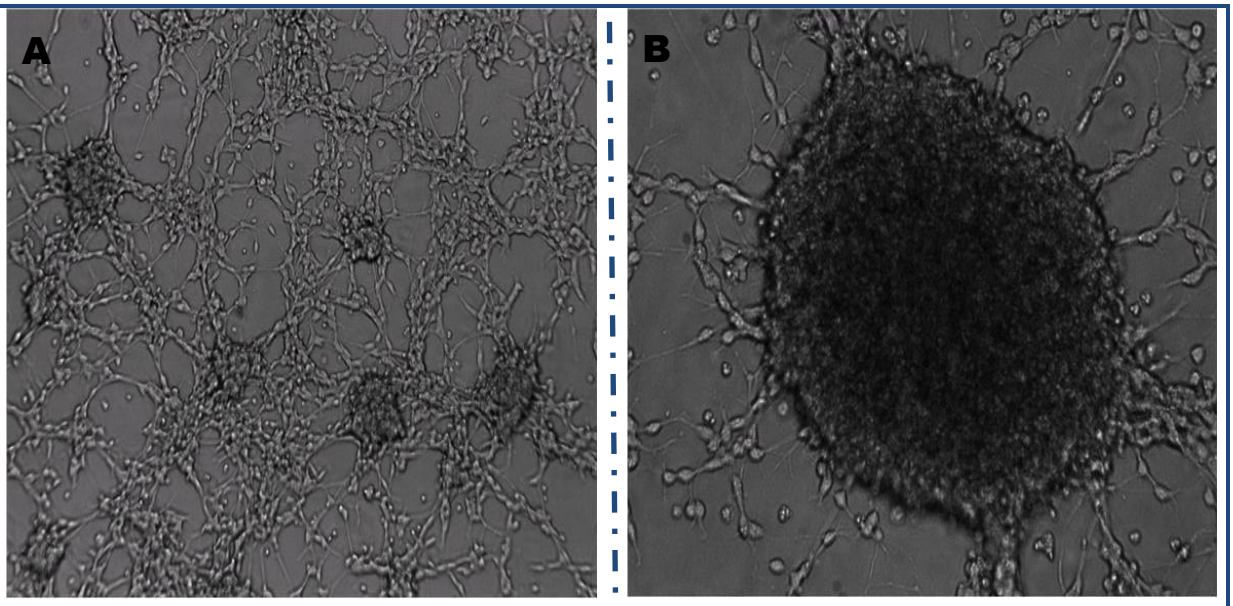

Figure 3.9 - Differentiation of mouse neural stem cells. The differentiation of NSCs was induced by incubating the cells in the NSC medium with differentiation supplements (Stem Cell Technologies). The early stages of the differentiation (**A** and **B**), where mixed neuronal cells are seen emerging from the neurospheres. Image magnifications are 10X and 40X for A and B, respectively.

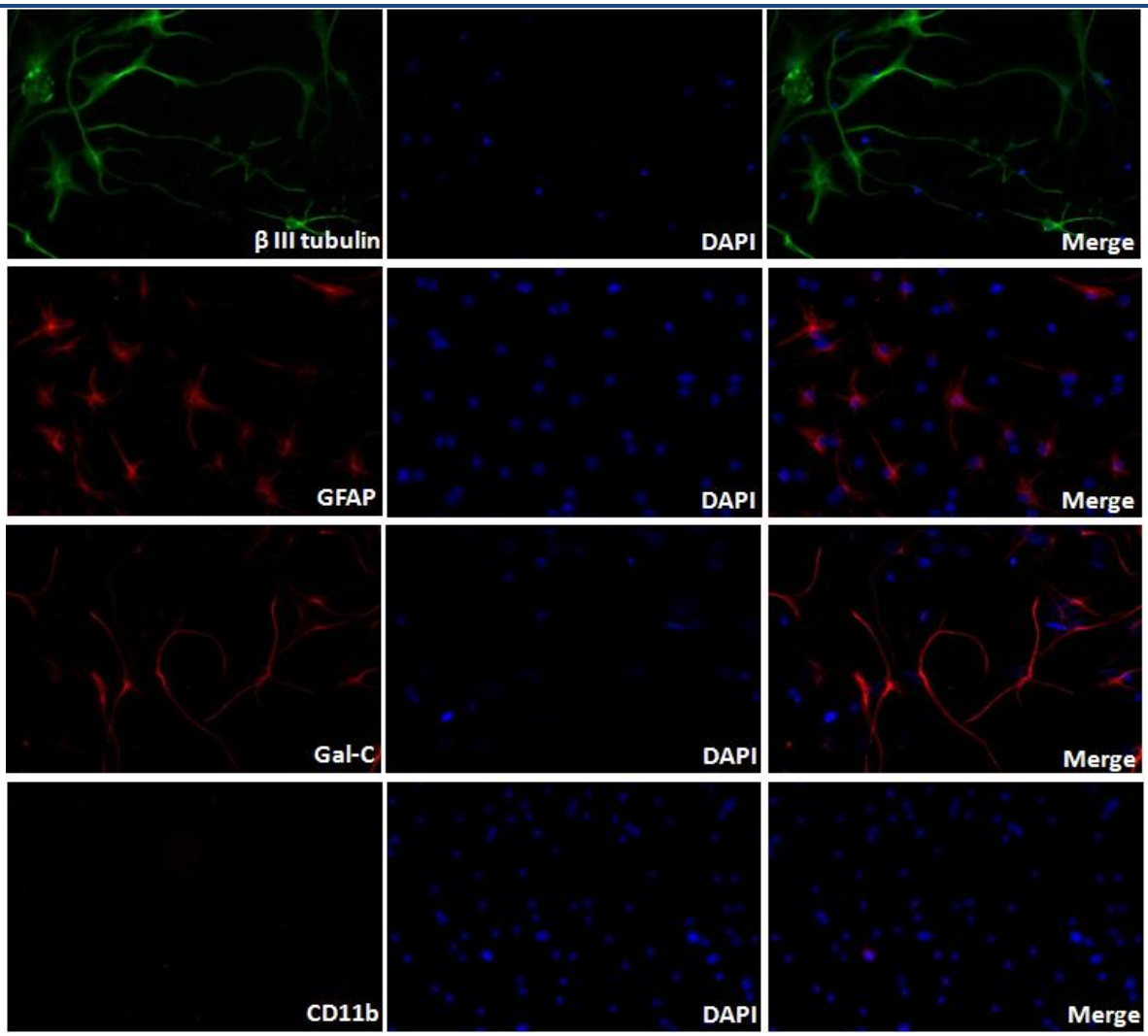

Figure 3.10 - Characterization of NSCs by immunofluorescence assay. NSCs were collected by centrifugation and dissociated by gently pipetting up and down several times until single cell suspension has been achieved followed by incubation with NSC dissociation medium for 48 hours on poly-D-lysine coated coverslips. After 48 hours in culture NSCs were positively stained with β III-tubulin (neuron), GFAP (astrocytes), and Gal-C (oligodendrocytes) and negatively stained with CD11b (microglia). The micrographs were taken at the magnification of 10X.

The immunofluorescence assays have clearly indicated the presence of neurons, oligodendrocytes and astrocytes in the differentiated NSCs. However, the labelling of differentiated NSCs with CD11b, a specific marker for microglia, was found to be absent in the differentiated NSCs, indicating that there are no microglia cells in NSCs (Figure 3.10), consistent with the previous results (Levison *et al.* 2003). These findings show that the neurospheres were able to differentiate into different neural and glial cell types and perhaps such cells can be isolated to serve as an essential source in understanding the pathogenesis of FRDA more precisely.

Recently, the existence of a fifth cell type in the CNS, called 'synantocyte', has been reported (Butt *et al.* 2005). Therefore, for future immunofluorescence assays, a synantocyte specific marker should be used to investigate the possible presence of this cell type differentiating from our NSCs.

Finally, in order to understand the molecular mechanism underlying FRDA pathogenesis, we are investigating ways to differentiate the NSCs to obtain pure cultures of differentiated neural cells. This will hopefully allow us to quantify *FXN* mRNA and protein from individual differentiated cell types rather than from an intact neurosphere.

Most importantly, thus far our investigations have mainly focused on determining the levels of *FXN* expression. However, for future experiments it is of primary importance to quantify frataxin protein levels from these cells, since such results may provide additional information. Furthermore, evaluating all of these results in comparison with Y47 mouse cells rather than WT cells, when they are available, should be of paramount importance.

Chapter 4 - Therapeutic approaches *in vitro*

4.1 - Therapeutic testing of DNA demethylating agents

4.1.1 - Introduction

Recognition of the role of epigenetics in human disease started with oncology, but it has now extended to other disciplines, such as neurodevelopment and neurodegenerative disorders like Alzheimer's disease, Parkinson's disease, Huntington's disease and FRDA. Epigenetic mechanisms, which involve DNA and histone modifications, result in the heritable silencing of genes without a change in their coding sequence. Chromatin had been viewed in the past as a static entity, which packaged DNA in a condensed form and maintained its integrity. A much more expanded view of epigenetics has recently emerged in which multiple mechanisms interact to collectively establish alternate states of chromatin structure, histone modification, associated protein composition, transcriptional activity, and in mammals, cytosine-5 DNA methylation at CpG dinucleotides (Ordway and Curran 2002; Felsenfeld and Groudine 2003; Freiman and Tjian 2003; Jaenisch and Bird 2003). Histone modifications regulate chromatin function either by altering the accessibility of DNA to different *trans*-acting factors, or by recruiting specific proteins that recognize a single or conformational set of modifications (Strahl and Allis 2000).

The methylation of DNA is a process shared by both eukaryotic and prokaryotic cells (Noyer-Weidner and Trautner 1993) and it serves as an epigenetic method of modulating gene expression. Methylation plays a role in genomic stability and carcinogenesis, and it offers a target for the treatment of malignancy (Colot and Rossignol 1999; Baylin and Herman 2000). The process of methylation is carried out by DNA methyltransferases (DNMT). These enzymes catalyze the covalent addition of a methyl group from a donor *S*-adenosylmethionine (SAM) to the 5 position of cytosine, predominantly within the CpG

dinucleotide (Momparler *et al.* 2000; Robertson 2001). Many lines of evidence demonstrate that the pattern of methylation can be stably inherited, through the action of a maintenance DNA methyltransferase (Holliday 1991; Holliday and Grigg 1993). Genetic analyses of the various DNMTs have established that DNA methylation is essential for vertebrate development. Loss of methylation causes apoptosis in embryos (Panning and Jaenisch 1996; Stancheva *et al.* 2001) and fibroblasts (Jackson-Grusby *et al.* 2001), but not in embryonic stem cells (Li *et al.* 1992; Lei *et al.* 1996; Albani *et al.* 2009) or in human cancer cells (Rhee *et al.* 2002).

4.1.2 - DNA methyltransferases (DNMTs)

The DNA methyltransferases (DNMTs) are enzymes which regulate DNA methylation and catalyse the transference of a methyl group from S-adenosyl-L-methionine (SAM) to a cytosine. In mammals, the DNMT family includes three functional proteins: DNMT1, DNMT3a and DNMT3b (Bestor 2000), the most abundant is the DNMT1 (Robertson 2001). DNMT1 preferentially methylates hemi-methylated DNA and is thus responsible for methylation during DNA replication (Pradhan *et al.* 1999). It plays a key role in imprinting and X-chromosome inactivation during embryogenesis (Beard *et al.* 1995). Other known functional methyltransferases are DNMT3a and DNMT3b, which are responsible for *de novo* methylation during embryogenesis (Okano *et al.* 1999). DNMT3a and DNMT3b have equal preference for hemi-methylated and non-methylated DNA, and so have been classified as *de novo* methyltransferases (Okano *et al.* 1998a).

Non-functional homologs of the methyltransferases have also been identified, such as TRDMT1 and DNMT3L. TRDMT1 (formally known as DNMT2) does not appear to have significant methyltransferase activity (Okano *et al.* 1998b; Yoder and Bestor 1998), but it was shown to methylate position 38 in aspartic acid tRNA and does not methylate DNA (Goll *et al.* 2006). Therefore, to reflect the different function of this enzyme, the name for this methyltransferase has been changed to TRDMT1 (tRNA aspartic acid methyltransferase 1) (TRDMT1 2006). TRDMT1 is the first RNA cytosine methyltransferase to be identified in a human. Similarly, DNMT3L has a mutated active site and is likely to be non-functional (Aapola *et al.* 2000). It has been speculated that it may antagonize functional methyltransferase activity (Robertson 2001).

4.1.3 - DNA methylation and transcriptional repression

Transcriptional repression is an essential mechanism in the precise control of gene expression. DNA methylation could control gene activity either at a local level through effects at a single promoter and enhancer, or through global mechanisms that influence many genes within an entire chromosome or genome (Kass *et al.* 1997). The most direct mechanism by which DNA methylation can interfere with transcription is to prevent the binding of basal transcriptional machinery or ubiquitous transcriptional factors that require contact with cytosine in the major groove of the double helix (Maldonado *et al.* 1999). Transcriptionally active chromatin is predominantly unmethylated and has high levels of acetylated histone tails.

Transcriptional repression takes place firstly by the deacetylation of histone tails followed by the methylation of CpG dinucleotides by one of the three human DNA methyltransferases (DNMT1, DNMT3a, and DNMT3b), resulting in DNA with high levels of CpG methylation (Razin 1998). CpG methylation induces chromatin remodelling and gene silencing through a transcription repressor complex that includes mSin3a and NURD complex with two HDAC enzymes, HDAC1 and HDAC2 (Zlatanova *et al.* 2000). The deacetylase activity, which accompanies the mSin3a complex renders the promoter of the gene inaccessible to transcription factors by deacetylating histone H3 and H4 (Razin 1998). DNA methylation-directed gene silencing can be alleviated by either inhibiting DNMT activity by DNA demethylating agents or by a specific inhibition of HDAC1 and/or HDAC2 activity by HDAC inhibitors.

4.1.4 - DNA demethylating agents

DNA demethylating agents are a class of substances that can inhibit methylation, resulting in expression of previously hypermethylated silenced genes. DNA demethylating agents are widely used in cancer therapy. Genes are silenced by a poorly understood process generally known as *de novo* DNA methylation. In many instances CpG islands that were originally unmethylated, with an associated active gene, become heavily methylated and inactivated, or silenced. Inhibitors of DNA methylation rapidly reactivate the expression of genes that have undergone epigenetic silencing, particularly if this silencing has occurred in a pathological situation. The prototype inhibitors, 5-azacytidine (5-aza-CR) and 5-aza-2'-deoxycytidine (5-aza-CdR), were initially developed as cytotoxic agents (Sorm *et al.* 1964), but it was subsequently discovered that they are powerful inhibitors of DNA methylation and induce gene expression and differentiation in cultured cells (Constantinides *et al.* 1977; Jones and Taylor 1980).

5-aza-CR and 5-aza-CdR are structurally related, but distinct, cytidine nucleoside analogs used clinically for the treatment of myelodysplastic syndromes (MDS) and acute myeloid leukemia (AML) (Saba 2007; Cataldo *et al.* 2009). Following cellular uptake and sequential phosphorylation, 5-aza-CR is incorporated into both RNA and DNA (Li *et al.* 1970; Glover and Leyland-Jones 1987; Stresemann *et al.* 2008), whereas 5-aza-CdR is incorporated solely into DNA (Stresemann *et al.* 2006)). Once incorporated, both compounds have related mechanisms of action, including depletion of DNMTs (Ghoshal *et al.* 2005; Stresemann *et al.* 2006), hypomethylation of DNA (Stresemann *et al.* 2006; Flotho *et al.* 2009), and induction of DNA damage (Kiziltepe *et al.* 2007; Palii *et al.* 2008).

In addition, other potential compounds have been developed that are able to reduce the level of DNA methylation, such as zebularine (Zhou *et al.* 2002), hydralazine (Rubin 2005; Sarzi-Puttini *et al.* 2005), procaine (Rubin 2005; Sarzi-Puttini *et al.* 2005), and an anti-sense oligonucleotide MG98 (Goffin and Eisenhauer 2002). However, the role of these compounds needs to be assessed where hypermethylation-induced gene silencing play a crucial role in disease pathology, like FRDA.

4.1.5 - DNA methylation and therapeutic testing in FRDA

Exactly how *FXN* transcriptional silencing is achieved in FRDA is not well understood, however recent evidence indicates that an epigenetic abnormality is an important underlying mechanism (Greene *et al.* 2007; Al-Mahdawi *et al.* 2008). In principle, changes in chromatin modifications in non-coding sequence could affect transcription by affecting RNA polymerase II elongation or by changing the accessibility of this region to regulatory factors important for transcription initiation (Lorincz *et al.* 2004). It has been reported that the first intron of many genes contains regulatory sequences which are important for gene expression (De Jaco *et al.* 2005; Lee *et al.* 2005; LeBlanc *et al.* 2006; Zhao *et al.* 2006). Therefore, in FRDA, the sequences adjacent to the *FXN* GAA repeat within intron 1 are likely to be affected by chromatin changes.

Greene *et al.* (2007) examined the DNA methylation status in intron 1 of the *FXN* gene in lymphoblast cells from unaffected individuals and individuals with FRDA. They reported that the region immediately upstream of GAA repeats showed increased DNA methylation in FRDA lymphoblast cells compared with cells derived from unaffected individuals. However, cultured cells are known to often develop non-physiological DNA methylation profiles. Furthermore, FRDA is a systemic disorder that is known to have differentially affected tissues and cell types. Therefore, Al-Mahdawi *et al.* (2008) investigated the DNA methylation status in brain and heart, two of the primary affected tissues in FRDA. Bisulfite sequence analysis of the *FXN* flanking GAA regions in these tissues revealed a shift in the FRDA DNA methylation profile, where upstream CpG sites were consistently hypermethylated and downstream CpG sites were hypomethylated (Figure 4.1) (Al-Mahdawi *et al.* 2008).

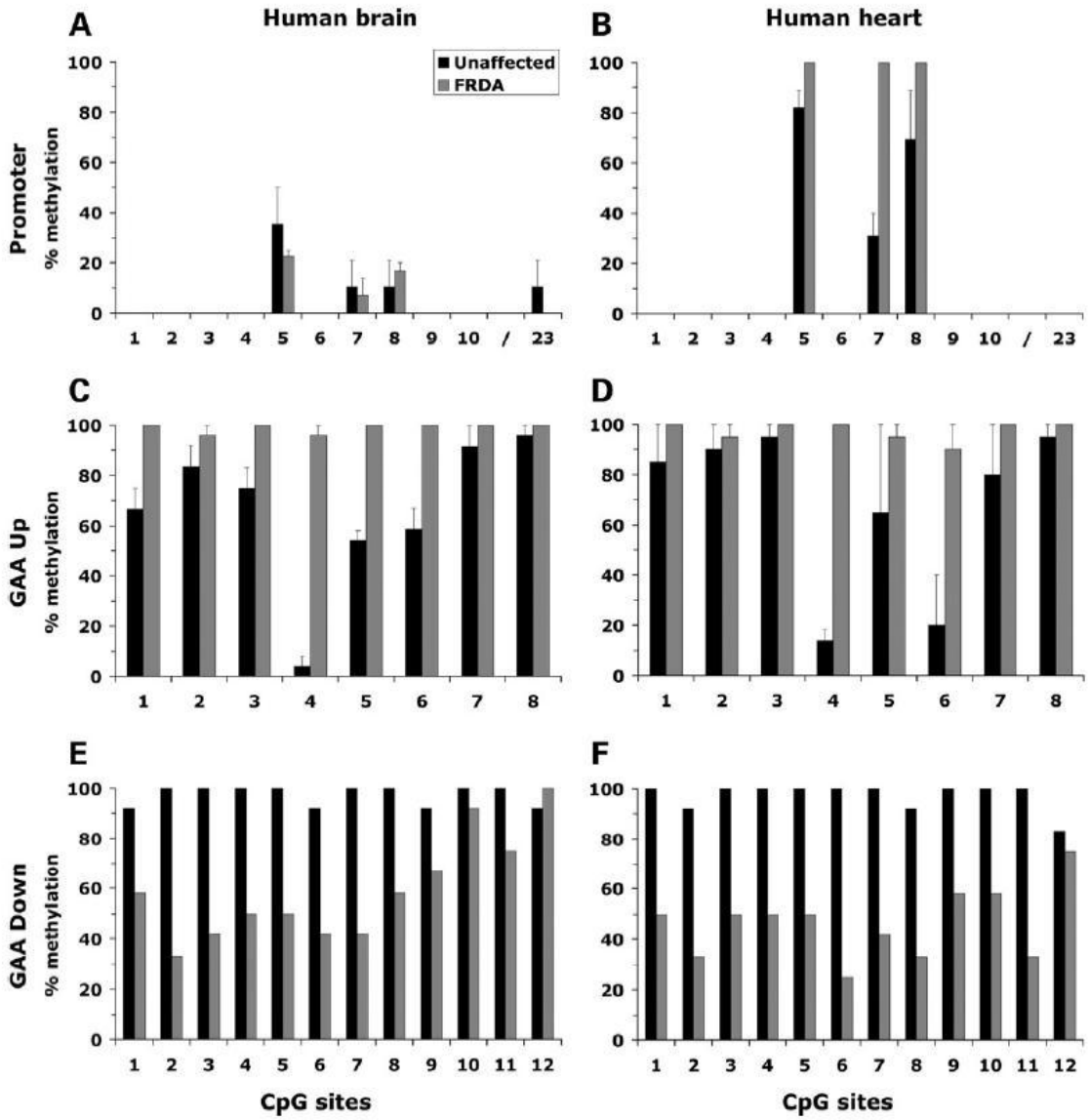

Figure 4.1 - DNA methylation analysis of the *FXN* promoter (**A** and **B**), upstream GAA (**C** and **D**) and downstream GAA (**E** and **F**) regions of human brain and heart tissues. In each case for the *FXN* promoter and upstream GAA regions the mean percentage (+/- SEM) of methylated CpG sites is shown as determined from the analysis of two FRDA patients and two unaffected individuals, with 7–12 independent cloned DNA sequences analysed for each (Al-Mahdawi *et al.* 2008).

Recently, De Biase *et al.* (2009) have reported that FRDA patients have high levels of FAST1 (frataxin antisense transcript 1) and heterochromatin protein 1 (HP1). In addition, they have also identified elevated levels of H3K9me3 and H3K27me3 at the +1 nucleosome region of *FXN* in primary fibroblasts from individuals with FRDA compared with normal individuals.

Nevertheless, so far there are no reports of using DNA demethylating agents as a therapeutic approach for FRDA to decrease the levels of DNA methylation and thereby increase *FXN* transcription. Therefore, we have investigated the efficacy of DNA demethylating agents 5-aza-CdR, zebularine and hydralazine on FRDA mouse and human primary fibroblasts. Following treatment with various DNA demethylating compounds, we have investigated *FXN* mRNA levels by QRT-PCR, and changes in DNA methylation by a methylscreen assay.

4.1.5.1 - Therapeutic testing of 5-aza-2'-deoxycytidine (5-aza-CdR)

The fact that many human diseases, including cancer, have an epigenetic aetiology has encouraged the development of a new therapeutic option that might be termed 'epigenetic therapy.' Many agents have been discovered that alter methylation patterns on DNA or the modification of histones, and several of these agents are currently being tested in clinical trials. 5-aza-2'-deoxycytidine (5-aza-CdR, or decitabine) has been tested in several Phase I, II and III clinical trials finding the most promising benefits in leukaemia patients (Jain *et al.* 2009), especially those affected by myelodysplastic syndrome (MDS) (Issa *et al.* 2004; Saba and Wijermans 2005; Mund *et al.* 2006; Saba 2007). For this reason 5-aza-CdR has been approved for the treatment of MDS showing excellent capability to reactivate the expression of several methylated genes.

As mentioned earlier, 5-aza-CdR only incorporates into DNA (Stresemann *et al.* 2006) in the place of cytosine into replicating DNA (Figure 4.2) (Egger *et al.* 2004). Therefore, it is active only in S-phase cells (Constantinides *et al.* 1977), where it serves as a powerful mechanism-based inhibitor of DNA methylation (Jones and Taylor 1980). DNMTs get trapped on DNA containing modified bases, resulting in the formation of heritably demethylated DNA (Jones and Taylor 1980; Zhou *et al.* 2002). Treatment of lymphoblastoid cells from FXS-patients with 5-aza-CdR alone (Chiurazzi *et al.* 1998) or in combination with HDAC inhibitors (Chiurazzi *et al.* 1999) efficiently reverse the *FMR1* promoter hypermethylation and restores mRNA and protein levels to baseline.

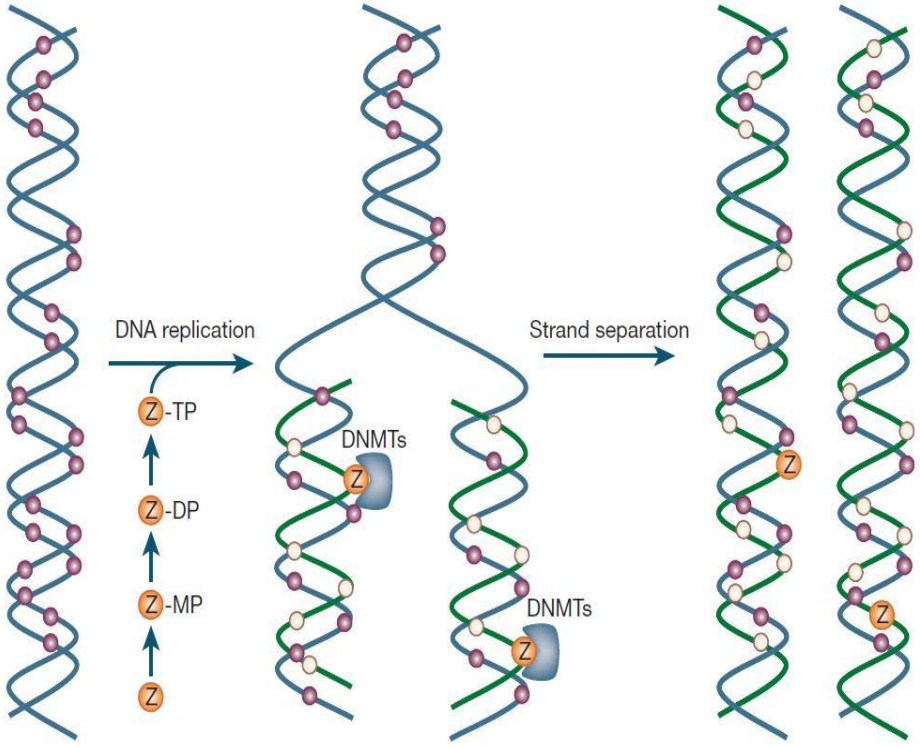

Figure 4.2 - Mechanism of action of nucleoside analogue inhibitors. Deoxynucleoside analogue, 5-aza-2'-deoxycytidine (depicted by Z) is converted into the triphosphate inside S-phase cells and are incorporated in place of cytosine into DNA (Egger *et al.* 2004).

In order to test the efficacy of the 5-aza-CdR in FRDA, we treated the mouse and human primary fibroblasts with 0.2µM and 1µM concentrations of 5-aza-CdR for 4 and 24 hours along with a mock treatment. After the treatment, *FXN* mRNA expression was quantified by QRT-PCR, and the level of DNA methylation for drug-treated and untreated samples was detected by a methylscreen assay. It is important to note that the methylscreen results presented in this thesis were centred on CpG site 4 in the upstream region of the GAA repeats where we find differential methylation between normal and FRDA patients' brain and heart tissues (Al-Mahdawi *et al.* 2008). In addition, in all our methylscreen results WT mice samples were excluded due to the absence of the human-specific CpG site 4 in such mice.

Interestingly, *FXN* mRNA levels increased with 5-aza-CdR compared to mock-treated sample. In particular, significantly increased levels were observed with 0.2µM of 5-aza-CdR after 24 hours (1.6-fold, $p<0.001$) (Figure 4.3A). These elevated levels were not observed with 1µM of drug at any time point (4 and 24h), suggesting that low concentrations of 5-aza-CdR are beneficial. Additionally, in order to find whether the endogenous control (*Gapdh*) that we are using is stable throughout the drug treatment we also quantified the *Gapdh* mRNA levels and found no difference (Figure A.2).

The methylscreen analysis revealed reduced DNA methylation levels in samples treated with 5-aza-CdR compared to vehicle-treated cells. Particularly, 0.2µM of 5-aza-CdR after 4 and 24 hours produced reduced levels of DNA methylation to 88% and 86%, respectively (Figure 4.3B). A 1µM (after 24 hours) concentration of 5-aza-CdR produced no significant effect compared to vehicle. At this concentration, trypan blue exclusion assay showed that the cell viability was reduced to 67% and 63% in WT and YG8 rescue mice, respectively, indicating that high concentration of this drug is toxic to the cells (Figure 4.4A). Interestingly, no differences in *FXN* expression were identified between vehicle and drug-treated WT cells, suggesting somewhat a specific effect of 5-aza-CdR.

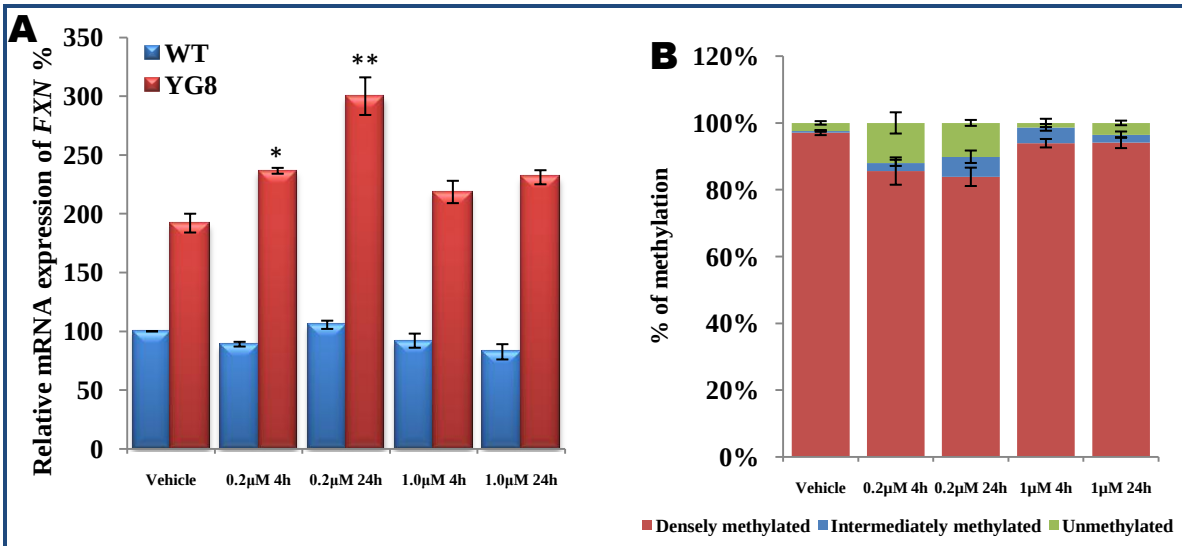

Figure 4.3 - The effect of 5-aza-CdR on mouse primary fibroblasts. **A)** Relative *FXN* mRNA expression, and **B)** change in methylation as determined by QRT-PCR and methylscreen assay, respectively following treatment with 5-aza-CdR. Each result displayed is the mean of two independent experiments. *FXN* mRNA expression was normalized to *Gapdh*. The values were expressed as a ratio to the corresponding untreated (vehicle) sample (* p<0.05, ** p<0.01, error bars ± 1 SEM).

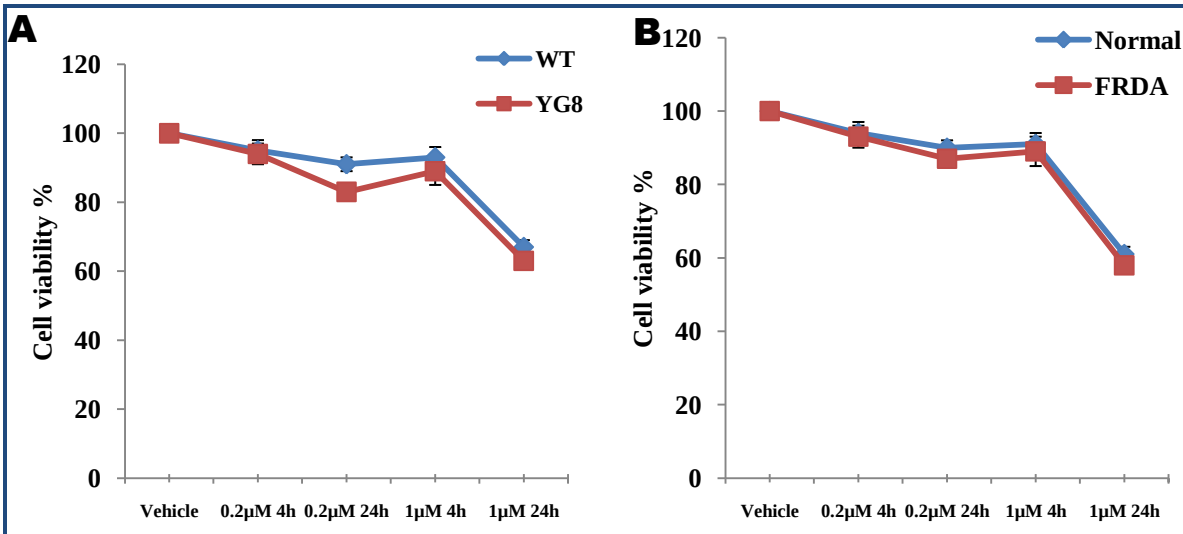

Figure 4.4 - Quantification of cell viability following treatment with 5-aza-CdR. The cell viability as determined by the trypan blue exclusion assay in **A)** mouse, and **B)** human primary fibroblasts (error bars ± 1 SEM).

Regarding human fibroblasts, obviously no apparent drug-induced effect in the level of *FXN* mRNA expression has been observed; rather reduced *FXN* expression was found in all samples treated with 5-aza-CdR. Particularly, statistically significantly reduced levels of *FXN* (50%) have been identified in cells treated with 1µM of 5-aza-CdR after 24 hours (Figure 4.5). The methylscreen assay clearly indicated reduced levels of DNA methylation in all samples treated with 5-aza-CdR in FRDA fibroblasts. Interestingly, the level of DNA methylation was reduced from 63% to 4.2% with 1µM of 5-aza-CdR after 24 hours and the unmethylated DNA levels rose from 2.1% to 72.4% in the FRDA fibroblasts (Figure 4.6B).

In the normal fibroblasts, a detrimental effect with 5-aza-CdR was observed, as increased levels of DNA methylation (at 0.2µM 4h) and reduced levels of unmethylated DNA were displayed at 0.2µM after 24 hours and 1µM after 4 hours time point (Figure 4.6A). In fact, no increases in *FXN* expression were found even when the DNA methylation was reduced to normal or below normal with 5-aza-CdR. Similar to murine fibroblasts, cell viability was also reduced with increasing concentrations of the drug. At 24 hours treatment with 1µM of 5-aza-CdR, an average, the cell viability was decreased to 61% and 58% in human normal and FRDA fibroblasts, respectively (Figure 4.4B).

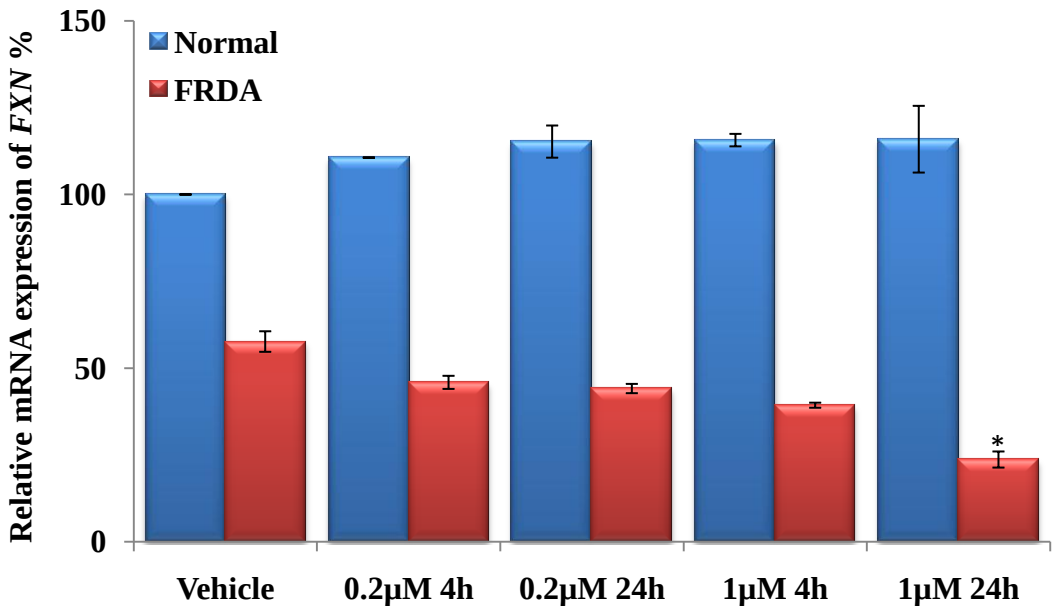

Figure 4.5 - Quantification of relative *FXN* mRNA expression in human normal and FRDA fibroblasts following treatment with 5-aza-CdR (*p<0.05, error bars ± 1 SEM).

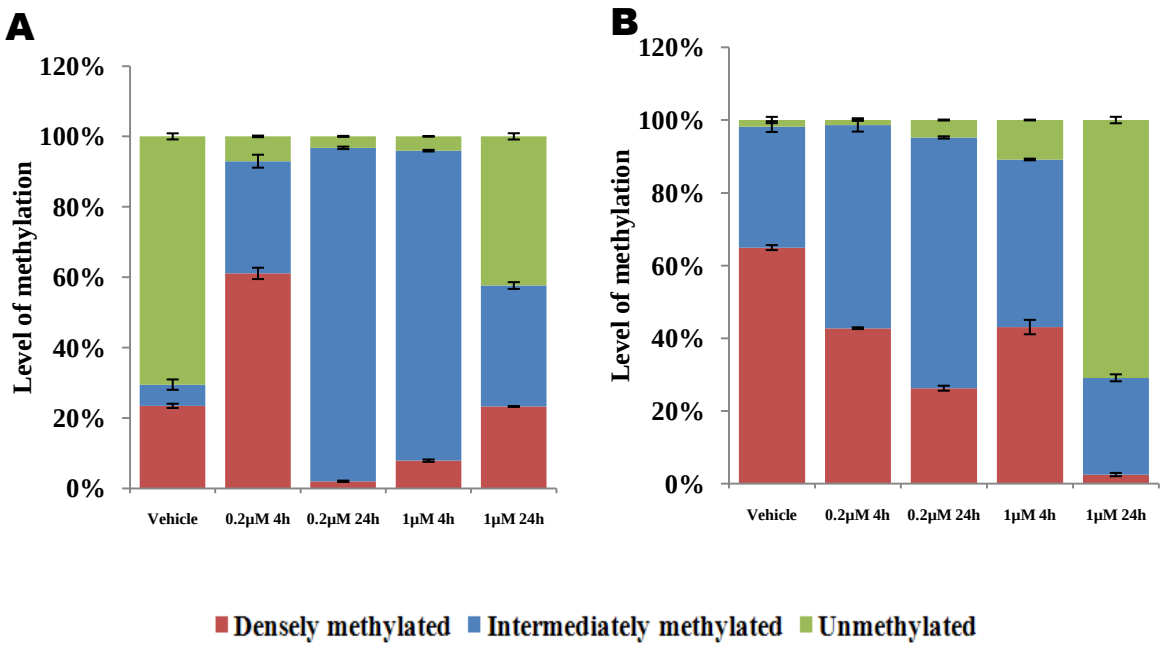

Figure 4.6 - The effect of 5-aza-CdR on DNA methylation. The analysis of changes in methylation as determined by methylscreen assay following treatment with increased concentrations of 5-aza-CdR (0-1µM) in **A)** normal, and **B)** FRDA primary fibroblasts (error bars ± 1 SEM).

4.1.5.2 - Therapeutic testing of zebularine

In the case of 5-aza-CdR, toxicity and instability under physiological conditions may complicate their use in the clinical trial. Therefore, we have considered using zebularine as another therapeutic approach to reduce DNA methylation in FRDA. Zebularine, a cytidine deaminase inhibitor, contains a 2-(1H)-pyrimidine ring, and has been recently demonstrated as an effective hypomethylating agent (Cheng *et al.* 2003). Unlike 5-aza-CdR, zebularine has the advantage of being stable in aqueous solutions and has half life of approximately 44 hours at 37°C in PBS at pH 1.0 and approximately 508 hours at pH 7.0 (Kelley *et al.* 1986). Furthermore, oral administration of zebularine has been shown to cause DNA demethylation and reactivation of a silenced and hypermethylated *p16* gene in human bladder tumour cells grown in nude mice (Cheng *et al.* 2004), suggesting that oral administration of the drug is possible.

In addition, it has been reported that zebularine was minimally toxic by both *in vitro* and *in vivo* studies (Cheng *et al.* 2003), indicating a safe administration of the drug. Particularly, recent evidence has shown that continuous administration of low doses of DNA demethylating agents are more efficient at reducing DNA methylation (Cheng *et al.* 2004), and this is possible with zebularine because of its low toxicity. Additionally, a combined study using 5-aza-cdR and zebularine has shown inhibition of DNA methylation and effective reactivation of silenced genes (Cheng *et al.* 2004). Therefore, in order to determine the efficacy of zebularine in FRDA, we have treated the human and mouse primary fibroblasts with 10µM and 100µM of zebularine for 24 and 48 hours, followed by *FXN* mRNA quantification, methylscreen analysis and cell viability assays.

Treatment of mouse fibroblasts with increased concentrations of zebularine (0-100µM) has revealed a significant increase in *FXN* expression in all samples treated with zebularine as compared to vehicle-treated cells. At a 10µM concentration, 24 and 48 hours after treatment *FXN* levels were increased to 1.3- and 1.4-fold compared to vehicle-treated cells, respectively (Figure 4.7A). Although a slight increase in *FXN* expression was seen in cells treated with 100µM of zebularine at both time points tested, no statistically significant difference was observed. The methylscreen analysis revealed that the DNA methylation levels were reduced from 92% to 54% with 100µM drug after 24 hours treatment (Figure 4.7B). Although slight fluctuations in DNA methylation were observed with 10µM of zebularine, no significant changes were detected. Also, no significant difference in DNA methylation was found at 48 hours treatment with 100µM of zebularine compared to vehicle-treated cells.

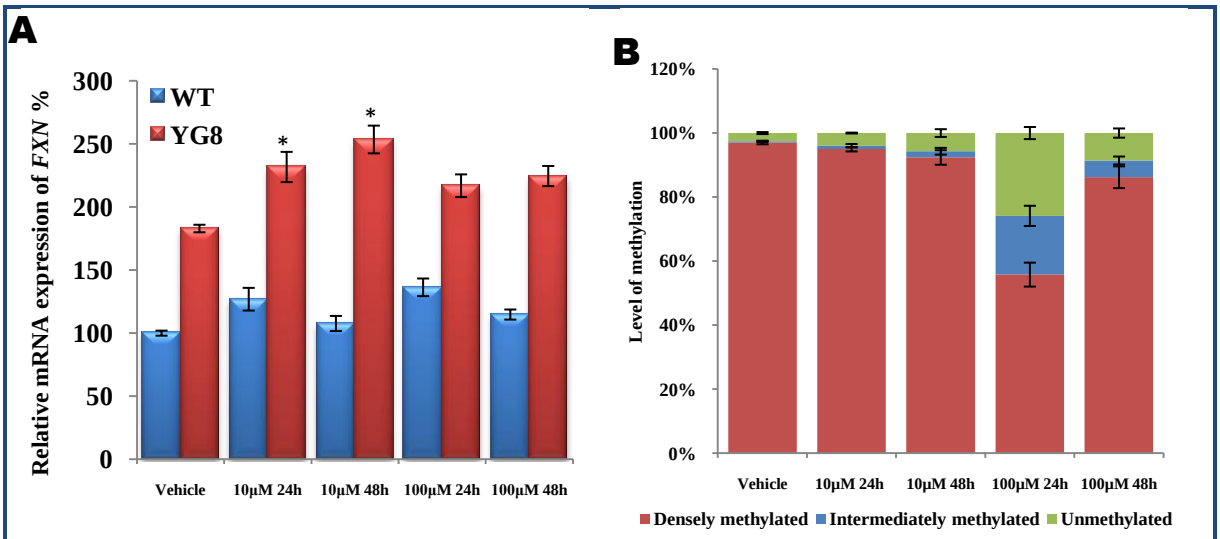

Figure 4.7 - The effect of zebularine on mouse primary fibroblasts following treatment with zebularine. **A)** Relative *FXN* mRNA expression, and **B)** change in methylation as determined by QRT-PCR and methylscreen assay, respectively. The *FXN* mRNA expression was normalized to *Gapdh*. The values were expressed as a ratio to the corresponding untreated sample (* $p<0.05$, error bars ± 1 SEM).

In order to assess whether zebularine is capable of upregulating *FXN* mRNA expression in human fibroblasts, QRT-PCR was performed with *GAPDH* as an internal control. Quantification of the *FXN* mRNA levels derived from the treated cell lines revealed reduced levels of *FXN* expression in FRDA fibroblasts. *FXN* mRNA was significantly downregulated in cells treated with 10µM zebularine for 24 hours and 100µM zebularine for 48 hours (Figure 4.8). In contrast, the normal fibroblasts showed an overall upregulation in *FXN* mRNA expression compared to vehicle-treated cells.

Regarding changes in DNA methylation as determined by methylscreen assay, the FRDA fibroblasts showed a reduction in DNA methylation to 42% and a 10-fold increase in the level of unmethylated DNA with 100µM of zebularine treatment for 48 hours as compared to vehicle-treated cells (Figure 4.9B). No changes were observed with other concentrations of the drug at any time points tested. In contrast, the level of DNA methylation increased in normal fibroblasts treated with 10µM of zebularine for 24 hours and 48 hours (Figure 4.9A). Similar to our previous findings with 5-aza-CdR, no correlation has been found between the level of DNA methylation and *FXN* expression at any concentration of drug and time point tested, suggesting that DNA methylation may be a secondary consequence in FRDA.

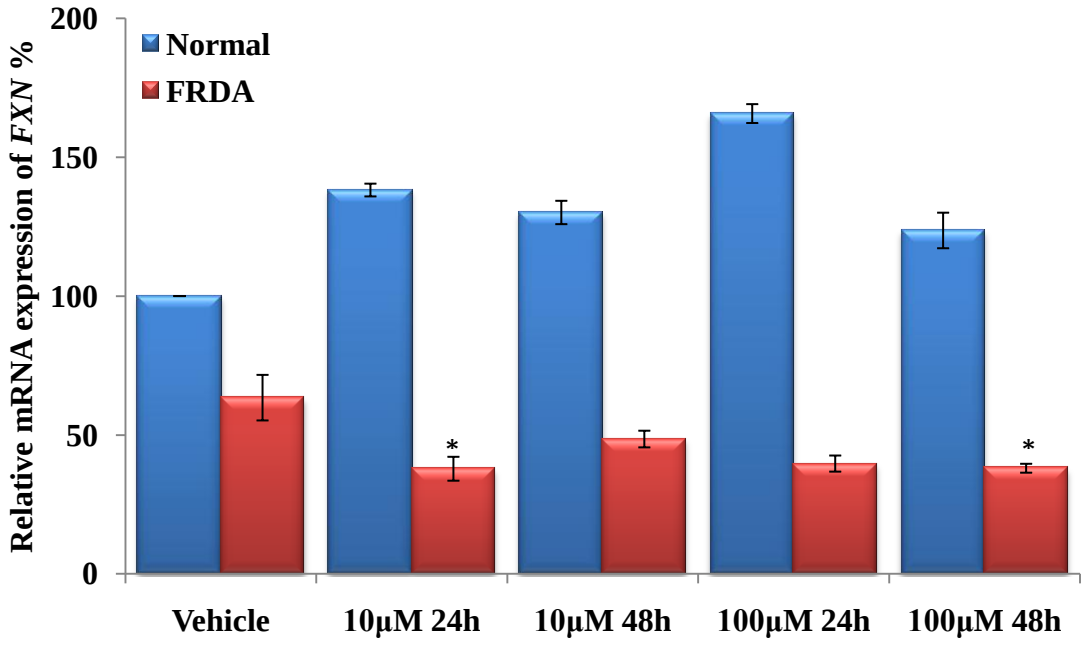

Figure 4.8 - Quantification of relative *FXN* mRNA expression in human normal and FRDA fibroblasts following treatment with zebularine (*p<0.05, error bars ± 1 SEM).

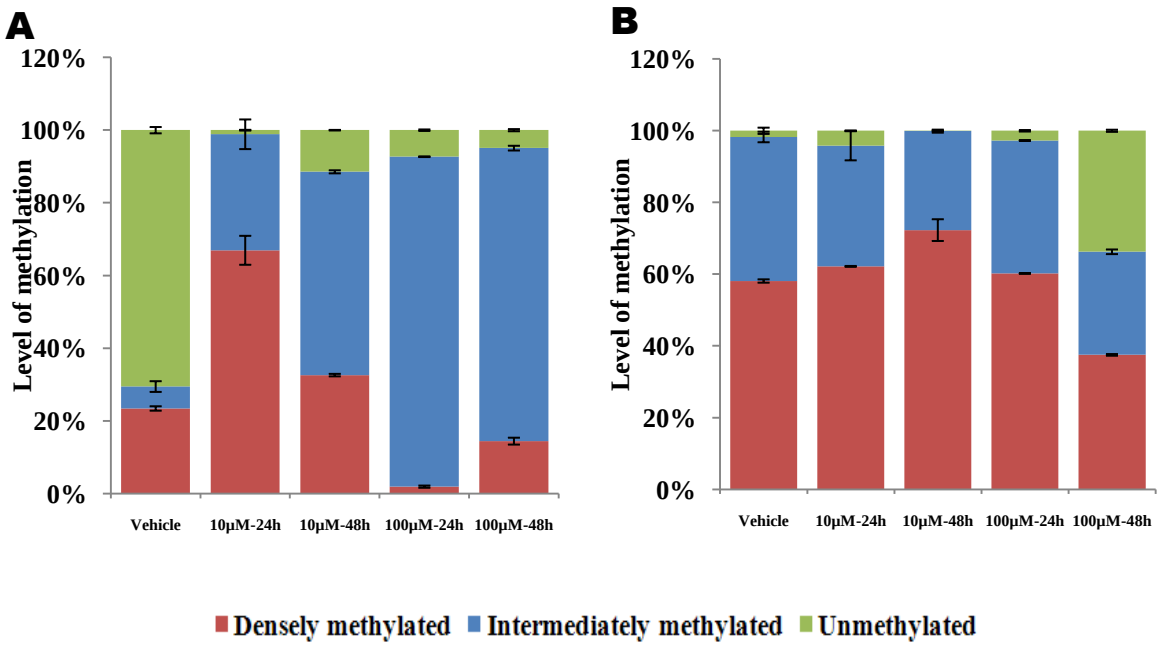

Figure 4.9 - The effect of zebularine on DNA methylation. The analysis of changes in methylation as determined by methylscreen assay following treatment with increased concentrations of zebularine (0-100µM) in **A)** normal, and **B)** FRDA primary fibroblasts (error bars ± 1 SEM).

4.1.5.3 - Therapeutic testing of hydralazine

Having obtained mixed results with the first two DNA demethylating agents, 5-aza-CdR and zebularine, we then tested the efficacy of hydralazine as a possible therapy for FRDA. Hydralazine (also known as apresoline) is a direct-acting smooth muscle relaxant used to treat hypertension by acting as a vasodilator (Herting and Hunter 1967; Klein *et al.* 2003). However, recently hydralazine has shown to inhibit the DNA methylation in various cancer cells, thereby reactivating the silenced genes (Segura-Pacheco *et al.* 2003; Zambrano *et al.* 2005; Segura-Pacheco *et al.* 2006). Phase I and II clinical trials with hydralazine in cervical cancers have evaluated its tolerability and efficacy upon administration (Zambrano *et al.* 2005; Candelaria *et al.* 2007). Despite many years of research, the mechanism of action of hydralazine has remained controversial, with uncertainty as to whether hydralazine directly inhibits DNMT enzymatic activity or not. However, recent findings have revealed reduced RNA methyltransferase 1 and 3a expression levels following treatment with hydralazine (Deng *et al.* 2003; Arce *et al.* 2006), suggesting that hydralazine does not directly inhibit DNA methyltransferase activities.

In this current study, we have evaluated the effect of hydralazine on reactivation of the *FXN* gene *in vitro*. To do this end, we have treated the human and mouse primary fibroblasts with 5µM and 10µM of hydralazine over a period of 48 and 72 hours, together with a mock treatment. After the treatment, cells were washed once with PBS and collected by centrifugation followed by QRT-PCR analysis. Cell viability was assessed by trypan blue assay. The passage numbers for all cell lines used in this study were ranged between 7 and 11.

The relative quantification of *FXN* by QRT-PCR following treatment with hydralazine in mouse fibroblasts revealed an overall increase in *FXN* expression in all samples treated with hydralazine as compared to mock-treated cells. Strikingly, significant upregulation of *FXN* has been observed in cells treated with 5µM of hydralazine for 48 hours (Figure 4.10A). Interestingly, hydralazine does not seem to have a positive effect on WT cells, as slightly reduced *FXN* mRNA expression levels were found in all drug-treated samples compared to vehicle-treated cells. Regarding methylscreen analysis, significant reduction in DNA methylation was identified in all samples treated with hydralazine. Particularly, cells treated with 5µM of hydralazine for 72 hours have displayed lowest level of methylation where it dropped from 87% to 22% ($p<0.001$) (Figure 4.10B).

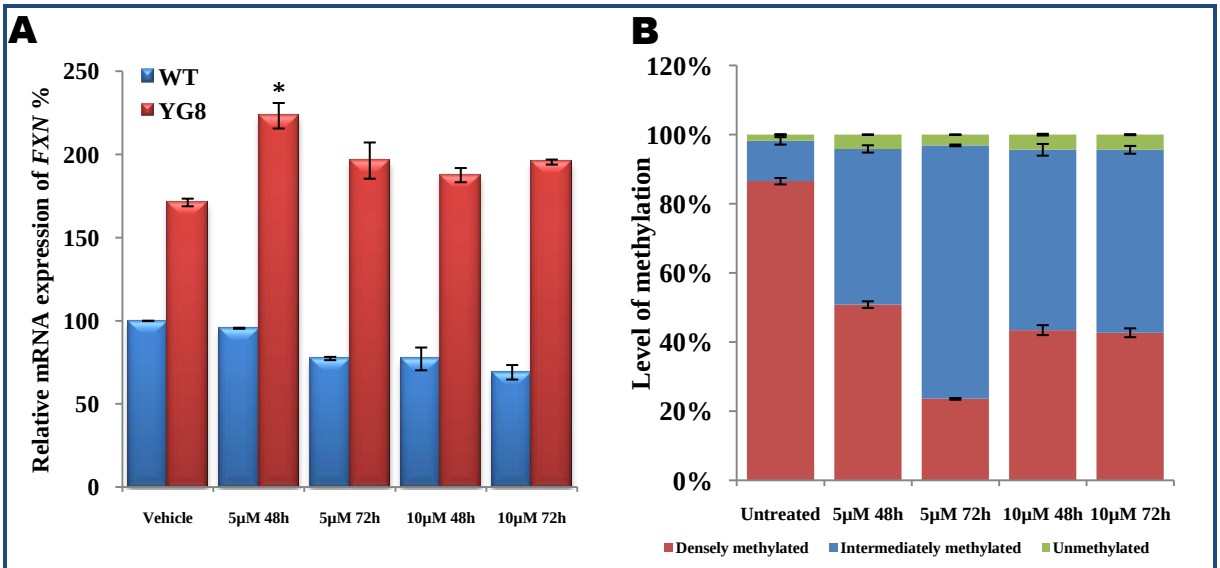

Figure 4.10 - Relative *FXN* mRNA and methylation changes following treatment with hydralazine in mouse primary fibroblasts. **A)** *FXN* mRNA expression in WT and YG8 mice, and **B)** level of methylation in YG8 mice as determined by QRT-PCR and methylscreen assay following treatment with hydralazine, respectively. Each result displayed is the mean of two independent experiments and mRNA expression was normalized to *Gapdh*. The values were expressed as a ratio to the corresponding untreated sample (* $p<0.05$, error bars ± 1 SEM).

Regarding the effect of hydralazine on *FXN* mRNA in human fibroblasts, after treatment the level of *FXN* mRNA was quantified and expressed relative to an internal control (*GAPDH*). After 48 hours there were decreases in *FXN* expression as seen previously with 5-aza-CdR and zebularine. However, by extending the time duration to 72 hours we detected increased *FXN* expression. Although there were slight fluctuations within each cell type, significantly elevated levels (1.6-fold, $p<0.05$) of *FXN* were observed in FRDA cells treated with 10µM of hydralazine for 72 hours (Figure 4.11). It is possible that a shorter duration of drug may be causing a negative effect on *FXN* expression, as at 5µM hydralazine, *FXN* levels dropped to 67% at 48 hours, whereas at 72 hours it was increased by approximately 127% compared to vehicle-treated sample. The same effect was also found with 10µM of hydralazine, where downregulation of *FXN* was identified at 48 hours (58%), whereas upregulation of *FXN* (159%) was displayed at 72 hours. In the normal fibroblasts, overall reduced levels of *FXN* (except at 5µM 48h) were produced, suggesting that there is a specific effect of hydralazine towards FRDA cells.

Regarding changes in DNA methylation, the methylscreen assay has revealed that normal fibroblasts have displayed increased DNA methylation in all cells treated with hydralazine compared to vehicle-treated cells (Figure 4.12A). In contrast, reduced methylation was displayed in FRDA fibroblasts treated with 5µM of hydralazine for 72 hours (dropping from 61% to 12%), but there was no change in DNA methylation with any other concentrations and time points tested (Figure 4.12B).

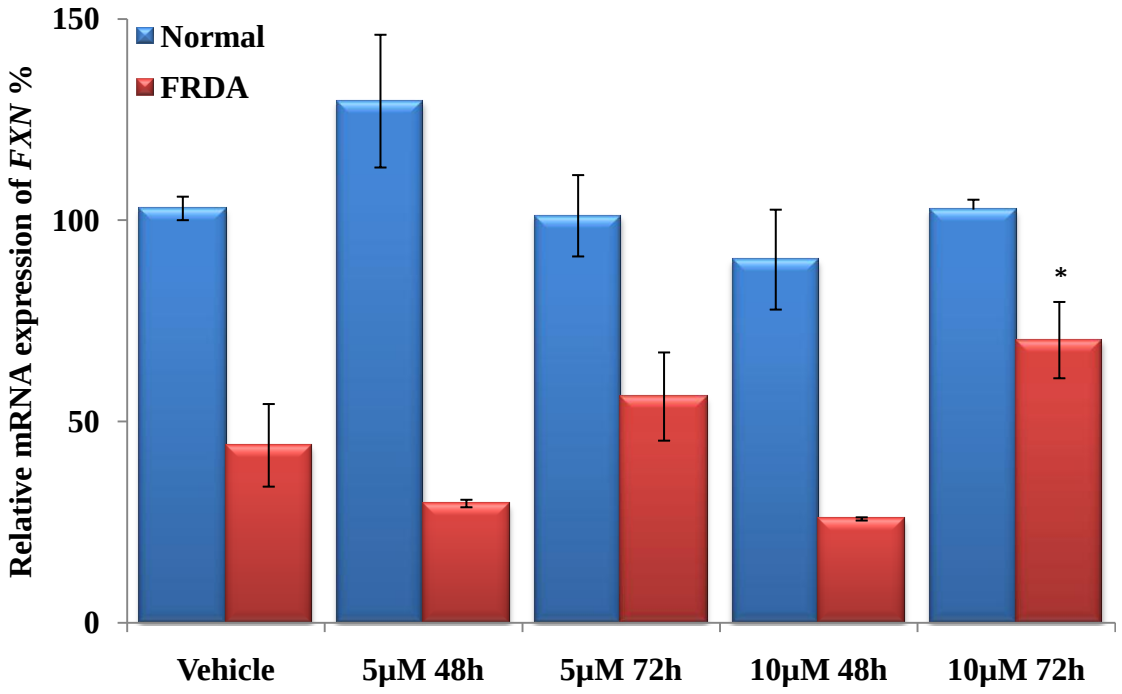

Figure 4.11 - Quantification of relative *FXN* mRNA expression in human normal and FRDA fibroblasts following treatment with hydralazine (*p<0.05, error bars ± 1 SE).

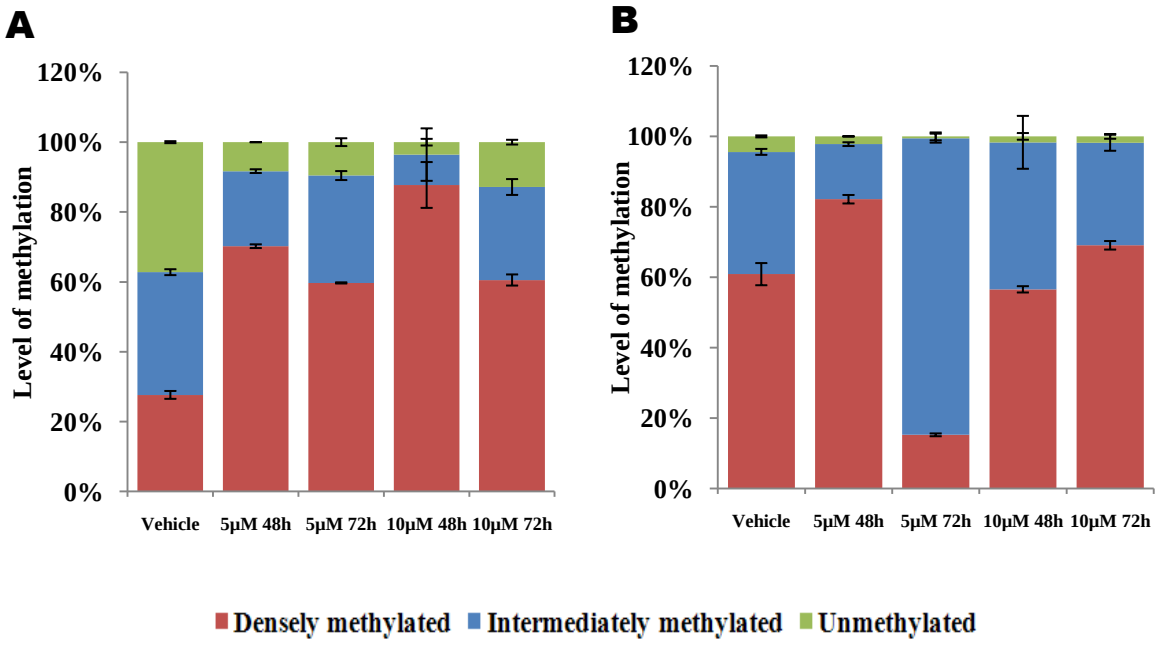

Figure 4.12 - The effect of hydralazine on DNA methylation. The analysis of changes in methylation as determined by methylscreen assay following treatment with increased concentrations of hydralazine (0-10µM) in **A)** normal, and **B)** FRDA primary fibroblasts.

4.1.6 - Discussion

Aberrant DNA methylation is recognized as a crucial component of the epigenetic mechanism underlying silencing of various genes. Despite many years of research, the precise mechanism of *FXN* gene silencing underlying FRDA is not yet understood, but it is currently generally accepted that FRDA may be caused by a heterochromatin-mediated silencing effect of the *FXN* gene (Festenstein 2006). This phenomenon is characterized by a differential DNA methylation profile accompanied by decreased histone acetylation and increased H3K9 trimethylation flanking the GAA repeat (Herman *et al.* 2006; Greene *et al.* 2007; Al-Mahdawi *et al.* 2008). The rapidly developing field of epigenetics has provided new hints as to what mechanisms might contribute to *FXN* gene silencing.

The mouse primary fibroblasts were derived from the FRDA YAC transgenic mouse (Al-Mahdawi *et al.* 2006), which exhibits epigenetic modifications similar to those observed in FRDA patients (Al-Mahdawi *et al.* 2008), suggesting that such mouse cells would be ideal for the *in vitro* investigation of epigenetic based therapeutic approaches for FRDA. Initial characterization of all cell lines which we used for these drug therapies were very well studied as mentioned before (Chapter 3).

The recently reported DNA demethylating agents, such as 5-aza-CdR, zebularine and hydralazine, alone or in combination with other compounds, have displayed encouraging results in cancer (Deng and Zhang 2009; Flotho *et al.* 2009; Wang *et al.* 2009) and in neurodegenerative disorders (Chiurazzi *et al.* 1999). Therefore, we have investigated such compounds in order to find their efficacy and tolerability as a possible therapy for FRDA.

The treatment of mouse cell lines with 5-aza-CdR has produced upregulation of *FXN* expression (at 0.2µM) in the YG8 rescue fibroblasts without any significant changes in the WT mice, suggesting a specific effect of this compound. The percentage of DNA methylation in YG8 rescue mice as studied by methylscreen assay revealed reduced levels of DNA methylation in a time dependent manner, especially with a low concentration of 0.2µM of 5-aza-CdR. Interestingly, we have found an inverse relationship between the level of methylation and *FXN* expression, where decreased DNA methylation levels were associated with increased *FXN* expression. This finding suggested that DNA demethylating agents are potential candidates for FRDA therapy.

Therefore, we further investigated the same compound in FRDA patient primary fibroblasts and found discrepant results between *FXN* expression levels and changes in DNA methylation. In contrast to the results found with mouse cell lines, reduced DNA methylation levels with 5-aza-CdR in the human FRDA fibroblasts did not seem to have promoted the *FXN* mRNA levels, rather *FXN* levels dropped. Although there is no obvious explanation for this effect, it could be due to many factors and one of the possibilities is that 5-aza-CdR may influence other genes which in turn perhaps negatively regulate the *FXN* expression. Recent microarray analysis on human fibroblasts following treatment with 5-aza-CdR has revealed 22 upregulated and 72 downregulated genes (Vallender and Lahn 2006). In view of this, we have quantified the endogenous control (*Gapdh*) mRNA levels of samples which shown highest *FXN* increase and found no difference in expression levels. Nevertheless, the observed DNA methylation at site 4 of GAA upstream region may be important for the correct transcription of *FXN.* Consequently, big changes in DNA methylation following treatment with 5-aza-CdR (like in the human FRDA cells) might negatively regulate the *FXN*

expression, as small changes in YG8 mice cells did not show such drastic effects on *FXN* expression. Furthermore, so far we have investigated the DNA methylation changes only centred around one out of three differentially methylated CpG sites in the upstream GAA repeat region of intron 1 (Al-Mahdawi *et al.* 2008). Therefore, in order to asses such compounds more precisely, future studies should be conducted taking more sites into the consideration from either side of the GAA repeats, such as downstream and upstream regions, along with the 5'-UTR region of the *FXN* gene.

Although we have found encouraging results with 5-aza-CdR, especially with mouse cell lines, in view of a prospective FRDA therapy in humans it has also been of paramount importance to select a stable and less toxic compounds. Therefore, we have subsequently investigated the ability of zebularine to inhibit the DNA methylation in the same way as 5-aza-CdR. The preliminary investigations and current knowledge on this compound has revealed zebularine is less toxic and more stable compound than 5-aza-CdR (Kelley *et al.* 1986). The treatment of varying concentrations of zebularine (0-100µM) in mouse cells significantly increased *FXN* expression, especially with low concentrations of zebularine (10µM) at both time-points tested. Interestingly, at these time-points no obvious changes in DNA methylation were identified. Although DNA methylation was reduced to 40% using 100µM of zebularine after 48 hours treatment, the *FXN* expression did not seem to be upregulated, which is in consistent with our previous findings with 5-aza-CdR. Subsequently, the effect of zebularine was investigated in human cells. Like 5-aza-CdR treatment, *FXN* expression was also reduced in FRDA fibroblasts treated with zebularine. It is important to note that, although the level of DNA methylation was reduced using 100µM of zebularine after 48 hours treatment, no apparent increase in *FXN* was reported. Indeed, it was

significantly reduced compared to vehicle-treated controls. Furthermore, surplus levels of DNA methylation (66%) induced by 10µM of zebularine at 24 hours treatment in normal fibroblasts did not seem to have any effect on *FXN* expression, indicating that *FXN* expression is primarily dependent on GAA repeat expansions not on DNA methylation. These findings support the hypothesis that DNA methylation and *FXN* expression are two independent mechanisms and perhaps DNA methylation is a secondary consequence of the disease.

Regarding hydralazine, we found interesting results in both mouse and human cell lines. In YG8 rescue mice cells *FXN* expression was significantly increased when the level of DNA methylation reduced (5µM at 48h). However, when the DNA methylation was reduced further, a slight drop in *FXN* was reported. In WT cells the *FXN* expression was reduced with hydralazine, indicating a specific effect of this compound. In human cell lines, hydralazine seems to have a positive effect, as *FXN* levels were elevated with hydralazine in a time-dependent manner. In FRDA fibroblasts, a significant 1.6-fold increase in *FXN* expression was achieved after 72 hours of treatment, although this result did not correspond with any DNA methylation change. Therefore, it would be interesting to also examine the effect of 5-aza-CdR and zebularine by conducting future experiments for more than 48 hours.

In summary, mixed results were seen in mouse and human *FXN* expression profiles following treatment with three DNA demethylating agents. Overall, increased *FXN* expression was seen in mouse cells (YG8) and decreased *FXN* levels were found in human cells (FRDA). This is possibly due to the tight regulation of *FXN* to ensure low levels of *FXN* transcription in human cells, as over expression of *FXN* has been suggested to be toxic (Fleming *et al.* 2005). It is possible that perhaps such mechanisms may not be available or

not strongly regulated in mouse cells, whereby slight activation of this transcription machinery may provoke more *FXN* expression. However, findings using frataxin over-expressing Y47 (Pook *et al.* 2001) and TgFxn mice (Miranda *et al.* 2004) indicate that increased *FXN* levels are not associated with any deleterious effects on phenotype. Therefore, the mechanism underlying these mouse and human cell line discrepancies should be assessed in future studies by taking more CpG sites into the consideration. Most importantly, fibroblasts from Y47 mice should be considered as an experimental control for future therapeutic testing of YG8 fibroblasts.

Finally, sequence specific DNA demethylating agents, such as the oligonucleotide antisense inhibitor MG98 (Stewart *et al.* 2003; Winquist *et al.* 2006; Amato 2007; Plummer *et al.* 2009), may be useful for future therapeutic approaches in reducing specific DNA methylation. In addition, naturally available green tea and their derivatives have also shown beneficial effects in reducing the DNA methylation in various cancers (Kato *et al.* 2008; Dou 2009; Yuasa *et al.* 2009; Pandey *et al.* 2010). Therefore, considering these compounds, which are already in clinical trials, for future FRDA therapy may be beneficial.

4.2 - Therapeutic testing of GAA interacting compounds

4.2.1 - Introduction

Recent advances in understanding of the molecular mechanisms involved in FRDA allow the development of a set of new potential therapeutic interventions aimed at ameliorating secondary disease effects such as oxidative stress and mitochondrial iron accumulation. Thus, FRDA preclinical and clinical trials using antioxidants and iron chelators have demonstrated some limited success (Schulz *et al.* 2009). At the same time, other studies have demonstrated that DNA binding compounds are effective at increasing transcription through GAA repeats. Therefore, more effective and specific overall therapy may be achieved by targeting the immediate effects of the GAA repeat expansion mutation.

Although the mechanisms by which the GAA repeat expansion leads to decreased levels of frataxin expression are currently not known, two distinct, but inter-related hypotheses have been put forward. In one model, it has been suggested that the GAA repeat expansion may adopt abnormal non-B DNA structures called 'triplexes (or sticky DNA)' or DNA•RNA hybrid structures that directly impede with *FXN* gene transcription elongation (Grabczyk *et al.* 2007; Wells 2008). In the other model, there is evidence originally from position effect variegation (PEV) studies in transgenic mice that GAA repeat expansions somehow produce a heterochromatin-mediated gene silencing effect (Saveliev *et al.* 2003). Therefore, compounds which specifically target these consequences in FRDA would be considered beneficial in order to find a potential therapy.

4.2.2 - Targeting the gene in FRDA

The accumulation of recent findings for a potential therapy of FRDA has revealed that certain compounds which specifically target the GAA repeats are capable of increasing transcription through GAA repeats. In addition, recent studies have revealed that some DNA binding compounds may displace proteins that promote heterochromatin formation, such as HP1, thereby resulting in a more open, transcriptionally active form of the *FXN* gene (reviewed by (Hebert 2008)). Although *FXN* transcription has been increased by recently described small molecules, such as hemin (Sarsero *et al.* 2003), cisplatin (Ghazizadeh 2003), 3-nitropropionic acid (Turano *et al.* 2003) and erythropoietin (Sturm *et al.* 2005), it has been postulated that this increase in *FXN* was due to the specific transcription factor activation, but not a direct consequence of increasing transcription through GAA repeats or inhibiting HDAC activity (Hebert 2008).

Therefore, in order to find specific therapeutic interventions for FRDA, Gottesfeld and colleagues (2006) have shown that polyamides that bind specifically to GAA repeats increased the *FXN* mRNA and protein levels in an FRDA lymphoblastoid cell lines. These compounds were also shown to reverse the sticky DNA conformation adopted by GAA·TTC repeats in supercoiled plasmid DNA (Burnett *et al.* 2006). Importantly, microarray analysis has revealed that the polyamides had a limited effect on global gene expression, suggesting more specific and safe administration of the drug. Herbert and colleagues (2006) have recently reported the results of a rational screen of small molecule DNA ligands to alleviate GAA·TTC repeat-mediated gene silencing. Although some compounds have exhibited cytotoxic nature, the other compounds, such as DAPI, Hoeschst 33258, distamycin and

pentamidine, were found more effective in upregulating the *FXN* expression in $(GAA{\cdot}TTC)^{148}$-EGFP cell line (Grant *et al.* 2006).

Subsequently, other compounds were also screened in order to find their specificity and potentiality towards an effective therapeutic approach for FRDA. As a result two classes of polyamides were identified for gene targeting, such as hairpin polyamides and linear β-alanine linked polyamides. Among them, β-linked polyamides have shown effective targeting of GAA·TTC repeats whereby enabling binding to different homopurine sequences *in vitro* (Janssen *et al.* 2000a; Urbach and Dervan 2001). In addition, these compounds also shown to interact with GAGAA repeats in *Drosophila* satellite DNA both *in vitro* and in *Drosophila* embryos (Janssen *et al.* 2000a). It has been reported that this satellite DNA-specific molecule induces chromatin opening and reverses heterochromatin-mediated PEV gene silencing when administered to *Drosophila* embryos (Janssen *et al.* 2000a; Janssen *et al.* 2000b), suggesting that similar molecules targeting GAA·TTC DNA could reverse *FXN* gene silencing.

In this chapter we have investigated the efficacy and tolerability of two GAA interacting compounds, DB221 and pentamidine. DB221 is a novel compound with unknown efficacy and toxicity. The advantage of pentamidine is that it has already been approved by FDA to help prevent pneumonia in AIDS patients.

4.2.2.1 - Therapeutic testing of DB221

DB221 is a novel, aromatic amidine and a specific DNA minor groove-binding compound (Figure 4.13). This compound was synthesized and kindly provided to us by Prof. David W. Boykin, Georgia State University, USA. Although little is known about this compound, preliminary investigation of DB221 on FRDA using a GAA_{148}-GFP construct has revealed a 28-fold increase in GFP protein expression (M.D. Herbert, personal communication), suggesting that it may be an effective compound for FRDA therapy. However, the exact mechanism by which this compound increases transcription is still unknown, and awaits further characterization. In addition, it has also been proposed that DB221 might disrupt the triplex structures formed as a result of large GAA repeat expansions and thereby reverse the heterochromatin-mediated gene silencing.

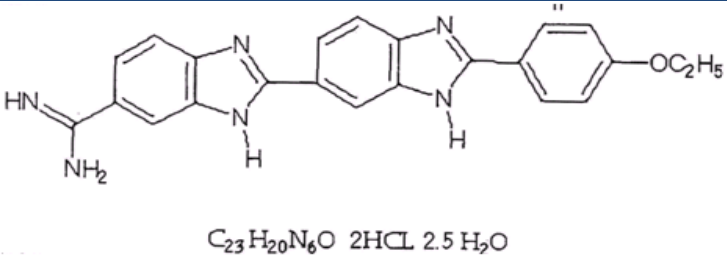

Figure 4.13 - The chemical structure of DB221.

In order to investigate the effect of DB221, WT and YG8 rescue mouse fibroblasts, and human normal and FRDA primary fibroblasts were treated with various concentrations of DB221 (0-5µM) for 4 and 24 hours. After the specified time, cells were collected by trypsinization and cell viability was determined by a trypan blue exclusion assay. Then, total RNA was extracted and converted into cDNA, followed by the quantification of *FXN* expression levels by QRT-PCR. In addition, changes in DNA methylation following treatment with DB221 were determined by methylscreen assay.

Quantification of *FXN* mRNA by QRT-PCR revealed a considerable increase in *FXN* expression levels in cells treated with DB221 (Figure 4.14). Especially, treatment of YG8 rescue fibroblasts with 1µM of DB221 for a period of 4 and 24 hours showed significant ($p<0.001$) upregulation in *FXN* expression of 1.9- and 1.6-fold compared to vehicle, respectively. However, somewhat surprisingly, downregulation of *FXN* was found with high concentration of DB221 in a time dependent manner. Thus, 5µM of DB221 decreased the *FXN* expression to 70% and 40% after 4 and 24 hours treatment compared to mock-treated cells, respectively. The methylscreen assay revealed significantly reduced levels of DNA methylation with DB221 treatment. At 1µM of DB221, the level of DNA methylation was reduced to 80% and 20% after 4 and 24 hours treatment compared to vehicle, respectively. No difference in methylation was detected with 5µM of DB221 at any time point tested (data not shown).

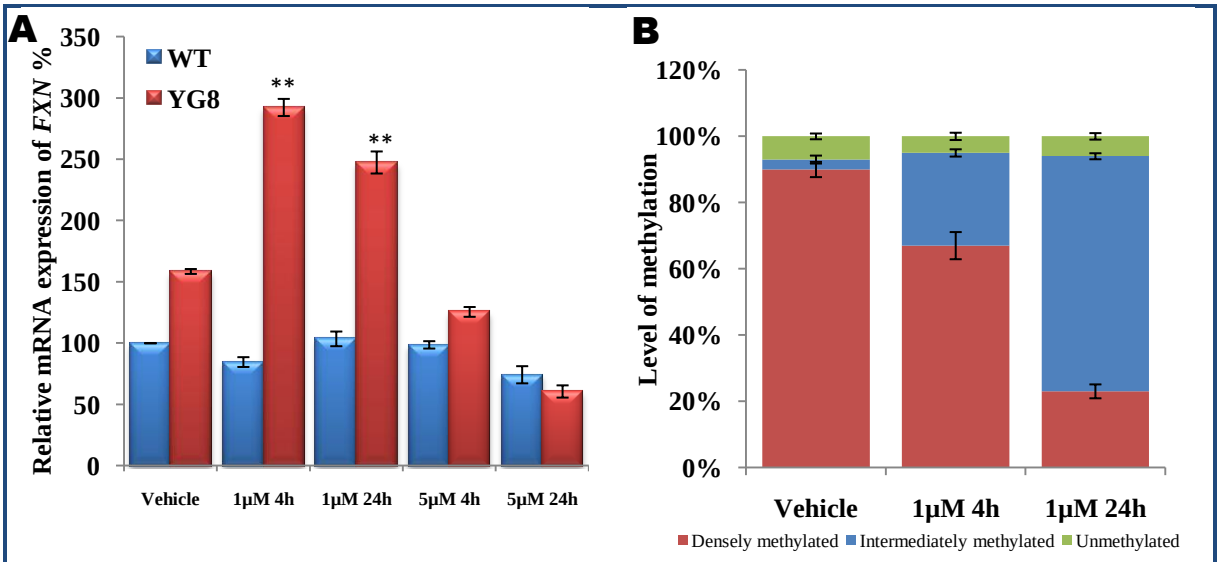

Figure 4.14 - Relative *FXN* mRNA and methylation levels following treatment with DB221 in mouse primary fibroblasts. **A)** *FXN* mRNA expression, and **B)** level of methylation as determined by QRT-PCR following treatment with DB221. Each result displayed is the mean of two independent experiments and mRNA expression was normalized to *Gapdh*. (** $p<0.01$, error bars ± 1 SEM).

Interestingly, no difference in *FXN* expression was identified in the WT mice fibroblasts at any concentration and time-point tested, suggesting a specific effect of DB221 in YG8, the GAA repeat expansion-containing rescue mice.

Regarding the human fibroblasts, we found encouraging results with DB221 (Figure 4.15). The QRT-PCR analysis following treatment with DB221 revealed increased *FXN* expression in all samples treated with DB221 in FRDA fibroblasts. The *FXN* expression was remarkably increased in cells treated with 1µM of DB221, where 2.2- and 2.9-fold increases in *FXN* expression were identified after 4 and 24 hours treatment compared to vehicle-treated cells, respectively (Figure 4.15).

With 5µM of DB221, lesser 1.7- and 1.2-fold increases in *FXN* expression were reported at 4 and 24 hours after treatment, respectively. Although it was unexpected, DB221 also showed an immense increase in *FXN* expression in human normal fibroblasts, especially 24 hours after treatment with 1µM and 5µM of DB221. It is possible that this is due to the presence of small GAA repeats (<9) in the normal fibroblasts compared to WT mice where there are no GAA repeats.

The methylscreen analysis demonstrated that DB221 was able to reduce the level of DNA methylation, especially in FRDA fibroblasts (Figure 4.16). At 4 and 24 hours treatment with 1µM of DB221, the level of DNA methylation was reduced from 53% (vehicle) to 5.5% and 0.5%, respectively. A similar effect was also found with 5µM of DB221, where the level of methylation was reduced to 1.5% and 16.4% at 4 and 24 hours after treatment (Figure 4.16).

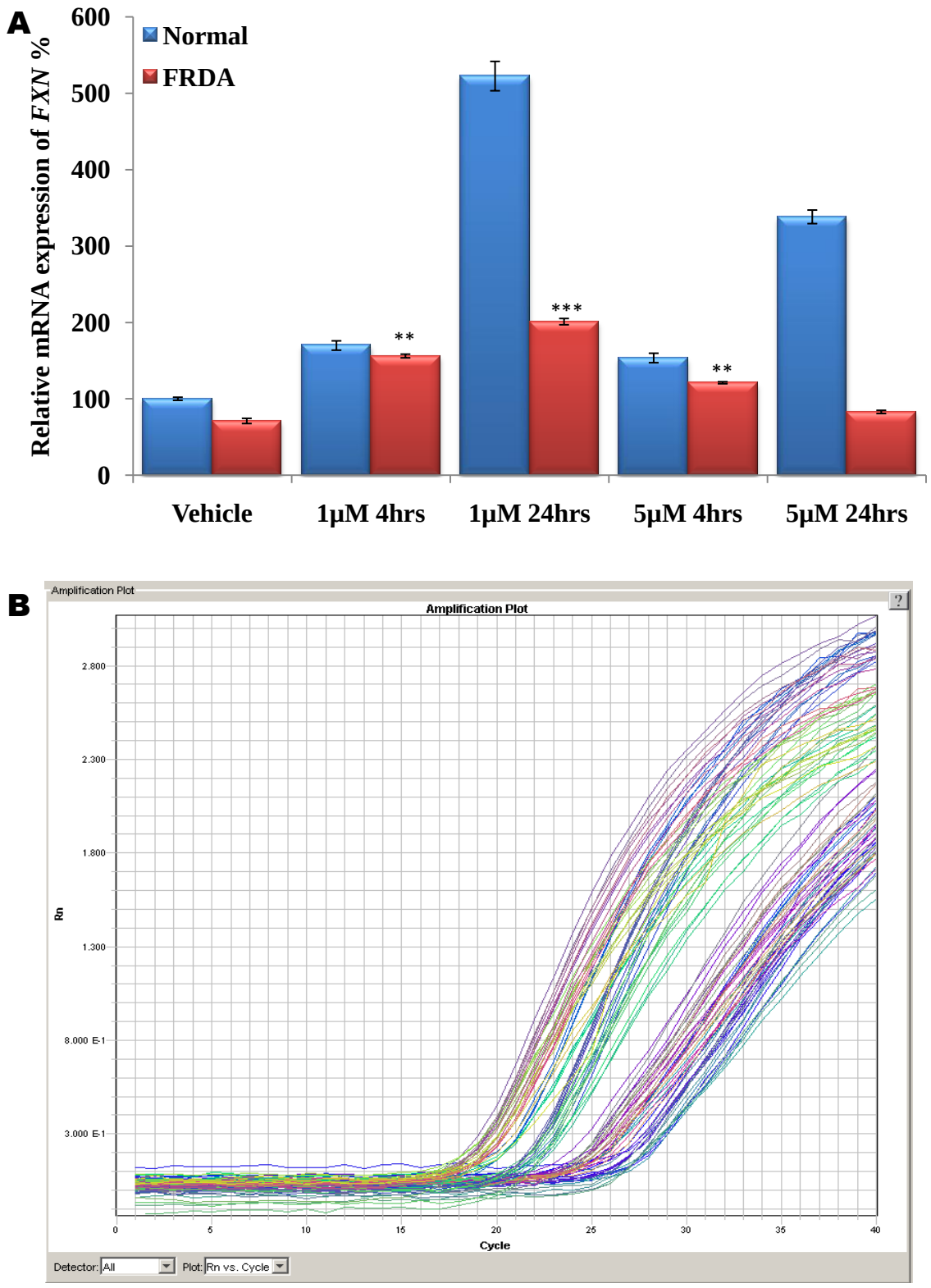

Figure 4.15 - Quantification of relative *FXN* mRNA expression in human normal and FRDA fibroblasts following treatment with DB221. **A)** Level of *FXN* expression, and **B)** QRT-PCR profile of DB221-treated normal and FRDA fibroblasts (*p<0.05, ** p<0.01, error bars ± 1 SEM).

In addition, the unmethylated DNA levels were significantly increased with DB221 after 4 (1µM and 5µM) and 24 hours (5µM) of the treatment, where 25-, 18- and 195-fold increases in unmethylated DNA were observed as compared to vehicle-treated samples, respectively. However, in contrast with our previous data using DNA demethylating agents, reduced levels of DNA methylation (or increased levels of unmethylated DNA) have a direct relationship with *FXN* upregulation in DB221-treated cells.

In normal human fibroblasts, the methylscreen analysis revealed increased levels of DNA methylation and decreased levels of unmethylated DNA with DB221, suggesting that there is somewhat specific effect of DB221 in FRDA cells.

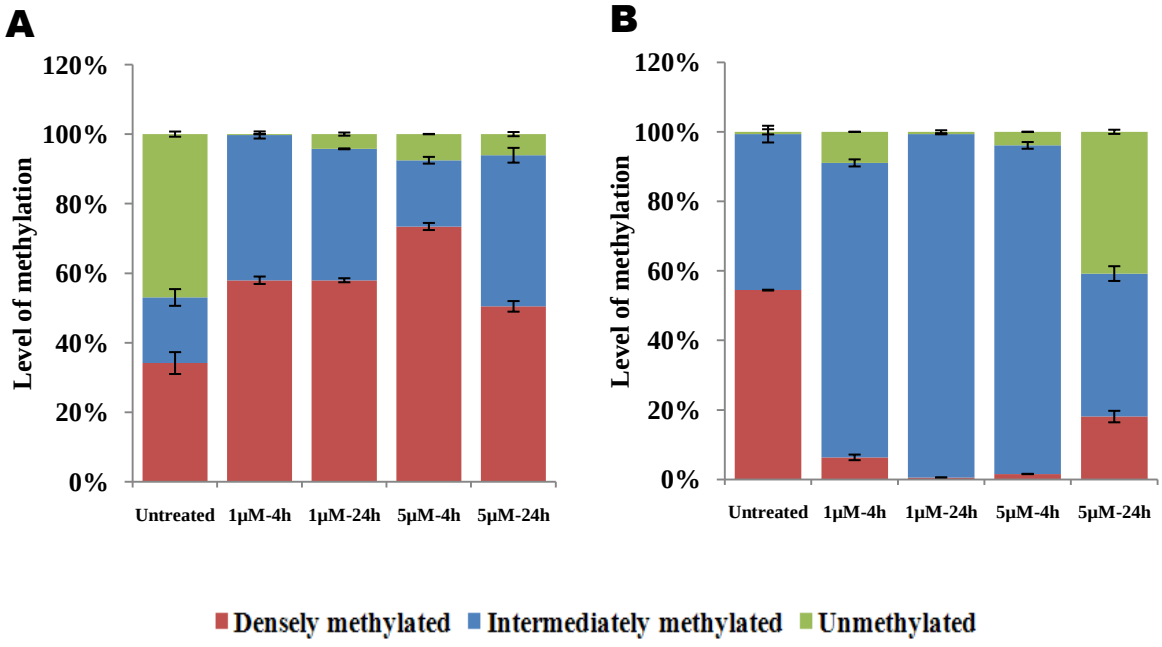

Figure 4.16 - The effect of DB221 on DNA methylation. The analysis of changes in methylation as determined by methylscreen assay following treatment with increased concentrations of Db221 (0-5µM) in **A)** normal, and **B)** FRDA primary fibroblasts (error bars ± 1 SEM).

4.2.2.2 - Therapeutic testing of pentamidine

Pentamidine (4,4'-[pentane-1,5-diylbis(oxy)]dibenzenecarboximidamide) (Figure 4.17) is one of the most successful agents against eukaryotic parasites and has been used clinically against *Pneumocystis pneumonia* (PCP), a severe interstitial type of pneumonia often seen in patients with HIV infection, for over 70 years (Burchmore *et al.* 2002; Wilson *et al.* 2008). It has been reported that pentamidine is capable of binding to the minor groove of double strand DNA but not single strand DNA and inhibits protein synthesis, DNA synthesis and the activity of endo-exonuclease in *Pneumocystis carini* (Hildebrandt *et al.* 1998). It has also been reported that pentamidine is able to upregulate the *FXN* expression in FRDA patients' lymphocytes (Grant *et al.* 2006).

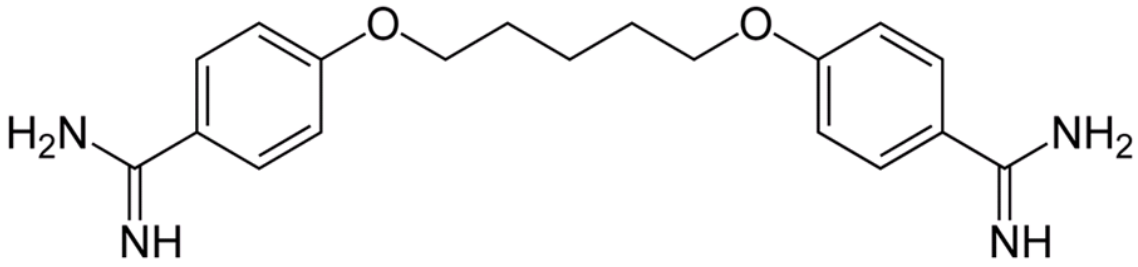

Figure 4.17 - Chemical structure of pentamidine.

However, to date the efficacy and tolerability of pentamidine has not yet been tested in other FRDA cell types. Therefore, we have investigated the effectiveness of pentamidine as a therapy for FRDA using human and mouse primary fibroblasts. We have used 0-20µM concentrations of pentamidine and incubated the cells with the drug for 48 hours. After the treatment, cell viability was determined by trypan blue exclusion assay. Total RNA was

extracted, and cDNA was synthesized using first strand cDNA synthesis kit (Invitrogen) followed by *FXN* specific QRT-PCR.

Generally there was little increase in *FXN* expression levels in drug-treated cells, but significant upregulation (1.3-fold) in *FXN* was identified in cells treated with 20µM of pentamidine compared with vehicle-treated cells in YG8 rescue mouse fibroblasts (Figure 4.18). The WT fibroblasts showed no difference in the *FXN* expression. In human fibroblasts, contradictory results were obtained, as normal fibroblasts showed an overall increase in *FXN* expression, whereas FRDA fibroblasts displayed a general decrease in *FXN* expression in all drug-treated cells compared to vehicle-treated cells.

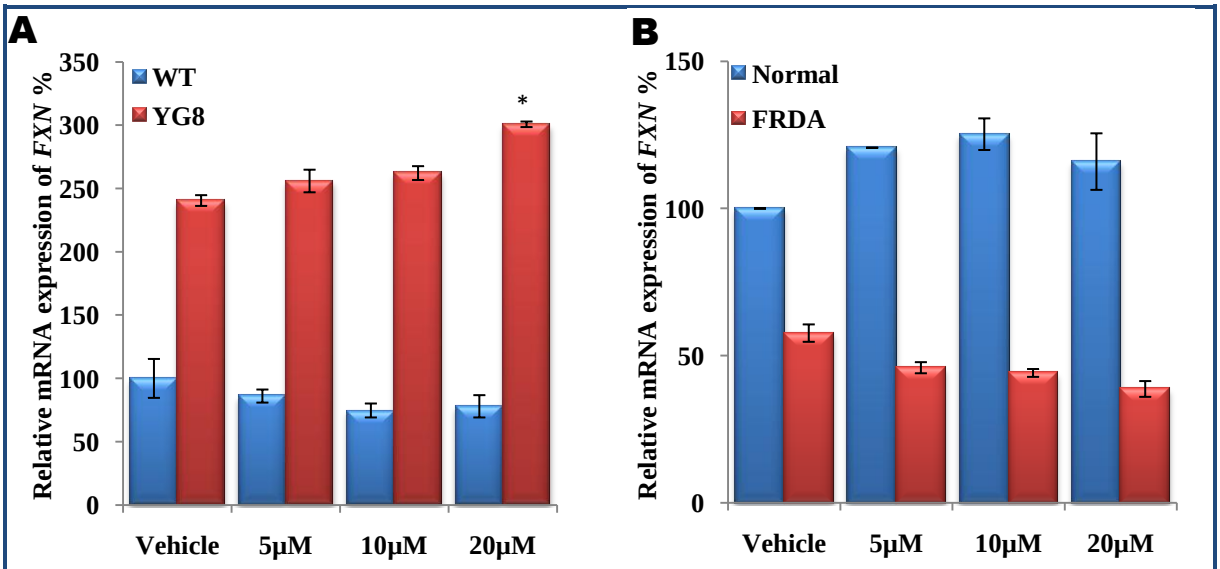

Figure 4.18 - Quantification of relative *FXN* mRNA levels following treatment with pentamidine in **A)** mouse, and **B)**human primary fibroblasts. Each result displayed is the mean of two independent experiments and mRNA expression was normalized to *Gapdh/GAPDH*. The values were expressed as a ratio to the corresponding untreated (vehicle) sample (* $p<0.05$, error bars ± 1 SEM).

4.2.3 - Discussion

Using rational selection and screening of potential FRDA therapeutic molecules GAA repeat specific compounds have been identified and are being investigated (Sarsero *et al.* 2005; Grant *et al.* 2006; Herman *et al.* 2006). Although the exact mechanism by which the GAA interacting compounds induce *FXN* expression is not known, it has been postulated that these compounds are able to disrupt the triple/sticky DNA structures formed as a result of GAA repeat expansion (Hebert and Whittom 2007; Hebert 2008). Another possibility may be that these compounds displace the proteins that promote the heterochromatin formation (HP1), thereby resulting in more open chromatin and transcriptionally accessible form of *FXN* gene (Hebert 2008). The analysis of data obtained from the first generation competition dialysis screening assay (Chaires 2005) has revealed the identification of several small molecules with the potential to bind selectively to the duplex form of the GAA repeat sequences. In which, the interactions of 126 compounds with 13 nucleic acid structures were studied (Grant *et al.* 2006).

We have tested two potential candidates, DB221 and pentamidine. These molecules are minor groove binders that prefer A-T rich duplex DNA over other DNA structures. Regarding DB221, we found most promising results in human and mouse cells with significant increase in *FXN* expression, especially with low concentrations of the drug (1µM). In mouse cells, a selective increase in *FXN* expression was seen only in YG8 rescue mice cells indicating a GAA repeat-specific effect of DB221. In addition, DB221 also produced reduced DNA methylation in mouse and human cell lines.

In contrast to DNA demethylating agents, the reduced DNA methylation with DB221 is associated with an increase in *FXN* expression in both mouse and human cells. Indeed, in human FRDA fibroblasts, the level of DNA methylation almost disappeared with DB221 treatment, which resulted in increased the *FXN* levels. The reason for this differing effect to DNA demethylating agents could be that DB221 specifically targets triplex/sticky GAA repeat DNA causing a specific local inhibition of DNA methylation rather than a more generalized DNA methylation inhibition as seen with DNA demethylating agents.

As DB221 is a GAA interacting compound, one can perhaps expect more *FXN* expression in treated cells that have more GAA repeats, like FRDA fibroblasts (>450 GAA repeats). However, we found a massive increase in *FXN* levels in cells with a normal number of GAA repeats (<9) rather than in cells with longer GAA repeats. This leads me to speculate that DB221 may selectively target the GAA repeats, causing transcriptional activation, in a way that is inversely dependent upon the number of GAA repeats. Thus, for large GAA repeat FRDA fibroblasts, transcription activation may require more time than for normal fibroblasts. This would be consistent with our findings where more *FXN* levels were produced with 1µM of DB221 after 24 hours treatment compared to 4 hours treatment with the same concentration of the drug. However, such an increase in *FXN* expression did not appeared with 5µM of DB221, but perhaps higher concentrations of DB221 negatively regulate *FXN* expression.

We next analysed the effect of pentamidine, used on the basis of its known DNA minor-groove binding properties (Neidle 2001) and previous gene expression activation results (Grant *et al.* 2006). In addition, pentamidine was chosen because it is a FDA approved drug for the treatment of infections in patients with HIV and thus can be easily tried in FRDA patients. No apparent effect was seen in human cells treated with pentamidine. However, in YG8 rescue mice a moderate but significant increase in *FXN* expression was produced only with high concentration of the drug (20μM). Therefore, we have investigated the effect of this compound with even higher concentration (30μM), but 90% of the cells died within 24 hours after the treatment, indicating that high concentrations of pentamidine are toxic to cells. Recently reported data using a GAA_{148}-GFP construct has demonstrated that pentamidine significantly increased the GFP signal in cells treated intermittently with pentamidine, compared to the cells treated with pentamidine continuously (Grant *et al.* 2006). Therefore, such a strategy could be applied in future drug therapy investigations with pentamidine.

Previous studies have indicated that healthy FRDA carriers show about 40% of the normal *FXN* mRNA levels (Pianese *et al.* 2004), suggesting that a modest increase in *FXN* levels, such as that induced by pentamidine (in mouse), may be sufficient to reverse the FRDA-associated phenotype. Herbert and colleagues (2006) reported that a DNA binding protein, Hoechst 33258, has significantly increased the GFP levels in a GAA_{148}-GFP construct. Although there are no explicit data for the preferential binding of Hoechst 33258 to GAA repeats, considering such compounds for future FRDA therapy may also be useful.

In summary, our findings suggest that the GAA interacting compounds we have investigated, especially DB221, may prove useful as therapeutics for FRDA. It seems to be that we do not have a simple scenario whereby DB221 can target non-B DNA forms specifically in FRDA cells, inducing *FXN* transcription and hence raising frataxin levels. Other unknown mechanisms must clearly be at play. Finally, although we have investigated the effect of DB221 in a preliminary short-term *in vivo* study and seen no effect (Appendix Figure B.5), it will be very important to consider long term *in vivo* studies in future to determine the bioavailability and efficacy of these compounds. Consequently, it will also be essential for future studies to ascertain the precise contribution of triplex/sticky GAA DNA structures and heterochromatin mechanisms in silencing the *FXN* gene.

4.3 - Therapeutic testing of histone deacetylase (HDAC) inhibitors

4.3.1 - Introduction

Epigenetic modifications are increasingly recognized as having a substantial role to play in both normal cellular physiology and disease processes. Histone deacetylases (HDAC) are enzymes involved in the remodelling of chromatin, and have a key role in the epigenetic regulation of gene expression. In mammalian cells, they are responsible for the deacetylation of N-terminal lysine residues in histones, particularly the core histones H2A, H2B, H3 and H4. Histones are also distinguished by the fact that they undergo abundant post-translational modifications to both the globular and tail domains. The combination of such histone modifications is indicative of whether a gene is transcriptionally active or inactive (Grant 2001; Goll and Bestor 2002). To date, more than 60 different modifications have been detected and these include acetylation, methylation, ubiquitynation, phosphorylation, and sumoylation (Table 4.1), all of which serve as epigenetic tags (reviewed by Kouzarides 2007).

Table 4.1 – Different classes of histone modifications (Kouzarides 2007)

Chromatin Modifications	**Residues Modified**	**Functions Regulated***
Acetylation	**K**-ac	Trans, Rep, Repli, Cond
Methylation (lysines)	**K**-ac1 **K**-me2 **K**-me3	Trans, Rep
Methylation (arginines))	**R**-ac1 **R**-me2 **R**-me3	Trans
Phosphorylation	**S**-ph **T**-ph	Trans, Rep, Cond
Ubiquitylation	**K**-ub	Trans, Rep
Sumoylation	**K**-su	Trans
ADP ribosylation	**E**-ar	Trans
Deimination	**R** > **Cit**	Trans
Proline Isomerization	**P-cis > P-trans**	Trans

* - Trans = Transcription, Rep = Repair, Repli = Replication, Cond = Condensation

4.3.2 - Classification of HDACs

Based on the homologies to yeast HDACs, 18 HDAC enzymes have been identified in mammals and divided into four classes (Table 4.2) (Blander and Guarente 2004; Bhalla 2005; Marks and Dokmanovic 2005; Glaser 2007); Class I HDACs include HDACs 1, 2, 3, and 8, which are related to yeast RPD3 deacetylase. Class II HDACs are related to yeast Hda1 and include HDACs 4, 5, 6, 7, 9, and 10. This class is further divided into class IIa, consisting of HDAC 4, 5, 7 and 9, and class IIb, consisting of HDAC6 and 10. All class I and II HDACs are zinc-dependent enzymes. Class III HDACs, sirtuins (sir 1-7), require NAD^+ for their enzyme activity (Blander and Guarente 2004). Class IV HDAC represented by HDAC 11, which, like yeast Had 1 similar 3.

Table 4.2 – Classification of HDACs in mammals (Pan *et al.* 2007)

Classification			Location	Function
Zn^{2+}-dependent	**Class I**	HDAC1	Nucleus	Participate in Sin3, NuRD (nucleosome remodeling and deacetylation) and Co-REST complex
		HDAC2	Nucleus	
		HDAC3	Nucleus, rarely in cytoplasm	Participate in SMRT (silencing mediator for retinoic acid and thyroid hormone receptors), N-CoR (nuclear receptor co-repressor) complex
		HDAC8	Nucleus	-
	Class IIa	HDAC4	Nucleus, cytoplasm	Interaction with SMRT/N-CoR and the co-repressors BcoR (Bcl-6-interacting co-repressor) and CtBP
		HDAC5	Nucleus, cytoplasm	
		HDAC7	Nucleus, cytoplasm	
		HDAC9	Nucleus, cytoplasm	Muscle differentiation
	Class IIb	HDAC6	Cytoplasm	Tubulin deacetylase
		HDAC10	Nucleus, cytoplasm	Recruitment other HDACs
	Class IV	HDAC11	Nucleus, cytoplasm	-
Zn^{2+}-independent	**Class III**	SIRT1-7		

4.3.3 - Mechanisms of histone modifications and transcriptional regulation

Histone modifications regulate gene expression in three mechanistic ways (Jenuwein and Allis 2001; Berger 2007; Kouzarides 2007). Firstly, they regulate chromatin structure, making genetic loci more or less accessible to the transcriptional machinery. Secondly, they serve as a signalling role by integrating responses to multiple biochemical signalling cascades and recruit or repel the transcriptional machinery and chromatin remodelling complexes (Abel and Zukin 2008). Thirdly, and perhaps more interestingly, histone modifications mediate epigenetic changes in gene expression that provide a mechanism by which neural function and behaviour are stably altered for long periods of time in response to transient experience or neuronal insult (Abel and Zukin 2008).

Histone modifications may affect higher-order chromatin structure by affecting the contact between different histones in adjacent nucleosome or the interaction of histones with DNA (Kouzarides 2007). Of all the known modifications, acetylation has the most potential to unfold chromatin since it neutralizes the basic charge of the lysine. This function is not easy to observe *in vivo*, but biophysical studies indicate that inter-nucleosome contacts are important for stabilization of higher-order chromatin structure (Kouzarides 2007; Abel and Zukin 2008).

Acetylation of core histones is catalyzed by transcriptional coactivators such as CREB-binding protein (CBP), which possess histone acetyl transferase (HAT) activity (Lee and Workman 2007). Histone acetylation remodels chromatin structure, thereby modulating transcription. Specificity of gene regulation is achieved by the recruitment of HATs by transcription factors to specific genetic loci, where they locally modify histones (Abel and

Zukin 2008). Importantly, HATS interact with a large number of transcription factors and thus serve as critical hubs, integrating the activity of multiple signalling cascades.

The activity of HATs can be reversed by HDACs, which remove acetyl groups from lysine/arginine residues in the amino-terminal tails of core histones. Deacetylation of histone proteins shifts the balance towards chromatin condensation and thereby silences gene expression (Abel and Zukin 2008). Unlike HATs, HDACs have a rich structural diversity, which confers diversity of function and renders HDACs promising targets for drug discovery and therapeutic intervention.

4.3.4 - Histone modifications in FRDA

Epigenetic mechanisms, such as histone deacetylation and methylation are known to affect gene expression by chromatin remodelling (Egger *et al.* 2004), and these epigenetic changes are likely to underpin any GAA repeat-induced heterochromatin-mediated gene silencing effects. Recent findings consensually implicate chromatin modifications in the aetiology of FRDA (Herman *et al.* 2006; Greene *et al.* 2007; Al-Mahdawi *et al.* 2008).

The histone acetylation state of the *FXN* gene in a lymphoblastoid cell line derived from a FRDA patient ($GAA_{650/1030}$) showed significantly lower levels of histone acetylation in H3K9, H3K14, H4K5, H4K8, H4K12 and H4K16 surrounding the GAA repeat, compared to a normal cell line (Figure 4.19a)(Herman *et al.* 2006). No significant difference was observed at the *FXN* promoter region. Additionally, the levels of H3K9 mono-, di- and trimethylation for the region upstream of the GAA repeat were also reported to be significantly higher in the FRDA cell line, particularly those of H3K9 trimethylation (Figure 4.19b). Similarly, Greene *et al*. (2007) reported significantly elevated levels of H3K9 dimethylation upstream of the GAA repeat in lymphoblasts from four FRDA patients, when compared to those of unaffected individuals.

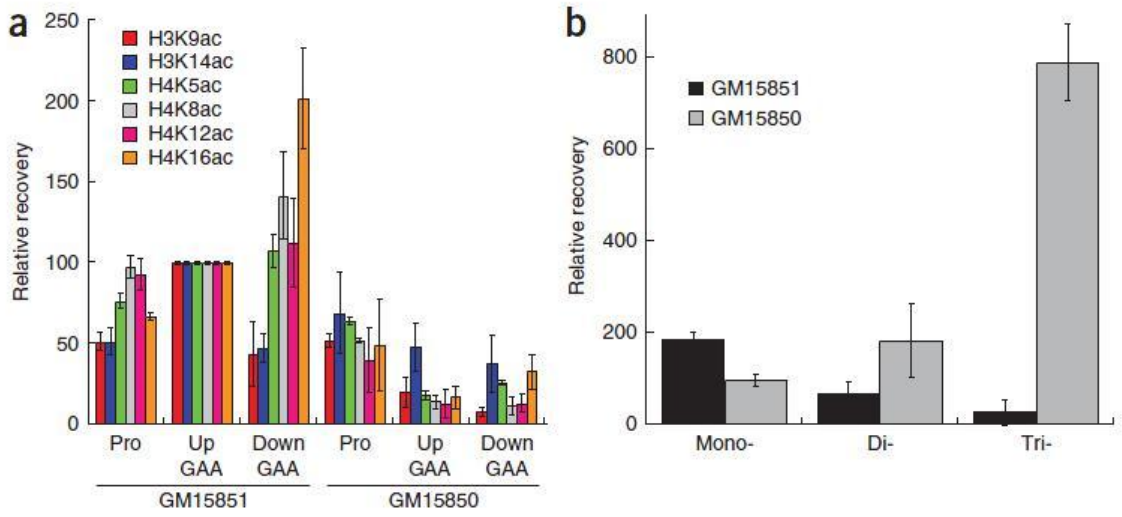

Figure 4.19 - Analysis of histone modifications in *FXN* gene by ChIP experiments in FRDA (GM15850) versus a normal (GM15851) individual lymphoblastoid cell lines. In FRDA, (**a**) histone acetylation levels at specified lysine residues are generally lower immediately upstream and downstream of the GAA repeat, (**b**) while levels of H3K9 methylation are significantly higher in upstream of the GAA., when compared to the normal cell line (Herman *et al.* 2006)

Later, Al-Mahdawi *et al.* (2008) investigated the acetylated histone H3 and H4 and methylated histone H3K9 by ChIP analysis of the *FXN* promoter, upstream GAA and downstream GAA regions in autopsy brain tissues from two FRDA and two unaffected individuals. Overall decreased acetylation of histone H3 and H4 was confirmed, particularly in the downstream GAA region. The six acetylated histone residues (H3: K9, K14, H4: K5, K8, K12, and K16), showed a GAA-induced gradient of comparative acetylation that is highest in the *FXN* 5'UTR and lowest in the downstream GAA region, with the single most altered residue being H3K9. Interestingly, H3K9 also showed consistently increased levels of di- and trimethylation in all three of the *FXN* regions (Figure 4.20) (Al-Mahdawi *et al.* 2008).

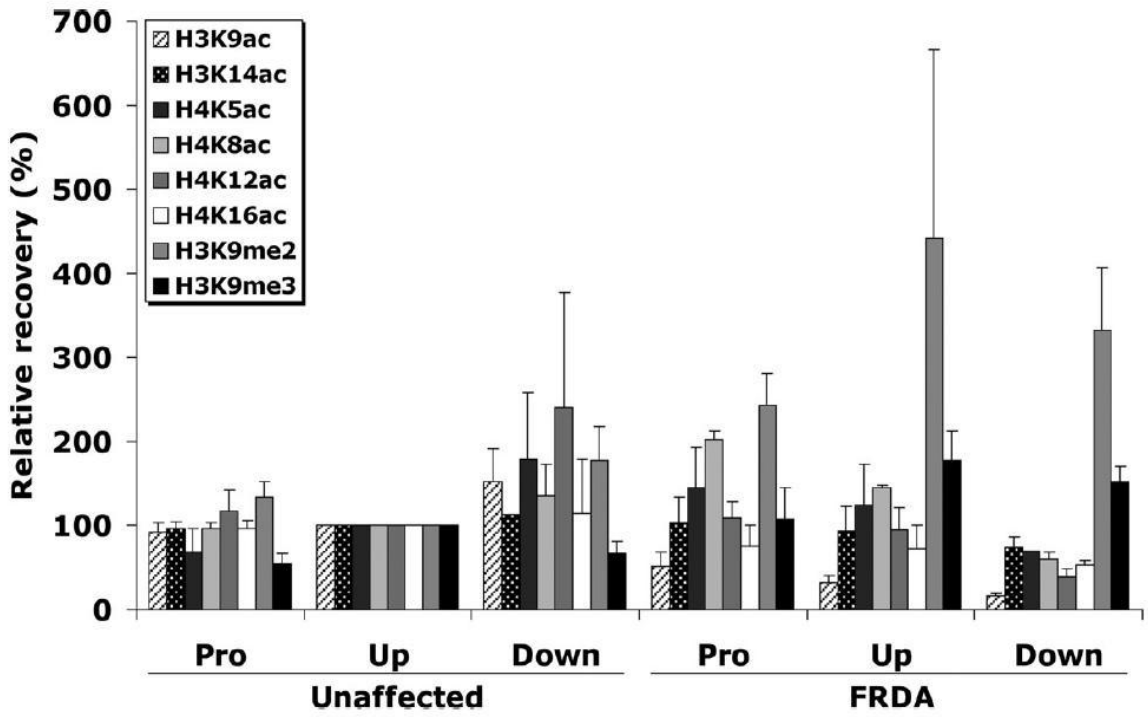

Figure 4.20 - Analysis of histone modifications in human brain tissue. ChIP quantitative PCR results for the *FXN* promoter/exon1 (Pro), upstream GAA (Up) and downstream GAA (Down) amplified regions are represented as the relative amount of immunoprecipitated DNA compared with input DNA, having taken negligible -Ab control values into account. *FXN* values were normalized with human *GAPDH* and all values have been adjusted so that all of the Upstream GAA mean values from the unaffected individuals are 100%. In each case two individual ChIP samples from two FRDA patients and two unaffected controls were analysed in triplicate. The means and SEMs of these values are shown (Al-Mahdawi *et al.* 2008).

4.3.5 - Use of HDAC inhibitors as a therapy in FRDA

There has been substantial progress in the development of drugs that target epigenetic control processes as a new class of mechanism-based therapeutics (McLaughlin and La Thangue 2004; Inche and La Thangue 2006), and one of the fastest moving areas is the development of HDAC inhibitors (HDACi). Acetylation and deacetylation of histones play an important role in transcription regulation of eukaryotic cell (Lehrmann *et al.* 2002; Mai *et al.* 2005). Over the last 10 years, many different types of HDAC inhibitors have been developed, ranging from complicated structures of bacterial or fungal origin (TSA) to the very simple butyrate. HDAC inhibitors can affect transcription by inducing acetylation of histones, transcription factors and other proteins regulating transcription (Glozak *et al.* 2005; Marks and Dokmanovic 2005; Bolden *et al.* 2006; Minucci and Pelicci 2006). Inhibition of HDACs can result in a general hyperacetylation of histones, which is followed by the transcriptional activation of certain genes through relaxation of DNA conformation (Suenaga *et al.* 2002). Chemically, the HDAC inhibitors can be classified into six structural groups: the small carboxylates, the hydroxamic acids, the benzamides, the epoxyketones, the cyclic peptides, and hybrid molecules containing cyclic peptide motifs and hydroxamic acid moieties (Drummond *et al.* 2005; also reviewed in Gottesfeld 2007).

Considering the recent identification of alterations in histone acetylation and methylation profile in FRDA, which resulted in heterochromatin mediated *FXN* gene silencing, it was postulated that the reversal or inhibition of these histone modifications could represent a potential therapeutic route for FRDA (Figure 4.21)(Herman *et al.* 2006). A number of studies have focused in the use of HDAC inhibitors as therapy for restoring histone acetylation and transcriptional activation in neurodegenerative mouse models

(Langley *et al.* 2005). HDAC inhibitors have been shown to cross blood-brain barrier, to ameliorate motor deficits in mouse models for Huntington disease (Ferrante *et al.* 2003; Hockly *et al.* 2003; Gardian *et al.* 2005), and to increase expression of the SMN2 gene in spinal muscular atrophy (Kernochan *et al.* 2005; Riessland *et al.* 2006). Thus, interest in this class of compounds as therapeutics for other neurological diseases has emerged (Di Prospero and Fischbeck 2005; reviewed in Gottesfeld 2007).

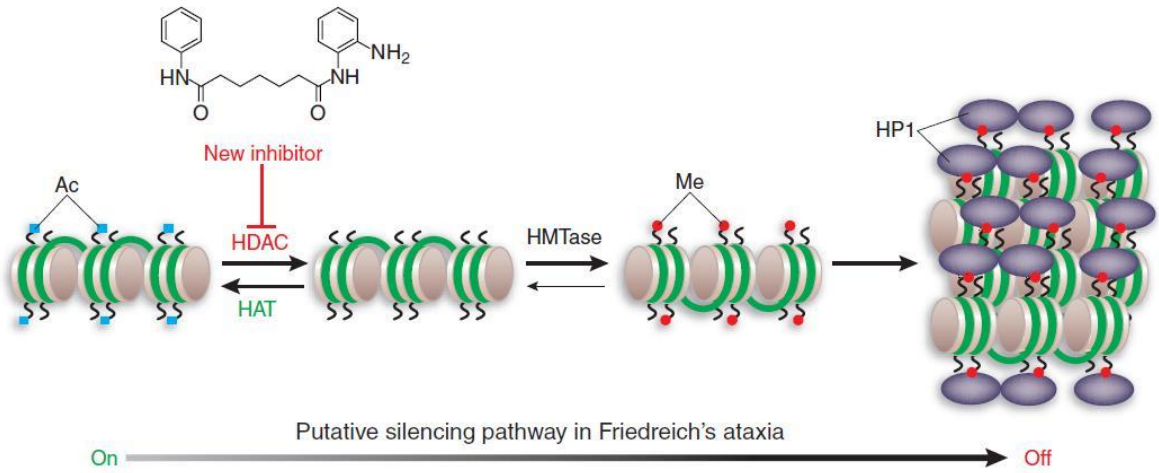

Figure 4.21 - Heterochromatin-mediated silencing pathway in FRDA may be reversed by HDAC inhibitor (Festenstein 2006).

An earlier study demonstrated a small effect of the general HDAC inhibitor, sodium butyrate, on *FXN* gene activity in an EGFP reporter cell line (Sarsero *et al.* 2003). Later, the potential of HDAC inhibitor use in FRDA therapy was investigated by monitoring the effects of a range of commercial HDAC inhibitors on both the levels of histone acetylation and *FXN* transcription in an FRDA lymphoblastoid cell line from donor FRDA patient blood (Herman *et al.* 2006). This study showed that of the tested compounds, the benzamide-type SAHA derivative BML-210 was the only HDAC inhibitors to significantly increase (~2-fold) the level

of *FXN* mRNA in the FRDA cell line (Figure 4.22b), even though other HDAC inhibitors produced much higher levels of total acetylated histone (Figure 4.22a).

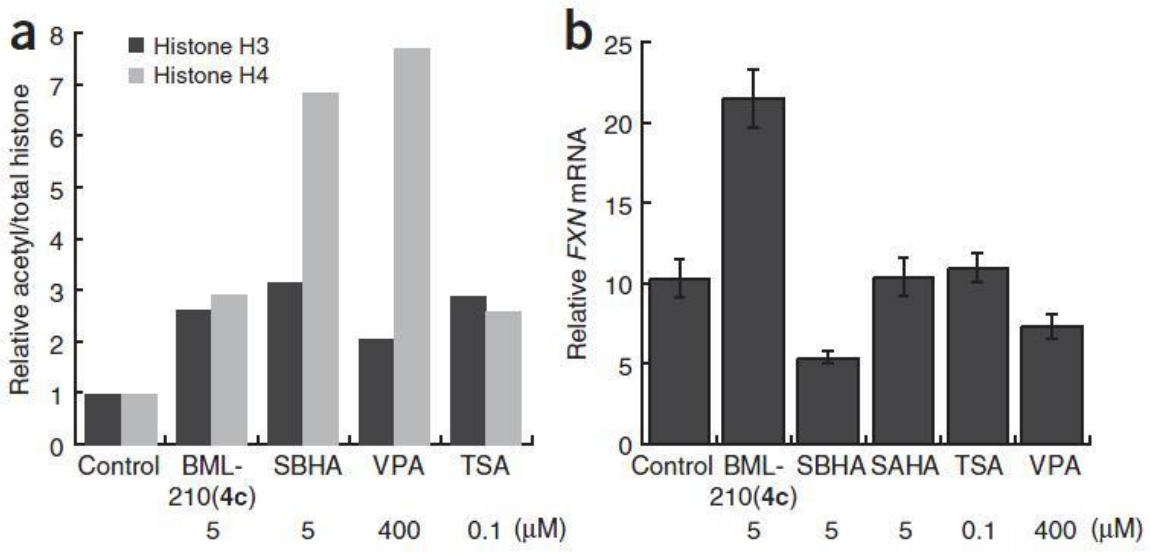

Figure 4.22 - Effect of HDAC inhibitor on acetylation and *FXN* mRNA in FRDA. a) The levels of H3 and H4 acetylation, b) *FXN* mRNA levels (Herman *et al.* 2006).

Subsequent synthesis of analogues of BML-210 identified a pimelic diphenylamide compound, **4b** (N^1-(2-aminophenyl)-N^7-phenylheptanediamide), that was shown to act on FRDA primary lymphocytes to significantly increase the acetylation levels of H3K14, H4K5 and H4K12 in the *FXN* upstream GAA region and to increase *FXN* mRNA levels by 2.5-fold, approximately 80% of that in unaffected individuals and to at least those of carriers, without apparent toxicity (Herman *et al.* 2006).

Recently, Rai *et al*. (2008) explored the use of HDAC inhibitors as a potential therapy in FRDA patients' primary lymphocytes, fibroblasts and mouse model of FRDA (KIKI, $GAA^{230/230}$). Initially they used the HDAC inhibitor 106, a derivative of 4b, and showed a significant increase in *FXN* mRNA expression, especially in the cerebellum and heart tissues of the KIKI

mice. Additionally, this compound resulted in increased acetylation of histone H3 and H4 in the mouse *Fxn* intron 1 region just upstream of the knocked-in GAA repeat (Rai *et al.* 2008). Interestingly, microarray analysis revealed that drug-treated mouse genes (67% in brain, 84% in cerebellum, and 67% in heart) showed coordinate changes towards normal levels after 106 treatment (Rai *et al.* 2008)

The same research group also investigated the efficacy of another two HDAC inhibitors in FRDA, 136 and 109, structurally similar novel pimelic diphenylamides, and found up regulation of frataxin mRNA and protein expression *in vitro* (Rai *et al.* 2010). In addition, an *in vivo* pilot study using the same compounds also showed significantly increased *FXN* mRNA and acetylation of histones H3K14 and H4K5 expression in the FRDA mouse model (Rai *et al.* 2010). However, long term *in vivo* studies are needed to confirm the effectiveness of these two compounds as a potential therapy for FRDA.

4.3.5.1 - Therapeutic testing of sirtinol

Since commonly used HDAC class I and II inhibitors such as TSA, VPA and SAHA are not effective in enhancing *FXN* transcription, we decided to investigate the effect of certain class III HDAC inhibitors. Sirtinol is an inhibitor of Sirt1, which is a mammalian NAD^+-dependent deacetylase that belongs to class III histone deacetylases (HDACs) (Imai *et al.* 2000; Landry *et al.* 2000b; Blander and Guarente 2004). These enzymes, also known as sirtuins, have multiple targets, act NAD+-dependently and are implicated in telomeric and rDNA silencing in humans (Grozinger *et al.* 2001). Most HDAC inhibitors, including the mammalian sirtuins, have a number of different targets, one of them being histones. The use of sirtinol in cancer therapy has been very well explored and shown promising results for use as an anticancer agent (Ota *et al.* 2006; Kojima *et al.* 2008).

Here, the focus will lie on the activity of sirtuins on histones, since opening up the chromatin structure via acetylation of *FXN* might facilitate its expression. So far, the most characterised histone target of sirtuins is the deacetylation of the H4K16 modification. In *Drosophila* it was shown that this modification correlates best with processes thought to "open" chromatin structure (Taipale and Akhtar 2005). Thus, it seemed reasonable to treat FRDA mouse and human cell lines with sirtuin inhibitors, despite their diverse functions, to determine whether simply "opening up" the *FXN* locus would be sufficient to relieve the hampered *FXN* transcription in FRDA patients.

In order to test the effect of sirtinol, mouse and human primary fibroblasts (normal and FRDA) were treated with a 10µM, 50µM and 100µM sirtinol for 48 hours followed by the quantification of *FXN* mRNA expression by QRT-PCR (Figure 4.23).

Treatment of cells with sirtinol significantly ($p<0.05$) up regulated the *FXN* mRNA expression in a dose dependent manner. At 50µM concentration of sirtinol, *FXN* expression levels were increased to approximately 1.8-fold in YG8 mouse fibroblasts and 3-fold in human FRDA fibroblasts, compared to their respective vehicle-treated cells. Surprisingly, sirtinol also produced a significant increase of *FXN* mRNA expression (~2-fold) in human normal primary fibroblasts, suggesting some non-specific activity. Nevertheless, high concentrations of the drug reduced the *FXN* mRNA expression in both WT and YG8 mouse and human FRDA primary fibroblasts. Finally, no cell toxicity was detected with any concentrations tested.

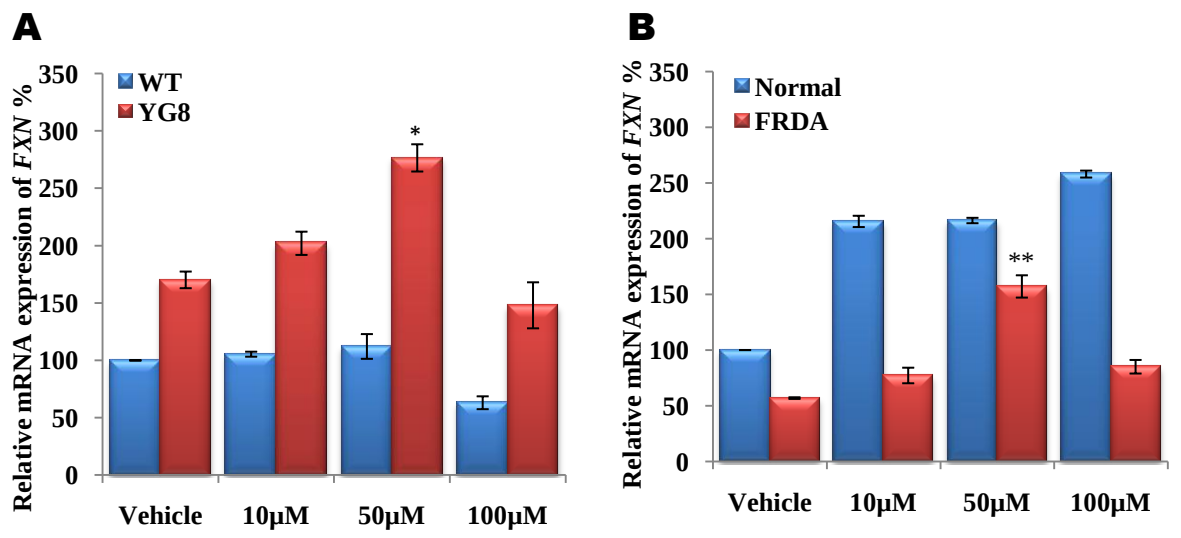

Figure 4.23 - Relative *FXN* mRNA levels following treatment with sirtinol in mouse and human primary fibroblasts. Displayed are the levels of *FXN* mRNA expression, as determined by QRT-PCR following treatment with sirtinol in **A)** mouse, and **B)** human. Each result displayed is the mean of two independent experiments and each sample was normalized to *Gapdh/GAPDH*. The values were expressed as a ratio to the corresponding untreated (vehicle) sample of WT/normal fibroblasts (* $p<0.05$, error bars ± 1 SEM).

4.3.5.2 - Therapeutic testing of splitomicin

Splitomicin, a compound with a saturated six-membered lactone ring, is a more specific inhibitor of Class III HDACs and is thought to have a mechanism distinct from that of other class III HDAC inhibitors, inhibiting these enzymes by competing for binding of the acetylated substrate (Da Costa *et al.* 1996; Bedalov *et al.* 2001; Posakony *et al.* 2004). It was initially recognized as a potent, selective inhibitor of SIR2, which is a member of the class III HDAC protein family (Frye 1999; North and Verdin 2004; Kruszewski and Szumiel 2005). Subsequently, it has been demonstrated that splitomicin is also able to inhibit Sirt2, whose biological functions are relevant to genomic stability, DNA repair, p53-mediated apoptosis and adipogenesis (Guarente 2006; Haigis and Guarente 2006; Longo and Kennedy 2006).

Biacsi *et al*. (2008) have recently reported that splitomicin has increased the *FMR1* mRNA expression by 200-600 fold in Fragile X mental retardation syndrome (FXS), alleviating the heterochromatin-mediated silencing effect in FXS. Since FRDA and FXS are both trinucleotide repeat disorders and share some common features, we considered using splitomicin as a potential therapy for FRDA.

In order to assess the effectiveness of splitomicin treatment, both mouse and human (normal and FRDA) primary fibroblast cells were cultured in DMEM medium with 0.5mM, 0.75mM and 1mM splitomicin (Figure 4.24) for 48 hours. After the treatment, the cells were collected and cell viability was tested, followed by quantification of *FXN* mRNA expression by QRT-PCR.

Splitomicin treatment of mouse primary fibroblasts produced a dose dependent increase of *FXN* mRNA expression at 0.5mM and 0.75mM concentrations in YG8 mouse cells with a maximal increase of ≈1.6-fold at 0.75mM. *FXN* levels then dropped when using 1mM. No significant differences in *FXN* mRNA expression were detected between vehicle and drug-treated samples in WT mouse fibroblasts (Figure 4.24), suggesting a specific effect of splitomicin on FRDA. Unexpectedly, splitomicin did not produce any increase in *FXN* expression in the human fibroblasts (Figure 4.24) at any concentration tested. This difference may possibly be due to the larger GAA repeats (>450) in human fibroblasts compared with YG8 (<250) mice fibroblasts. However, no cell toxicity was detected with splitomicin, proposing a safe administering of the drug.

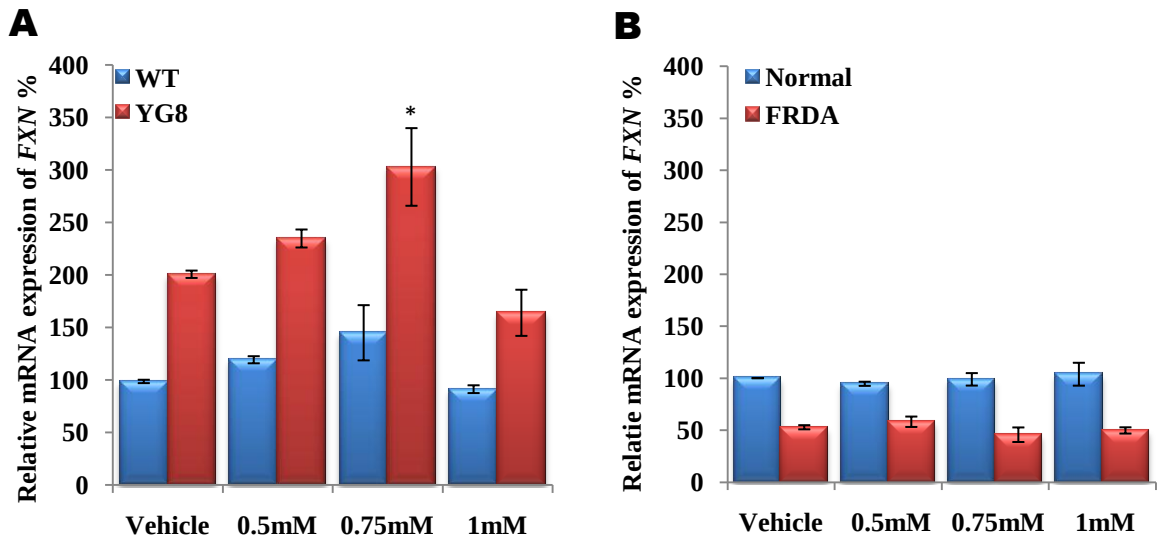

Figure 4.24 - Relative *FXN* mRNA levels following treatment with splitomicin in mouse and human primary fibroblasts. Displayed are the increases in *FXN* mRNA expression in **A)** mice, and **B)** human primary fibroblasts as determined by QRT-PCR following treatment with splitomicin. Each result displayed is the mean of two independent experiments and each sample was normalized to *Gapdh*. The values were expressed as a ratio to the corresponding untreated (vehicle) sample of WT/normal fibroblasts (* $p<0.05$, error bars ± 1 SEM).

4.3.5.3 - Therapeutic testing of nicotinamide

Nicotinamide is a precursor of nicotinamide adenine dinucleotide (NADH), which is a substrate for complex I of the electron transport chain. Nicotinamide is an inhibitor of the NAD^+-dependent or Class III HDAC sirtuin family and is the biologically active form of niacin (vitamin B3) (Fuller and Dietrich 1971), which has been widely used clinically for >40 years (Knip *et al.* 2000). Ghosh *et al.* (2004) reported that nicotinamide substantially rescued the neuronal loss in a *drosophila* model of spinocerebellar ataxia-3. Furthermore, nicotinamide is currently in clinical trials as a therapy for cancer and type I diabetes (Kaanders *et al.* 2002). However, the long term safety of the high doses used in these treatments has been questioned (Knip *et al.* 2000).

Treatment of cardiomyocytes with nicotinamide significantly increased the acetylation of histone H3 and H4 (Imai *et al.* 2000). As sirtuins act NAD^+-dependently, nicotinamide can also inhibit the deacetylation of H4K16ac, a product of the SIRT- mediated deacetylation reaction. Here, nicotinamide directly competes with NAD^+ for binding to the pocket of the Sir2-family catalytic domain (Landry *et al.* 2000a; Landry *et al.* 2000b). Nicotinamide is also thought to be more stable under cell culture conditions than splitomicin or sirtinol (Posakony *et al.* 2004).

The effect of nicotinamide on FRDA was subsequently investigated by treating the mouse and human primary fibroblasts with a range of drug concentrations (0 - 10mM) for 72 hours. After drug treatment, *FXN* mRNA expression was quantified with QRT-PCR.

Nicotinamide produced no change in *FXN* expression at lower concentrations, but 10mM nicotinamide produced significant increase of approximately 1.8-fold in YG8 mouse fibroblasts and 2-fold in human FRDA cells (Figure 4.25). No *FXN* upregulation was found in either mouse (WT) or human normal fibroblasts, indicating a specific effect of nicotinamide on FRDA. However, a major concern with nicotinamide is the high concentrations of the drug needed to upregulate the *FXN* mRNA expression, as highlighted by the adverse effects seen in previous clinical trials of nicotinamide for cancer and type I diabetes (Knip *et al.* 2000). However, in our testing no cell toxicity was detected even with the highest tested concentration (10mM) of nicotinamide.

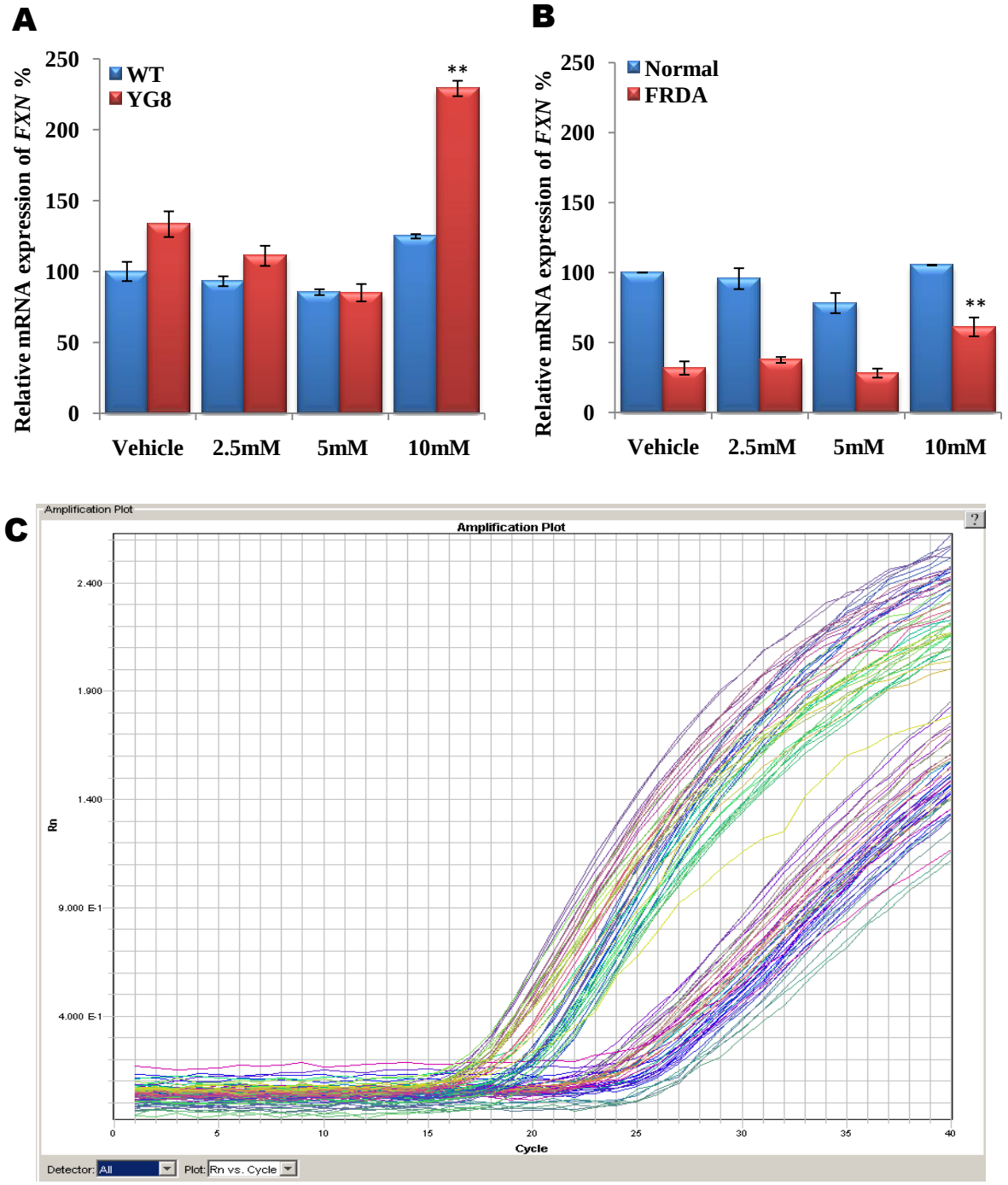

Figure 4.25 - Relative *FXN* mRNA levels following treatment with nicotinamide in mouse and human primary fibroblasts. Percentage changes in *FXN* mRNA expression, as determined by QRT-PCR following treatment with nicotinamide in **A)** mice, and **B)** human were displayed. **C)** QRT-PCR profile of nicotinamide-treated mouse and human fibroblasts. Each result displayed is the mean of two independent experiments and each sample was normalized to *Gapdh/GAPDH*. The values were expressed as a ratio to the corresponding untreated (vehicle) sample of WT/normal fibroblasts (** $p<0.01$, error bars ± 1 SEM).

4.3.5.4 - Therapeutic testing of oxamflatin

Oxamflatin is an aromatic sulfonamide derivative with a hydroxamic acid group. The use of oxamflatin as an anti-cancer agent has been very well studied in breast cancer (Restall *et al.* 2009) and uterine cancer (Jiang *et al.* 2007). Oxamflatin induces transcriptional activation of JunD and morphological reversion in various NIH3T3-derived transformed cell lines (Sonoda *et al.* 1996). Oxamflatin induces morphological change of HeLa cells similar to that induced by the HDAC inhibitor TSA, and indeed showed inhibition of HDAC activity *in vivo* and *in vitro* (Kim *et al.* 1999).

Recently, Soragni *et al*. (2008) reported that oxamflatin significantly increased ($P<0.05$) the expression of the GFP_ $(GAA{\cdot}TTC)_{560}$ reporter 1.4- to 2.5-fold. Also, this compound induced expression of the *FXN* gene harbouring expanded GAA·TTC repeats in the two lymphoblastoid cell lines derived from FRDA patients ($P<0.05$) (Soragni *et al.* 2008). However, the molecular mechanism of oxamflatin is still unknown and more *in vitro* and *in vivo* long term studies are needed to confirm the efficacy of this novel HDAC inhibitor as a therapy for FRDA.

Mouse and human primary fibroblasts were treated with oxamflatin at 50nM, 100nM and 500nM concentrations (Figure 4.26) for 72 hours followed by the *FXN* mRNA quantification by QRT-PCR. Cell viability was measured by trypan blue exclusion assay and no difference in cell viability was detected in between vehicle and drug-treated samples.

Oxamflatin selectively increased *FXN* expression in the YG8 FRDA mouse model and no effect on *FXN* expression was observed in human FRDA primary fibroblasts (Figure 4.26). A significant increase (≈1.5-fold) in *FXN* expression was identified with 100nM of oxamflatin in YG8 mouse cells, and with high concentration of drug (500nM) these levels dropped to 66% of those observed in vehicle-treated cells. Interestingly, a slightly reduced (but not significant) *FXN* expression was identified in WT mouse primary fibroblasts. This indicates that oxamflatin may have a specific effect in mouse FRDA cells with smaller GAA repeats and not the human FRDA cells with larger GAA repeats. Similar to splitomicin, *FXN* mRNA expression was significantly increased in human normal primary fibroblasts with oxamflatin and this is possibly due to fewer GAA repeats in human normal fibroblasts.

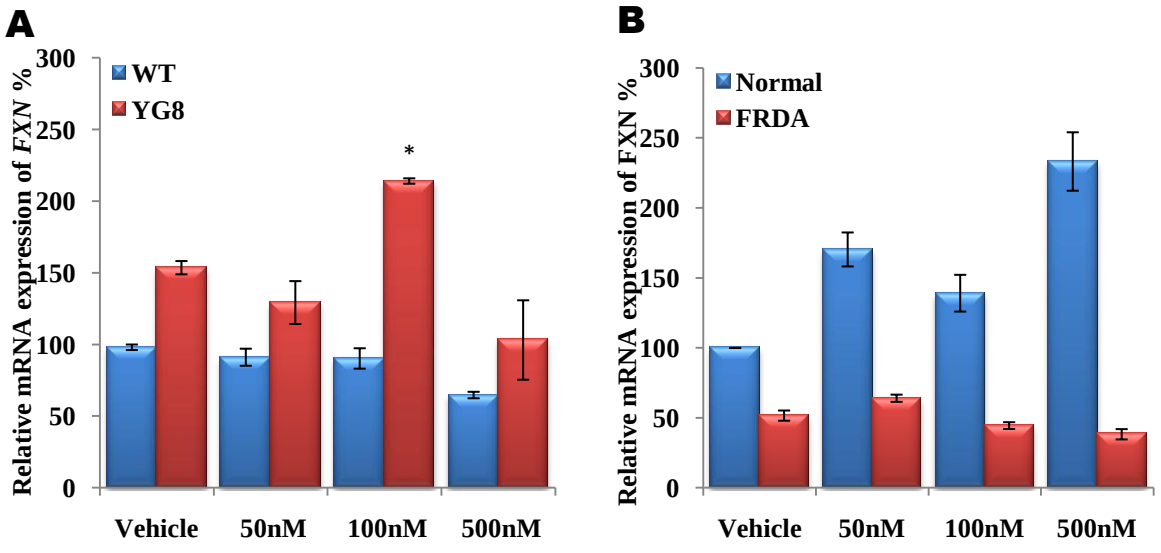

Figure 4.26 - Oxamflatin treatment of normal and FRDA primary fibroblasts of **A)** mouse and **B)** human. *FXN* mRNA expression was determined by QRT-PCR following treatment with oxamflatin. Each QRT-PCR was done twice in triplicate. All values were normalized to *Gapdh/GAPDH* and the values were expressed as a ratio to the corresponding untreated (vehicle) sample of WT/normal fibroblasts (* $p<0.05$, error bars ± 1 SEM).

4.3.6 - Discussion

Acetylation and deacetylation of histone proteins play crucial roles in transcriptional regulation thereby regulating the gene expression. Recent studies show that in FRDA transcriptional repression of the *FXN* gene is consistent with heterochromatin-mediated silencing, as indicated by increased trimethylation of H3 and decreased acetylation of H3 and H4 histone tails immediately surrounding the expanded GAA repeats (Herman *et al.* 2006; Greene *et al.* 2007; Al-Mahdawi *et al.* 2008).

Over the past ten years, numerous HDAC inhibitors have been clinically evaluated for the treatment of cancer and these are proving to be generally well tolerated (Cang *et al.* 2009; Prince *et al.* 2009). New uses of HDAC inhibitors appear to confer significant neuroprotection in several experimental models of neurodegenerative diseases such as spinal muscular atrophy (Riessland *et al.* 2006; Garbes *et al.* 2009), Huntington disease (Hockly *et al.* 2003; Butler and Bates 2006; Thomas *et al.* 2008), cardiac hypertrophy (Antos *et al.* 2003) and cystic fibrosis (Hutt *et al.* 2010). Therefore, there is ample evidence to propose the use of HDAC inhibitors to reverse *FXN* gene silencing as a potential FRDA therapy.

Recent studies using FRDA patient cell lines have suggested that common inhibitors targeting HDAC class I and II enzymes are generally not sufficient to reverse the downregulation of *FXN* (Herman *et al.* 2006 and see review Gottesfeld 2007). Therefore, in this study we have tested the efficacy of class III HDAC inhibitors such as sirtinol, splitomicin and nicotinamide, and the novel HDAC inhibitor, oxamflatin, as potential therapeutic approaches for FRDA. All of our preliminary cell culture experiments with these HDAC

inhibitors resulted in a significant increase in *FXN* expression in mouse and/or human fibroblasts.

We have shown that sirtinol increases *FXN* mRNA expression in mouse and human fibroblasts. In YG8 rescue mouse cells, the *FXN* expression was increased in a dose dependant manner. However, such an effect was not seen in human FRDA cell lines and this is probably due to the more number of GAA repeats (<450) in FRDA fibroblasts compared to YG8 rescue fibroblasts (>250). In human FRDA fibroblasts, increased *FXN* expression (~1.5-fold) was achieved only with 50µM concentration and this was again reduced to baseline levels with higher concentration (100µM) of drug. Surprisingly, the level of *FXN* expression in normal cell lines was increased by approximately 2-fold, with the lowest concentration (10µM) of sirtinol maintaining the same level throughout.

Like sirtinol, splitomicin also increased *FXN* expression significantly ($p<0.05$) in mouse cell lines, displaying an almost linear dose-response relation. With WT and human normal fibroblasts, no detectable changes in *FXN* expression were found between drug-treated and vehicle-treated samples. Importantly, no cell toxicity was found at any concentration tested with both sirtinol and splitomicin, suggesting a safe administration of these compounds. However, to confirm that the observed effect in *FXN* expression is due to solely to Sirt1 inhibition, future RNA interference-mediated knockdown of the *Sirt1* gene in FRDA cells could be investigated.

The exact mechanism by which Sirt1 inhibitors leads to increased *FXN* expression is unknown. Since most Sirt1 inhibitors do not require DNA replication to be effective, these compounds may have a better therapeutic potential than DNA demethylating agents in increasing *FXN* expression in neurons, which no longer divide and where *FXN* expression is

more essential. The controversial role of Sirt1 activity is a hindrance to finding the exact mechanism of how Sirt1 inhibition upregulates *FXN* expression and thereby could be used to reverse FRDA pathology. Indeed, a large number of studies using pharmacological and/or genetic manipulation of Sirt1 activity have revealed that Sirt1 activation, rather than inhibition, could be a general neuroprotective outcome. Thus, resveratrol, a Sirt1 activator, has displayed beneficial effects in various *in vitro* and *in vivo* models of central nervous system (CNS) neuron death and degeneration (Kiziltepe *et al.* 2004; Kaplan *et al.* 2005; Tsai *et al.* 2007). As explained earlier, Sirt1 inhibitors have also been shown neuroprotective effect. These conflicting results leave us with an apparently irreconcilable paradox of how the Sirt1 activators and inhibitors are both able to ameliorate the neurodegeneration in certain neurodegenerative disorders. However, recent studies of resveratrol have clearly indicated that resveratrol is not a direct activator of Sirt1, but does increase AMPK activity (Dasgupta and Milbrandt 2007; Beher *et al.* 2009; Tang 2010). Furthermore, it has been reported that AMPK enhances Sirt1 activity indirectly by increasing cellular NAD^+ levels (Canto and Auwerx 2009; Canto *et al.* 2009).

Although sirtinol and splitomicin have produced increased *FXN* expression, these expression levels were either non-statistically significant or just above the significance levels. Therefore, we investigated the effect of nicotinamide using our novel cell culture system and we found encouraging results. Treatment of mouse and human fibroblast cells with 10mM nicotinamide for 72 hours successfully upregulated *FXN* expression by ~2-fold in YG8 mouse and FRDA fibroblasts. Interestingly, no differences in *FXN* expression were detected in the normal fibroblasts suggesting that nicotinamide exhibits a specific effect in FRDA cells. However, the use of such a high concentration of nicotinamide may be a major disadvantage

in using this drug for FRDA therapy. In the present study, the specific mechanism whereby nicotinamide enhances *FXN* expression remains to be determined. A recent study has shown that physiological concentrations of nicotinamide noncompetitively inhibit Sirt1 *in vitro,* suggesting that nicotinamide is a physiologically relevant regulator of Sirt1 enzymes (Bitterman *et al.* 2002). In addition, nicotinamide, as precursor of NAD synthesis, acts to maintain NAD^+ levels and the bioenergetics state of neurons.

The other HDAC inhibitor used in this study, oxamflatin, also showed interesting results, especially in the mouse cell lines. 100nM oxamflatin significantly ($p<0.05$) increased *FXN* mRNA expression by approximately 150% and this level dropped to 86% and 73% with 50nM and 500nM of drug, respectively. This indicates that the ideal concentration to stimulate *FXN* expression seems to be 100nM. On the other hand, oxamflatin did not show any effect on FRDA human cell lines. However, a non-specific effect of oxamflatin was identified in human normal cells, where it significantly increased the *FXN* mRNA expression levels by almost 2-fold compared with vehicle.

HDAC inhibitors are believed to act by increasing global histone acetylation and thereby reactivating epigenetically silenced genes. However, the accumulation of recent epigenetic studies has revealed that certain HDAC inhibitors have also been reported to decrease histone acetylation and down-regulate genes (Rada-Iglesias *et al.* 2007). Thus, HDAC inhibitors can both increase and decrease gene transcription (Drummond *et al.* 2005; Reid *et al.* 2005; Rai *et al.* 2008), and this may include up-regulation of certain HDACs themselves (Reid *et al.* 2005).

Recent studies of Sirt1 have revealed that it also deacetylates the peroxisome proliferator-activated receptor gamma (PPAR-γ) (Picard *et al.* 2004) and its transcriptional coactivators PPAR-γ coactivator-1α (PGC-1α) (Nemoto *et al.* 2005; Rodgers *et al.* 2005; Lagouge *et al.* 2006), which regulate a wide range of metabolic activities. Furthermore, in a recent study using human fibroblasts it was revealed that PGC-1α expression was downregulated when the *FXN* expression was specifically inhibited by *sh*RNA (Coppola *et al.* 2009) and vice versa (Marmolino *et al.* 2010). This indicates the likelihood that a direct mechanism may exist between PGC-1α and *FXN* expression. In addition, increased *FXN* expression was achieved by the treatment of PPAR-γ agonist compounds in FRDA cells (Marmolino *et al.* 2009). In this scenario, consistent with our data, it has been suggested that Sirt1 inhibitors such as sirtinol, splitomicin and nicotinamide presumably increase acetylation of PGC-1α by inhibiting Sirt1 activity, thereby increasing the PGC-1α function, which in turn can increase *FXN* expression.

However, there are significant barriers to using Sirt1 inhibitors for FRDA therapy. Firstly, the yeast Sir2p protein, a homologue of Sirt1, extends the life span in yeast (Kaeberlein *et al.* 1999) raising the concern that inhibition of Sirt1 may shorten the lifespan in humans. In contrast, Chua *et al*. (2005) has showed that Sirt1 actually limits the life span in mammals in response to genotoxic stress. In addition, it could be possible that HDAC inhibition may lead to inappropriate expression of other genes, which may be quite deleterious.

Recently, high throughput chromatin immunoprecipitation (ChIP) experiments have shown that HDAC inhibitors can, somewhat surprisingly, elicit decreases of histone acetylation rather than the expected increases of histone acetylation (Rada-Iglesias *et al.*

2007). Although we have not yet quantified the frataxin protein levels following treatment(s) with HDAC inhibitors, it was clear that certain HDAC inhibitors have also been able to increase protein levels by enhancing stability (Garbes *et al.* 2009) or conversely decrease protein levels by suppressing translation (Kawamata *et al.* 2007). Furthermore, HDAC inhibitors also have the capability of affecting the acetylation status of non-histone proteins including transcription factors and transcription co-regulators (Butler and Bates 2006). Further studies will be required to uncover any such mechanisms of action of Sirt1 inhibitors with regard to frataxin expression.

So far, our analysis of HDAC inhibitors has focused on their potential to upregulate *FXN* mRNA expression. Therefore, future investigations should be performed to characterize the potential effects of HDAC inhibitors at the post-transcriptional level and their effect on local histone modifications in the *FXN* gene. To begin with, frataxin protein quantification and ChIP analysis using antibodies specific for individual histone modifications (e.g. H3K9ac, H4K12ac, H4K16ac and H3K9me3) should be performed. DNA methylation alterations, as secondary effects, should also be considered either by “bisulfite sequencing” or “methylscreen” approaches.

In conclusion, all of our results clearly confirm that HDAC inhibitors are able to upregulate the *FXN* expression, particularly nicotinamide. Therefore, a future *in vivo* study with nicotinamide will be performed to monitor the efficacy of such compounds in long term studies. Although we obtained some encouraging results with human fibroblasts using HDAC inhibitors, the *FXN* levels did not seem to be increased as high as they were in mouse cells. Therefore, to investigate the upregulation of *FXN* expression in human cell lines more

efficiently, further studies are in progress using drug concentrations on either side of the optimal concentration found in mouse fibroblasts.

Finally, the GAA repeat sizes within our mouse cells are comparatively small (90 to 200) and longer GAA repeats in FRDA patients are associated with a more severe phenotype and greater histone modifications (Saveliev *et al.* 2003; Rai *et al.* 2008; Soragni *et al.* 2008). Therefore, for future *in vivo* or *in vitro* studies the use of a model containing larger GAA repeats is of paramount importance and this will hopefully be achieved soon in our laboratory as studies are ongoing to develop such an FRDA model.

Chapter 5 - Therapeutic approaches *in vivo*

5.1 - RGFA 136 therapeutic testing in FRDA mice

5.1.1 - Introduction

It is essential to understand the mechanism of GAA-induced inhibition of *FXN* gene transcription for the consideration of future FRDA therapy. Previous studies have implicated epigenetic changes, including increased DNA methylation of specific CpG sites upstream of the GAA repeat and histone modifications in regions flanking the GAA repeat that are both consistent with transcription inhibition (Herman *et al.* 2006; Greene *et al.* 2007). HDAC inhibitors are a structurally diverse group of compounds that are believed to act by increasing global histone acetylation and thereby reactivating epigenetically silenced genes, although some HDAC inhibitors have been reported to decrease histone acetylation and down-regulate genes (Rada-Iglesias *et al.* 2007). Thus far HDAC inhibitors have primarily been used in the treatment of various human cancers (Monneret 2005; Cang *et al.* 2009; Prince *et al.* 2009).

We have generated a GAA repeat expansion mutation-based mouse model of FRDA in a null mouse frataxin background, designated YG8 (Al-Mahdawi *et al.* 2006). Although the YG8 mice do not appear to show any marked reduction of *FXN* mRNA or frataxin protein compared to wild type mice, they show decreased frataxin mRNA and protein levels compared to Y47 mice that contain a normal-sized GAA *FXN* transgene (Al-Mahdawi *et al.* 2008). Furthermore, YG8 mice also display progressive functional FRDA-like deficits, including impaired coordination ability, together with biochemical and histopathological features consistent with FRDA (Al-Mahdawi *et al.* 2006). In addition, YG8 rescue mice exhibit an FRDA-like molecular disease phenotype that includes intergenerational and somatic instability of the GAA repeat expansion mutation (Al-Mahdawi *et al.* 2004; Clark *et al.* 2007),

together with increased DNA methylation, reduced histone H3 and H4 acetylation and increased di- and trimethylated H3K9 at the *FXN* upstream GAA region (Al-Mahdawi *et al.* 2008). Therefore, we consider YG8 mice to be a suitable mouse model in which to investigate potential FRDA therapies.

Although encouraging results have been obtained using HDAC inhibitors *in vitro* by ourselves (in chapter 4) or others (Herman *et al.* 2006), and *in vivo* pilot studies (Rai *et al.* 2008; Rai *et al.* 2010) using mouse models (KIKI), the lack of long-term studies has been a drawback in understanding the long-term efficacy of these compounds. Therefore, initial long term studies were performed on our FRDA YAC transgenic mice with the class I HDAC inhibitor 106. After the 106 treatment period, we observed increased histone H3 and H4 acetylation in brain, consistent with the previous observation in acute FRDA KIKI mouse studies (Rai *et al.* 2008) that 106 can cross the blood-brain barrier to exert its effect. In addition, we identified general 106-induced increases in brain frataxin expression, together with improved motor coordination performance, both beneficial effects for FRDA therapy (R. Mouro Pinto, PhD thesis).

Recent investigations have determined that 106 has a slow and potent inhibitory effect on class I HDACs, particularly on HDAC3 (Chou *et al.* 2008). Thus it is possible that specific inhibition of HDAC3 may have a significant impact on the expression of many genes other than *FXN.* Therefore, novel formulations of 106 are currently being developed in order to improve the specificity and potency (Hu *et al.* 2009). As a result, two derivatives of 106, designated RGFA 136 and RGFP 109, have recently been generated and subsequently used in our FRDA YAC transgenic mice.

5.1.2 - Materials and methods

5.1.2.1 - RGFA 136 structure and drug preparation

RGFA 136, *N*-(6-(2-amino-4-fluorophenylamino)-6-oxohexyl)-4-methylbenzamide, is a novel pimelic diphenylamide compound and structurally similar to HDAC inhibitor 106 (Figure 5.1).

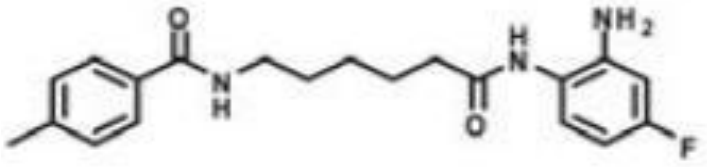

Figure 5.1 - Chemical structure of RGFA 136

The IC_{50} and K_i values of RGFA 136 as determined by purified recombinant HDAC enzymes with a fluorescent substrate indicated that the IC_{50} values of RGFA 136 for HDAC1 and HDAC3 are 1.14µM and 560nM, respectively (Rai *et al.* 2010). The K_i (dissociation constant) values of RGFA 136 were expressed as a ratio of HDAC1/HDAC3 activity and mentioned in Table 5.1. RGFA 136 was synthesized and made available to us by Repligen Corporation (USA). The drug was provided in the form solid HCl powder and stored at -80°C until required to use.

Table 5.1 - Kinetic properties of RGFA 136

IC_{50} HDAC1	1.14µM
IC_{50} HDAC3	560nM
K_i HDAC1	630nM
K_i HDAC3	196nM

5.1.2.2 - Formulation of the drug

All the drug formulations were carried out according to the manufacturers' recommendations and were freshly prepared in a weekly basis. Initially, 200mg of RGFA 136 was weighed and resuspended in 1 ml of DMSO (prewarmed at 37°C). Then, the required amount of diluent (20% glycerol, 20% PEG 400, 20% propylene glycol and 100mM acetate buffer) was added to the solution to make a final volume of 20ml drug solution (10mg/ml stock). A placebo/vehicle solution was also prepared in the same way by mixing 1ml of DMSO and 19ml of diluent without drug. Both drug and vehicle solutions were stored at 4°C.

5.1.2.3 - Study design: drug administration and sample collection

A long term study with RGFA 136 was performed on WT and YG8 rescue mice. The average ages of the mice subjected to this treatment were 3-4 months of old. 10 WT mice and 20 YG8 rescue mice were used in each group (vehicle and drug) (Table 5.2) and all the mice were matched to their age, sex and initial functional studies. RGFA 136 (50mg/kg/d and 150mg/kg/d) has previously been administered subcutaneously to KIKI mice in a pilot study without any toxic effects (Rai *et al.* 2010). We wanted to determine if this lack of acute toxicity could be maintained throughout a long-term RGFA 136 dosing regimen. Therefore, we injected the mice with 50mg/kg RGFA 136 (10mg/ml) 5 times per week. A corresponding volume of vehicle solution was administered to the control group of mice. Such long-term administrations of 50mg/kg RGFA 136 were well tolerated. No overt toxicity was observed in any of the mice given subcutaneous dosing throughout the entire 5-month period of this study.

After treatment, several tissues were collected from the drug- and vehicle-treated mice for molecular biology, biochemistry and histological analysis. It is important to note that the whole RGFA 136 study was repeated to validate our findings and very consistent results were obtained (see appendix B).

Table 5.2 - Long term Study design of RGFA 136 in WT and YG8 rescue mice

Group	Genotype	Male	Female
Vehicle	WT	5	5
	YG8 R	10	10
RGFA 136 - 50mg/kg	WT	5	5
	YG8 R	10	10

5.1.3 - Results

5.1.3.1 - Functional studies during the drug treatment

Functional studies such as weight, rotarod, locomotor and beam breaker measurements were taken just before the start of the drug treatment and were repeated on a monthly basis until completion of the treatment. All procedures were carried out in accordance with the UK Home Office 'Animals (Scientific Procedures) Act 1986'. The analysis of functional data was measured as fold change taking the initial value as 1 (Table 5.3).

Table 5.3 - Absolute values of functional data (RGFA 136).

Parameter	Group	Initial Value	Final Value
Weight (g)	WT vehicle	27.4	34.9
	WT RGFA 136	26.6	33.4
	YG8 Vehicle	27.3	33.3
	YG8 RGFA 136	26.0	30.8
Rotarod (s)	WT vehicle	284	276
	WT RGFA 136	293	331
	YG8 Vehicle	269	231
	YG8 RGFA 136	270	280
Locomotor (no. squares in 30s)	WT vehicle	N/A	N/A
	WT RGFA 136	N/A	N/A
	YG8 Vehicle	9.60	8.70
	YG8 RGFA 136	9.50	10.90
Average velocity (cm/s)	WT vehicle	21.20	21.38
	WT RGFA 136	21.81	23.35
	YG8 Vehicle	21.55	21.15
	YG8 RGFA 136	21.49	24.42
Ambulatory distance (cm)	WT vehicle	527.11	366.96
	WT RGFA 136	628.84	411.95
	YG8 Vehicle	516.42	301.17
	YG8 RGFA 136	518.00	411.87
Vertical counts	WT vehicle	16.20	12.00
	WT RGFA 136	23.85	9.25
	YG8 Vehicle	14.85	6.10
	YG8 RGFA 136	16.05	16.87

Weight analysis

At the start of drug treatment, vehicle and drug-treated mice showed similar weight distributions. However, considerable differences were noticed between the vehicle and drug-treated YG8 mice over time (Figure 5.2), but no obvious differences were detected in between vehicle-treated and drug-treated WT mice. Two-factor ANOVA with replication analysis confirmed that the age of the mice (time point) had a significant effect on the weight gain on both WT ($F=6.1$, $p<0.001$) and YG8 mice ($F=6.3$, $p<0.001$). However, a significant drug-induced effect (treatment) over the time point was identified in the YG8 mice ($F=5.01$, $p=0.02$) (Table B.1).

Subsequently, the difference in male and female weight gain/loss was also analysed within each group (Figure 5.3). Body weight analysis of male and female mice by two way ANOVA confirmed that the age of the mice (time point) and treatment effect was significantly different in both the YG8 male ($F=10.7$, 9.3, $p<0.001$ and $p<0.002$) and YG8 female mice ($F=8.4$, 3.8, $P<0.001$ and $p=0.05$). However, the WT male and female mice only displayed a significant effect with time point ($F=18.4$, 9.5, both $p<0.001$) (Figure 5.3A-B), but not with treatment, suggesting a specific effect of RGFA 136.

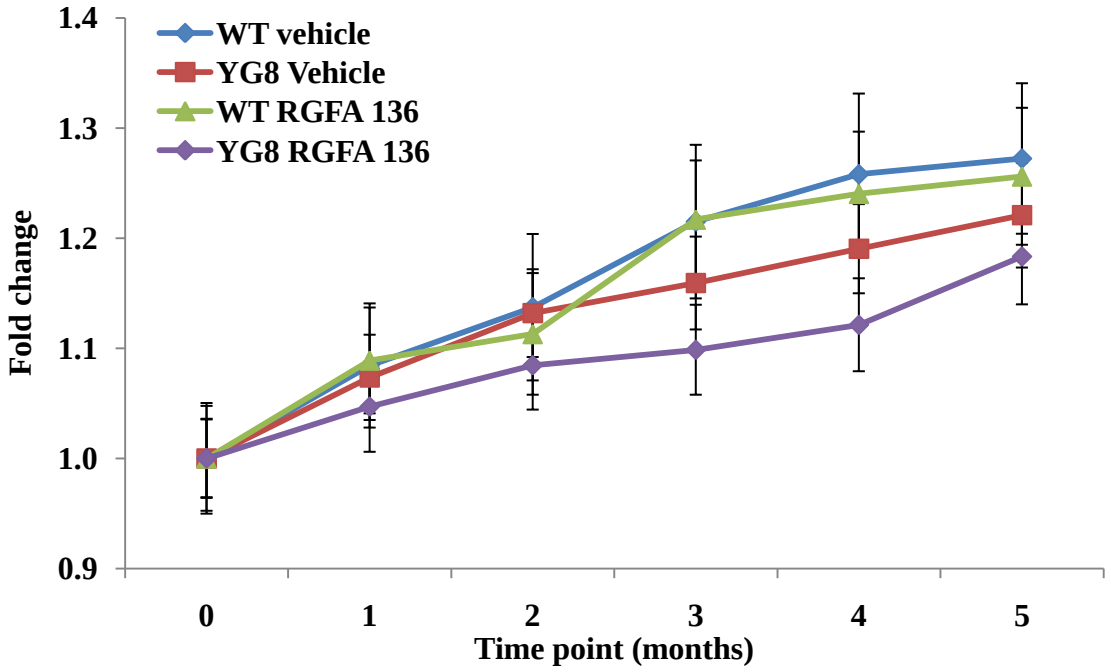

Figure 5.2 - Body weight analysis during treatment with RGFA 136 in WT and YG8 rescue mice showing vehicle and drug-treated groups (error bars represents SEM).

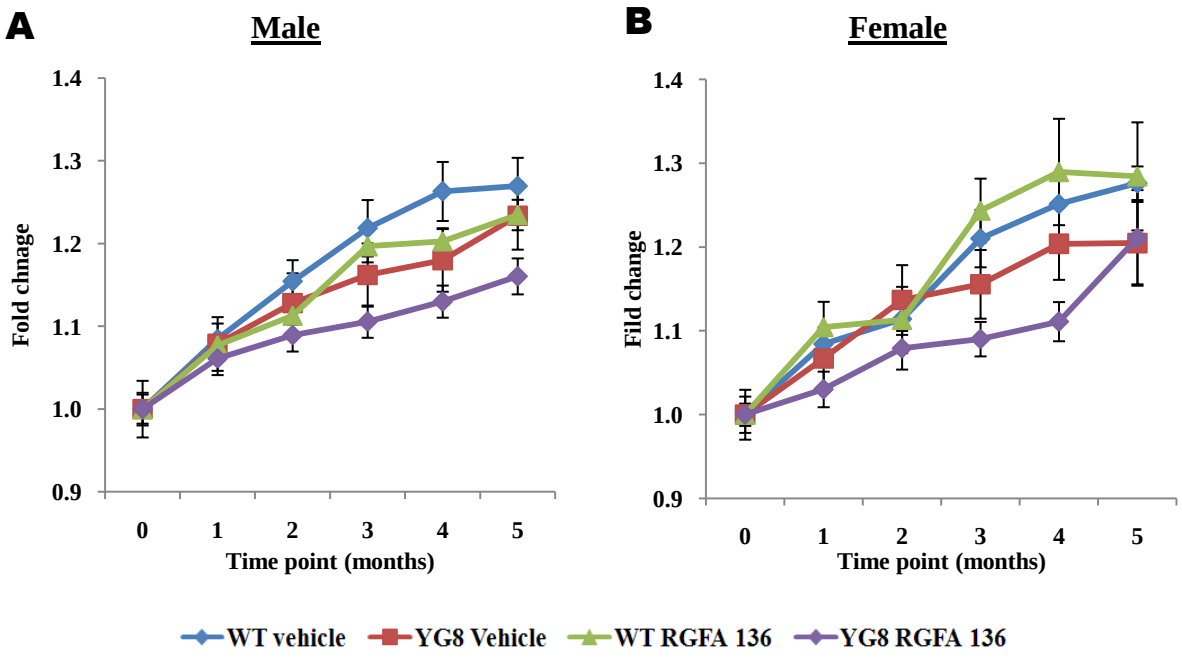

Figure 5.3 - Body weight analysis of male and female mice during treatment with RGFA 136. The average fold changes of weight in **A)** male and **B)** female WT and YG8 rescue mice are shown (error bars represents SEM).

Rotarod analysis

The motor coordination performances of both WT and YG8 mice were determined by change in rotarod performance (fold change) at time points throughout the treatment period. Up to the 2-month time point, no detectable changes were observed between YG8 vehicle and RGFA 136-treated mice. After this time, drug-treated YG8 mice showed a significant improvement in rotarod performance, compared to vehicle group (F=9.09, p=0.002) (Figure 5.4). Although performance then slightly declined, the RGFA 136-treated mice always performed better than the vehicle-treated controls. The similar effect was also observed between WT vehicle and drug-treated mice, with exceptions that the significant differences were found from the beginning (at 1 month) of the experiment and maintained throughout.

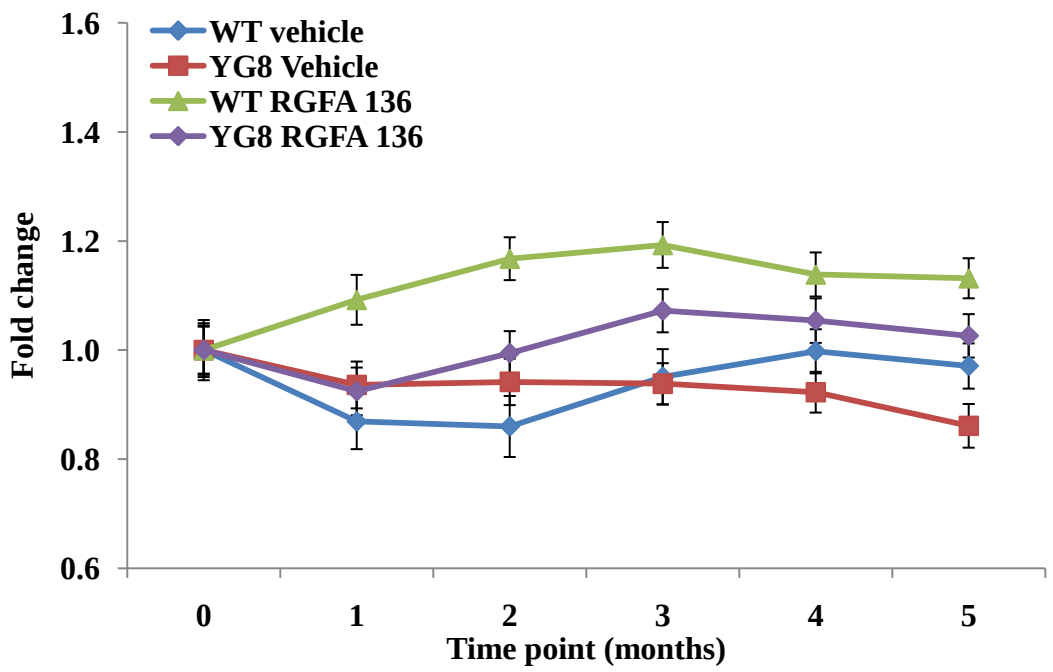

Figure 5.4 - Rotarod analysis during treatment with RGFA 136 in WT and YG8 rescue mice showing mean fold change values of vehicle and drug-treated groups (error bars represents SEM).

Both WT and YG8 vehicle groups showed a similar rotarod performance with interchangeable values. Somewhat surprisingly, the rotarod performance of WT vehicle-treated mice slightly declined (but not significantly) at some time points compared to YG8 vehicle group. In fact, although the age of the mice (time point) produced a significant increase in rotarod performance over 5 month time point, a significant genotype effect (WT vs YG8) was observed in mice treated with RGFA 136 ($F=22$, $p<0.001$), but not in the vehicle-treated mice (Table B.2).

The possible differences between male and female mice within each group were then analysed and a significant gender effect on rotarod performance was detected. In the male mice, continual decline of rotarod performance in both vehicle-treated WT and YG8 mice was detected across time. However, treatment with RGFA 136 not only ameliorated the decline, but actually induced an initial improvement in rotarod performance at the 2-month time point, and the maximum rotarod performance (1.3-fold, $p<0.001$) was observed at the 3-month time point in both WT and YG8 mice (Figure 5.5A). Although rotarod performance then slightly declined, significant changes were maintained between vehicle and RGFA 136-treated mice throughout the treatment.

In contrast, female YG8 vehicle-treated mice had a much worse rotarod performance compared to the female WT vehicle group, indicating a specific disease effect in the YG8 female mice (Figure 5.5B). Two way ANOVA confirmed a significant gender effect on rotarod performance between WT ($F=9.3$, $p<0.002$) and YG8 mice ($F=53.9$, $p<0.001$) (Table B.5). In contrast, no major changes were observed between vehicle and RGFA 136-treated female WT and YG8 mice, indicating that there was little drug effect on these female mice.

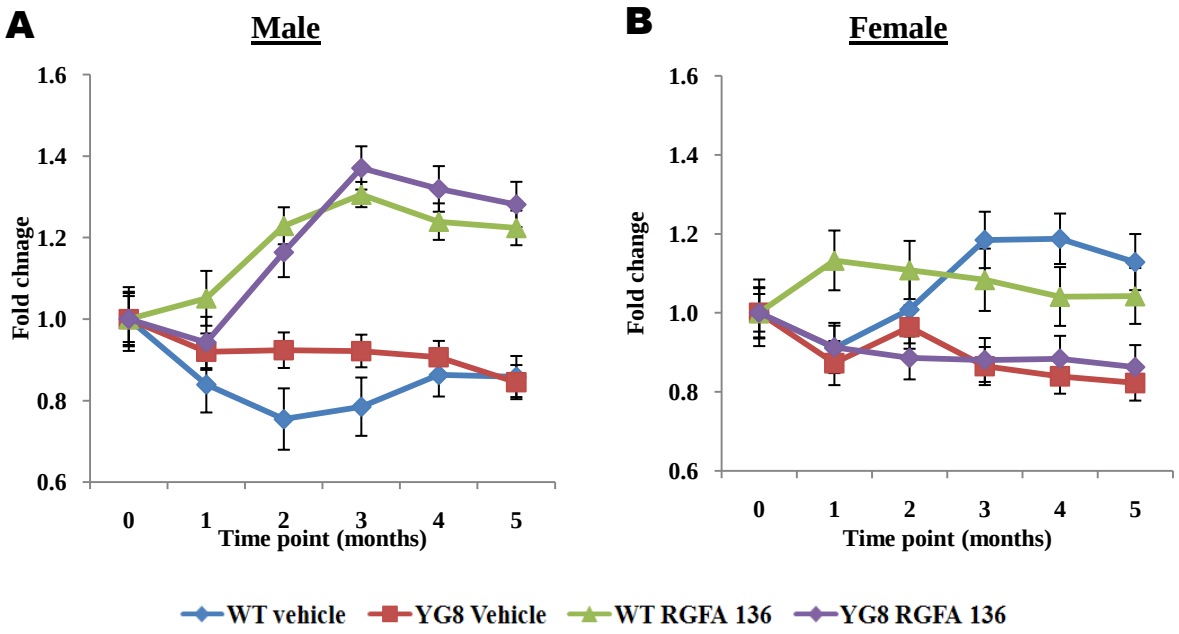

Figure 5.5 - Rotarod analysis of male and female mice during treatment with RGFA 136. The average fold changes of rotarod performance in **A)** male and **B)** female WT and YG8 rescue mice are shown (error bars represents SEM).

Locomotor analysis

Locomotor activity analysis was performed only with YG8 mice for a direct comparison with previous RGFA 136 long-term studies, which did not contain any WT mice. Analysis confirmed significant increases in locomotor activity in the RGFA 136-treated YG8 mice compared to vehicle-treated mice ($F=17.7$, $p<0.001$) (Figure 5.6). Especially from the 2-month time point, RGFA 136-treated mice displayed a significant effect on locomotor performance and this persisted throughout the experiment.

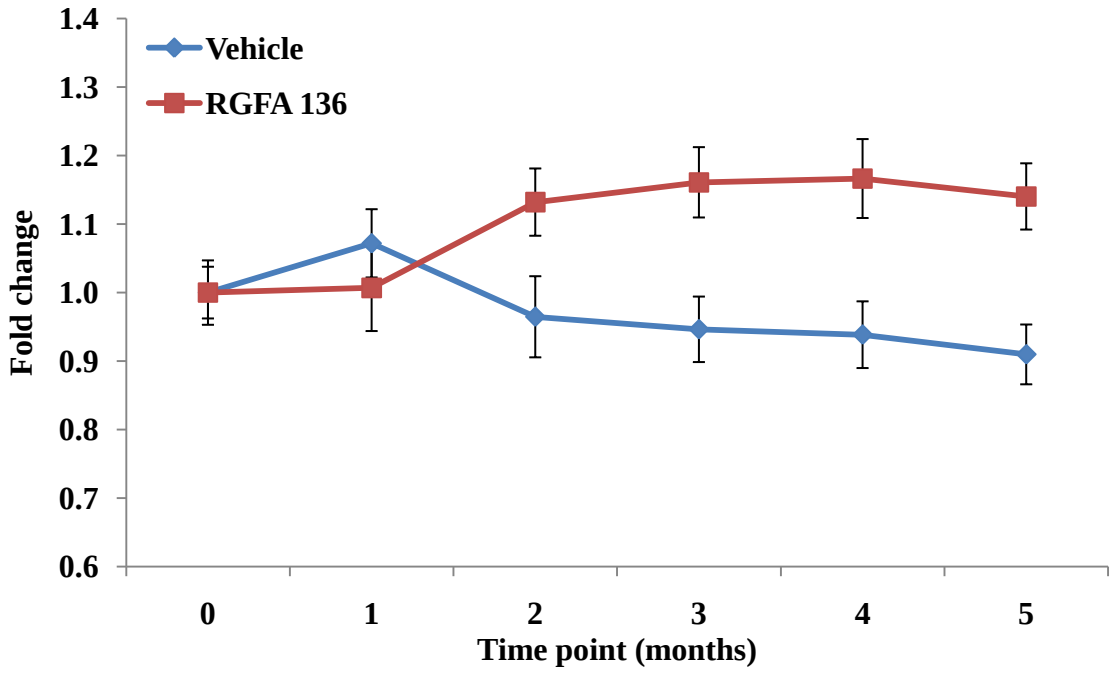

Figure 5.6 - Locomotor activity analysis during treatment with RGFA 136 in YG8 rescue mice showing mean fold change values of vehicle and drug-treated groups (error bars represents SEM).

Interesting results were found with male and female mice segregation analysis (Figure 5.7). RGFA 136 had a more significant effect on locomotor activity in male mice ($F=14.3$, $p<0.001$) than female mice ($F=5.8$, $p=0.016$), compared to vehicle-treated mice.

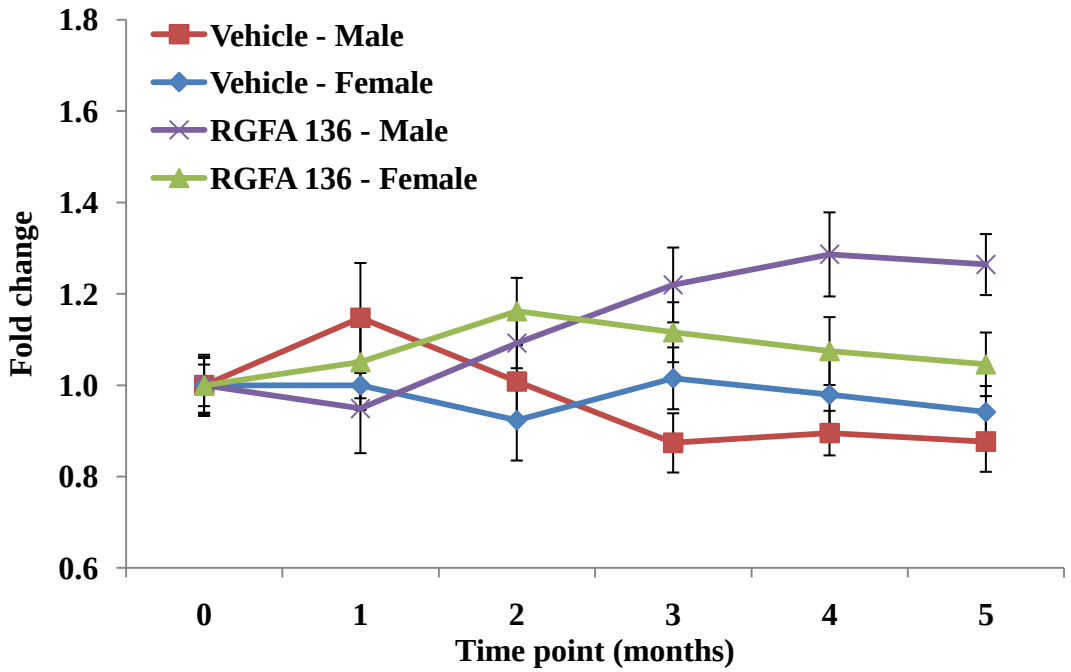

Figure 5.7 - Locomotor activity analysis of male and female mice during treatment with RGFA 136. The average fold changes of activity in male and female YG8 rescue mice are shown (error bars represents SEM).

5.1.3.2 - Open-field activity monitor

All mice were subsequently analysed by using a more precise and sophisticated method for effective monitoring of the functional data, called 'open-field activity monitor' or 'beam-breaker'. By using open-field activity monitor functional measurements, such as average velocity, ambulatory distance and vertical counts of the mice were examined.

Average velocity

The average velocity is defined as 'the total distance covered divided by the total time elapsed'. This can be expressed either by meters per second (m/s) or inches/s. The average velocity was calculated by using beam breaker apparatus as mentioned earlier (section 2.5).

In general, the average velocity was significantly improved throughout the study in YG8 RGFA 136-treated mice ($F=28.9$, $p<0.001$) compared to WT vehicle control mice (Figure 5.8), suggesting a specific effect of RGFA 136 in YG8 mice. Although RGFA 136-treated WT mice performed better than the vehicle-treated WT mice, no statistical significant difference was observed at any time point tested compared to YG8 RGFA 136-treated mice.

The gender specific analysis of average velocity showed that RGFA 136-treated YG8 male and female mice showed an overall increased performance across the time compared to their respective vehicle-treated YG8 mice ($F=15$, 12.7, both $p<0.001$) (Figure 5.9A-B). In addition, two way ANOVA also confirmed that the genotype had a significant effect on average velocity (Table B.7-B.9).

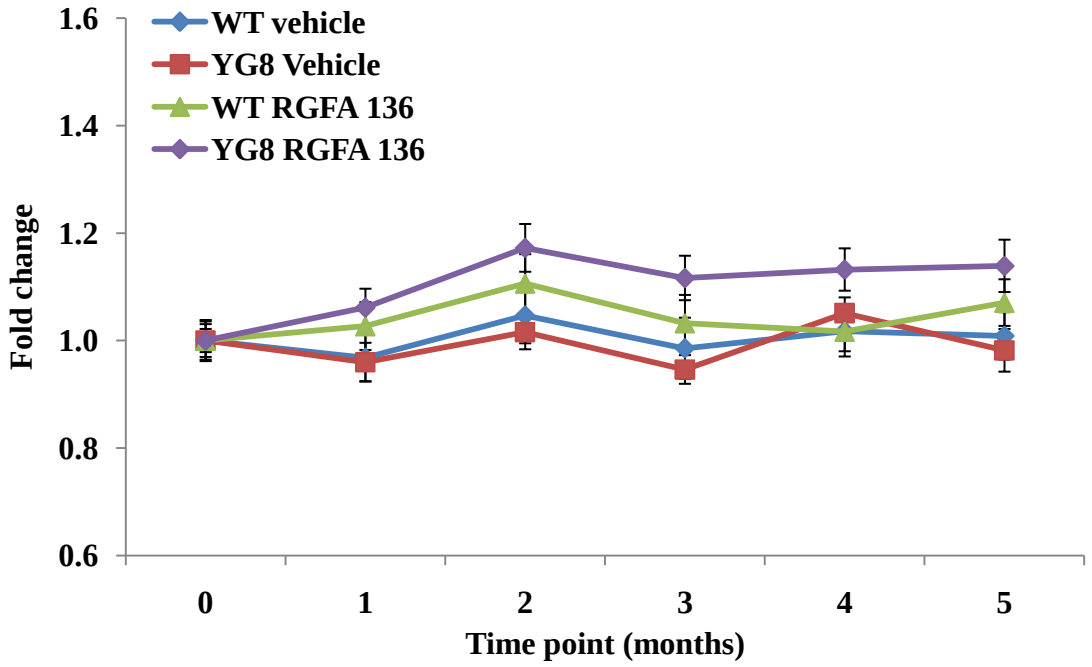

Figure 5.8 - Average velocity analysis during treatment with RGFA 136 in WT and YG8 rescue mice showing vehicle and drug-treated groups (error bars represents SEM).

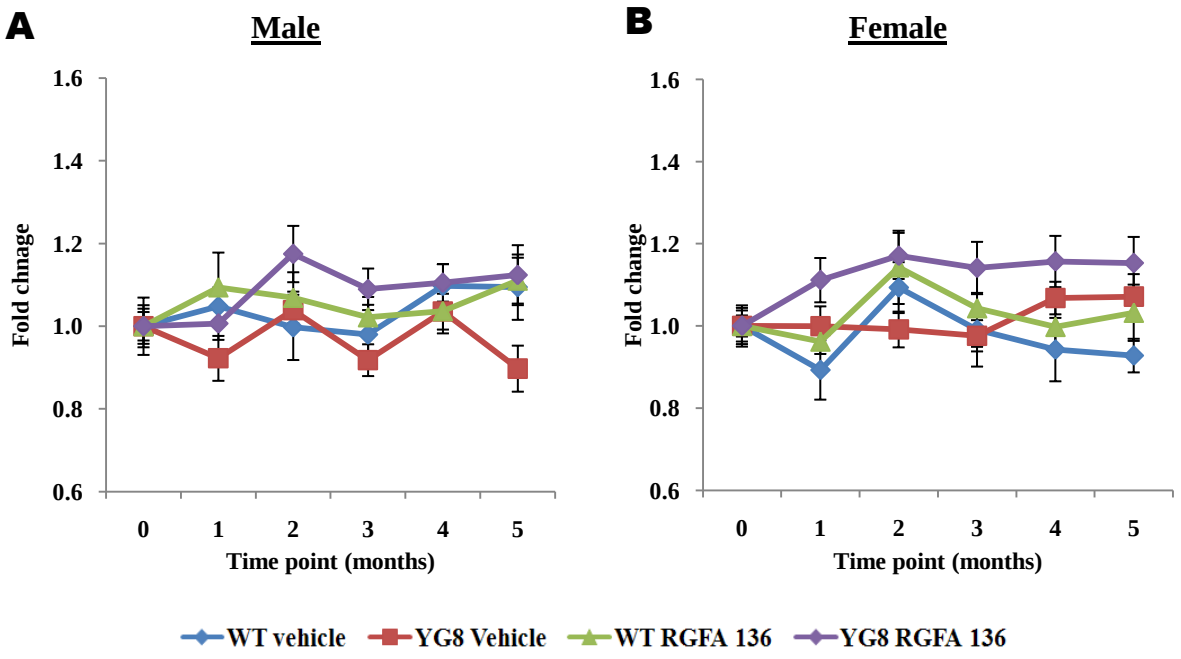

Figure 5.9 - Average velocity analysis of male and female mice during treatment with RGFA 136. The average fold changes of average velocity in **A)** male and **B)** female WT and YG8 rescue mice are shown (error bars represents SEM).

Ambulatory distance

Ambulatory distance is the total distance covered by the mice within a specific time, expressed in terms of centimetres (cm). Regarding ambulatory distance, two factor ANOVA analysis revealed a significant increase in ambulatory distance in RGFA 136-treated YG8 mice ($F=13.5$, $p<0.001$) from the 2-month time point and persisting throughout the treatment, compared to vehicle-treated YG8 mice (Figure 5.10). Interestingly, no difference in ambulatory distance was identified between the drug-treated and vehicle-treated WT mice, suggesting a specific effect of RGFA 136 on YG8 mice.

Subsequently, the effects of RGFA 136 on separate groups of male or female mice were analysed. Although male and female drug-treated YG8 mice showed better ambulatory distance compared to the vehicle-treated mice, significantly improved ambulatory distance was mainly seen in female mice ($F=15.2$, $p<0.01$) (Figure 5.11A).. However, none of these mice sustained their initial perform. A similar effect was also displayed by the WT mice. RGFA 136-treated WT female mice showed a constant decline in ambulatory distance compared to vehicle-treated WT mice (Figure 5.11B). Although the age of the mice (time point) had a significant effect on the ambulatory distance of both WT and YG8 mice ($p<0.001$), the drug-induced effect was mainly observed in the YG8 mice (genotype), suggesting a strong genotype effect on the performance.

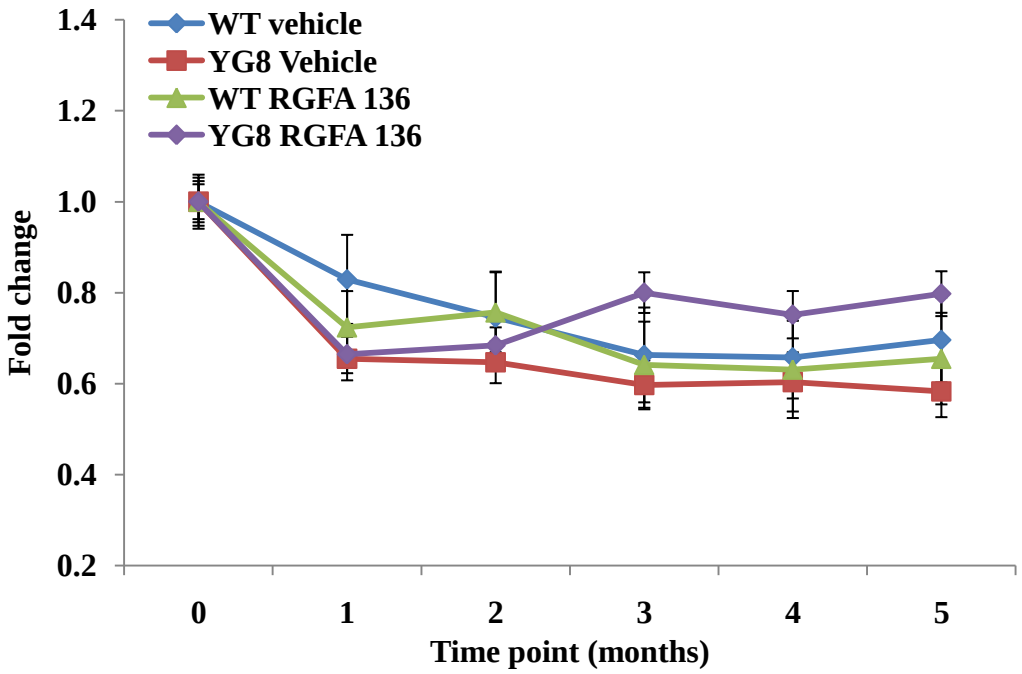

Figure 5.10 - Ambulatory distance analysis during treatment with RGFA 136 in WT and YG8 rescue mice showing vehicle and drug-treated groups (error bars represents SEM).

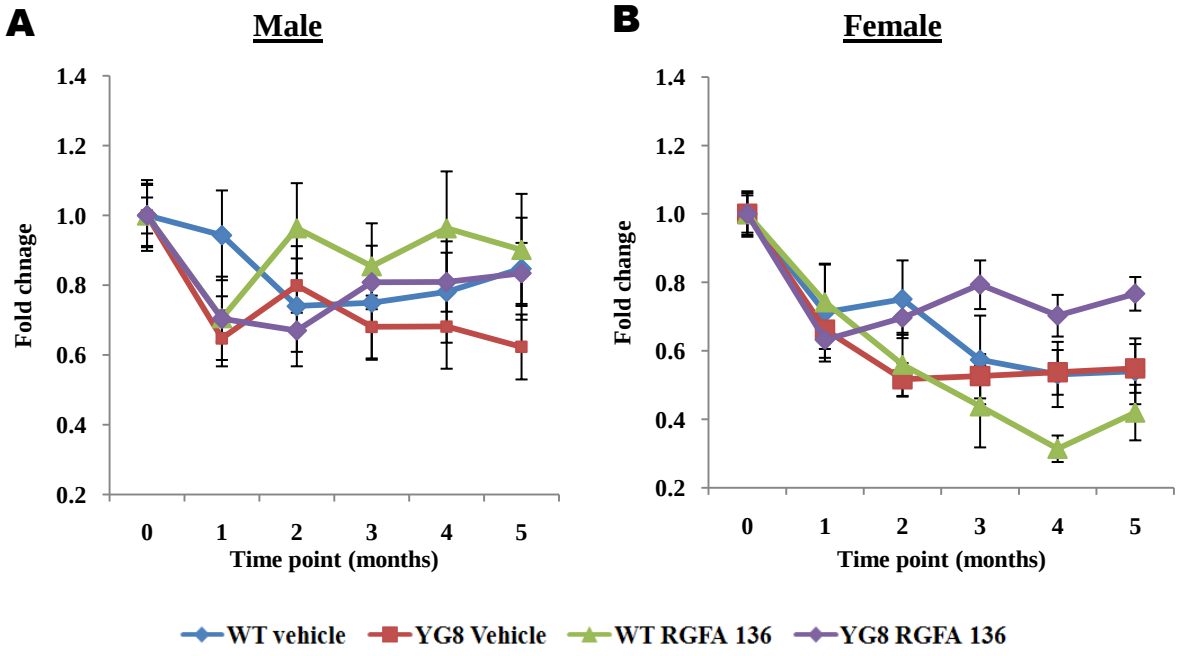

Figure 5.11 - Ambulatory distance analysis of male and female mice during treatment with RGFA 136. The average fold changes of ambulatory distance in **A)** male and **B)** female WT and YG8 rescue mice are shown (error bars represents SEM).

Vertical counts

The vertical counts are the continuous beam breaks reported by the 'Z' I/R array strips, which occurs when the mouse stands with the hind legs. A significant increase of vertical counts was detected in RGFA 136-treated YG8 mice ($F=67.3$, $p<0.001$) compared to YG8 vehicle-treated mice, and this effect was maintained throughout the treatment period. However, the greatest variability was found at the 3-month time point where RGFA 136-treated YG8 mice showed 3.2-fold increase ($p<0.001$) in vertical counts compared to vehicle group (Figure 5.12). Interestingly, the RGFA 136-treated WT mice showed a constant drop in vertical counts, even lower than the vehicle-treated WT mice. At the end of the treatment period, the vertical counts of RGFA 136-treated WT mice were reduced to 48%, compared to the WT vehicle-treated mice ($F=8.6$, $p=0.004$). However, the WT vehicle group always performed better than ($p<0.05$) the YG8 vehicle group.

The analysis of separate male and female groups of mice demonstrated significantly increased number of vertical counts in both male ($F=9.4$, $p=0.002$) and female ($F=78.2$, $p<0.001$) RGFA 136-treated YG8 mice, compared to their respective vehicle control mice (Figure 5.13A-B). In contrast, RGFA 136-treated WT male and female mice showed reduced number of vertical counts compared to the WT vehicle-treated mice, suggesting a specific effect of RGFA 136 on YG8 mice. The comparison between the male and female RGFA 136-treated WT mice has revealed that a significant drop in vertical counts was observed in the female mice compared to the male mice ($F=48.2$, $p<0.001$) (Table B.10).

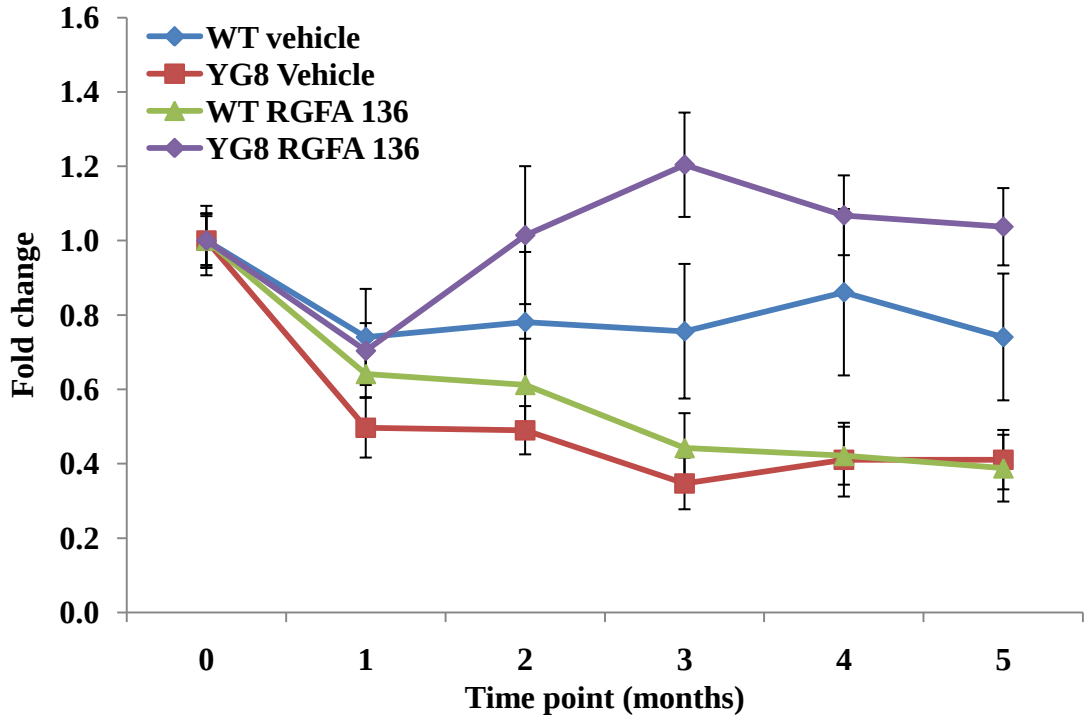

Figure 5.12 - Vertical count analysis during treatment with RGFA 136 in WT and YG8 rescue mice showing vehicle and drug-treated groups (error bars represents SEM).

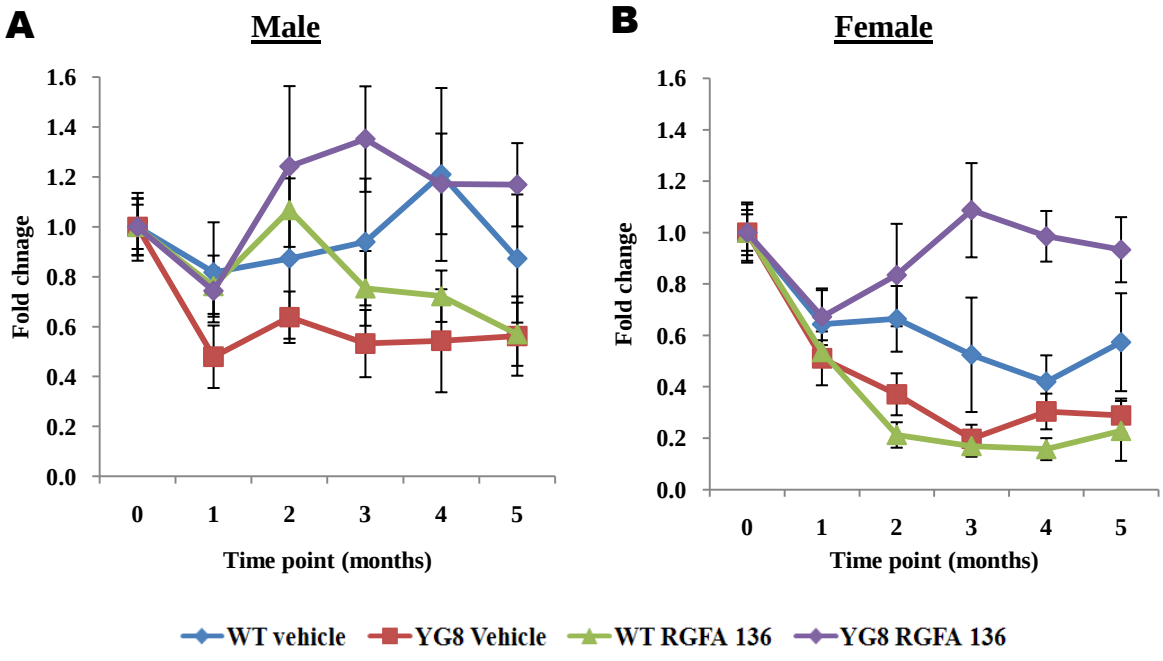

Figure 5.13 - Vertical count analysis of male and female mice during treatment with RGFA 136. The average fold change of vertical count in **A)** male and **B)** female WT and YG8 rescue mice are shown (error bars represents SEM).

5.1.3.3 - Investigation of *FXN* mRNA

Following treatment with RGFA 136, the levels of *FXN* mRNA expression were measured in brain, cerebellum, spinal cord and DRG of the drug-treated and vehicle-treated mice by QRT-PCR analysis. The relative *FXN* expression level was quantified using mRNA-specific primers for *FXN,* and mouse *Gapdh* was used as an endogenous control. Relative quantification values were determined by the $2^{-\Delta\Delta Ct}$ method using SDS 2.1 software (Applied Biosystems). Four mice from each group were used for the analysis (Table 5.4) and triplicate QRT-PCRs were performed for each sample. However, due to the limited availability of DRG, all of the DRGs from 4 mice were pooled and then subjected to the mRNA analysis.

Table 5.4 - Number of mice investigated for the *FXN* mRNA quantification

Group	Genotype	Brain	Spinal cord	DRG*	Cerebellum
Vehicle	WT	4	4	4	4
	YG8 R	4	4	4	4
RGFA 136 - 50mg/kg	WT	4	4	4	4
	YG8 R	4	4	4	4

*-Collective DRGs from 4 mice

The *FXN* QRT-PCR analysis following sub-cutaneous treatment with RGFA 136 in WT and YG8 mice revealed reduced *FXN* mRNA expression in the drug-treated WT mice compared to the vehicle-treated WT mice. Although the level of *FXN* expression was slightly reduced in the brain, spinal cord and cerebellum in RGFA 136-treated WT mice, significantly reduced level of *FXN* expression (23% lower than vehicle, $P<0.05$) was reported in the DRG (Figure 5.14). In contrast, *FXN* mRNA expression levels were slightly increased in all tissues

(except brain) from the RGFA 136-treated YG8 mice compared to the vehicle-treated mice. However, none of these increases reached a level of statistical significance (Figure 5.15).

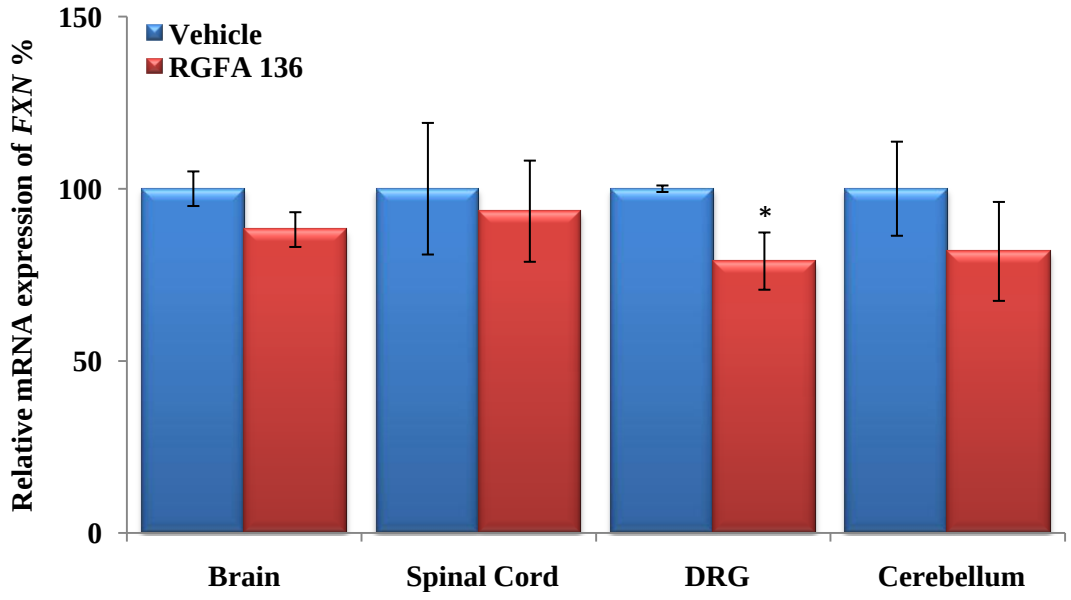

Figure 5.14 - Relative *FXN* mRNA levels in WT mice following treatment with RGFA 136 in brain, spinal cord, DRG and cerebellum (n=4, *p<0.05, error bars ± 1 SEM).

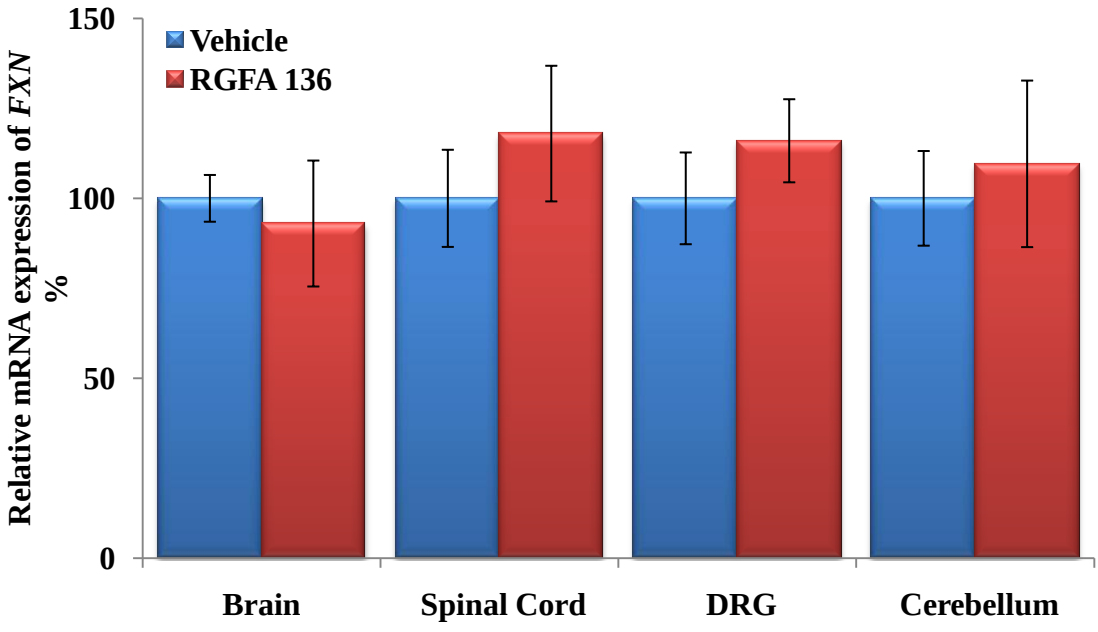

Figure 5.15 - Relative *FXN* mRNA levels in YG8 mice following treatment with RGFA 136 in brain, spinal cord, DRG and cerebellum (n=4, error bars ± 1 SEM).

5.1.3.4 - Investigation of frataxin protein

The comparative levels of human frataxin protein expression were determined from the brain tissues of WT and YG8 vehicle and RGFA 136 treated mice by western blot analysis (experiments were performed by Dr. Sahar Al-Mahdawi). The frataxin western blot analysis was carried out using an anti-frataxin rabbit polyclonal antibody (Santa Cruz) and the values were normalized to an anti-tubulin rabbit polyclonal antibody (Sigma). Densitometry was carried out using UN-SCAN-IT software (Silk Scientific Corporation) and in all cases n=4.

The western blot analysis revealed no difference in frataxin protein levels between the vehicle and drug-treated YG8 mice. However, somewhat unexpectedly, the frataxin protein levels were significantly increased (1.8-fold, $p<0.05$) in RGFA 136-treated WT mice compared to vehicle-treated mice (Figure 5.16), suggesting a non-specific effect of RGFA 136. Furthermore, reduced *FXN* mRNA expression associated with increased frataxin protein in RGFA 136-treated WT mice (Figure 5.14 and Figure 5.16) suggests that RGFA 136 may perhaps act at a post-transcriptional level and has limited activity at the transcriptional level.

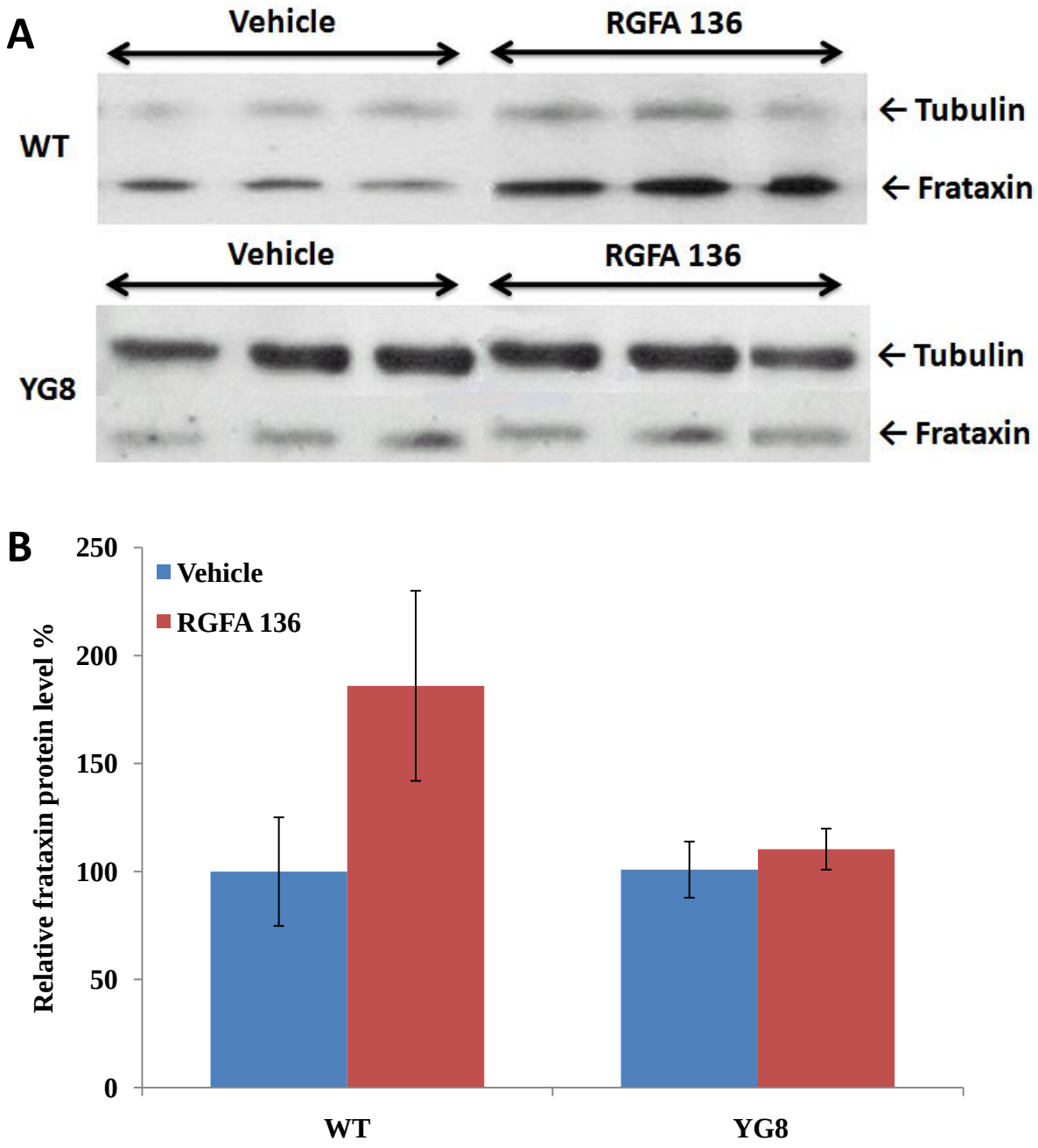

Figure 5.16 - Relative frataxin protein levels in brain tissues from WT and YG8 mice following treatment with RGFA 136. **A)** Western blot showing frataxin protein expression together with α-tubulin controls, and **B)** densitometry calculations of frataxin levels are shown for vehicle and RGFA 136-treated WT and YG8 rescue mice (n=3, error bars ± 1 SEM).

5.1.3.5 - Investigation of global histone acetylation changes

To examine the effects of chronic subcutaneous dosing of RGFA 136 on global histone acetylation within the brain tissue of WT and YG8 rescue mice throughout the treatment, H3 acetylation and H4 acetylation levels were determined by western blotting analysis (experiments were performed by Dr. Sahar Al-Mahdawi). Histone H3 and H4 acetylation levels were determined using anti-acetyl-histone H3 (Upstate) and anti-acetyl-histone H4 (Upstate) antibodies, respectively.

The analysis, which was carried out on four mice from each of vehicle and drug-treated groups, revealed no significant difference in H3 acetylated histone protein levels between the vehicle and RGFA 136-treated YG8 mice. However, in the WT mice reduced levels of acetylated H3 protein (81%) were observed in RGFA 136-treated mice compared to vehicle group. Regarding acetylated H4 protein, although no difference was seen between vehicle and drug-treated WT mice, H4 acetylated protein levels were significantly increased (32%, $p<0.05$) in the RGFA 136-treated YG8 samples compared to vehicle-treated YG8 mice (Figure 5.17).

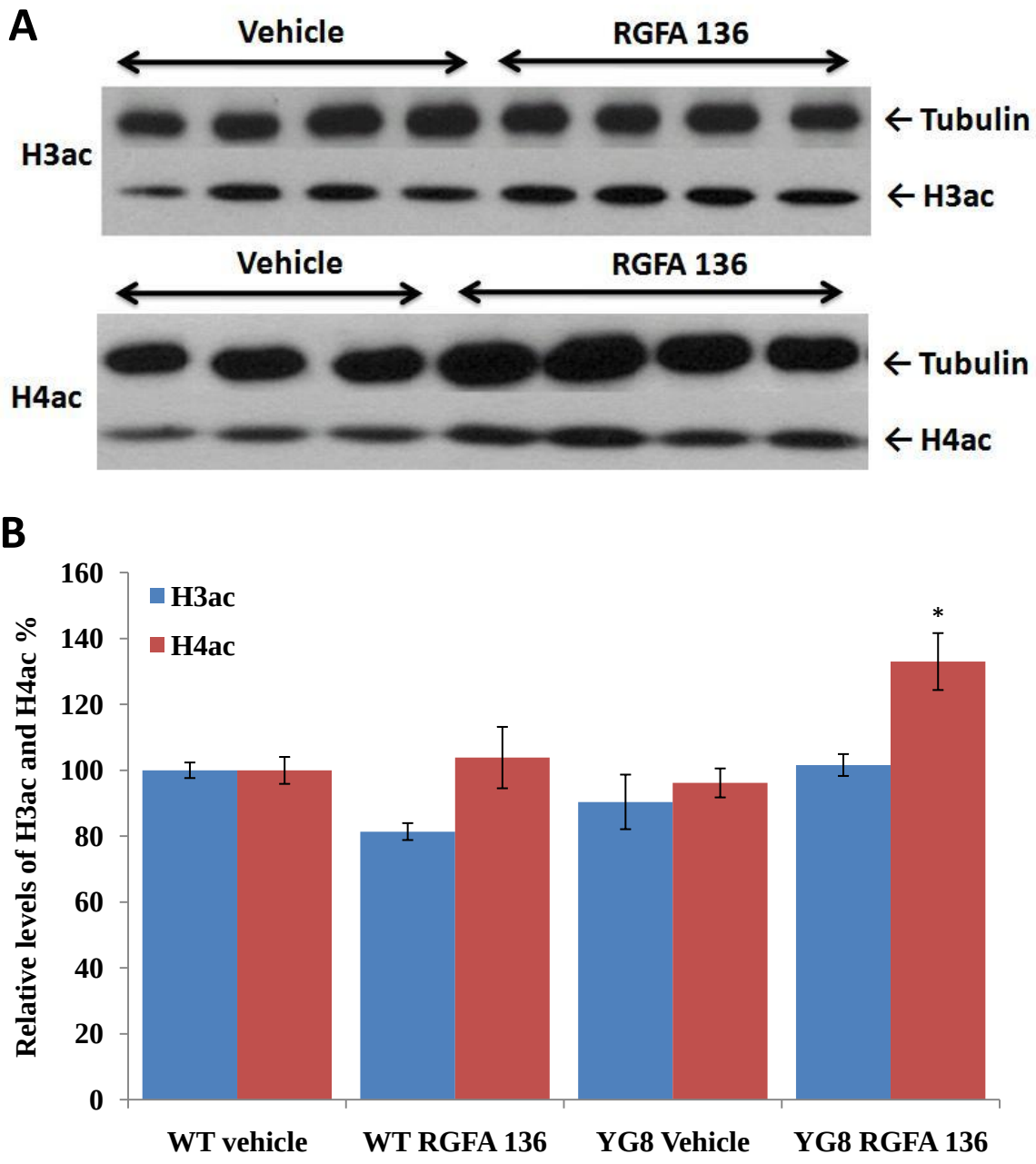

Figure 5.17 - Relative levels of acetylated H3 and acetylated H4 histone proteins in WT and YG8 mice following treatment with RGFA 136 in brain tissues. **A)** Western blot showing acetylated H3 histones (H3ac) and acetylated H4 histones (H4ac) of YG8 rescue mice only. Densitometry calculations of H3ac and H4ac **(B)** are shown for vehicle-treated and RGFA 136-treated WT and YG8 rescue mice (n=4, *p<0.05, error bars ± 1 SEM).

5.1.3.6 - Biochemical analysis following treatment with RGFA 136

It has been reported that FRDA patient and mouse model tissues have exhibited impaired activities of several Fe-S containing enzymes, such as aconitase and MRC complexes I, II, and III (Bradley *et al.* 2000; Puccio *et al.* 2001). Therefore, we have investigated whether RGFA 136 treatment is able to ameliorate such abnormalities in the YG8 mice by assessing aconitase enzyme activity in the brain tissues of WT and YG8 mice (experiments were performed by Dr. Sahar Al-Mahdawi).

The assay consisted of four mice from each vehicle and drug-treated group and the experiment was repeated twice with values being expressed relative to citrate synthase activity. Our findings showed significantly decrease in aconitase activity in the YG8 vehicle mice by approximately 18% compared to WT vehicle mice (Figure 5.18) resembling with our previous results of aconitase activity in YG8 heart tissue (Al-Mahdawi *et al.* 2006). Although this level of activity slightly increased in RGFA 136-treated mice, no statistically significant effect was observed. Interestingly, the relative aconitase activity was decreased in the RGFA 136-treated WT mice by approximately 16% (non-significant) compared to WT vehicle control mice (Figure 5.18) suggesting a specific effect of RGFA 136 in YG8 mice.

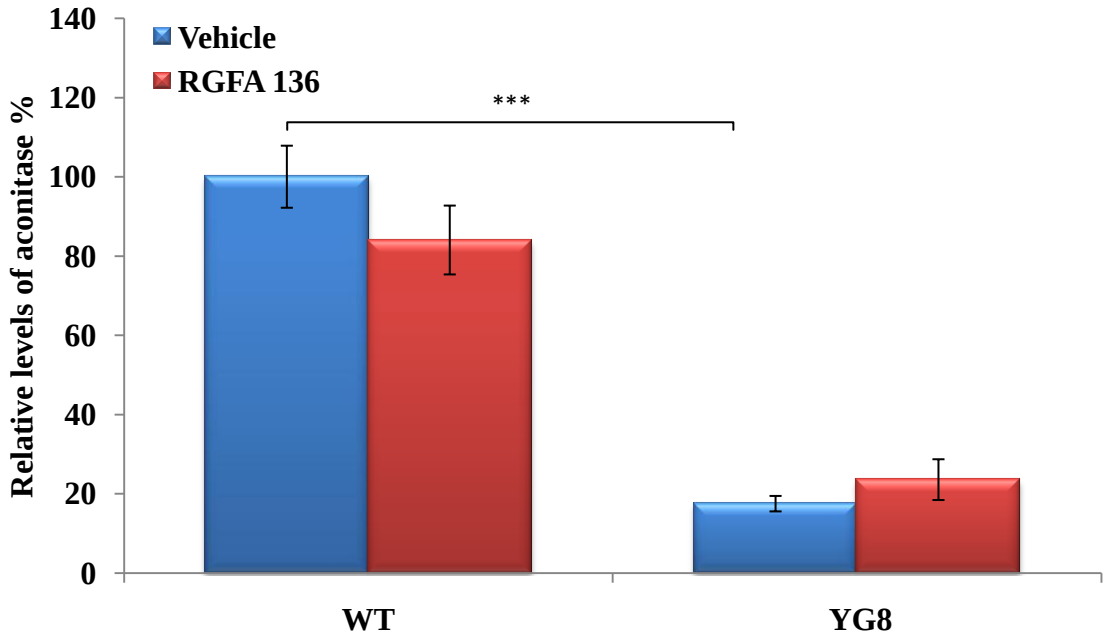

Figure 5.18 - The relative levels of aconitase in WT and YG8 mice brain tissues following treatment with RGFA 136 (n=4, ***p<0.001, error bars ± 1 SEM).

5.1.3.7 - Histological analysis following treatment with RGFA 136

In order to find possible histopathology changes following treatment with RGFA 136, we have analysed DRG paraffin-embedded sections by standard H&E histology. This investigation was carried out only on two mice from each group. The selected mice were culled immediately after the treatment and fixed in the 4% paraformaldehyde. The level of neurodegeneration was determined by counting the number of vacuoles within each DRG neuronal cell body and representing this as a percentage of all DRG cells counted.

The histological analysis following treatment with RGFA 136 revealed a significant reduction ($p<0.05$) in the number of vacuoles in the DRG of RGFA 136-treated YG8 mice compared to vehicle-treated YG8 mice, suggesting that RGFA 136 has to certain extent successfully ameliorated the FRDA pathology by reducing the DRG neurodegeneration (Figure 5.20). Although the number of vacuoles was reduced in the RGFA 136-treated mice, it was not reduced sufficiently to reach the WT mice levels. We also found a significantly higher number of vacuoles in the DRG of YG8 vehicle mice compared to WT mice (Figure 5.19), in agreement with our previous findings (Al-Mahdawi *et al.* 2006). Interestingly, RGFA 136-treated WT mice showed an approximately 4-fold increase in the number of vacuoles compared to vehicle-treated WT mice (Figure 5.20). These contradictory RGFA 136 effects, such as reduced DRG neurodegeneration in YG8 mice and increased DRG neurodegeneration in WT mice, indicate that RGFA 136 may have detrimental as well as beneficial effect, although the overall effect in the YG8 disease state is beneficial.

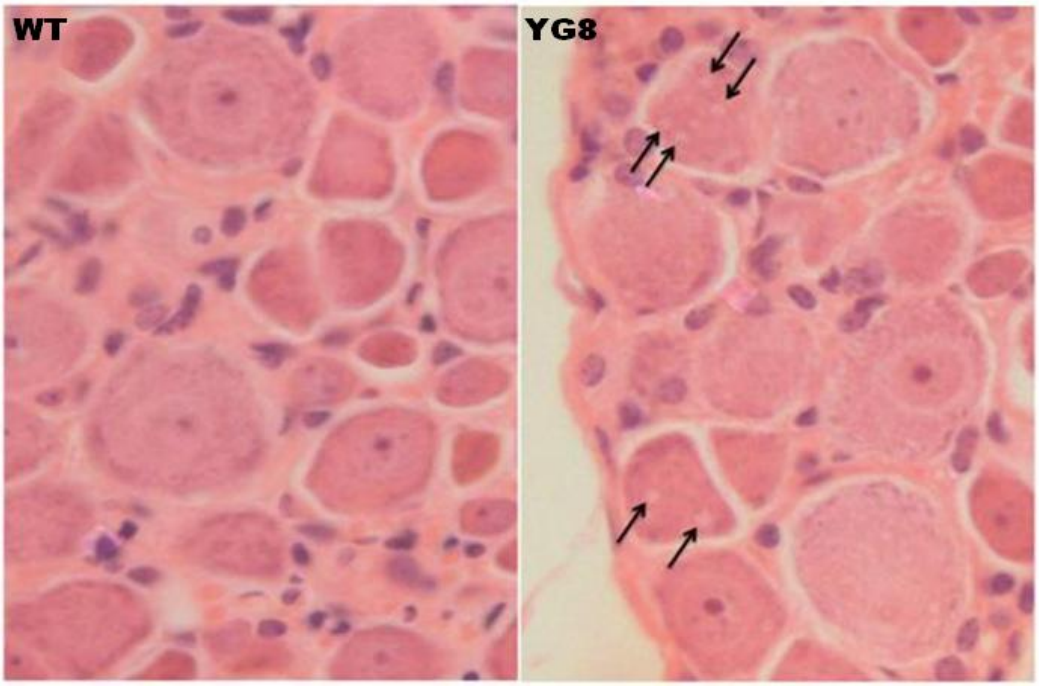

Figure 5.19 - The paraffin embedded H&E stained DRG sections of WT and YG8 mice. Arrow heads indicate the position of vacuoles in the DRG cell bodies (40X).

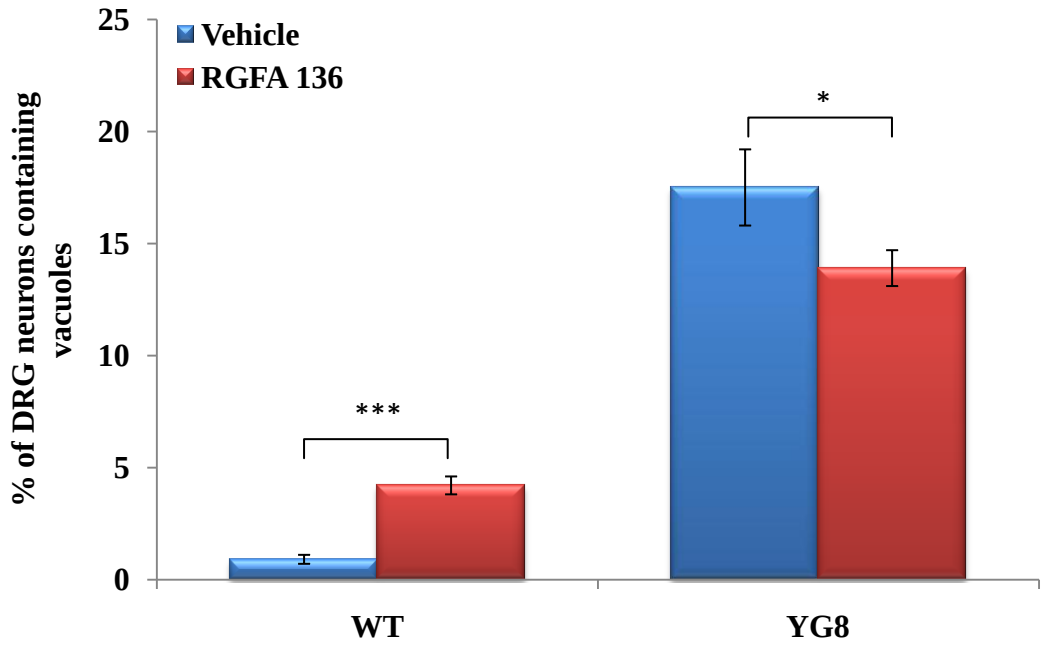

Figure 5.20 - The level of DRG neurodegeneration following treatment with RGFA 136 (n=2, ***p<0.0001, *p<0.05, error bars represents SEM).

5.2 - RGFP 109 therapeutic testing in FRDA mice

5.2.1 - Introduction

In an effort to further improve the pharmacological profile of HDAC inhibitors as a potential therapy for FRDA, we have investigated several HDAC inhibitors *in vitro* and *in vivo.* The recently described RGFA 136 has displayed promising results in long term *in vivo* studies. Therefore, we have investigated the efficacy and toxicity of the other derivative of 106, RGFP 109, in our FRDA YAC transgenic mice. A previous study using RGFP 109 in FRDA patients PBMCs and KIKI mice indicated a significant increase in frataxin mRNA, protein and global histone acetylation of H3 and H4 histone proteins (Rai *et al.* 2010). In the same study, the lack of effect of RGFP 109 on expression levels in wild type mice again indicated specificity of RGFP 109 towards GAA repeat expansion-containing *FXN* sequence.

Treatment of FRDA KIKI mice with 150mg/kg RGFP 109 subcutaneously showed RGFP 109 to be non-toxic and able to cross the blood-brain barrier, as determined by increases in *FXN* mRNA and acetylation of histone H3 and H4 proteins in mouse brain tissue (Rai *et al.* 2010). Thus, many of the outcomes from short-term treatments with the HDAC inhibitor RGFP 109 indicated that this compound should be investigated further for long-term FRDA therapy. Therefore, this project aimed to examine both the short-term and long-term efficacy of HDAC inhibitor RGFP 109 in the FRDA YAC transgenic mice.

5.2.2 - Materials and methods

5.2.2.1 - RGFP 109 structure

RGFP 109, *N*-(6-(2-aminophenylamino)-6-oxohexyl)-4-methylbenzamide, is also a novel pimelic diphenylamide compound and structurally similar to HDAC inhibitor RGFA 136 and 106 (Figure 5.21).

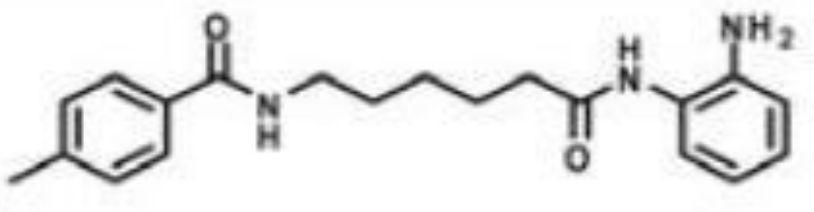

Figure 5.21 - The chemical structure of RGFP 109.

Similar to HDAC inhibitor RGFA 136, the K_i and IC_{50} values for RGFP 109 were also identified and expressed as a ratio of HDAC1/HDAC3 by using recombinant HDAC enzymes with a fluorescent substrate. This finding has revealed RGFP 109 shown to have doubled the Ki value and reduced IC_{50} value compared to RGFA 136 (Table 5.5) (Rai *et al.* 2010), indicating that RGFP 109 is more effective even with small concentrations of the drug.

Table 5.5 - Kinetic properties of RGFP 109

IC_{50} HDAC1	60nM
IC_{50} HDAC3	50nM
K_i HDAC1	32nM
K_i HDAC3	5nM

5.2.2.2 - Formulation of the drug

RGFP 109 was also synthesized and provided to us by Repligen Corporation (USA). The drug was supplied in the form solid HCl powder and stored at -80°C until required to use. All the drug formulations were carried out according to the manufacturer's recommendations and were freshly prepared in a weekly basis. RGFP 109 was administered in two different concentrations, such as 100mg/kg/day and 150mg/kg/day.

Preparation of 150mg/kg/day of RGFP 109

At first, 600mg of RGFP 109 was weighed and resuspended in 1ml of DMSO (prewarmed to 37°C), followed by 19ml of diluent (prewarmed to 37°C) resulting in 30mg/ml RGFP 109 solution and stored at 4°C until required to use. The diluent for RGFP 109 is the same as RGFA 136 diluent (see 5.1.1.2).

Preparation of 100mg/kg/day of RGFP 109

To begin with, the drug stock (30mg/ml) prepared above was diluted 1.5 times with diluent resulting in 20mg/ml RGFP 109 solution and stored at 4°C until required to use. A placebo/vehicle solution was also prepared in the same way by mixing 1ml of DMSO and 19ml of diluent without drug. Both drug and vehicle solutions were stored at 4°C.

5.2.2.3 - Study design: drug administration and sample collection

Preliminary studies

Initial short-term studies were performed only on YG8 rescue mice exploring sub-cutaneous injection of RGFP 109 with two different concentrations, 15mg/kg and 50mg/kg, along with a vehicle group. In each group 10 mice were included with an average age of 6-7 months old and treatment consisted of 3 consecutive daily doses of RGFP 109 sub-cutaneous injection. The drug was prepared in dilutions of 10mg/ml for 50mg/kg concentration and 3mg/ml for 15mg/kg concentration of RGFP 109. A corresponding volume of diluent was injected into vehicle control YG8 mice. The RGFP 109 compound was found to be well tolerated, with no mouse deaths or adverse effects noticed.

Long-term studies

Based on the previous study with RGFA 136, we have carried out treatment of RGFP 109 on groups of 20 YG8 mice and 10 WT mice (Table 5.6). At the start of the experiment, the average age of the mice was in between 3.4 to 3.9 months. All mice were matched by their age, sex and initial functional studies. As the short-term sub-cutaneous administration of RGFP 109 into our FRDA YAC transgenic mice and also into KIKI mice (Rai *et al.* 2010) have previously been well tolerated, we wanted to find if this could be maintained in a long term dosing regimen. Therefore, we injected the mice subcutaneously with 100mg/kg 5 times per week or 150mg/kg 3 times per week. A corresponding volume of vehicle solution was administered to a control group. Such long-term administrations of 100mg/kg or 150mg/kg of RGFP 109 were well tolerated. No toxicity was observed in any of the mice given subcutaneous dosing throughout the entire 5-month period of this study.

Table 5.6 - Long term Study design of RGFP 109 in WT and YG8 rescue mice

Group	Genotype	Male	Female
Vehicle	WT	5	5
	YG8 R	10	10
RGFP 109 100mg/kg	WT	5	5
	YG8 R	10	10
RGFP 109 150mg/kg	WT	-	-
	YG8 R	10	10

At the end of the treatment in both short-term and long-term treatments, the mice were culled and all the required tissues were collected and processed for molecular biology, biochemistry and histological analysis.

5.2.3 - Results - preliminary short-term RGFP 109 studies

5.2.3.1 - Investigation of *FXN* mRNA expression

Short-term preliminary studies were performed on a relatively small number of YG8 rescue mice (n=10). Following 3 consecutive sub-cutaneous injections of RGFP 109 the level of *FXN* mRNA expression was investigated in the brain and cerebellum tissues of vehicle-treated and both concentrations of RGFP 109 treated samples by QRT-PCR. This analysis revealed an increased *FXN* expression in 15mg/kg treated mice by approximately 34% and 31% in the brain and cerebellum tissues, respectively compared to vehicle control mice (Figure 5.22). In contrast, the *FXN* levels were slightly reduced (~6%-10%) with 50mg/kg of RGFP 109, suggesting that a high concentration of the drug is not beneficial on *FXN* mRNA expression.

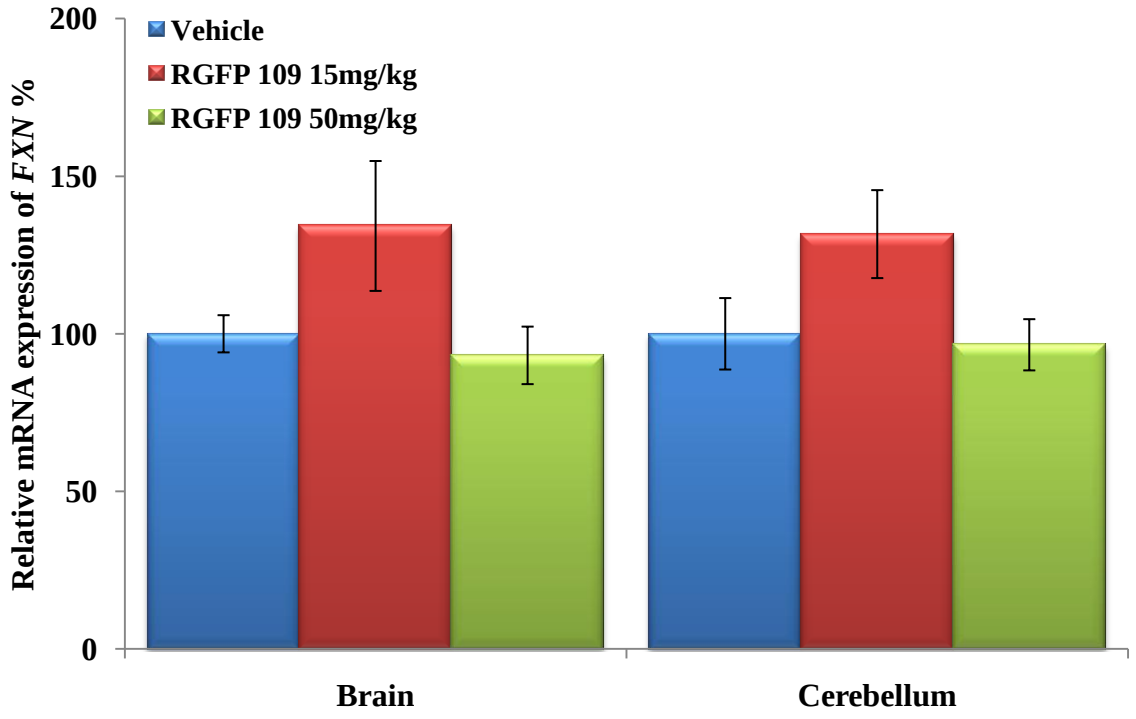

Figure 5.22 - Relative *FXN* mRNA quantification in YG8 rescue mice following short-term treatment of vehicle and RGFP 109 in YG8 rescue mice (error bars represents SEM).

5.2.3.2 - Investigation of frataxin protein

Subsequently, we also quantified the amount of frataxin protein in YG8 brain samples by western blot analysis (experiments were performed by Dr. Sahar Al-Mahdawi). The sub-cutaneous injection of RGFP 109 revealed a slight (but not significant) increase (17%) of frataxin protein in mice treated with 50mg/kg concentration of the drug. However, with low concentration of the drug (15mg/kg) the protein levels dropped by approximately 12%. These contradictory results displayed by RGFP 109 such as mice expressing more *FXN* mRNA showing reduced frataxin protein and vice versa have questioned the exact effect of this compound. Further studies on KIKI mice and advice from Repligen Corporation suggested that doses of RGFP 109 higher than 50mg/kg may be more effective. Therefore, we have investigated RGFP 109 with even higher concentrations of 100mg/kg and 150mg/kg per day on our subsequent long-term studies.

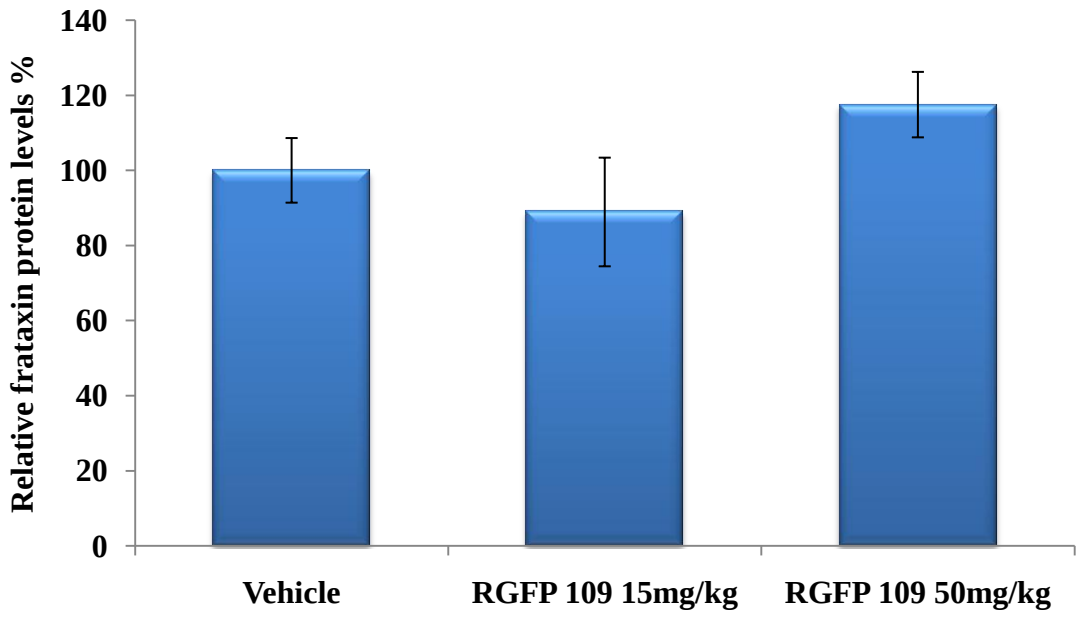

Figure 5.23 - Relative frataxin protein quantification in YG8 rescue mouse brain tissue following short-term treatment of vehicle and RGFP 109 in YG8 rescue mice (error bars represents SEM).

5.2.4 - Results - long-term RGFP 109 studies

5.2.4.1 - Functional studies during the drug treatment

The functional studies, such as weight, rotarod analysis, locomotor activity, and beam breaker measurements were taken just before the start of the treatment and repeated monthly during the entire 5-month RGFP 109 treatment period. As mentioned earlier that all functional data were measured as fold change considering the initial value as 1 (Table 5.7).

Table 5.7 - Absolute values of functional data (RGFP 109).

Parameter	Group	Initial Value	Final Value
Weight (g)	WT vehicle	27.4	34.9
	WT RGFA 109 (100mg/kg)	27.1	32.9
	YG8 Vehicle	27.3	33.3
	YG8 RGFP 109 (100mg/kg)	28.9	35.1
	YG8 RGFP 109 (150mg/kg)	27.3	31.7
Rotarod (s)	WT vehicle	284	276
	WT RGFA 109 (100mg/kg)	303	296
	YG8 Vehicle	269	231
	YG8 RGFP 109 (100mg/kg)	269	236
	YG8 RGFP 109 (150mg/kg)	265	251
Average velocity (cm/s)	WT vehicle	21.20	21.38
	WT RGFA 109 (100mg/kg)	22.20	21.80
	YG8 Vehicle	21.55	21.15
	YG8 RGFP 109 (100mg/kg)	22.85	19.93
	YG8 RGFP 109 (150mg/kg)	22.80	21.20
Ambulatory distance (cm)	WT vehicle	527.11	366.96
	WT RGFA 109 (100mg/kg)	612.55	475.35
	YG8 Vehicle	516.42	301.17
	YG8 RGFP 109 (100mg/kg)	367.00	256.74
	YG8 RGFP 109 (150mg/kg)	401.00	242.70
Vertical counts	WT vehicle	16.20	12.00
	WT RGFA 109 (100mg/kg)	26.20	16.69
	YG8 Vehicle	14.85	6.10
	YG8 RGFP 109 (100mg/kg)	14.44	5.41
	YG8 RGFP 109 (150mg/kg)	14.18	6.05

Weight analysis

All mice were showed similar weight distributions at the start of the experiment. However, when the drug treatment progressed, significant variations in weights were observed between the groups. In general, the WT vehicle mice showed significantly increased weight gain compared with the remaining groups. The analysis of body weight by two way ANOVA revealed that age of the mice (time point) had a significant effect on weight gain on both WT ($F=3.5$, $p=0.006$) and both YG8 groups of mice ($F=5.2$, 7.4, both $p<0.001$, Table B.11) (Figure 5.24). However, significantly reduced weight gain during the treatment was mainly seen in YG8 mice treated with 150mg/kg of RGFP 109 compared to vehicle-treated YG8 mice ($F=4.7$, $p<0.001$).

The weight analysis of male and female mice demonstrated a similar effect between the male and female mice showing a significant effect in weight gain over the time point ($p<0.001$). However, during the treatment significantly less weight gain was mainly observed in WT female mice ($F=4.8$, $p=0.033$) (Table B.13) and RGFP 109 (150mg/kg)-treated YG8 male mice ($F=6.8$, $p=0.01$) (Figure 5.25A-B).

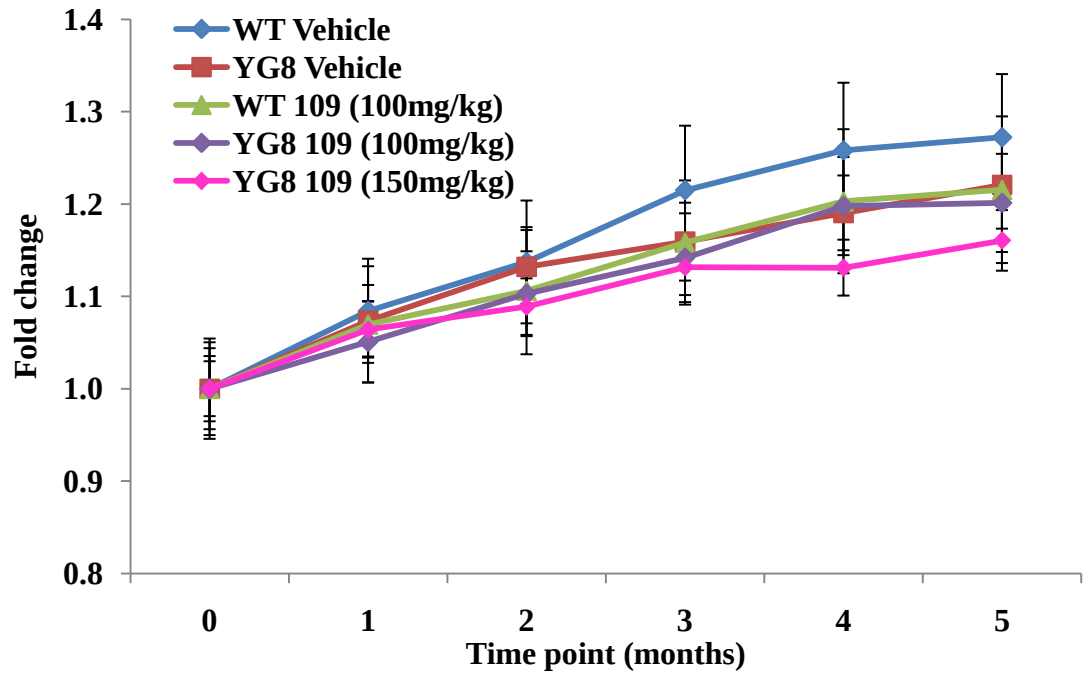

Figure 5.24 - Body weight analysis during treatment with RGFP 109 in WT and YG8 rescue mice comparing vehicle and drug-treated groups (error bars represents SEM).

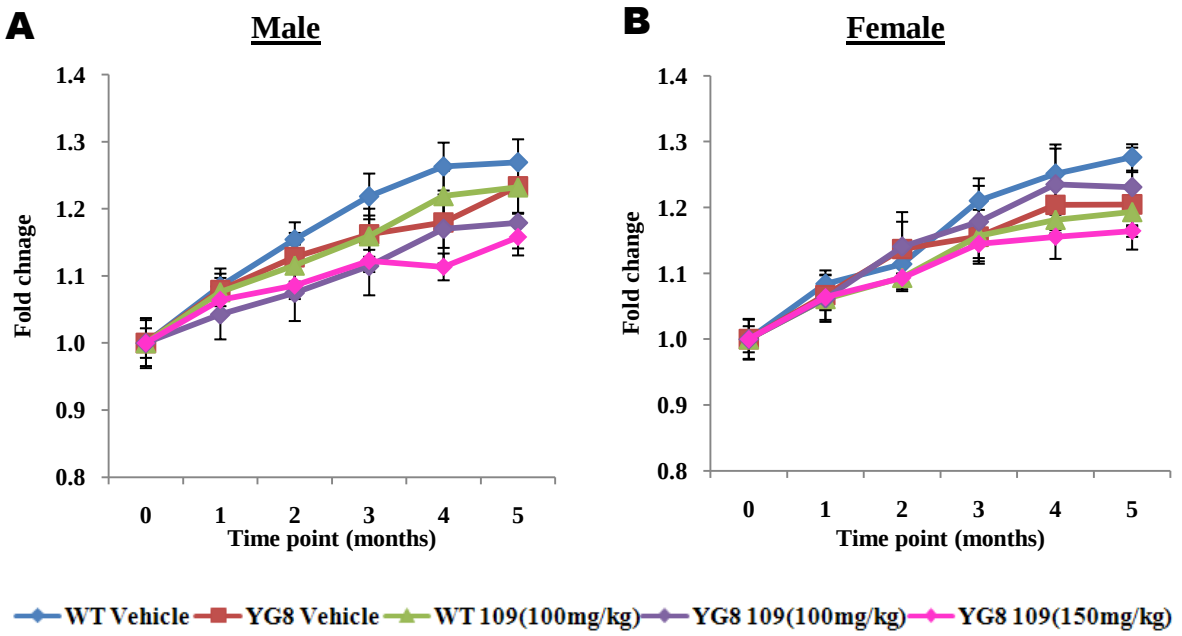

Figure 5.25 - Body weight analysis of male and female mice during treatment with RGFP 109. The average fold changes of weight in **A)** male and **B)** female WT and YG8 rescue mice are shown (error bars represents SEM).

Rotarod analysis

The motor coordination performances of RGFP 109-treated WT and YG8 mice were determined by rotarod analysis at time points throughout the treatment period. The vehicle-treated WT and YG8 mice exhibited a decline in rotarod performance, which was significantly ameliorated (WT $p=0.004$ and YG8 both $p<0.001$) (Table B.11) by both concentrations of RGFP 109 treatment (Figure 5.26). Although both the vehicle-treated mice (WT and YG8) showed reduced rotarod performance, at some time-points the WT mice displayed somewhat reduced rotarod performance compared to YG8 vehicle (not significant).

Subsequently, we have also analysed the possible differences between male and female mouse rotarod performances. This revealed a drastic decline in rotarod performance in male WT vehicle control mice, significantly lower than that of YG8 vehicle group ($F=15.6$, $p<0.001$). In contrast, female WT vehicle-treated mice showed improved rotarod performance, significantly higher than all drug-treated mice ($F=35.9$, $p<0.001$), suggesting that the overall drop in rotarod performance was originally due to the male mice (Figure 5.27A-B). Remarkably, a constantly improved rotarod performance was observed in both male ($F=0.65$, $p<0.05$) and female ($F=20$, $p<0.001$) RGFP 109 (100mg/kg)-treated YG8 mice, compared to their respective vehicle-treated controls (Figure 5.27A-B). However, with RGFP 109 (150mg/kg) treatment, significantly increased rotarod performance was seen only in the female mice ($F=8.6$, $p<0.001$), suggesting a gender specific effect of this compound. In fact, two way ANOVA confirmed a significant genotype effect over the time point on rotarod performance following RGFP 109 treatment only in male mice ($F=6.4$, $p=0.011$, Table B.12).

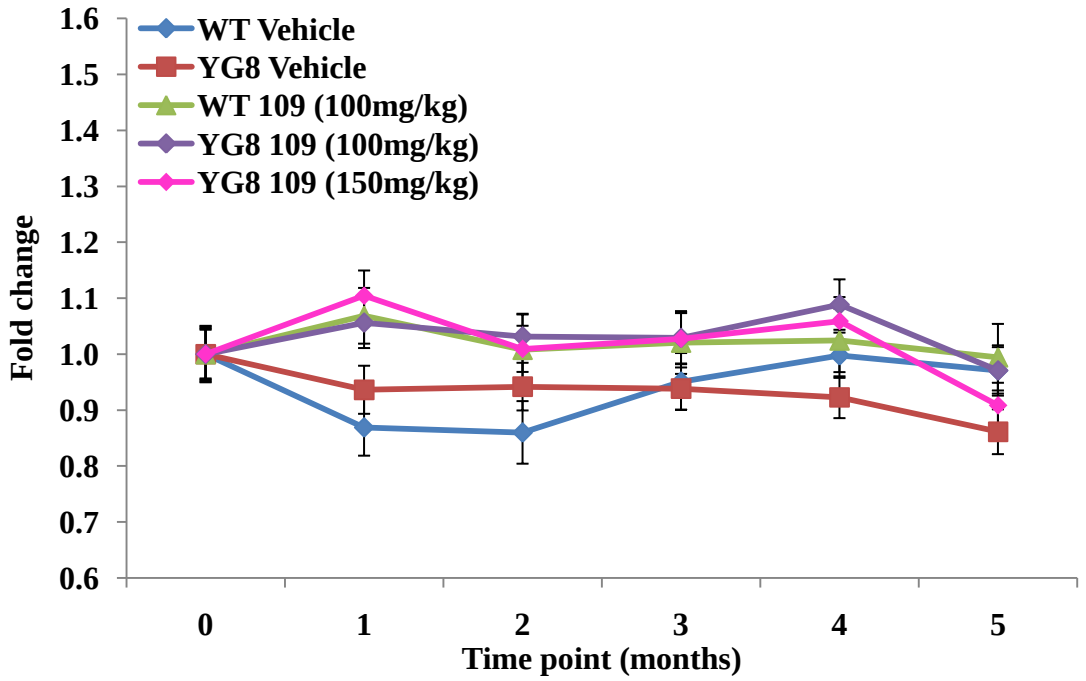

Figure 5.26 - Rotarod analysis during treatment with RGFP 109 in WT and YG8 rescue mice comparing vehicle and drug-treated groups (error bars represents SEM).

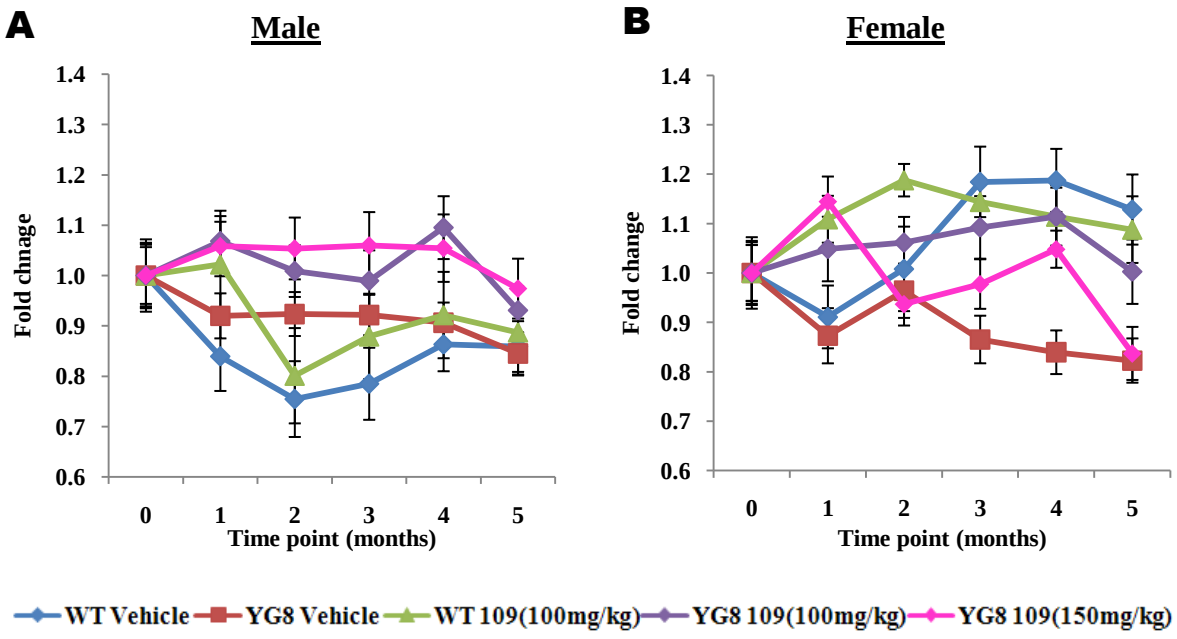

Figure 5.27 - Rotarod analysis of male and female mice during treatment with RGFP 109. The average fold changes of rotarod in **A)** male and **B)** female WT and YG8 rescue mice are shown (error bars represents SEM).

5.2.4.2 - Open-field activity monitor

Average velocity

The average velocity during the treatment with RGFP 109 did not reveal any obvious changes between the vehicle and drug-treated WT mice (Figure 5.28). However, RGFP 109 (150mg/kg)-treated YG8 mice showed significantly reduced average velocity compared to the YG8 vehicle control group (F=4.1, p=0.042). The analysis by two way ANOVA confirmed that neither the time point nor the genotype had a significant effect on the average velocity performance (Table B.16-B20). Although slight changes were observed between the vehicle and drug-treated male and female mice, none of them reached a significant effect (Figure 5.29A-B). However, a significantly gender specific effect was mainly observed between the male and female WT mice (F=6.5, p=0.011) (Figure 5.29A-B).

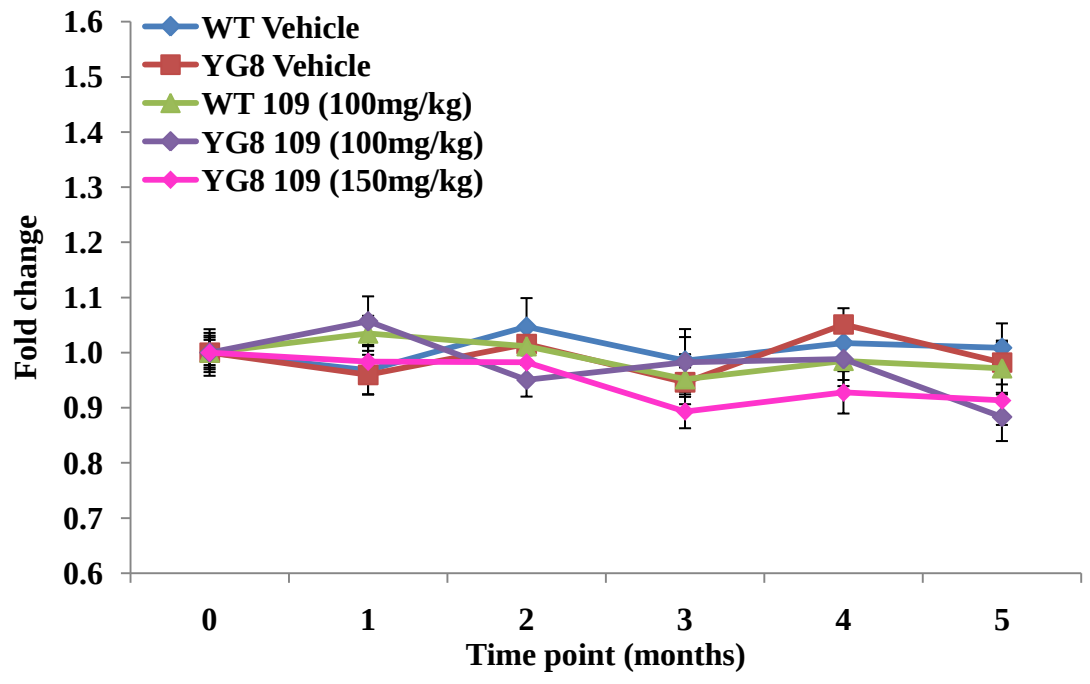

Figure 5.28 - Average velocity analysis during treatment with RGFP 109 in WT and YG8 rescue mice comparing vehicle and drug-treated groups (error bars represents SEM).

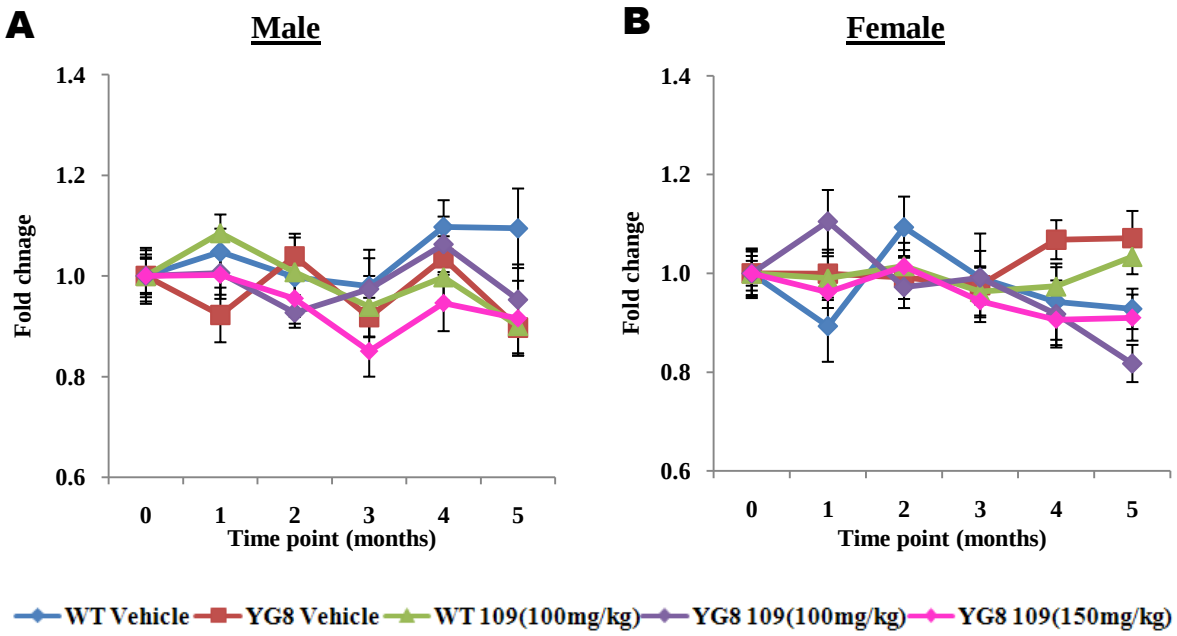

Figure 5.29 - Average velocity analysis of male and female mice during treatment with RGFP 109. The average fold changes of average velocity in **A)** male and **B)** female WT and YG8 rescue mice are shown (error bars represents SEM).

Ambulatory distance

Both the YG8 groups of mice treated with RGFP 109 (100mg/kg and 150mg/kg) showed significantly increased ambulatory distance compared to the YG8 vehicle control mice (F=22.2, 19.8, both p<0.001) (Figure 5.30). However, none of these mice sustained their initial levels of performance. Interestingly, no obvious changes were observed between the vehicle and drug-treated WT mice.

The analysis of male and female mice following treatment with RGFP 109 revealed that female mice displayed interesting results compared to male mice for both WT and YG8 mice. In the female mice, both the vehicle groups (WT and YG8) showed constant decline in ambulatory distance and this was successfully ameliorated with RGFP 109 treatments (Figure 5.31B). Although, RGFP 109 (150mg/kg)-treated YG8 female mice displayed significantly improved ambulatory distance (F=26.3, p<0.001) compared to YG8 vehicle-treated mice, no significant effect in male mice was observed. In contrast, a significant improvement in ambulatory distance was observed in RGFP 109 (100mg/kg)-treated YG8 male (F=6.3, both p=0.01) and female mice (F=9.3, p=0.02) (Table B.18), suggesting that a low concentration of RGFP 109 is beneficial (Figure 5.31A-B). Two way ANOVA confirmed that the age of the mice (time point) had a significant effect on ambulatory distance in both male and female YG8 mice (Table B.18).

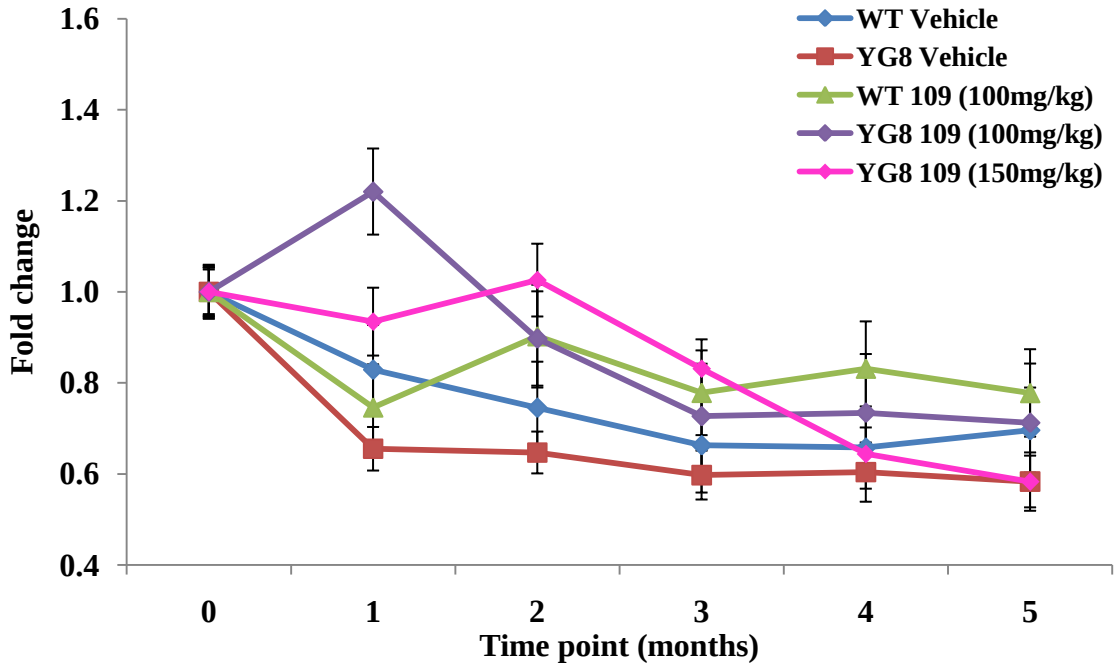

Figure 5.30 - Ambulatory distance analysis during treatment with RGFP 109 in WT and YG8 rescue mice comparing vehicle and drug-treated groups (error bars represents SEM).

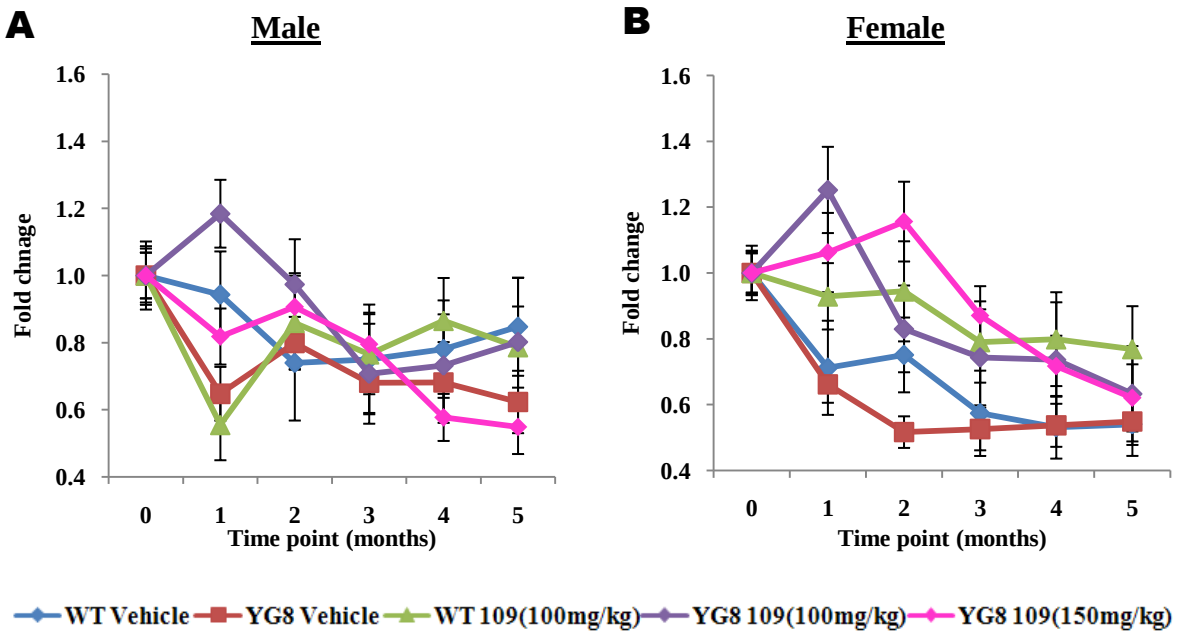

Figure 5.31 - Ambulatory distance analysis of male and female mice during treatment with RGFP 109. The average fold changes of ambulatory distance in **A)** male and **B)** female WT and YG8 rescue mice are shown (error bars represents SEM).

Vertical counts analysis

Regarding the vertical counts, WT and YG8 vehicle-treated mice displayed significantly different performances. The YG8 vehicle-treated mice showed considerable reduction in vertical counts compared to the WT vehicle-treated control mice ($F=24.5$, $P<0.001$) (Figure 5.32), indicating an FRDA-like disease effect. No evidence of a drug effect was detected with any concentration of RGFP 109 used in the YG8 mice.

However, interesting results were displayed by female mice when the data was analysed for male and female mice. The WT male vehicle mice displayed an overall increased number of vertical counts, even higher than the initial performance, and higher than the remaining three groups (Figure 5.31A). In the female mice, a significant effect of the drug was observed in the YG8 mice treated with RGFP 109 (150mg/kg) ($F=9.1$, $p=0.002$). However, the performance of these mice reduced to the level of vehicle-treated female mice when the treatment reached the 4-month time point (Figure 5.31B).

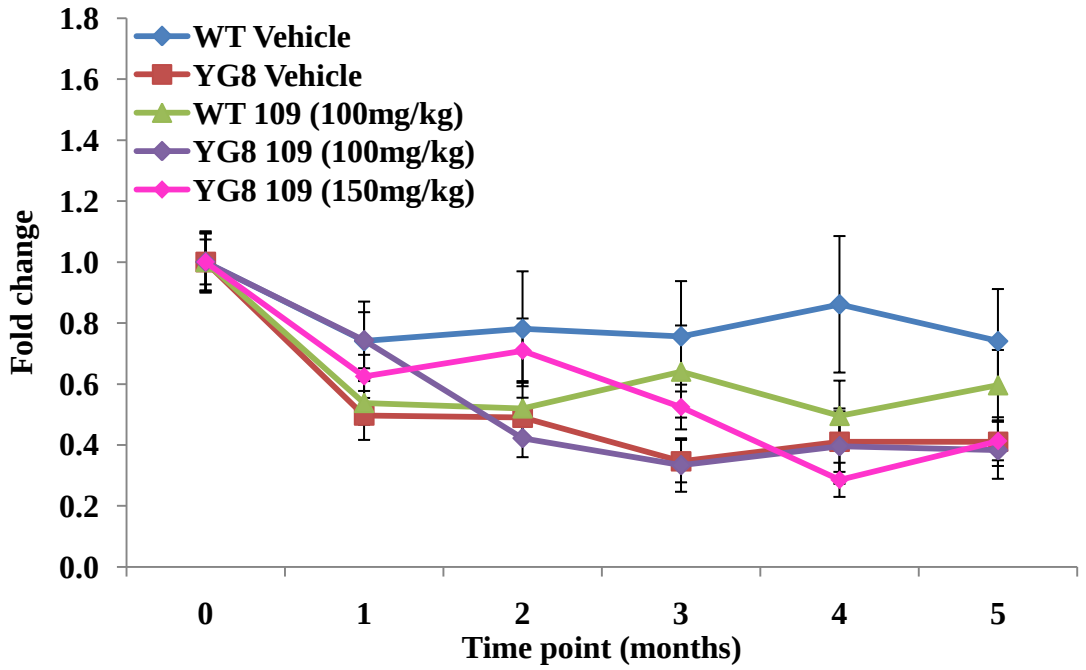

Figure 5.32 - Vertical count analysis during treatment with RGFP 109 in WT and YG8 rescue mice comparing vehicle and drug-treated group (error bars represents SEM).

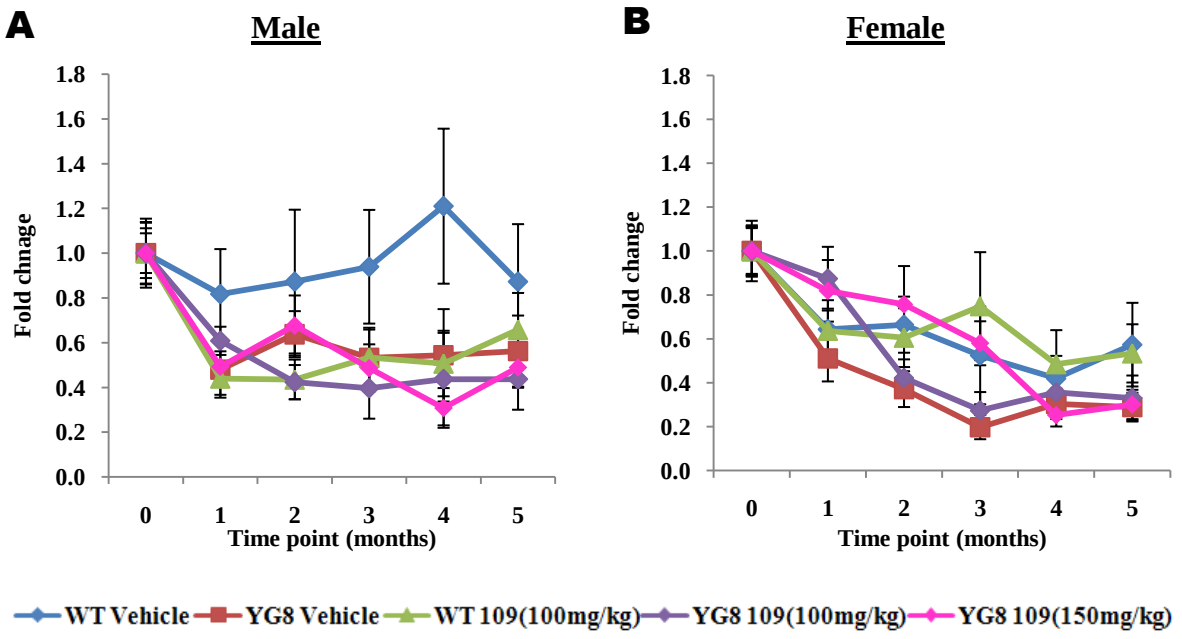

Figure 5.33 - Vertical count analysis of male and female mice during treatment with RGFP 109. The average fold changes of vertical count in **A)** male and **B)** female WT and YG8 rescue mice are shown (error bars represents SEM).

5.2.4.3 - Investigation of *FXN* mRNA following treatment with RGFP 109

FXN mRNA expression levels following treatment with RGFP 109 were investigated in brain, spinal cord, DRG and cerebellum tissues of vehicle and drug-treated WT and YG8 mice by QRT-PCR. In general, the *FXN* levels were reduced in WT RGFP 109 (100mg/kg) treated mice compared to the vehicle-treated mice by approximately 76%, 78% and 71% in the brain, DRG and cerebellum tissues, respectively (Figure 5.34). These findings suggest that RGFP 109, to some extent, had a detrimental effect in the normal mice. In contrast, a slight increase (not significant) in *FXN* expression (121%) was noticed in the spinal cord tissues of WT RGFP 109 (100mg/kg) treated mice.

No significant drug-induced effects were observed in the YG8 mice tissues tested. However, rather surprisingly, reduced *FXN* mRNA expression levels were obtained in the brain tissues of mice treated with both concentrations of RGFP 109. In addition, the cerebellum tissues also showed a decrease in *FXN* levels in the RGFP 109 (150mg/kg) treated mice to approximately 77% of those observed in the vehicle-treated cerebellum tissues (Figure 5.35). We also assessed the brain *Gapdh* levels, but detected no significant changes between the vehicle-treated and drug-treated mice (Figure B.6).

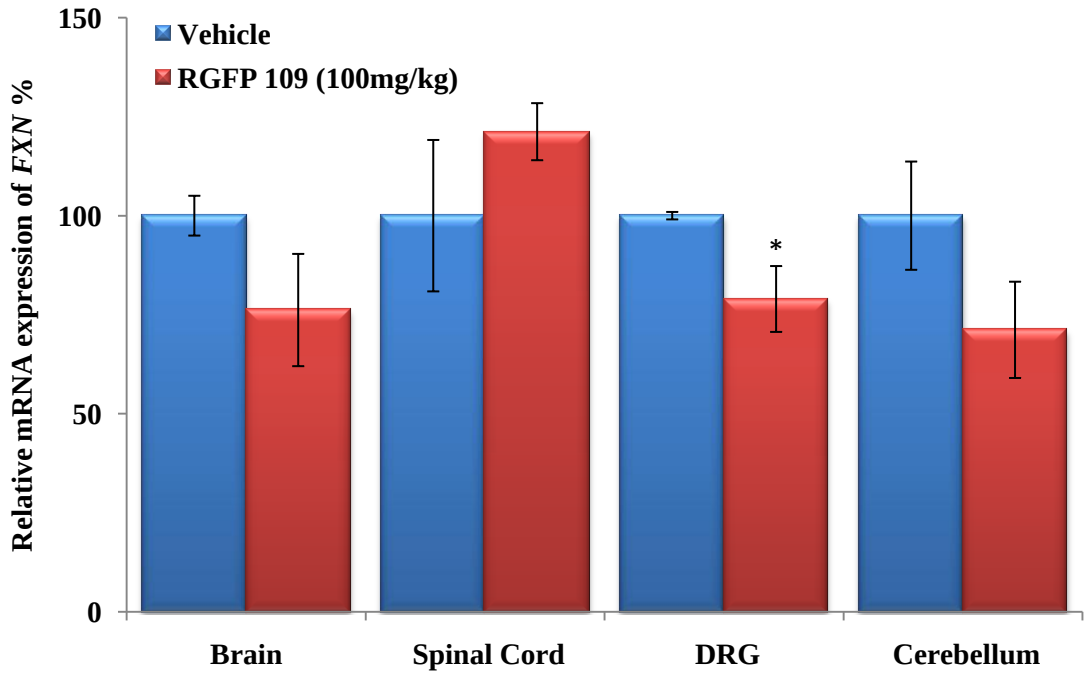

Figure 5.34 - Relative *FXN* mRNA levels in WT mice following treatment with RGFP 109 in brain, spinal cord, DRG and cerebellum tissues (n=4, *p<0.05, error bars ± 1 SEM).

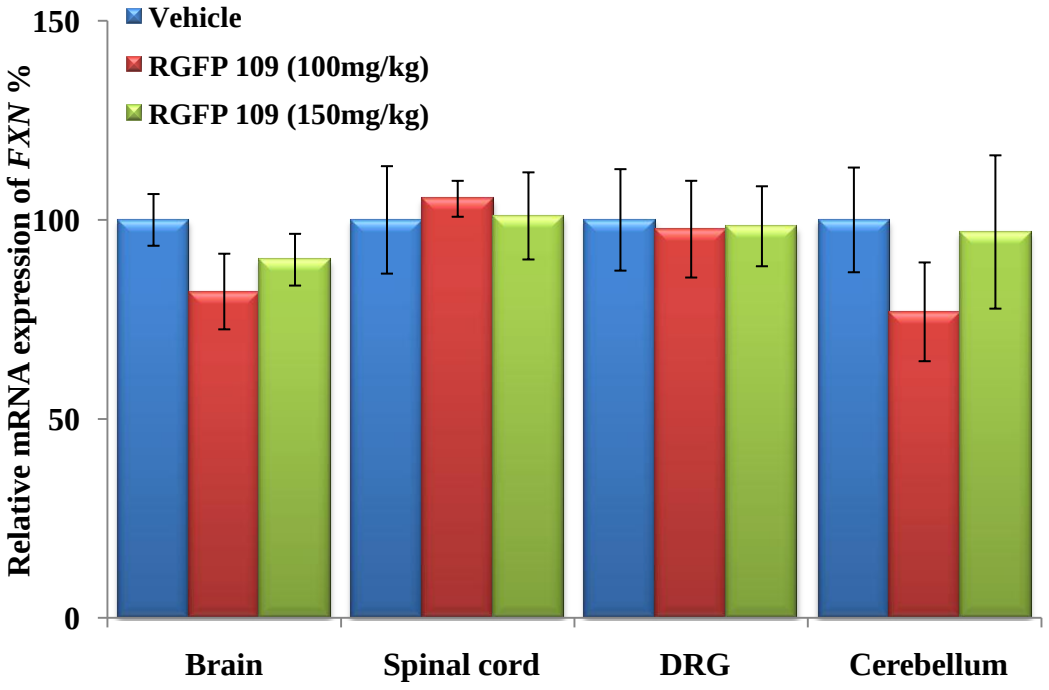

Figure 5.35 - Relative *FXN* mRNA levels in YG8 rescue mice following treatment with RGFP 109 in brain, spinal cord, DRG and cerebellum tissues (n=4, error bars ± 1 SEM).

5.2.4.4 - Investigation of frataxin protein

The relative levels of frataxin protein expression were investigated from the brain tissues of WT and YG8 mice by western blot analysis. The frataxin western blot analysis was carried out using an anti-frataxin rabbit polyclonal antibody (Santa Cruz) and the values were normalized to an anti-tubulin rabbit polyclonal antibody (Sigma) (experiments were performed by Dr. Sahar Al-Mahdawi). Densitometry was carried out using UN-SCAN-IT software (Silk Scientific Corporation). The western blot analysis, using 4 mice from each group, identified a significant increase in frataxin protein levels in both the YG8 groups treated with RGFP 109 (100mg/kg) and RGFP 109 (150mg/kg) compared to the WT vehicle group by approximately 1.6-fold ($p<0.05$) and 1.8-fold ($p<0.001$), respectively (Figure 5.36). Lesser increases in endogenous mouse frataxin levels were also seen in RGFP 109 (100mg/kg)-treated WT mice, indicating a general frataxin-increasing effect of these drugs. No obvious changes were identified between the WT and YG8 vehicle groups.

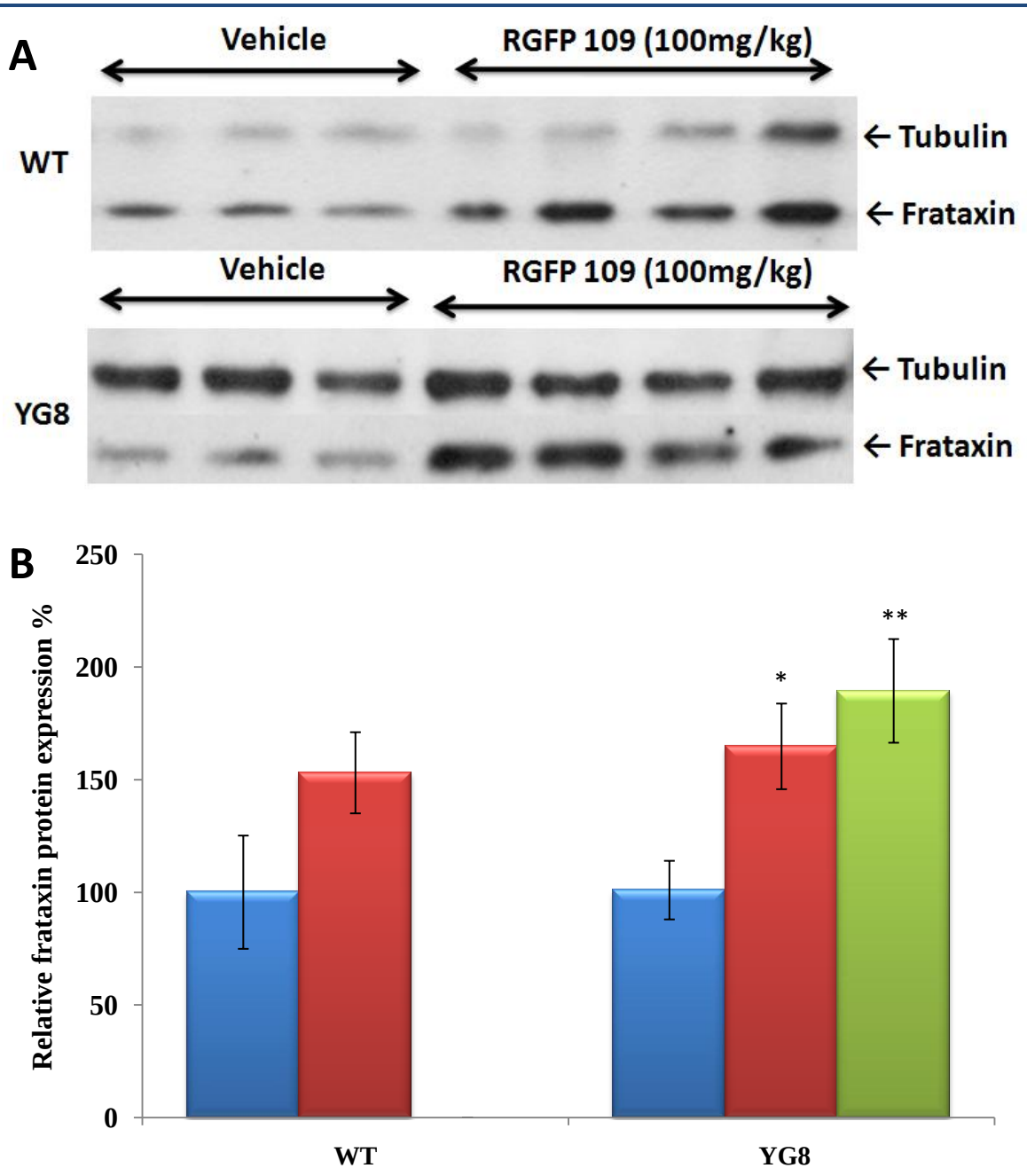

Figure 5.36 - Relative frataxin protein levels in brain tissues from WT and YG8 mice following treatment with RGFP 109. **A)** Western blot showing frataxin protein expression together with α-tubulin controls, and **B)** densitometry calculations of frataxin levels are shown for vehicle and RGFP 109-treated WT and YG8 rescue mice (n=3-4, error bars ± 1 SEM, *p<0.05, **p<0.01).

5.2.4.5 - Investigation of global histone acetylation changes

In order to find the long-term effect of RGFP 109 on histone acetylation changes, we have investigated the changes in global histone protein levels by western blot analysis. The analysis was carried out on brain tissues from four mice from each group. The western blotting analysis for global histone changes showed small decreases (non-significant) in both acetylated H3 and acetylated H4 protein of YG8 vehicle-treated mice compared with WT vehicle-treated mice (experiments were performed by Dr. Sahar Al-Mahdawi).

Increased acetylated histone H3 protein levels were found in both RGFP 109-treated YG8 mice with increases of 52% and 41% higher than vehicle-treated YG8 mice, respectively ($p<0.05$ for RGFP 109 (150mg/kg)) (Figure 5.37). Acetylated H4 histone proteins showed non-significant increases of 14% and 36% higher than vehicle-treated YG8 mice in both of RGFP 109-treated YG8 mice, respectively (Figure 5.37). Overall, these results are consistent with RGFP 109 crossing the blood brain-barrier to cause global increases in histone acetylation.

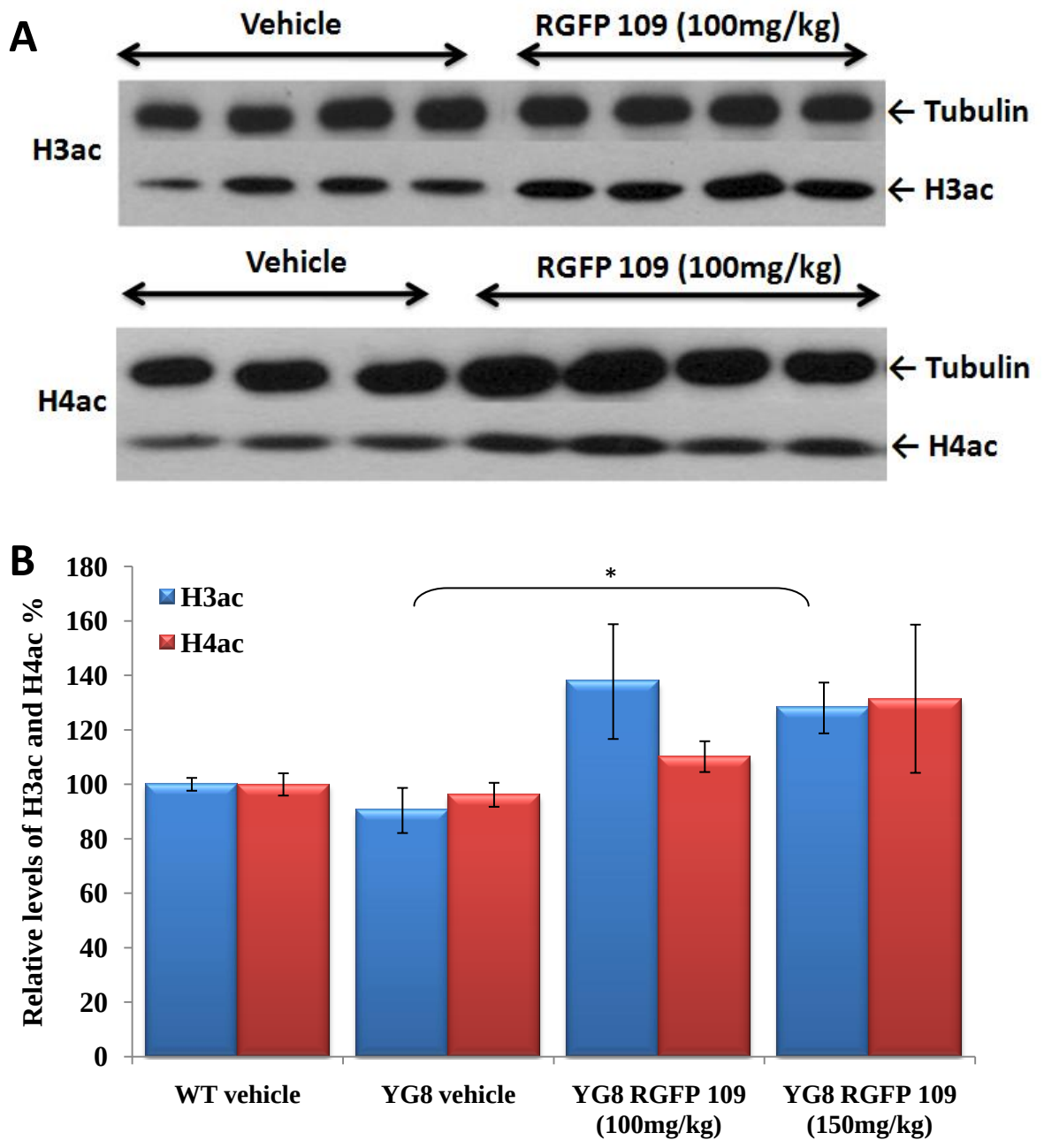

Figure 5.37 - Relative levels of acetylated H3 and acetylated H4 histone proteins in WT and YG8 mice following treatment with RGFP 109 in brain tissues. **A)** Western blot showing acetylated H3 histones (H3ac) and acetylated H4 histones (H4ac) of RGFP 109 (100mg/kg)-treated YG8 rescue mice. Densitometry calculations of H3ac and H4ac **(B)** are shown for vehicle-treated and RGFP 109-treated WT and YG8 rescue mice (n=3-4, *p<0.05, error bars ± 1 SEM).

5.2.4.6 - Biochemical studies following treatment with RGFP 109

Subsequently, we have also investigated the possible biochemical changes of aconitase enzyme activity following treatment with RGFP 109 in the brain tissues of WT (vehicle only) and YG8 mice. The aconitase assay showed significantly reduced levels of aconitase enzyme in the vehicle-treated YG8 mice to approximately 18% ($p<0.001$) of the WT vehicle control mouse levels. Treatment with RGFP 109 significantly increased the aconitase levels to 67% and 57% of WT vehicle levels in mice treated with 100mg/kg and 150mg/kg of RGFP 109, respectively (both $p<0.001$) (Figure 5.38). These levels are approximately 3.8 and 3.2-fold higher than YG8 vehicle mice indicating beneficial effect of RGFP 109 on aconitase enzyme activity.

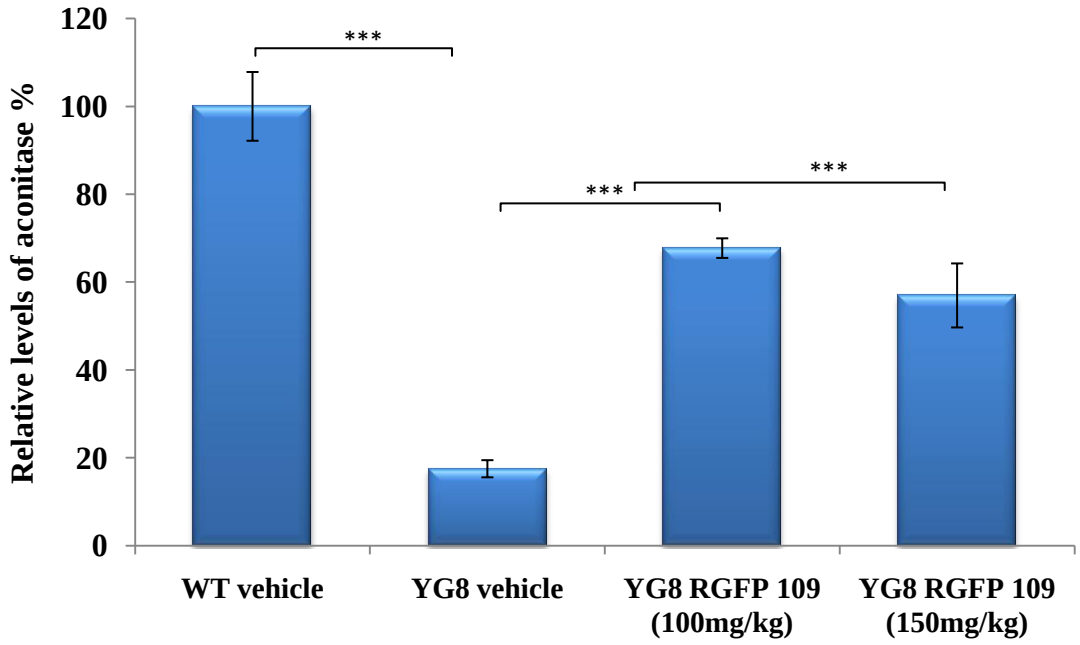

Figure 5.38 - The relative levels of aconitase activity following treatment with RGFP 109 in WT (vehicle only) and YG8 mice (n=4, ***$p<0.01$, error bars ± 1 SEM).

5.2.4.7 - Histological analysis following treatment with RGFP 109

In order to find whether the long-term treatment of RGFP 109 is able to ameliorate the FRDA-associated pathology of DRG neurodegeneration, we have analysed the DRG paraffin embedded sections by standard H&E staining. The levels of DRG neurodegeneration were determined by counting the number vacuoles in neuronal cell bodies as a percentage of the total number of DRG cells counted (Figure 5.19).

Subsequent analysis revealed that YG8 vehicle-treated mice showed an increased number of vacuoles in the DRG cells by approximately 19-fold higher than in the WT vehicle-treated mice ($p<0.001$) (Figure 5.39), in agreement with our previous results (Al-Mahdawi *et al.* 2006). Treatment with RGFP 109 successfully ameliorated this FRDA-associated phenotype to a large extent by reducing the number of vacuoles significantly by approximately 5.2-fold (to 28% of YG8 vehicle values) and 5.4-fold (to 26% of YG8 vehicle values) with 100mg/kg and 150mg/kg, respectively (Figure 5.39). Although the number of vacuoles was significantly reduced with RGFP 109 treatments, none of the values have reached the WT level, so amelioration of the neurodegenerative disease effect is not complete.

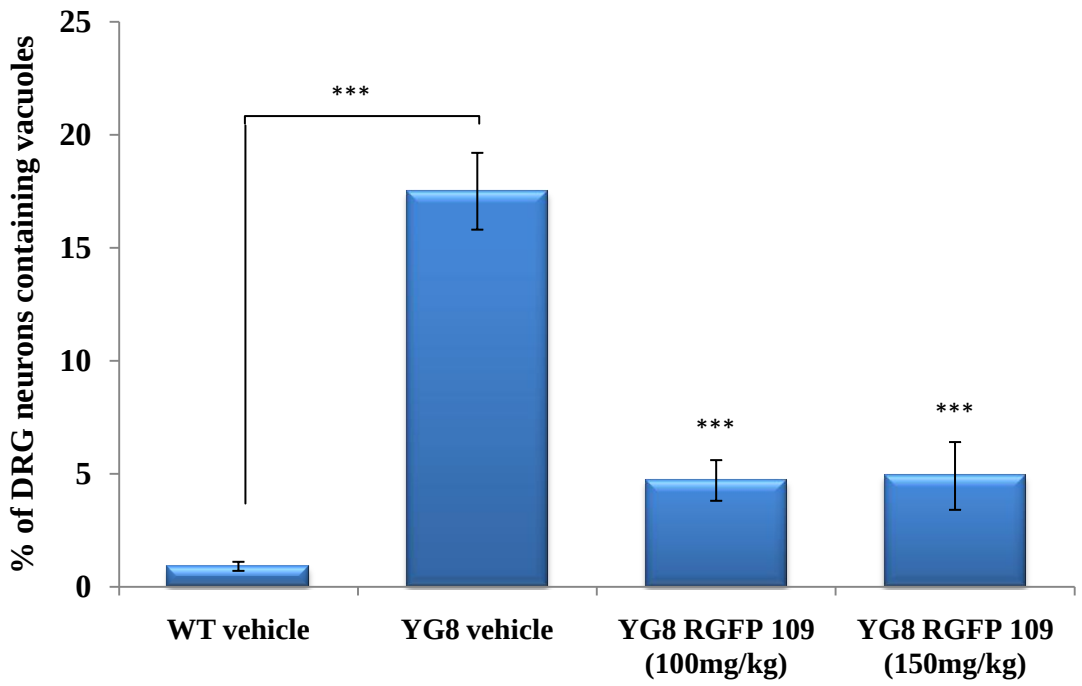

Figure 5.39 - The level of DRG neurodegeneration in WT and YG8 rescue mice as quantified by the percentage of vacuole-containing DRG cells following treatment with RGFP 109 (n=2, ***p<0.001, error bars represents SEM).

5.2.5 - Discussion

It has been shown that 98% of the FRDA patients have hyper-expanded GAA repeats in the intron 1 of the *FXN* gene, leading to reduced expression of frataxin (Campuzano *et al.* 1996). Although the mechanisms by which the GAA repeat expansion leads to decreased levels of frataxin expression are currently not known, it is generally currently accepted that FRDA may be caused by a heterochromatin-mediated silencing effect of the *FXN* gene (Saveliev *et al.* 2003; Festenstein 2006). In support of this hypothesis, differential DNA methylation in FRDA patients accompanied by decreased levels of acetylated H3 and H4 histone proteins were identified flanking the GAA repeats (Herman *et al.* 2006; Greene *et al.* 2007; Al-Mahdawi *et al.* 2008).

In addition, there is also evidence that the GAA repeat expansion may adopt abnormal non-B DNA structures (triplexes or "sticky DNA") or DNA•RNA hybrid structures that directly interfere with *FXN* gene transcription elongation (Grabczyk *et al.* 2007; Wells 2008). Therefore, any therapies aiming to target these consequences may prove to be of benefit.

Recently, epigenetic therapies using DNA demethylating agents and HDAC inhibitors have received considerable attention as potential therapeutics for cancer (Marks and Dokmanovic 2005) and for wide variety of neurological and neurodegenerative diseases (Kazantsev and Thompson 2008).

In the present study we have demonstrated the *in vivo* feasibility of using two HDAC inhibitors, RGFA 136 and RGFP 109, in long-term sub-cutaneous dosing regimens to potentially activate the *FXN* gene and ameliorate the disease phenotype in a mouse model that recapitulates the genetic and epigenetic features of FRDA. Previous short-term studies using these two compounds had already demonstrated increased frataxin mRNA and protein

expression along with elevated levels of acetylated H3 and H4 histone proteins in the brain and heart tissues of KIKI mouse (Rai *et al.* 2010), indicating the ability of these two compounds to cross the blood-brain barrier.

An initial long-term study with RGFA 136 and a short-term study with RGFP 109 showed no signs of toxicity indicating the safe administration of these two compounds. Therefore, we have used the same sub-cutaneous regimen throughout the long-term RGFA 136 and RGFP 109 treatments (5 months). Such long-term administration of RGFA 136 (50mg/kg) or RGFP 109 (100mg/kg and 150mg/kg) were well tolerated. No apparent toxicity was observed in any of the mice given subcutaneous dosing throughout the entire 5-month period of this study.

We previously reported that the WT mice have mean decreased weight gain compared to YG8 rescue mice (Al-Mahdawi *et al.* 2006). In contrast, the analysis of body weight by two-way ANOVA in this present study detected increased weight gain in WT mice and this was significantly reduced in YG8 rescue mice in both RGFA 136 and RGFP 109 treatment groups. In particular, we found considerably less weight gain in RGFA 136- and RGFP 109 (150mg/kg)-treated YG8 rescue mice throughout the treatment. The similar effect in body weight was also seen in male and female mice of RGFA 136 and RGFP 109 treatment groups. At this time the most likely explanation for such a discrepancy in weight gain/loss between WT and YG8 rescue mice is the fact that the initially reported WT mice were YG8 littermates of mixed CBA/C57BL6/J genetic background, whereas the WT mice used in this thesis were exclusively C57BL6/J.

The additional weight loss observed in RGFA 136 and RGFP 109-treated YG8 mice may be due to several possible drug effects. One of the possibilities is that since FRDA is

associated with diabetes (Pandolfo 2003; Ristow *et al.* 2003), the YG8 mice are actually overweight, as previously reported (Al-Mahdawi *et al.* 2006). Treatment with either RGFA 136 or RGFP 109 may perhaps reverse the diabetes effects (obesity), and consequently reduced weight gain is observed in the drug-treated YG8 mice compared to vehicle-treated YG8 mice. Additionally, HDAC inhibitors are likely to affect many genes that are involved in general body metabolism, with the overall effect being weight loss.

The motor coordination performance as determined by rotarod analysis confirmed a significant drug-induced effect by both drugs, particularly with RGFA 136. Interestingly, we found a strong gender effect on the rotarod performance, which has not been previously reported. Although the rotarod performance was significantly increased in the drug-treated YG8 rescue male mice, it was also significantly increased in WT male mice, suggesting a non-specific effect. Furthermore, no significant changes were detected between the WT vehicle and YG8 vehicle, indicating no overt FRDA-associated motor coordination deficit in these male mice. However, it is possible that a potential YG8 motor coordination deficit is masked by the weight differences between WT and YG8 male mice, with the heavier WT male mice performing worse on the rotarod due to an obesity problem and not a coordination problem.

In contrast, YG8 female vehicle mice have shown reduced rotarod performance compared to WT vehicle mice and this reduction in rotarod performance was successfully ameliorated by both RGFP 109 treatments and no explicit difference was observed with RGFA 136. Therefore, treatment with 109 may prove beneficial to improve the ataxic motor coordination deficits associated with FRDA. Furthermore, as a consequence of these studies, it is proposed that YG8 female mice should be used for any future rotarod experiments

rather than using YG8 male mice, since they alone show a motor coordination deficit compared to WT mice. Locomotor activity was investigated only in the YG8 mice (RGFA 136 only) and a significant drug-induced effect was observed in both male and female mice, suggesting that RGFA 136 is a potential therapeutic drug to improve locomotor deficits in FRDA.

The average velocity and ambulatory distance (measures of muscle strength and stamina) as determined by open-field monitor machine (beam-breaker) both showed significantly improved performances by RGFA 136 treatment. In comparison, 109 treatment had no effect on average velocity, but significantly improved ambulatory distance. Analyses of vertical counts (measures hind limb muscle strength) produced some interesting results. The YG8 vehicle-treated mice displayed continuous decline and significantly reduced number of vertical counts compared to WT vehicle control mice. Treatment with RGFA 136 not only ameliorated this decline, but actually induced significant improvement in vertical counts. A similar significant effect was also seen in male and female mice when analysed separately. No explicit effect of RGFP 109 was observed in the performance of vertical counts, although some improvement was observed in the separately analysed female mice. Therefore, both RGFA 136 and RGFP 109 may prove to be beneficial in improving the muscle strength and stamina deficits associated with FRDA.

In summary both drugs exhibited some improved performances with rotarod, manual activity or beam-breaker based functional measurements. RGFA 136 perhaps elicited the more substantial improvements, which were consistent with the previous study. Importantly, a strong gender effect was revealed, particularly with rotarod performance. Therefore, future rotarod analysis should only be carried out with YG8 female mice. In

addition, quite high levels of variability were observed within the same group (same gender) in these functional measurements. Therefore, more sensitive and accurate methods of functional measurements which are specifically designed to measure ataxia in mice such as the "parallel rod floor" apparatus (Kamens *et al.* 2005; Kamens and Crabbe 2007) should also be considered for any future experiments.

After RGFA 136 and RGFP 109 treatments, we observed general decrease in *FXN* mRNA expression in drug-treated WT mice compared to vehicle-treated WT mice suggesting these drugs have a negative effect on normal mice. Surprisingly, although some slight increases in *FXN* mRNA expression were observed in the drug-treated YG8 mice, none of these values reached significant difference after 5 months of treatment, in contrast to results from a recent short-term study (Rai *et al.* 2010). In addition, no explicit difference in frataxin protein has been observed between RGFA 136-treated and vehicle-treated YG8 mice. However, the frataxin protein levels were significantly increased in the RGFP 109 treated YG8 mice with both 100mg/kg and 150mg/kg concentrations, suggesting RGFP 109 may perhaps involve, as yet undetermined, post-transcriptional or translational levels.

The discrepancies between RGFP 109-treated *FXN* mRNA and frataxin expression levels may be explained by the fact that HDAC inhibitors can both increase and decrease gene transcription (Drummond *et al.* 2005; Reid *et al.* 2005; Rai *et al.* 2008), and this may include up-regulation of certain HDACs themselves (Reid *et al.* 2005). In addition, certain HDAC inhibitors have also been shown to increase protein levels by enhancing stability (Garbes *et al.* 2009) or conversely decrease protein levels by inhibition of translation or some post-transcription RNA processing steps (Kawamata *et al.* 2007). Furthermore, it has recently been suggested that intermittent dosing of HDAC inhibitors may preferentially

increased frataxin mRNA and protein levels (Rai *et al.* 2010). Therefore, intermittent administration of drug, possibly once or twice a week, should be considered for any future experiments. Such dosing regimen would minimize any toxic side effects by reducing drug exposure and may hopefully be associated with sustained upregulation of frataxin mRNA and protein. In support of this, we found more frataxin protein expression with intermittent dosing of RGFP 109 (150mg/kg) than with daily doses of RGFP 109 (100mg/kg), although no overt difference in *FXN* mRNA expression observed. However, whether this increase in frataxin protein with RGFP 109 (150mg/kg) is exclusively due to the intermittent dosage or due to use of high concentration of drug has, yet to be determined.

We also identified increased global acetylated H3 and H4 histone proteins in brain tissue, particularly with RGFP 109 treatment of the YG8 mice. However, with RGFA 136 these levels were also increased marginally to just above the minimum statistical significance (p=0.05). This suggests that RGFP 109 may be a more potent HDAC inhibitor than RGFA 136 or is better at crossing blood brain-barrier. Additionally, the histone acetylation levels that were measured are general and not specific for *FXN* locus. Therefore, specific histone acetylation changes particularly for H3K9, H4K5 and H4K16, the main histone changes of FRDA, flanking either side of the GAA repeats and at the 5'-UTR region could be investigated by future ChIP experiments. Particularly, investigating these changes in brain tissue confirm the ability to cross the blood brain-barrier of such compounds.

In general, HDAC inhibitors are believed to act by increasing global histone acetylation and thereby reactivating epigenetically silenced genes. However, some HDAC inhibitors have also been reported to decrease histone acetylation and down-regulate genes (Rada-Iglesias *et al.* 2007). Additionally, it has also been described that global histone acetylation and

deacetylation is associated with upregulation and downregulation of several specific genes (Vogelauer *et al.* 2000), one of which could be a negative regulator of *FXN* expression. Therefore, further studies, such as microarray expression analysis, will be required to uncover any such mechanisms of action of RGFA 136 and RGFP 109 with regard to *FXN* expression.

As known, reduced frataxin expression is associated with impaired activity of mitochondrial and cytosolic aconitases (Rotig *et al.* 1997; Puccio *et al.* 2001; Stehling *et al.* 2004). Therefore, we have investigated the effect of RGFA 136 and RGFP 109 on aconitase activity following treatment and we found significantly reduced levels of aconitase activity in the YG8 vehicle-treated mice compared to WT vehicle-treated control mice, in agreement with our previous findings (Al-Mahdawi *et al.* 2006). Notably, the aconitase activity levels were significantly increased by RGFP 109 treatment (both concentrations) and marginally increased by RGFA 136 treatment in the YG8 mice, suggesting that RGFP 109 is a somewhat more potent drug in ameliorating the FRDA-associated phenotype than RGFA 136. These findings give an additional support to the idea that aconitase activity is dependent on frataxin expression, since RGFP 109-treated mice with elevated levels of frataxin protein also had more aconitase activity compared to RGFA 136-treated mice.

Neurodegeneration is a hallmark of the FRDA pathology, particularly in DRG, the primary site of the disease. The investigation of DRG neurodegeneration following treatments with RGFA 136 and RGFP 109 by H&E staining of paraffin embedded DRG sections have shown higher levels of DRG neurodegeneration in YG8 mice compared to WT mice, consistent with our previous data (Al-Mahdawi *et al.* 2006). These levels were significantly reduced with HDAC inhibitors RGFA 136 and RGFP 109 treatments, but more

efficiently with RGFP 109. These findings indicate that both drugs may be capable of ameliorating the "dying-back" neurodegenerative phenomenon as seen in FRDA patients, with RGFP 109 again likely being more potent than RGFA 136.

Overall, although functional rotarod and activity improvements have been obtained with both drugs, higher levels of significance were mainly achieved in RGFA 136-treated mice. In contrast, the molecular, biochemical and histological abnormalities which are associated with FRDA-pathology were successfully ameliorated by RGFP 109 treatment and very little improvement was displayed by RGFA 136. The discrepancies between the effects of these two compounds indicate that although these two compounds have structural similarities, their mode of action seems to differ. It has been reported that the synergistic use of DNA demethylating agents and HDAC inhibitors have produced promising results in various cancer (Cecconi *et al.* 2009; Chen *et al.* 2009) and neurodegenerative disorders (Chiurazzi *et al.* 1999). Therefore, it is also speculated that the use of these two HDAC inhibitors together rather than individually for future experiment(s) could be beneficial in simultaneously improving functional and molecular abnormalities of FRDA.

Recent findings have suggested that HDAC3 is the main target for RGFA 136 and RGFP 109, and therefore HDAC3 may also be involved in the silencing of *FXN* gene (Herman *et al.* 2006; Chou *et al.* 2008; Rai *et al.* 2008). However, this conclusion does not exclude the possible involvement of other HDACs. The kinetic properties of RGFA 136 and RGFP 109 have shown 3-fold and 6-fold specificity towards HDAC3 over HDAC1, respectively (Rai *et al.* 2008) and perhaps this can explain how HDAC inhibitor RGFP 109 is more effective in reversing FRDA-associated abnormalities than RGFA 136. Recently, Gottesfeld and colleagues have reported the synthesis and use of specific HDAC3 inhibitor, **HDACi 3**. Although this

compound has been shown to increase the acetylation of H3 histone proteins, no overt effect in increasing either frataxin mRNA or protein were found (Xu *et al.* 2009). Therefore, future investigation should be focused on the compounds which can specifically inhibit the HDAC3 activity as well as increase the frataxin mRNA and protein levels.

In conclusion, the benzamide group of class I HDAC inhibitors are generally well tolerated and they elicit improved motor coordination and locomotor activity deficits, together with elevated levels of frataxin protein, global acetylated histone proteins (H3 and H4), aconitase enzyme activity, and a significant decrease in DRG neurodegeneration. Therefore, together with previous data (Rai *et al.* 2010), the present findings support the use of such compounds, particularly RGFP 109, in clinical development in order to provide potential therapeutics for FRDA.

Finally, since larger expanded GAA repeat tracts are associated with greater heterochromatin mediated silencing of the *FXN* gene and a more severe phenotype in FRDA (Saveliev *et al.* 2003; Soragni *et al.* 2008), it is of paramount importance to use a larger GAA repeat-containing mouse model for future *in vivo* experiments. As mentioned earlier we are currently investigating possible methods of increasing GAA repeats within our FRDA YAC transgenic mouse model and this will hopefully be achieved soon. Validating any future experiments with Y47 mice rather than WT mice should also be considered essential.

Summary and future plans

Friedreich ataxia is an autosomal recessive neurodegenerative disease affecting the central and peripheral nervous system (Harding 1981; Harding 1993) for which currently there is no therapy. Although FRDA has been classified as a rare disorder, the carrier frequency is approximately 1:120 individuals (Cossee *et al.* 1999). The most common mutation causing the disease is a large trinucleotide GAA repeat expansion in the first intron of *FXN* gene encoding 'frataxin', a mitochondrial protein. Although the mechanism by which the GAA repeat expansion induces silencing of *FXN* gene is currently not known, recent *in vitro* and *in vivo* investigations has been put forward that FRDA is associated with non-B DNA conformation (Ohshima *et al.* 1998) and/or heterochromatin-mediated *FXN* gene silencing (Saveliev *et al.* 2003; Festenstein 2006). In support to the later hypothesis, differential DNA methylation of CpG islands and histone modifications such as increased DNA methylation and decreased acetylation have been reported in FRDA (Herman *et al.* 2006; Greene *et al.* 2007; Al-Mahdawi *et al.* 2008).

The above mentioned consequences in association with FRDA have encouraged us to test compounds which can potentially directly reverse the abnormal phenotype of FRDA. Therefore, in order to find an effective therapy for FRDA we have investigated several DNA demethylating agents, HDAC inhibitors and GAA interacting compounds using our *in vitro* and/or *in vivo* model systems.

In order to hasten the drug screening and to find any molecular abnormalities associated with FRDA pathogenesis, we have established cell culture systems which include primary fibroblasts from unaffected human individuals and FRDA patients, mouse fibroblasts and neural stem cells (fetal and adult) from WT, YG8 and YG22 mice. Using mouse primary fibroblats we have shown that both YG8 and YG22 rescue mouse cells are more sensitive to

hydrogen peroxide induced oxidative stress, as seen in FRDA patient fibroblasts (Wong *et al.* 1999). Furthermore, we have also described the differentiation of NSC in to various neural cells such as neurons, oligodendrocytes and astrocytes and the presence of these cells has been confirmed using cell specific antibodies by immunoflourescence assay.

To date, the mechanism(s) responsible for the demyelination and neurodegeneration of DRG neurons in FRDA are poorly understood. Recently, it has been reported that frataxin deficiency results in significant inhibition of proliferation of Schwann cells, myelinating supporting cells of the PNS, without affecting DRG neural cells (Lu *et al.* 2009), indicating the importance of supporting cells in FRDA pathology. Therefore, future work should be focused on the quantification of GAA repeat expansions and frataxin mRNA and protein levels in each individual neural cell type to unravel any such mechanisms in the FRDA YAC transgenic mice.

The use of DNA demethylating agents, such as 5-aza-CdR, zebularine and hydralazine, have shown significantly increased *FXN* expression and reduced DNA methylation, particularly in mouse cells. However, the elevated levels of *FXN* expression were produced independent of DNA methylation, suggesting DNA methylation in FRDA is a secondary consequence of the disease. In addition, since the DNA demethylating agents used in these experiments are non-specific, they are likely to reduce global DNA methylation and perhaps affect the regulation of several genes, concurring with previous results (Vallender and Lahn 2006). Therefore, use of sequence specific DNA demethylating agents such as MG98 (antisense oligonucleotide) should be considered for future experiments. Additionally, since we only quantified *FXN* mRNA expression at the transcription level following treatment with

DNA demethylating agents, it is also essential to find any post-transcriptional effects of DNA demethylating agents and this could be done by future frataxin protein quantification.

The use of GAA interacting compounds, such as DB221 and pentamidine, has also given interesting results. Particularly, with DB221 we found a significant increase in *FXN* mRNA expression in both mouse and human fibroblasts together with reduced DNA methylation. This finding adds support the hypothesized association between GAA repeat expansions, DNA methylation and *FXN* expression (Saveliev *et al.* 2003; Al-Mahdawi *et al.* 2008). Curiously, we also investigated the efficacy of DB221 in a short-term preliminary study using 10mg/kg of DB221 along with a mock treatment. No obvious changes in *FXN* mRNA expression were detected in both brain and heart tissues tested between vehicle and drug-treated mice (Figure B.5). It could be possible that a sub-optimal concentration of the drug was incapable of provoking *FXN* expression in such a short period of time (3-days consecutive injection). Therefore, further DB221 treatments need to be assessed in future, possibly with longer-term *in vivo* experiments.

Although the mechanism by which the GAA interacting compounds increase *FXN* expression is currently not known, it is believed to involve reversing the non-B DNA structures associated with FRDA-pathology (Grant *et al.* 2006; Hebert and Whittom 2007; Hebert 2008; Bergquist *et al.* 2009). In future experiments these compounds could be tested for their ability to possibly result in histone modification changes to help unravel any FRDA-associated disease mechanisms. If these compounds do not give significantly increased the levels of acetylated histones in FRDA cells or patients, but do cause increased *FXN* expression, this could be imply that the *FXN* silencing in FRDA is a direct effect on non-B DNA structure formation. On the other hand, if these compounds are able to increase the *FXN*

expression and also acetylate histones in FRDA then it could be postulated that non-B DNA structures trigger deacetylated histone-induced heterochromatin-mediated silencing in FRDA, in agreement with previously proposed hypothesis (Saveliev *et al.* 2003).

Since the investigation of DNA demethylating agents revealed that DNA methylation is likely a secondary consequence in FRDA, we further investigated the possible therapy for FRDA using HDAC inhibitors. We found encouraging results using class III HDAC inhibitors particularly in mouse cells and probably this is due to small number of GAA repeats (<250) in mouse cells compared to human FRDA fibroblasts (>450). In contrast, we obtained similar results in mouse and human fibroblasts cells with nicotinamide, where *FXN* expression was increased by approximately 2-fold. However, the necessary use of high concentrations of nicotinamide (≥10mM) to induce the *FXN* expression strongly limits the use of such compound in a clinical setting.

Additionally, we have also investigated the long-term efficacy of two class I HDAC inhibitors, RGFA 136 and RGFP 109, which have previously been shown increased frataxin mRNA and protein levels, together with significant increases in acetylated H3 and H4 histones in brain tissues of KIKI mice and FRDA patient primary lymphocytes (Rai *et al.* 2010). These findings suggested to us that such compounds would be capable of crossing blood-brain barrier and induce drug-mediated effect. During the drug treatments with both compounds, we monitored the functional analysis of the mice in regular intervals by rotarod, locomotor activity and beam-breaker testing. The analysis by two way ANOVA detected a significant improvement in functional analysis with both drugs, but mainly RGFA 136, suggesting that these drugs are effective in ameliorating the FRDA-associated YG8 mouse phenotype.

However, none of these compounds significantly increased the *FXN* mRNA expression in brain tissues indicating little effect of these compounds at the transcriptional level. It is also possible that the activity of RGFA 136 and RGFP 109 to cross the blood brain-barrier is not as good as has been inferred from the previous KIKI mouse studies (Rai *et al.* 2010). Therefore, future studies should also investigate the frataxin mRNA and protein levels in non-CNS tissues of the YG8 mouse such as heart, liver and skeletal muscle. A potential beneficial effect of RGFA 136 and RGFP 109 in skeletal muscle tissue is certainly implied by the improvements observed in locomotor activity and beam-breaker measurements, which involve muscle strength.

Nevertheless, significant increases in frataxin protein, aconitase enzyme activity and considerably reduced DRG neurodegeneration were observed in the brain tissues of mice, particularly when treated with RGFP 109. In contrast, such parameters were only marginally increased in mice treated with RGFA 136, suggesting that RGFP 109 treatment may be better at crossing blood brain-barrier and may be potentially beneficial in reversing the FRDA pathology. RGFA 136 and RGFP 109 have shown distinctly different effects when taking both the functional and molecular analysis into the consideration. Therefore, it may be beneficial to use these two compounds together for any future experiments in order to hopefully obtain a much more prominent synergistic effect.

In order to find an effective drug screening use of positive controls is of paramount importance. The positive control confirms that the given drug is competent in observing the effect therefore it reduces the false negatives. The lack of use of positive controls may be perhaps a negative aspect in our drug screening tests. Therefore, for any future therapeutic testing use of positive control(s) need to be considered essential.

In conclusion, a number of compounds tested as part of this thesis show good promise for FRDA therapy. It is hoped that at least one of these compounds will soon be taken forward into FRDA clinical trials and may eventually help to cure this disease.

List of references

Aapola U, Kawasaki K*, et al.* (2000). "Isolation and initial characterization of a novel zinc finger gene, DNMT3L, on 21q22.3, related to the cytosine-5-methyltransferase 3 gene family." Genomics **65**(3): 293-298.

Abel T and Zukin RS (2008). "Epigenetic targets of HDAC inhibition in neurodegenerative and psychiatric disorders." Curr Opin Pharmacol **8**(1): 57-64.

Abeliovich A and Doege CA (2009). "Reprogramming therapeutics: iPS cell prospects for neurodegenerative disease." Neuron **61**(3): 337-339.

Abematsu M, Tsujimura K*, et al.* (2010). "Neurons derived from transplanted neural stem cells restore disrupted neuronal circuitry in a mouse model of spinal cord injury." J Clin Invest.

Acquaviva F, De Biase I*, et al.* (2005). "Extra-mitochondrial localisation of frataxin and its association with IscU1 during enterocyte-like differentiation of the human colon adenocarcinoma cell line Caco-2." J Cell Sci **118**(Pt 17): 3917-3924.

Acquaviva F, Castaldo I*, et al.* (2008). "Recombinant human erythropoietin increases frataxin protein expression without increasing mRNA expression." Cerebellum **7**(3): 360-365.

Adinolfi S, Iannuzzi C*, et al.* (2009). "Bacterial frataxin CyaY is the gatekeeper of iron-sulfur cluster formation catalyzed by IscS." Nat Struct Mol Biol **16**(4): 390-396.

Al-Mahdawi S, Pinto RM*, et al.* (2004). "GAA repeat instability in Friedreich ataxia YAC transgenic mice." Genomics **84**(2): 301-310.

Al-Mahdawi S, Pinto RM*, et al.* (2006). "GAA repeat expansion mutation mouse models of Friedreich ataxia exhibit oxidative stress leading to progressive neuronal and cardiac pathology." Genomics **88**(5): 580-590.

Al-Mahdawi S, Pinto RM*, et al.* (2008). "The Friedreich ataxia GAA repeat expansion mutation induces comparable epigenetic changes in human and transgenic mouse brain and heart tissues." Hum Mol Genet **17**(5): 735-746.

Albani D, Polito L*, et al.* (2009). "The SIRT1 activator resveratrol protects SK-N-BE cells from oxidative stress and against toxicity caused by alpha-synuclein or amyloid-beta (1-42) peptide." J Neurochem **110**(5): 1445-1456.

Amato RJ (2007). "Inhibition of DNA methylation by antisense oligonucleotide MG98 as cancer therapy." Clin Genitourin Cancer **5**(7): 422-426.

Anderson PR, Kirby K*, et al.* (2005). "RNAi-mediated suppression of the mitochondrial iron chaperone, frataxin, in Drosophila." Hum Mol Genet **14**(22): 3397-3405.

Antos CL, McKinsey TA*, et al.* (2003). "Dose-dependent blockade to cardiomyocyte hypertrophy by histone deacetylase inhibitors." J Biol Chem **278**(31): 28930-28937.

Arce C, Segura-Pacheco B*, et al.* (2006). "Hydralazine target: from blood vessels to the epigenome." J Transl Med **4**: 10.

Babcock M, de Silva D*, et al.* (1997). "Regulation of mitochondrial iron accumulation by Yfh1p, a putative homolog of frataxin." Science **276**(5319): 1709-1712.

Baralle M, Pastor T*, et al.* (2008). "Influence of Friedreich ataxia GAA noncoding repeat expansions on pre-mRNA processing." Am J Hum Genet **83**(1): 77-88.

Baylin SB and Herman JG (2000). "DNA hypermethylation in tumorigenesis: epigenetics joins genetics." Trends Genet **16**(4): 168-174.

Beard C, Li E*, et al.* (1995). "Loss of methylation activates Xist in somatic but not in embryonic cells." Genes Dev **9**(19): 2325-2334.

Bedalov A, Gatbonton T*, et al.* (2001). "Identification of a small molecule inhibitor of Sir2p." Proc Natl Acad Sci U S A **98**(26): 15113-15118.

Beher D, Wu J*, et al.* (2009). "Resveratrol is not a direct activator of SIRT1 enzyme activity." Chem Biol Drug Des **74**(6): 619-624.

Berciano J, Mateo I*, et al.* (2002). "Friedreich ataxia with minimal GAA expansion presenting as adult-onset spastic ataxia." J Neurol Sci **194**(1): 75-82.

Berger SL (2007). "The complex language of chromatin regulation during transcription." Nature **447**(7143): 407-412.

Bergquist H, Nikravesh A*, et al.* (2009). "Structure-specific recognition of Friedreich's ataxia (GAA)n repeats by benzoquinoquinoxaline derivatives." Chembiochem **10**(16): 2629-2637.

Bestor TH (2000). "The DNA methyltransferases of mammals." Hum Mol Genet **9**(16): 2395-2402.

Bhalla KN (2005). "Epigenetic and chromatin modifiers as targeted therapy of hematologic malignancies." J Clin Oncol **23**(17): 3971-3993.

Biacsi R, Kumari D*, et al.* (2008). "SIRT1 inhibition alleviates gene silencing in Fragile X mental retardation syndrome." PLoS Genet **4**(3): e1000017.

Bidichandani SI, Ashizawa T*, et al.* (1998). "The GAA triplet-repeat expansion in Friedreich ataxia interferes with transcription and may be associated with an unusual DNA structure." Am J Hum Genet **62**(1): 111-121.

Bidichandani SI, Garcia CA*, et al.* (2000). "Very late-onset Friedreich ataxia despite large GAA triplet repeat expansions." Arch Neurol **57**(2): 246-251.

Bitterman KJ, Anderson RM*, et al.* (2002). "Inhibition of silencing and accelerated aging by nicotinamide, a putative negative regulator of yeast sir2 and human SIRT1." J Biol Chem **277**(47): 45099-45107.

Blander G and Guarente L (2004). "The Sir2 family of protein deacetylases." Annu Rev Biochem **73**: 417-435.

Boddaert N, Le Quan Sang KH*, et al.* (2007). "Selective iron chelation in Friedreich ataxia: biologic and clinical implications." Blood **110**(1): 401-408.

Boehm T, Scheiber-Mojdehkar B*, et al.* (2010). "Variations of frataxin protein levels in normal individuals." Neurol Sci.

Boesch S, Sturm B*, et al.* (2007). "Friedreich's ataxia: clinical pilot trial with recombinant human erythropoietin." Ann Neurol **62**(5): 521-524.

Boesch S, Sturm B*, et al.* (2008). "Neurological effects of recombinant human erythropoietin in Friedreich's ataxia: a clinical pilot trial." Mov Disord **23**(13): 1940-1944.

Bogoyevitch MA (2004). "An update on the cardiac effects of erythropoietin cardioprotection by erythropoietin and the lessons learnt from studies in neuroprotection." Cardiovasc Res **63**(2): 208-216.

Bolden JE, Peart MJ*, et al.* (2006). "Anticancer activities of histone deacetylase inhibitors." Nat Rev Drug Discov **5**(9): 769-784.

Bradley JL, Blake JC*, et al.* (2000). "Clinical, biochemical and molecular genetic correlations in Friedreich's ataxia." Hum Mol Genet **9**(2): 275-282.

Bradley JL, Homayoun S*, et al.* (2004). "Role of oxidative damage in Friedreich's ataxia." Neurochem Res **29**(3): 561-567.

Burchmore RJ, Ogbunude PO*, et al.* (2002). "Chemotherapy of human African trypanosomiasis." Curr Pharm Des **8**(4): 256-267.

Burnett R, Melander C*, et al.* (2006). "DNA sequence-specific polyamides alleviate transcription inhibition associated with long GAA.TTC repeats in Friedreich's ataxia." Proc Natl Acad Sci U S A **103**(31): 11497-11502.

Butler R and Bates GP (2006). "Histone deacetylase inhibitors as therapeutics for polyglutamine disorders." Nat Rev Neurosci **7**(10): 784-796.

Butt AM, Hamilton N*, et al.* (2005). "Synantocytes: the fifth element." J Anat **207**(6): 695-706.

Calmels N, Schmucker S*, et al.* (2009). "The first cellular models based on frataxin missense mutations that reproduce spontaneously the defects associated with Friedreich ataxia." PLoS ONE **4**(7): e6379.

Campuzano V, Montermini L*, et al.* (1996). "Friedreich's ataxia: autosomal recessive disease caused by an intronic GAA triplet repeat expansion." Science **271**(5254): 1423-1427.

Campuzano V, Montermini L*, et al.* (1997). "Frataxin is reduced in Friedreich ataxia patients and is associated with mitochondrial membranes." Hum Mol Genet **6**(11): 1771-1780.

Candelaria M, Gallardo-Rincon D*, et al.* (2007). "A phase II study of epigenetic therapy with hydralazine and magnesium valproate to overcome chemotherapy resistance in refractory solid tumors." Ann Oncol **18**(9): 1529-1538.

Cang S, Ma Y*, et al.* (2009). "New clinical developments in histone deacetylase inhibitors for epigenetic therapy of cancer." J Hematol Oncol **2**: 22.

Canto C and Auwerx J (2009). "PGC-1alpha, SIRT1 and AMPK, an energy sensing network that controls energy expenditure." Curr Opin Lipidol **20**(2): 98-105.

Canto C, Gerhart-Hines Z*, et al.* (2009). "AMPK regulates energy expenditure by modulating NAD+ metabolism and SIRT1 activity." Nature **458**(7241): 1056-1060.

Cataldo VD, Cortes J*, et al.* (2009). "Azacitidine for the treatment of myelodysplastic syndrome." Expert Rev Anticancer Ther **9**(7): 875-884.

Cavadini P, Gellera C*, et al.* (2000). "Human frataxin maintains mitochondrial iron homeostasis in Saccharomyces cerevisiae." Hum Mol Genet **9**(17): 2523-2530.

Cecconi D, Donadelli M*, et al.* (2009). "Synergistic effect of trichostatin A and 5-aza-2'-deoxycytidine on growth inhibition of pancreatic endocrine tumour cell lines: a proteomic study." Proteomics **9**(7): 1952-1966.

Cemal CK, Huxley C*, et al.* (1999). "Insertion of expanded CAG trinucleotide repeat motifs into a yeast artificial chromosome containing the human Machado-Joseph disease gene." Gene **236**(1): 53-61.

Chaires JB (2005). "Competition dialysis: an assay to measure the structural selectivity of drug-nucleic acid interactions." Curr Med Chem Anticancer Agents **5**(4): 339-352.

Chamberlain S, Shaw J*, et al.* (1988). "Mapping of mutation causing Friedreich's ataxia to human chromosome 9." Nature **334**(6179): 248-250.

Chantrel-Groussard K, Geromel V*, et al.* (2001). "Disabled early recruitment of antioxidant defenses in Friedreich's ataxia." Hum Mol Genet **10**(19): 2061-2067.

Chen G, Wang Y*, et al.* (2009). "Combination of DNA methylation inhibitor 5-azacytidine and arsenic trioxide has synergistic activity in myeloma." Eur J Haematol **82**(3): 176-183.

Cheng JC, Matsen CB*, et al.* (2003). "Inhibition of DNA methylation and reactivation of silenced genes by zebularine." J Natl Cancer Inst **95**(5): 399-409.

Cheng JC, Weisenberger DJ*, et al.* (2004). "Continuous zebularine treatment effectively sustains demethylation in human bladder cancer cells." Mol Cell Biol **24**(3): 1270-1278.

Chiurazzi P, Pomponi MG*, et al.* (1998). "In vitro reactivation of the FMR1 gene involved in fragile X syndrome." Hum Mol Genet **7**(1): 109-113.

Chiurazzi P, Pomponi MG*, et al.* (1999). "Synergistic effect of histone hyperacetylation and DNA demethylation in the reactivation of the FMR1 gene." Hum Mol Genet **8**(12): 2317-2323.

Cho SJ, Lee MG*, et al.* (2000). "Crystal structure of Escherichia coli CyaY protein reveals a previously unidentified fold for the evolutionarily conserved frataxin family." Proc Natl Acad Sci U S A **97**(16): 8932-8937.

Chou CJ, Herman D*, et al.* (2008). "Pimelic diphenylamide 106 is a slow, tight-binding inhibitor of class I histone deacetylases." J Biol Chem **283**(51): 35402-35409.

Christodoulou K, Deymeer F*, et al.* (2001). "Mapping of the second Friedreich's ataxia (FRDA2) locus to chromosome 9p23-p11: evidence for further locus heterogeneity." Neurogenetics **3**(3): 127-132.

Chua KF, Mostoslavsky R*, et al.* (2005). "Mammalian SIRT1 limits replicative life span in response to chronic genotoxic stress." Cell Metab **2**(1): 67-76.

Clark RM, De Biase I*, et al.* (2007). "The GAA triplet-repeat is unstable in the context of the human FXN locus and displays age-dependent expansions in cerebellum and DRG in a transgenic mouse model." Hum Genet **120**(5): 633-640.

Colot V and Rossignol JL (1999). "Eukaryotic DNA methylation as an evolutionary device." Bioessays **21**(5): 402-411.

Condo I, Ventura N*, et al.* (2006). "A pool of extramitochondrial frataxin that promotes cell survival." J Biol Chem **281**(24): 16750-16756.

Condo I, Ventura N*, et al.* (2007). "In vivo maturation of human frataxin." Hum Mol Genet **16**(13): 1534-1540.

Condo I, Malisan F*, et al.* (2010). "Molecular control of the cytosolic aconitase/IRP1 switch by extramitochondrial frataxin." Hum Mol Genet **19**(7): 1221-1229.

Constantinides PG, Jones PA*, et al.* (1977). "Functional striated muscle cells from non-myoblast precursors following 5-azacytidine treatment." Nature **267**(5609): 364-366.

Cooper JM, Korlipara LV*, et al.* (2008). "Coenzyme Q10 and vitamin E deficiency in Friedreich's ataxia: predictor of efficacy of vitamin E and coenzyme Q10 therapy." Eur J Neurol **15**(12): 1371-1379.

Coppola G, Choi SH*, et al.* (2006). "Gene expression profiling in frataxin deficient mice: microarray evidence for significant expression changes without detectable neurodegeneration." Neurobiol Dis **22**(2): 302-311.

Coppola G, Marmolino D*, et al.* (2009). "Functional genomic analysis of frataxin deficiency reveals tissue-specific alterations and identifies the PPARgamma pathway as a therapeutic target in Friedreich's ataxia." Hum Mol Genet **18**(13): 2452-2461.

Cossee M, Campuzano V*, et al.* (1997a). "Frataxin fracas." Nat Genet **15**(4): 337-338.

Cossee M, Schmitt M*, et al.* (1997b). "Evolution of the Friedreich's ataxia trinucleotide repeat expansion: founder effect and premutations." Proc Natl Acad Sci U S A **94**(14): 7452-7457.

Cossee M, Durr A*, et al.* (1999). "Friedreich's ataxia: point mutations and clinical presentation of compound heterozygotes." Ann Neurol **45**(2): 200-206.

Cossee M, Puccio H*, et al.* (2000). "Inactivation of the Friedreich ataxia mouse gene leads to early embryonic lethality without iron accumulation." Hum Mol Genet **9**(8): 1219-1226.

Cummings CJ and Zoghbi HY (2000). "Fourteen and counting: unraveling trinucleotide repeat diseases." Hum Mol Genet **9**(6): 909-916.

Da Costa LT, Jen J*, et al.* (1996). "Converting cancer genes into killer genes." Proc Natl Acad Sci U S A **93**(9): 4192-4196.

Dasgupta B and Milbrandt J (2007). "Resveratrol stimulates AMP kinase activity in neurons." Proc Natl Acad Sci U S A **104**(17): 7217-7222.

De Biase I, Rasmussen A*, et al.* (2007a). "Progressive GAA expansions in dorsal root ganglia of Friedreich's ataxia patients." Ann Neurol **61**(1): 55-60.

De Biase I, Rasmussen A*, et al.* (2007b). "Somatic instability of the expanded GAA triplet-repeat sequence in Friedreich ataxia progresses throughout life." Genomics **90**(1): 1-5.

De Biase I, Chutake YK*, et al.* (2009). "Epigenetic Silencing in Friedreich Ataxia Is Associated with Depletion of CTCF (CCCTC-Binding Factor) and Antisense Transcription." PLoS ONE **4**(11): e7914.

De Jaco A, Camp S*, et al.* (2005). "Influence of the 5' intron in the control of acetylcholinesterase gene expression during myogenesis." Chem Biol Interact **157-158**: 372-373.

de Wind N, Dekker M*, et al.* (1995). "Inactivation of the mouse Msh2 gene results in mismatch repair deficiency, methylation tolerance, hyperrecombination, and predisposition to cancer." Cell **82**(2): 321-330.

Delatycki MB, Paris D*, et al.* (1998). "Sperm DNA analysis in a Friedreich ataxia premutation carrier suggests both meiotic and mitotic expansion in the FRDA gene." J Med Genet **35**(9): 713-716.

Delatycki MB, Williamson R*, et al.* (2000). "Friedreich ataxia: an overview." J Med Genet **37**(1): 1-8.

Deng C, Lu Q*, et al.* (2003). "Hydralazine may induce autoimmunity by inhibiting extracellular signal-regulated kinase pathway signaling." Arthritis Rheum **48**(3): 746-756.

Deng T and Zhang Y (2009). "5-Aza-2'-deoxycytidine reactivates expression of RUNX3 by deletion of DNA methyltransferases leading to caspase independent apoptosis in colorectal cancer Lovo cells." Biomed Pharmacother **63**(7): 492-500.

Dhe-Paganon S, Shigeta R*, et al.* (2000). "Crystal structure of human frataxin." J Biol Chem **275**(40): 30753-30756.

Di Prospero NA and Fischbeck KH (2005). "Therapeutics development for triplet repeat expansion diseases." Nat Rev Genet **6**(10): 756-765.

Di Prospero NA, Baker A*, et al.* (2007a). "Neurological effects of high-dose idebenone in patients with Friedreich's ataxia: a randomised, placebo-controlled trial." Lancet Neurol **6**(10): 878-886.

Di Prospero NA, Sumner CJ*, et al.* (2007b). "Safety, tolerability, and pharmacokinetics of high-dose idebenone in patients with Friedreich ataxia." Arch Neurol **64**(6): 803-808.

Dillin A, Hsu AL*, et al.* (2002). "Rates of behavior and aging specified by mitochondrial function during development." Science **298**(5602): 2398-2401.

Dillon N and Festenstein R (2002). "Unravelling heterochromatin: competition between positive and negative factors regulates accessibility." Trends Genet **18**(5): 252-258.

Dou QP (2009). "Molecular mechanisms of green tea polyphenols." Nutr Cancer **61**(6): 827-835.

Drummond DC, Noble CO*, et al.* (2005). "Clinical development of histone deacetylase inhibitors as anticancer agents." Annu Rev Pharmacol Toxicol **45**: 495-528.

Durr A, Cossee M*, et al.* (1996). "Clinical and genetic abnormalities in patients with Friedreich's ataxia." N Engl J Med **335**(16): 1169-1175.

Egger G, Liang G*, et al.* (2004). "Epigenetics in human disease and prospects for epigenetic therapy." Nature **429**(6990): 457-463.

Eissenberg JC, Morris GD*, et al.* (1992). "The heterochromatin-associated protein HP-1 is an essential protein in Drosophila with dosage-dependent effects on position-effect variegation." Genetics **131**(2): 345-352.

Elgin SC (1996). "Heterochromatin and gene regulation in Drosophila." Curr Opin Genet Dev **6**(2): 193-202.

Elgin SC and Grewal SI (2003). "Heterochromatin: silence is golden." Curr Biol **13**(23): R895-898.

Emond M, Lepage G*, et al.* (2000). "Increased levels of plasma malondialdehyde in Friedreich ataxia." Neurology **55**(11): 1752-1753.

Ensembl (2006). "Human Contig View, accessed October 2006 URL<http://www.ensembl.org/Homo_sapiens/Search/Results?species=Homo_sapiens;idx=;q=frataxin>."

Felsenfeld G and Groudine M (2003). "Controlling the double helix." Nature **421**(6921): 448-453.

Feng J, Bussiere F*, et al.* (2001). "Mitochondrial electron transport is a key determinant of life span in Caenorhabditis elegans." Dev Cell **1**(5): 633-644.

Ferrante RJ, Kubilus JK*, et al.* (2003). "Histone deacetylase inhibition by sodium butyrate chemotherapy ameliorates the neurodegenerative phenotype in Huntington's disease mice." J Neurosci **23**(28): 9418-9427.

Festenstein R, Sharghi-Namini S*, et al.* (1999). "Heterochromatin protein 1 modifies mammalian PEV in a dose- and chromosomal-context-dependent manner." Nat Genet **23**(4): 457-461.

Festenstein R (2006). "Breaking the silence in Friedreich's ataxia." Nat Chem Biol **2**(10): 512-513.

Filla A, De Michele G*, et al.* (1996). "The relationship between trinucleotide (GAA) repeat length and clinical features in Friedreich ataxia." Am J Hum Genet **59**(3): 554-560.

Fleming J, Spinoulas A*, et al.* (2005). "Partial correction of sensitivity to oxidant stress in Friedreich ataxia patient fibroblasts by frataxin-encoding adeno-associated virus and lentivirus vectors." Hum Gene Ther **16**(8): 947-956.

Flotho C, Claus R*, et al.* (2009). "The DNA methyltransferase inhibitors azacitidine, decitabine and zebularine exert differential effects on cancer gene expression in acute myeloid leukemia cells." Leukemia **23**(6): 1019-1028.

Foury F and Cazzalini O (1997). "Deletion of the yeast homologue of the human gene associated with Friedreich's ataxia elicits iron accumulation in mitochondria." FEBS Lett **411**(2-3): 373-377.

Foury F (1999). "Low iron concentration and aconitase deficiency in a yeast frataxin homologue deficient strain." FEBS Lett **456**(2): 281-284.

Foury F and Talibi D (2001). "Mitochondrial control of iron homeostasis. A genome wide analysis of gene expression in a yeast frataxin-deficient strain." J Biol Chem **276**(11): 7762-7768.

Frank-Kamenetskii MD and Mirkin SM (1995). "Triplex DNA structures." Annu Rev Biochem **64**: 65-95.

Freiman RN and Tjian R (2003). "Regulating the regulators: lysine modifications make their mark." Cell **112**(1): 11-17.

Frye RA (1999). "Characterization of five human cDNAs with homology to the yeast SIR2 gene: Sir2-like proteins (sirtuins) metabolize NAD and may have protein ADP-ribosyltransferase activity." Biochem Biophys Res Commun **260**(1): 273-279.

Fuller L and Dietrich LS (1971). "Comments on the detemmination of nicotinamide." Anal Biochem **39**(2): 538-539.

Garbes L, Riessland M*, et al.* (2009). "LBH589 induces up to 10-fold SMN protein levels by several independent mechanisms and is effective even in cells from SMA patients non-responsive to valproate." Hum Mol Genet **18**(19): 3645-3658.

Gardian G, Browne SE*, et al.* (2005). "Neuroprotective effects of phenylbutyrate in the N171-82Q transgenic mouse model of Huntington's disease." J Biol Chem **280**(1): 556-563.

Gerber J, Muhlenhoff U*, et al.* (2003). "An interaction between frataxin and Isu1/Nfs1 that is crucial for Fe/S cluster synthesis on Isu1." EMBO Rep **4**(9): 906-911.

Ghazizadeh M (2003). "Cisplatin may induce frataxin expression." J Nippon Med Sch **70**(4): 367-371.

Ghosh S and Feany MB (2004). "Comparison of pathways controlling toxicity in the eye and brain in Drosophila models of human neurodegenerative diseases." Hum Mol Genet **13**(18): 2011-2018.

Ghoshal K, Datta J*, et al.* (2005). "5-Aza-deoxycytidine induces selective degradation of DNA methyltransferase 1 by a proteasomal pathway that requires the KEN box, bromo-adjacent homology domain, and nuclear localization signal." Mol Cell Biol **25**(11): 4727-4741.

Glaser KB (2007). "HDAC inhibitors: clinical update and mechanism-based potential." Biochem Pharmacol **74**(5): 659-671.

Glover AB and Leyland-Jones B (1987). "Biochemistry of azacitidine: a review." Cancer Treat Rep **71**(10): 959-964.

Glozak MA, Sengupta N*, et al.* (2005). "Acetylation and deacetylation of non-histone proteins." Gene **363**: 15-23.

Goffin J and Eisenhauer E (2002). "DNA methyltransferase inhibitors-state of the art." Ann Oncol **13**(11): 1699-1716.

Goll MG and Bestor TH (2002). "Histone modification and replacement in chromatin activation." Genes Dev **16**(14): 1739-1742.

Goll MG, Kirpekar F*, et al.* (2006). "Methylation of tRNAAsp by the DNA methyltransferase homolog Dnmt2." Science **311**(5759): 395-398.

Gomes-Pereira M and Monckton DG (2004). "Mouse tissue culture models of unstable triplet repeats." Methods Mol Biol **277**: 215-227.

Gomez-Sebastian S, Gimenez-Cassina A*, et al.* (2007). "Infectious delivery and expression of a 135 kb human FRDA genomic DNA locus complements Friedreich's ataxia deficiency in human cells." Mol Ther **15**(2): 248-254.

Goncalves S, Paupe V*, et al.* (2008). "Deferiprone targets aconitase: implication for Friedreich's ataxia treatment." BMC Neurol **8**: 20.

Gordon DM, Shi Q*, et al.* (1999). "Maturation of frataxin within mammalian and yeast mitochondria: one-step processing by matrix processing peptidase." Hum Mol Genet **8**(12): 2255-2262.

Gottesfeld JM (2007). "Small molecules affecting transcription in Friedreich ataxia." Pharmacol Ther **116**(2): 236-248.

Grabczyk E and Usdin K (2000). "The GAA*TTC triplet repeat expanded in Friedreich's ataxia impedes transcription elongation by T7 RNA polymerase in a length and supercoil dependent manner." Nucleic Acids Res **28**(14): 2815-2822.

Grabczyk E, Mancuso M*, et al.* (2007). "A persistent RNA.DNA hybrid formed by transcription of the Friedreich ataxia triplet repeat in live bacteria, and by T7 RNAP in vitro." Nucleic Acids Res **35**(16): 5351-5359.

Grant L, Sun J*, et al.* (2006). "Rational selection of small molecules that increase transcription through the GAA repeats found in Friedreich's ataxia." FEBS Lett **580**(22): 5399-5405.

Grant PA (2001). "A tale of histone modifications." Genome Biol **2**(4): REVIEWS0003.

Greene E, Mahishi L*, et al.* (2007). "Repeat-induced epigenetic changes in intron 1 of the frataxin gene and its consequences in Friedreich ataxia." Nucleic Acids Res **35**(10): 3383-3390.

Grozinger CM, Chao ED*, et al.* (2001). "Identification of a class of small molecule inhibitors of the sirtuin family of NAD-dependent deacetylases by phenotypic screening." J Biol Chem **276**(42): 38837-38843.

Guarente L (2006). "Sirtuins as potential targets for metabolic syndrome." Nature **444**(7121): 868-874.

Haigis MC and Guarente LP (2006). "Mammalian sirtuins--emerging roles in physiology, aging, and calorie restriction." Genes Dev **20**(21): 2913-2921.

Harding AE (1981). "Friedreich's ataxia: a clinical and genetic study of 90 families with an analysis of early diagnostic criteria and intrafamilial clustering of clinical features." Brain **104**(3): 589-620.

Harding AE (1993). "Clinical features and classification of inherited ataxias." Adv Neurol **61**: 1-14.

Harrison RG, Greenman, M. J., Mall, F.M., Jackson, C. M. (1907). "Observations of the living develping nerve fibre." The Anatomical Record **1**: 116-128.

Hart PE, Lodi R*, et al.* (2005). "Antioxidant treatment of patients with Friedreich ataxia: four-year follow-up." Arch Neurol **62**(4): 621-626.

Haugen AC, Di Prospero NA*, et al.* (2010). "Altered gene expression and DNA damage in peripheral blood cells from Friedreich's ataxia patients: cellular model of pathology." PLoS Genet **6**(1): e1000812.

Hausse AO, Aggoun Y*, et al.* (2002). "Idebenone and reduced cardiac hypertrophy in Friedreich's ataxia." Heart **87**(4): 346-349.

Hebert MD and Whittom AA (2007). "Gene-based approaches toward Friedreich ataxia therapeutics." Cell Mol Life Sci **64**(23): 3034-3043.

Hebert MD (2008). "Targeting the gene in Friedreich ataxia." Biochimie **90**(8): 1131-1139.

Heneka MT and Landreth GE (2007). "PPARs in the brain." Biochim Biophys Acta **1771**(8): 1031-1045.

Herman D, Jenssen K*, et al.* (2006). "Histone deacetylase inhibitors reverse gene silencing in Friedreich's ataxia." Nat Chem Biol **2**(10): 551-558.

Herting RL and Hunter HL (1967). "The physiologic and pharmacologic basis for the clinical treatment of hypertension." Med Clin North Am **51**(1): 25-37.

Hildebrandt E, Boykin DW*, et al.* (1998). "Identification and characterization of an endo/exonuclease in Pneumocystis carinii that is inhibited by dicationic diarylfurans with efficacy against Pneumocystis pneumonia." J Eukaryot Microbiol **45**(1): 112-121.

Hockly E, Richon VM*, et al.* (2003). "Suberoylanilide hydroxamic acid, a histone deacetylase inhibitor, ameliorates motor deficits in a mouse model of Huntington's disease." Proc Natl Acad Sci U S A **100**(4): 2041-2046.

Holemon H, Korshunova Y*, et al.* (2007). "MethylScreen: DNA methylation density monitoring using quantitative PCR." Biotechniques **43**(5): 683-693.

Holliday R (1991). "Mutations and epimutations in mammalian cells." Mutat Res **250**(1-2): 351-363.

Holliday R and Grigg GW (1993). "DNA methylation and mutation." Mutat Res **285**(1): 61-67.

Hu F, Chou CJ*, et al.* (2009). "Design and synthesis of novel hybrid benzamide-peptide histone deacetylase inhibitors." Bioorg Med Chem Lett **19**(14): 3928-3931.

Hutt DM, Herman D*, et al.* (2010). "Reduced histone deacetylase 7 activity restores function to misfolded CFTR in cystic fibrosis." Nat Chem Biol **6**(1): 25-33.

Imai S, Armstrong CM*, et al.* (2000). "Transcriptional silencing and longevity protein Sir2 is an NAD-dependent histone deacetylase." Nature **403**(6771): 795-800.

Imbert G, Kretz C*, et al.* (1993). "Origin of the expansion mutation in myotonic dystrophy." Nat Genet **4**(1): 72-76.

Inche AG and La Thangue NB (2006). "Chromatin control and cancer-drug discovery: realizing the promise." Drug Discov Today **11**(3-4): 97-109.

Issa JP, Garcia-Manero G*, et al.* (2004). "Phase 1 study of low-dose prolonged exposure schedules of the hypomethylating agent 5-aza-2'-deoxycytidine (decitabine) in hematopoietic malignancies." Blood **103**(5): 1635-1640.

Jackson-Grusby L, Beard C*, et al.* (2001). "Loss of genomic methylation causes p53-dependent apoptosis and epigenetic deregulation." Nat Genet **27**(1): 31-39.

Jaenisch R and Bird A (2003). "Epigenetic regulation of gene expression: how the genome integrates intrinsic and environmental signals." Nat Genet **33 Suppl**: 245-254.

Jain A, Rajeswari MR*, et al.* (2002). "Formation and thermodynamic stability of intermolecular (R*R*Y) DNA triplex in GAA/TTC repeats associated with Freidreich's ataxia." J Biomol Struct Dyn **19**(4): 691-699.

Jain N, Rossi A*, et al.* (2009). "Epigenetic therapy of leukemia: An update." Int J Biochem Cell Biol **41**(1): 72-80.

Jana M, Jana A*, et al.* (2007). "A simplified method for isolating highly purified neurons, oligodendrocytes, astrocytes, and microglia from the same human fetal brain tissue." Neurochem Res **32**(12): 2015-2022.

Janssen S, Cuvier O*, et al.* (2000a). "Specific gain- and loss-of-function phenotypes induced by satellite-specific DNA-binding drugs fed to Drosophila melanogaster." Mol Cell **6**(5): 1013-1024.

Janssen S, Durussel T*, et al.* (2000b). "Chromatin opening of DNA satellites by targeted sequence-specific drugs." Mol Cell **6**(5): 999-1011.

Jauslin ML, Meier T*, et al.* (2003). "Mitochondria-targeted antioxidants protect Friedreich Ataxia fibroblasts from endogenous oxidative stress more effectively than untargeted antioxidants." Faseb J **17**(13): 1972-1974.

Jenuwein T and Allis CD (2001). "Translating the histone code." Science **293**(5532): 1074-1080.

Jiang S, Dowdy SC*, et al.* (2007). "Histone deacetylase inhibitors induce apoptosis in both Type I and Type II endometrial cancer cells." Gynecol Oncol **105**(2): 493-500.

Jones PA and Taylor SM (1980). "Cellular differentiation, cytidine analogs and DNA methylation." Cell **20**(1): 85-93.

Kaanders JH, Pop LA*, et al.* (2002). "ARCON: experience in 215 patients with advanced head-and-neck cancer." Int J Radiat Oncol Biol Phys **52**(3): 769-778.

Kaeberlein M, McVey M*, et al.* (1999). "The SIR2/3/4 complex and SIR2 alone promote longevity in Saccharomyces cerevisiae by two different mechanisms." Genes Dev **13**(19): 2570-2580.

Kamens HM, Phillips TJ*, et al.* (2005). "Characterization of the parallel rod floor apparatus to test motor incoordination in mice." Genes Brain Behav **4**(4): 253-266.

Kamens HM and Crabbe JC (2007). "The parallel rod floor test: a measure of ataxia in mice." Nat Protoc **2**(2): 277-281.

Kaplan S, Bisleri G*, et al.* (2005). "Resveratrol, a natural red wine polyphenol, reduces ischemia-reperfusion-induced spinal cord injury." Ann Thorac Surg **80**(6): 2242-2249.

Kass SU, Pruss D*, et al.* (1997). "How does DNA methylation repress transcription?" Trends Genet **13**(11): 444-449.

Kato K, Long NK*, et al.* (2008). "Effects of green tea polyphenol on methylation status of RECK gene and cancer cell invasion in oral squamous cell carcinoma cells." Br J Cancer **99**(4): 647-654.

Kawamata N, Chen J*, et al.* (2007). "Suberoylanilide hydroxamic acid (SAHA; vorinostat) suppresses translation of cyclin D1 in mantle cell lymphoma cells." Blood **110**(7): 2667-2673.

Kazantsev AG and Thompson LM (2008). "Therapeutic application of histone deacetylase inhibitors for central nervous system disorders." Nat Rev Drug Discov **7**(10): 854-868.

Kelley JA, Driscoll JS*, et al.* (1986). "Furanose-pyranose isomerization of reduced pyrimidine and cyclic urea ribosides." J Med Chem **29**(11): 2351-2358.

Kelso GF, Porteous CM*, et al.* (2001). "Selective targeting of a redox-active ubiquinone to mitochondria within cells: antioxidant and antiapoptotic properties." J Biol Chem **276**(7): 4588-4596.

Kernochan LE, Russo ML*, et al.* (2005). "The role of histone acetylation in SMN gene expression." Hum Mol Genet **14**(9): 1171-1182.

Kim YB, Lee KH*, et al.* (1999). "Oxamflatin is a novel antitumor compound that inhibits mammalian histone deacetylase." Oncogene **18**(15): 2461-2470.

Kiziltepe T, Hideshima T*, et al.* (2007). "5-Azacytidine, a DNA methyltransferase inhibitor, induces ATR-mediated DNA double-strand break responses, apoptosis, and synergistic cytotoxicity with doxorubicin and bortezomib against multiple myeloma cells." Mol Cancer Ther **6**(6): 1718-1727.

Kiziltepe U, Turan NN*, et al.* (2004). "Resveratrol, a red wine polyphenol, protects spinal cord from ischemia-reperfusion injury." J Vasc Surg **40**(1): 138-145.

Klein L, O'Connor CM*, et al.* (2003). "Pharmacologic therapy for patients with chronic heart failure and reduced systolic function: review of trials and practical considerations." Am J Cardiol **91**(9A): 18F-40F.

Knip M, Douek IF*, et al.* (2000). "Safety of high-dose nicotinamide: a review." Diabetologia **43**(11): 1337-1345.

Koeppen AH, Michael SC*, et al.* (2007). "The dentate nucleus in Friedreich's ataxia: the role of iron-responsive proteins." Acta Neuropathol **114**(2): 163-173.

Koeppen AH, Morral JA*, et al.* (2009). "The dorsal root ganglion in Friedreich's ataxia." Acta Neuropathol **118**(6): 763-776.

Kojima K, Ohhashi R*, et al.* (2008). "A role for SIRT1 in cell growth and chemoresistance in prostate cancer PC3 and DU145 cells." Biochem Biophys Res Commun **373**(3): 423-428.

Koutnikova H, Campuzano V*, et al.* (1997). "Studies of human, mouse and yeast homologues indicate a mitochondrial function for frataxin." Nat Genet **16**(4): 345-351.

Koutnikova H, Campuzano V*, et al.* (1998). "Maturation of wild-type and mutated frataxin by the mitochondrial processing peptidase." Hum Mol Genet **7**(9): 1485-1489.

Kouzarides T (2007). "Chromatin modifications and their function." Cell **128**(4): 693-705.

Krasilnikova MM and Mirkin SM (2004). "Replication stalling at Friedreich's ataxia (GAA)n repeats in vivo." Mol Cell Biol **24**(6): 2286-2295.

Kruszewski M and Szumiel I (2005). "Sirtuins (histone deacetylases III) in the cellular response to DNA damage--facts and hypotheses." DNA Repair (Amst) **4**(11): 1306-1313.

Ku S, Soragni E*, et al.* (2010). "Friedreich's Ataxia Induced Pluripotent Stem Cells Model Intergenerational GAATTC Triplet Repeat Instability." Cell Stem Cell **7**(5): 631-637.

Kumari D, Biacsi RE*, et al.* (2010). "Repeat expansion affects both transcription initiation and elongation in friedreich ataxia cells." J Biol Chem.

Kumari D and Usdin K (2010). "The distribution of repressive histone modifications on silenced FMR1 alleles provides clues to the mechanism of gene silencing in fragile X syndrome." Hum Mol Genet **19**(23): 4634-4642.

Lagouge M, Argmann C*, et al.* (2006). "Resveratrol improves mitochondrial function and protects against metabolic disease by activating SIRT1 and PGC-1alpha." Cell **127**(6): 1109-1122.

Landry J, Slama JT*, et al.* (2000a). "Role of NAD(+) in the deacetylase activity of the SIR2-like proteins." Biochem Biophys Res Commun **278**(3): 685-690.

Landry J, Sutton A*, et al.* (2000b). "The silencing protein SIR2 and its homologs are NAD-dependent protein deacetylases." Proc Natl Acad Sci U S A **97**(11): 5807-5811.

Langley B, Gensert JM*, et al.* (2005). "Remodeling chromatin and stress resistance in the central nervous system: histone deacetylase inhibitors as novel and broadly effective neuroprotective agents." Curr Drug Targets CNS Neurol Disord **4**(1): 41-50.

LeBlanc SE, Jang SW*, et al.* (2006). "Direct regulation of myelin protein zero expression by the Egr2 transactivator." J Biol Chem **281**(9): 5453-5460.

Lee JG, Dahi S*, et al.* (2005). "Intronic regulation of matrix metalloproteinase-2 revealed by in vivo transcriptional analysis in ischemia." Proc Natl Acad Sci U S A **102**(45): 16345-16350.

Lee KK and Workman JL (2007). "Histone acetyltransferase complexes: one size doesn't fit all." Nat Rev Mol Cell Biol **8**(4): 284-295.

Lee SS, Lee RY*, et al.* (2003). "A systematic RNAi screen identifies a critical role for mitochondria in C. elegans longevity." Nat Genet **33**(1): 40-48.

Lehrmann H, Pritchard LL*, et al.* (2002). "Histone acetyltransferases and deacetylases in the control of cell proliferation and differentiation." Adv Cancer Res **86**: 41-65.

Lei H, Oh SP*, et al.* (1996). "De novo DNA cytosine methyltransferase activities in mouse embryonic stem cells." Development **122**(10): 3195-3205.

Lenaz G, Bovina C*, et al.* (2002). "Role of mitochondria in oxidative stress and aging." Ann N Y Acad Sci **959**: 199-213.

Levison SW, Druckman SK*, et al.* (2003). "Neural stem cells in the subventricular zone are a source of astrocytes and oligodendrocytes, but not microglia." Dev Neurosci **25**(2-4): 184-196.

Li E, Bestor TH*, et al.* (1992). "Targeted mutation of the DNA methyltransferase gene results in embryonic lethality." Cell **69**(6): 915-926.

Li K, Besse EK*, et al.* (2008). "Iron-dependent regulation of frataxin expression: implications for treatment of Friedreich ataxia." Hum Mol Genet **17**(15): 2265-2273.

Li LH, Olin EJ*, et al.* (1970). "Cytotoxicity and mode of action of 5-azacytidine on L1210 leukemia." Cancer Res **30**(11): 2760-2769.

Li W, Maeda Y*, et al.* (2004). "Beneficial effect of erythropoietin on experimental allergic encephalomyelitis." Ann Neurol **56**(6): 767-777.

Liao MJ, Yin C*, et al.* (1999). "Atm is dispensable for p53 apoptosis and tumor suppression triggered by cell cycle dysfunction." Mol Cell Biol **19**(4): 3095-3102.

Lim F, Palomo GM*, et al.* (2007). "Functional recovery in a Friedreich's ataxia mouse model by frataxin gene transfer using an HSV-1 amplicon vector." Mol Ther **15**(6): 1072-1078.

Llorens JV, Navarro JA*, et al.* (2007). "Causative role of oxidative stress in a Drosophila model of Friedreich ataxia." FASEB J **21**(2): 333-344.

Lodi R, Hart PE*, et al.* (2001a). "Antioxidant treatment improves in vivo cardiac and skeletal muscle bioenergetics in patients with Friedreich's ataxia." Ann Neurol **49**(5): 590-596.

Lodi R, Taylor DJ*, et al.* (2001b). "Mitochondrial dysfunction in friedreich's ataxia." Biol Signals Recept **10**(3-4): 263-270.

Lodi R, Rajagopalan B*, et al.* (2002). "Mitochondrial dysfunction in Friedreich's ataxia: from pathogenesis to treatment perspectives." Free Radic Res **36**(4): 461-466.

Longo VD and Kennedy BK (2006). "Sirtuins in aging and age-related disease." Cell **126**(2): 257-268.

Lorincz MC, Dickerson DR*, et al.* (2004). "Intragenic DNA methylation alters chromatin structure and elongation efficiency in mammalian cells." Nat Struct Mol Biol **11**(11): 1068-1075.

Lu C, Schoenfeld R*, et al.* (2009). "Frataxin deficiency induces Schwann cell inflammation and death." Biochim Biophys Acta **1792**(11): 1052-1061.

Mai A, Massa S*, et al.* (2005). "Histone deacetylation in epigenetics: an attractive target for anticancer therapy." Med Res Rev **25**(3): 261-309.

Maldonado E, Hampsey M*, et al.* (1999). "Repression: targeting the heart of the matter." Cell **99**(5): 455-458.

Mariappan SV, Catasti P*, et al.* (1999). "The high-resolution structure of the triplex formed by the GAA/TTC triplet repeat associated with Friedreich's ataxia." J Mol Biol **285**(5): 2035-2052.

Mariotti C, Solari A*, et al.* (2003). "Idebenone treatment in Friedreich patients: one-year-long randomized placebo-controlled trial." Neurology **60**(10): 1676-1679.

Marks PA and Dokmanovic M (2005). "Histone deacetylase inhibitors: discovery and development as anticancer agents." Expert Opin Investig Drugs **14**(12): 1497-1511.

Marmolino D, Acquaviva F*, et al.* (2009). "PPAR-gamma agonist Azelaoyl PAF increases frataxin protein and mRNA expression: new implications for the Friedreich's ataxia therapy." Cerebellum **8**(2): 98-103.

Marmolino D, Manto M*, et al.* (2010). "PGC-1alpha down-regulation affects the antioxidant response in Friedreich's ataxia." PLoS One **5**(4): e10025.

McLaughlin F and La Thangue NB (2004). "Histone deacetylase inhibitors open new doors in cancer therapy." Biochem Pharmacol **68**(6): 1139-1144.

Minucci S and Pelicci PG (2006). "Histone deacetylase inhibitors and the promise of epigenetic (and more) treatments for cancer." Nat Rev Cancer **6**(1): 38-51.

Miranda CJ, Santos MM*, et al.* (2002). "Frataxin knockin mouse." FEBS Lett **512**(1-3): 291-297.

Miranda CJ, Santos MM*, et al.* (2004). "Frataxin overexpressing mice." FEBS Lett **572**(1-3): 281-288.

Mirkin SM (2007). "Expandable DNA repeats and human disease." Nature **447**(7147): 932-940.

Momparler RL, Eliopoulos N*, et al.* (2000). "Evaluation of an inhibitor of DNA methylation, 5-aza-2'-deoxycytidine, for the treatment of lung cancer and the future role of gene therapy." Adv Exp Med Biol **465**: 433-446.

Monneret C (2005). "Histone deacetylase inhibitors." Eur J Med Chem **40**(1): 1-13.

Monros E, Molto MD*, et al.* (1997). "Phenotype correlation and intergenerational dynamics of the Friedreich ataxia GAA trinucleotide repeat." Am J Hum Genet **61**(1): 101-110.

Montermini L, Andermann E*, et al.* (1997a). "The Friedreich ataxia GAA triplet repeat: premutation and normal alleles." Hum Mol Genet **6**(8): 1261-1266.

Montermini L, Richter A*, et al.* (1997b). "Phenotypic variability in Friedreich ataxia: role of the associated GAA triplet repeat expansion." Ann Neurol **41**(5): 675-682.

Muhlenhoff U, Richhardt N*, et al.* (2002). "The yeast frataxin homolog Yfh1p plays a specific role in the maturation of cellular Fe/S proteins." Hum Mol Genet **11**(17): 2025-2036.

Mund C, Brueckner B*, et al.* (2006). "Reactivation of epigenetically silenced genes by DNA methyltransferase inhibitors: basic concepts and clinical applications." Epigenetics **1**(1): 7-13.

Murphy MP (1997). "Selective targeting of bioactive compounds to mitochondria." Trends Biotechnol **15**(8): 326-330.

Murphy MP and Smith RA (2000). "Drug delivery to mitochondria: the key to mitochondrial medicine." Adv Drug Deliv Rev **41**(2): 235-250.

Musco G, Stier G*, et al.* (2000). "Towards a structural understanding of Friedreich's ataxia: the solution structure of frataxin." Structure **8**(7): 695-707.

Nair M, Adinolfi S*, et al.* (2004). "Solution structure of the bacterial frataxin ortholog, CyaY: mapping the iron binding sites." Structure **12**(11): 2037-2048.

Navarro JA, Ohmann E*, et al.* (2010). "Altered lipid metabolism in a Drosophila model of Friedreich's ataxia." Hum Mol Genet.

Neidle S (2001). "DNA minor-groove recognition by small molecules." Nat Prod Rep **18**(3): 291-309.

Nemoto S, Razeghi P*, et al.* (2005). "PPAR-gamma agonist rosiglitazone ameliorates ventricular dysfunction in experimental chronic mitral regurgitation." Am J Physiol Heart Circ Physiol **288**(1): H77-82.

North BJ and Verdin E (2004). "Sirtuins: Sir2-related NAD-dependent protein deacetylases." Genome Biol **5**(5): 224.

Noyer-Weidner M and Trautner TA (1993). "Methylation of DNA in prokaryotes." EXS **64**: 39-108.

Ohshima K, Montermini L*, et al.* (1998). "Inhibitory effects of expanded GAA.TTC triplet repeats from intron I of the Friedreich ataxia gene on transcription and replication in vivo." J Biol Chem **273**(23): 14588-14595.

Okano M, Xie S*, et al.* (1998a). "Cloning and characterization of a family of novel mammalian DNA (cytosine-5) methyltransferases." Nat Genet **19**(3): 219-220.

Okano M, Xie S*, et al.* (1998b). "Dnmt2 is not required for de novo and maintenance methylation of viral DNA in embryonic stem cells." Nucleic Acids Res **26**(11): 2536-2540.

Okano M, Bell DW*, et al.* (1999). "DNA methyltransferases Dnmt3a and Dnmt3b are essential for de novo methylation and mammalian development." Cell **99**(3): 247-257.

Ordway JM and Curran T (2002). "Methylation matters: modeling a manageable genome." Cell Growth Differ **13**(4): 149-162.

Ota H, Tokunaga E*, et al.* (2006). "Sirt1 inhibitor, Sirtinol, induces senescence-like growth arrest with attenuated Ras-MAPK signaling in human cancer cells." Oncogene **25**(2): 176-185.

Palii SS, Van Emburgh BO*, et al.* (2008). "DNA methylation inhibitor 5-Aza-2'-deoxycytidine induces reversible genome-wide DNA damage that is distinctly influenced by DNA methyltransferases 1 and 3B." Mol Cell Biol **28**(2): 752-771.

Pan LN, Lu J*, et al.* (2007). "HDAC inhibitors: a potential new category of anti-tumor agents." Cell Mol Immunol **4**(5): 337-343.

Pandey M, Shukla S*, et al.* (2010). "Promoter demethylation and chromatin remodeling by green tea polyphenols leads to re-expression of GSTP1 in human prostate cancer cells." Int J Cancer **126**(11): 2520-2533.

Pandolfo M (1998). "Molecular genetics and pathogenesis of Friedreich ataxia." Neuromuscul Disord **8**(6): 409-415.

Pandolfo M (2002). "The molecular basis of Friedreich ataxia." Adv Exp Med Biol **516**: 99-118.

Pandolfo M (2003). "Friedreich ataxia." Semin Pediatr Neurol **10**(3): 163-172.

Panning B and Jaenisch R (1996). "DNA hypomethylation can activate Xist expression and silence X-linked genes." Genes Dev **10**(16): 1991-2002.

Pianese L, Cavalcanti F*, et al.* (1997). "The effect of parental gender on the GAA dynamic mutation in the FRDA gene." Am J Hum Genet **60**(2): 460-463.

Pianese L, Turano M*, et al.* (2004). "Real time PCR quantification of frataxin mRNA in the peripheral blood leucocytes of Friedreich ataxia patients and carriers." J Neurol Neurosurg Psychiatry **75**(7): 1061-1063.

Picard F, Kurtev M*, et al.* (2004). "Sirt1 promotes fat mobilization in white adipocytes by repressing PPAR-gamma." Nature **429**(6993): 771-776.

Plummer R, Vidal L*, et al.* (2009). "Phase I study of MG98, an oligonucleotide antisense inhibitor of human DNA methyltransferase 1, given as a 7-day infusion in patients with advanced solid tumors." Clin Cancer Res **15**(9): 3177-3183.

Pook MA, Al-Mahdawi S*, et al.* (2001). "Rescue of the Friedreich's ataxia knockout mouse by human YAC transgenesis." Neurogenetics **3**(4): 185-193.

Posakony J, Hirao M*, et al.* (2004). "Inhibitors of Sir2: evaluation of splitomicin analogues." J Med Chem **47**(10): 2635-2644.

Pradhan S, Bacolla A*, et al.* (1999). "Recombinant human DNA (cytosine-5) methyltransferase. I. Expression, purification, and comparison of de novo and maintenance methylation." J Biol Chem **274**(46): 33002-33010.

Prince HM, Bishton MJ*, et al.* (2009). "Clinical studies of histone deacetylase inhibitors." Clin Cancer Res **15**(12): 3958-3969.

Puccio H and Koenig M (2000). "Recent advances in the molecular pathogenesis of Friedreich ataxia." Hum Mol Genet **9**(6): 887-892.

Puccio H, Simon D*, et al.* (2001). "Mouse models for Friedreich ataxia exhibit cardiomyopathy, sensory nerve defect and Fe-S enzyme deficiency followed by intramitochondrial iron deposits." Nat Genet **27**(2): 181-186.

Puccio H (2009). "Multicellular models of Friedreich ataxia." J Neurol **256 Suppl 1**: 18-24.

Punga T and Buhler M (2010). "Long intronic GAA repeats causing Friedreich ataxia impede transcription elongation." EMBO Mol Med **2**(4): 120-129.

Rada-Iglesias A, Enroth S*, et al.* (2007). "Butyrate mediates decrease of histone acetylation centered on transcription start sites and down-regulation of associated genes." Genome Res **17**(6): 708-719.

Radisky DC, Babcock MC*, et al.* (1999). "The yeast frataxin homologue mediates mitochondrial iron efflux. Evidence for a mitochondrial iron cycle." J Biol Chem **274**(8): 4497-4499.

Rai M, Soragni E*, et al.* (2008). "HDAC inhibitors correct frataxin deficiency in a Friedreich ataxia mouse model." PLoS ONE **3**(4): e1958.

Rai M, Soragni E*, et al.* (2010). "Two new pimelic diphenylamide HDAC inhibitors induce sustained frataxin upregulation in cells from Friedreich's ataxia patients and in a mouse model." PLoS One **5**(1): e8825.

Razin A (1998). "CpG methylation, chromatin structure and gene silencing-a three-way connection." EMBO J **17**(17): 4905-4908.

Rea S and Johnson TE (2003). "A metabolic model for life span determination in Caenorhabditis elegans." Dev Cell **5**(2): 197-203.

Rea SL, Ventura N*, et al.* (2007). "Relationship between mitochondrial electron transport chain dysfunction, development, and life extension in Caenorhabditis elegans." PLoS Biol **5**(10): e259.

Reid G, Metivier R*, et al.* (2005). "Multiple mechanisms induce transcriptional silencing of a subset of genes, including oestrogen receptor alpha, in response to deacetylase inhibition by valproic acid and trichostatin A." Oncogene **24**(31): 4894-4907.

Restall C, Doherty J*, et al.* (2009). "A novel histone deacetylase inhibitor augments tamoxifen-mediated attenuation of breast carcinoma growth." Int J Cancer **125**(2): 483-487.

Reynolds BA and Rietze RL (2005). "Neural stem cells and neurospheres--re-evaluating the relationship." Nat Methods **2**(5): 333-336.

Rhee I, Bachman KE*, et al.* (2002). "DNMT1 and DNMT3b cooperate to silence genes in human cancer cells." Nature **416**(6880): 552-556.

Ribai P, Pousset F*, et al.* (2007). "Neurological, cardiological, and oculomotor progression in 104 patients with Friedreich ataxia during long-term follow-up." Arch Neurol **64**(4): 558-564.

Richardson DR, Mouralian C*, et al.* (2001). "Development of potential iron chelators for the treatment of Friedreich's ataxia: ligands that mobilize mitochondrial iron." Biochim Biophys Acta **1536**(2-3): 133-140.

Richardson DR (2003). "Friedreich's ataxia: iron chelators that target the mitochondrion as a therapeutic strategy?" Expert Opin Investig Drugs **12**(2): 235-245.

Richter B, Bandeira-Echtler E*, et al.* (2007). "Rosiglitazone for type 2 diabetes mellitus." Cochrane Database Syst Rev(3): CD006063.

Riessland M, Brichta L*, et al.* (2006). "The benzamide M344, a novel histone deacetylase inhibitor, significantly increases SMN2 RNA/protein levels in spinal muscular atrophy cells." Hum Genet **120**(1): 101-110.

Ristow M, Mulder H*, et al.* (2003). "Frataxin deficiency in pancreatic islets causes diabetes due to loss of beta cell mass." J Clin Invest **112**(4): 527-534.

Robertson KD (2001). "DNA methylation, methyltransferases, and cancer." Oncogene **20**(24): 3139-3155.

Rodgers JT, Lerin C*, et al.* (2005). "Nutrient control of glucose homeostasis through a complex of PGC-1alpha and SIRT1." Nature **434**(7029): 113-118.

Rotig A, de Lonlay P*, et al.* (1997). "Aconitase and mitochondrial iron-sulphur protein deficiency in Friedreich ataxia." Nat Genet **17**(2): 215-217.

Rozen S and Skaletsky H (2000). "Primer3 on the WWW for general users and for biologist programmers." Methods Mol Biol **132**: 365-386.

Rubin RL (2005). "Drug-induced lupus." Toxicology **209**(2): 135-147.

Rustin P, von Kleist-Retzow JC*, et al.* (1999). "Effect of idebenone on cardiomyopathy in Friedreich's ataxia: a preliminary study." Lancet **354**(9177): 477-479.

Saba HI and Wijermans PW (2005). "Decitabine in myelodysplastic syndromes." Semin Hematol **42**(3 Suppl 2): S23-31.

Saba HI (2007). "Decitabine in the treatment of myelodysplastic syndromes." Ther Clin Risk Manag **3**(5): 807-817.

Sakamoto N, Chastain PD*, et al.* (1999). "Sticky DNA: self-association properties of long GAA.TTC repeats in R.R.Y triplex structures from Friedreich's ataxia." Mol Cell **3**(4): 465-475.

Sakamoto N, Ohshima K*, et al.* (2001). "Sticky DNA, a self-associated complex formed at long GAA*TTC repeats in intron 1 of the frataxin gene, inhibits transcription." J Biol Chem **276**(29): 27171-27177.

Sarsero JP, Li L*, et al.* (2003). "Upregulation of expression from the FRDA genomic locus for the therapy of Friedreich ataxia." J Gene Med **5**(1): 72-81.

Sarsero JP, Li L*, et al.* (2004). "Human BAC-mediated rescue of the Friedreich ataxia knockout mutation in transgenic mice." Mamm Genome **15**(5): 370-382.

Sarsero JP, Holloway TP*, et al.* (2005). "Evaluation of an FRDA-EGFP genomic reporter assay in transgenic mice." Mamm Genome **16**(4): 228-241.

Sarzi-Puttini P, Atzeni F*, et al.* (2005). "Drug-induced lupus erythematosus." Autoimmunity **38**(7): 507-518.

Saveliev A, Everett C*, et al.* (2003). "DNA triplet repeats mediate heterochromatin-protein-1-sensitive variegated gene silencing." Nature **422**(6934): 909-913.

Schapira AH, Cooper JM*, et al.* (1990). "Mitochondrial myopathy with a defect of mitochondrial-protein transport." N Engl J Med **323**(1): 37-42.

Schmucker S, Argentini M*, et al.* (2008). "The in vivo mitochondrial two-step maturation of human frataxin." Hum Mol Genet.

Schmucker S and Puccio H (2010). "Understanding the molecular mechanisms of Friedreich's ataxia to develop therapeutic approaches." Hum Mol Genet **19**(R1): R103-110.

Schulz JB, Dehmer T*, et al.* (2000). "Oxidative stress in patients with Friedreich ataxia." Neurology **55**(11): 1719-1721.

Schulz JB, Boesch S*, et al.* (2009). "Diagnosis and treatment of Friedreich ataxia: a European perspective." Nat Rev Neurol **5**(4): 222-234.

Segura-Pacheco B, Trejo-Becerril C*, et al.* (2003). "Reactivation of tumor suppressor genes by the cardiovascular drugs hydralazine and procainamide and their potential use in cancer therapy." Clin Cancer Res **9**(5): 1596-1603.

Segura-Pacheco B, Perez-Cardenas E*, et al.* (2006). "Global DNA hypermethylation-associated cancer chemotherapy resistance and its reversion with the demethylating agent hydralazine." J Transl Med **4**: 32.

Seznec H, Simon D*, et al.* (2005). "Friedreich ataxia: the oxidative stress paradox." Hum Mol Genet **14**(4): 463-474.

Shogren-Knaak M, Ishii H*, et al.* (2006). "Histone H4-K16 acetylation controls chromatin structure and protein interactions." Science **311**(5762): 844-847.

Simon D, Seznec H*, et al.* (2004). "Friedreich ataxia mouse models with progressive cerebellar and sensory ataxia reveal autophagic neurodegeneration in dorsal root ganglia." J Neurosci **24**(8): 1987-1995.

Smith RA, Porteous CM*, et al.* (1999). "Selective targeting of an antioxidant to mitochondria." Eur J Biochem **263**(3): 709-716.

Smith RA, Porteous CM*, et al.* (2003). "Delivery of bioactive molecules to mitochondria in vivo." Proc Natl Acad Sci U S A **100**(9): 5407-5412.

Son LS, Bacolla A*, et al.* (2006). "Sticky DNA: in vivo formation in E. coli and in vitro association of long GAA*TTC tracts to generate two independent supercoiled domains." J Mol Biol **360**(2): 267-284.

Sonoda H, Nishida K*, et al.* (1996). "Oxamflatin: a novel compound which reverses malignant phenotype to normal one via induction of JunD." Oncogene **13**(1): 143-149.

Soragni E, Herman D*, et al.* (2008). "Long intronic GAA*TTC repeats induce epigenetic changes and reporter gene silencing in a molecular model of Friedreich ataxia." Nucleic Acids Res **36**(19): 6056-6065.

Sorm F, Piskala A*, et al.* (1964). "5-Azacytidine, a new, highly effective cancerostatic." Experientia **20**(4): 202-203.

Stancheva I, Hensey C*, et al.* (2001). "Loss of the maintenance methyltransferase, xDnmt1, induces apoptosis in Xenopus embryos." EMBO J **20**(8): 1963-1973.

Stehling O, Elsasser HP*, et al.* (2004). "Iron-sulfur protein maturation in human cells: evidence for a function of frataxin." Hum Mol Genet **13**(23): 3007-3015.

Stewart DJ, Donehower RC*, et al.* (2003). "A phase I pharmacokinetic and pharmacodynamic study of the DNA methyltransferase 1 inhibitor MG98 administered twice weekly." Ann Oncol **14**(5): 766-774.

Strahl BD and Allis CD (2000). "The language of covalent histone modifications." Nature **403**(6765): 41-45.

Stresemann C, Brueckner B*, et al.* (2006). "Functional diversity of DNA methyltransferase inhibitors in human cancer cell lines." Cancer Res **66**(5): 2794-2800.

Stresemann C, Bokelmann I*, et al.* (2008). "Azacytidine causes complex DNA methylation responses in myeloid leukemia." Mol Cancer Ther **7**(9): 2998-3005.

Sturm B, Stupphann D*, et al.* (2005). "Recombinant human erythropoietin: effects on frataxin expression in vitro." Eur J Clin Invest **35**(11): 711-717.

Suenaga M, Soda H*, et al.* (2002). "Histone deacetylase inhibitors suppress telomerase reverse transcriptase mRNA expression in prostate cancer cells." Int J Cancer **97**(5): 621-625.

Taipale M and Akhtar A (2005). "Chromatin mechanisms in Drosophila dosage compensation." Prog Mol Subcell Biol **38**: 123-149.

Tan G, Napoli E*, et al.* (2003). "Decreased expression of genes involved in sulfur amino acid metabolism in frataxin-deficient cells." Hum Mol Genet **12**(14): 1699-1711.

Tang BL (2010). "Resveratrol is neuroprotective because it is not a direct activator of Sirt1-A hypothesis." Brain Res Bull **81**(4-5): 359-361.

Stem Cell Technologies. (2006). "NeuroCult® Chemical Dissociation Kit (Mouse)." 2008, from http://www.stemcell.com/product_catalog/product_catalog_index.aspx?type=catalog_item&id=641.

Theocharis S, Margeli A*, et al.* (2004). "Peroxisome proliferator-activated receptor-gamma ligands as cell-cycle modulators." Cancer Treat Rev **30**(6): 545-554.

Thomas EA, Coppola G*, et al.* (2008). "The HDAC inhibitor 4b ameliorates the disease phenotype and transcriptional abnormalities in Huntington's disease transgenic mice." Proc Natl Acad Sci U S A **105**(40): 15564-15569.

Toft NJ, Winton DJ*, et al.* (1999). "Msh2 status modulates both apoptosis and mutation frequency in the murine small intestine." Proc Natl Acad Sci U S A **96**(7): 3911-3915.

TRDMT1 (2006). "TRDMT1 tRNA aspartic acid methyltransferase 1 http://www.ncbi.nlm.nih.gov/sites/entrez?Db=gene&Cmd=ShowDetailView&TermToSearch=1787."

Tsai SK, Hung LM*, et al.* (2007). "Resveratrol neuroprotective effects during focal cerebral ischemia injury via nitric oxide mechanism in rats." J Vasc Surg **46**(2): 346-353.

Turano M, Tammaro A*, et al.* (2003). "3-Nitropropionic acid increases frataxin expression in human lymphoblasts and in transgenic rat PC12 cells." Neurosci Lett **350**(3): 184-186.

Urbach AR and Dervan PB (2001). "Toward rules for 1:1 polyamide:DNA recognition." Proc Natl Acad Sci U S A **98**(8): 4343-4348.

Vallender TW and Lahn BT (2006). "Localized methylation in the key regulator gene endothelin-1 is associated with cell type-specific transcriptional silencing." FEBS Lett **580**(18): 4560-4566.

Vazquez-Manrique RP, Gonzalez-Cabo P*, et al.* (2006). "Reduction of Caenorhabditis elegans frataxin increases sensitivity to oxidative stress, reduces lifespan, and causes lethality in a mitochondrial complex II mutant." FASEB J **20**(1): 172-174.

Ventura N, Rea S*, et al.* (2005). "Reduced expression of frataxin extends the lifespan of Caenorhabditis elegans." Aging Cell **4**(2): 109-112.

Voest EE, Vreugdenhil G*, et al.* (1994). "Iron-chelating agents in non-iron overload conditions." Ann Intern Med **120**(6): 490-499.

Vogelauer M, Wu J*, et al.* (2000). "Global histone acetylation and deacetylation in yeast." Nature **408**(6811): 495-498.

Voncken M, Ioannou P*, et al.* (2004). "Friedreich ataxia-update on pathogenesis and possible therapies." Neurogenetics **5**(1): 1-8.

Waldvogel D, van Gelderen P*, et al.* (1999). "Increased iron in the dentate nucleus of patients with Friedrich's ataxia." Ann Neurol **46**(1): 123-125.

Wang X, Chao L*, et al.* (2009). "Association between CpG island methylation of the WWOX gene and its expression in breast cancers." Tumour Biol **30**(1): 8-14.

Wells RD (2008). "DNA triplexes and Friedreich ataxia." FASEB J **22**(6): 1625-1634.

Wilson RB and Roof DM (1997). "Respiratory deficiency due to loss of mitochondrial DNA in yeast lacking the frataxin homologue." Nat Genet **16**(4): 352-357.

Wilson RB (2003). "Frataxin and frataxin deficiency in Friedreich's ataxia." J Neurol Sci **207**(1-2): 103-105.

Wilson WD, Tanious FA*, et al.* (2008). "Antiparasitic compounds that target DNA." Biochimie **90**(7): 999-1014.

Winquist E, Knox J*, et al.* (2006). "Phase II trial of DNA methyltransferase 1 inhibition with the antisense oligonucleotide MG98 in patients with metastatic renal carcinoma: a National Cancer Institute of Canada Clinical Trials Group investigational new drug study." Invest New Drugs **24**(2): 159-167.

Wong A, Yang J*, et al.* (1999). "The Friedreich's ataxia mutation confers cellular sensitivity to oxidant stress which is rescued by chelators of iron and calcium and inhibitors of apoptosis." Hum Mol Genet **8**(3): 425-430.

Wong A, Yang J*, et al.* (2000). "Sensitivity of FRDA lymphoblasts to salts of transition metal ions." Antioxid Redox Signal **2**(3): 461-465.

Xu C, Soragni E*, et al.* (2009). "Chemical probes identify a role for histone deacetylase 3 in Friedreich's ataxia gene silencing." Chem Biol **16**(9): 980-989.

Yoder JA and Bestor TH (1998). "A candidate mammalian DNA methyltransferase related to pmt1p of fission yeast." Hum Mol Genet **7**(2): 279-284.

Yoon T, Dizin E*, et al.* (2007). "N-terminal iron-mediated self-cleavage of human frataxin: regulation of iron binding and complex formation with target proteins." J Biol Inorg Chem **12**(4): 535-542.

Yuasa Y, Nagasaki H*, et al.* (2009). "DNA methylation status is inversely correlated with green tea intake and physical activity in gastric cancer patients." Int J Cancer **124**(11): 2677-2682.

Zambrano P, Segura-Pacheco B*, et al.* (2005). "A phase I study of hydralazine to demethylate and reactivate the expression of tumor suppressor genes." BMC Cancer **5**: 44.

Zhao P, Caretti G*, et al.* (2006). "Fgfr4 is required for effective muscle regeneration in vivo. Delineation of a MyoD-Tead2-Fgfr4 transcriptional pathway." J Biol Chem **281**(1): 429-438.

Zhou L, Cheng X*, et al.* (2002). "Zebularine: a novel DNA methylation inhibitor that forms a covalent complex with DNA methyltransferases." J Mol Biol **321**(4): 591-599.

Zlatanova J, Caiafa P*, et al.* (2000). "Linker histone binding and displacement: versatile mechanism for transcriptional regulation." FASEB J **14**(12): 1697-1704.

Journal publications

Al-Mahdawi S, Pinto RM, Ismail O, Varshney D, Lymperi S, **Sandi C**, Trabzuni D and Pook M (2008) The Friedreich ataxia GAA repeat expansion mutation induces comparable epigenetic changes in human and transgenic mouse brain and heart tissues. *Hum Mol Genet*, 17 (5): 735-46.

Sandi C, Pinto RM, Al-Mahdawi S, Ezzatizadeh V, Barnes G, Jones S, Rusche JR, Gottesfeld J.M and Pook M (2010) Histone Deacetylase Inhibitors Provide Long-term Therapeutic Benefit to a Friedreich Ataxia Mouse Model (manuscript in preparation).

Sandi C, Al-Mahdawi S, Pinto RM, Ezzatizadeh V and Pook M (2010) The Therapeutic Role of Class III Histone Deacetylase Inhibitors and DNA demethylating agents in Friedreich Ataxia (manuscript in preparation).

Sandi C, Al-Mahdawi S, Pinto RM, Ezzatizadeh V and Pook M (2010) GAA Interacting Compounds as Therapeutics for Friedreich Ataxia (manuscript in preparation).

Posters presented

Sandi C, Al-Mahdawi S, Pinto RM and Pook M (2008) Investigating the pathogenesis and therapies of Friedreich ataxia using mouse model cell lines – poster presented at "58th ASHG annual meeting", Philadelphia, USA.

Sandi C, Al-Mahdawi S, Pinto RM, Ezzatizadeh V and Pook M (2009) Investigating the pathogenesis and therapy of Friedreich ataxia – poster presented at "59th ASHG annual meeting", Hawaii, USA.

Appendix A - Extra data from *in vitro* studies

A.1 - Negative control staining of NSCs

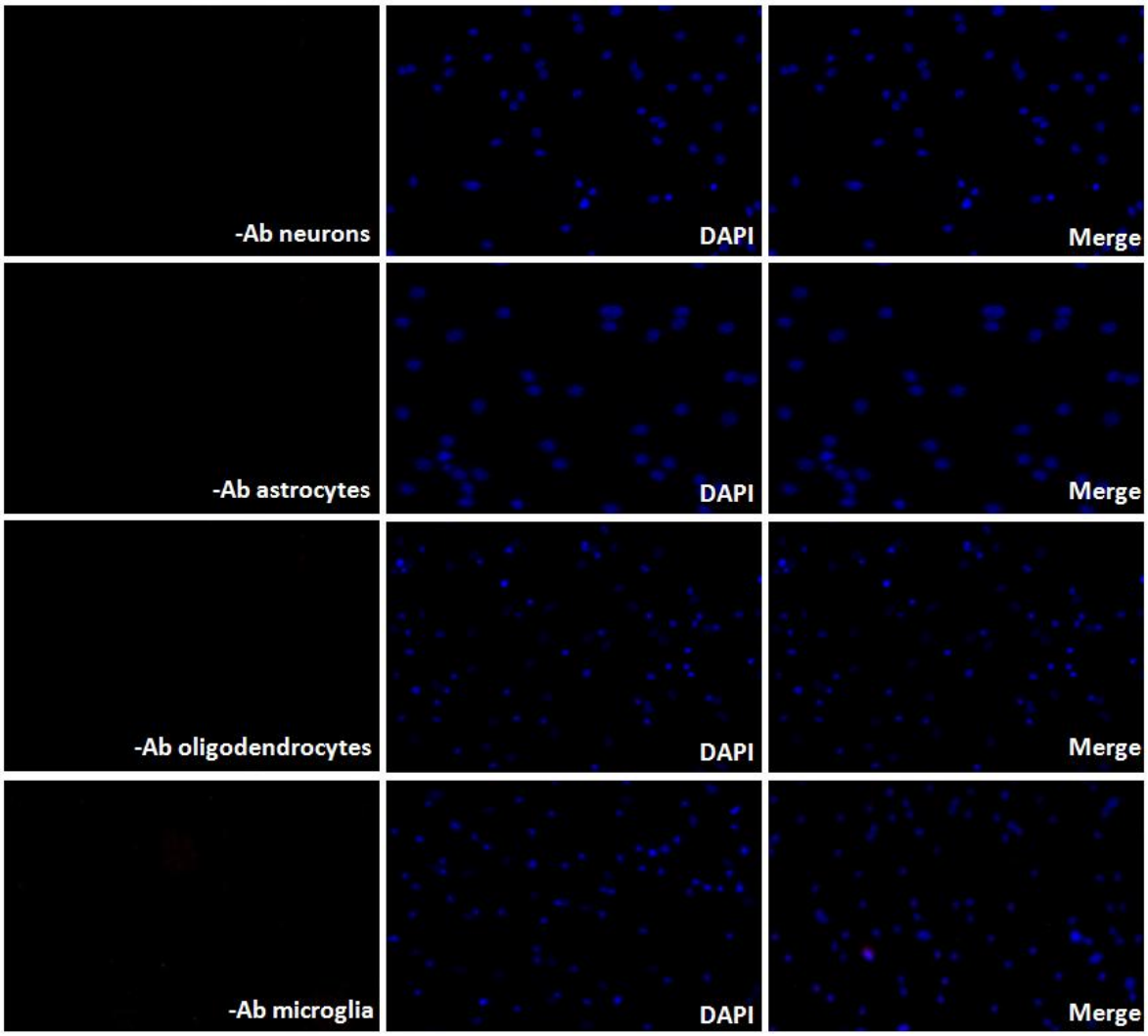

Figure A.1 - Negative antibody staining of NSCs.
NSCs were collected by centrifugation and dissociated by gently pipetting up and down several times until single cell suspension has been achieved followed by incubation with NSC dissociation medium for 48 hours on poly-D-lysine coated coverslips. After 48 hours in culture, NSCs were stained with secondary antibodies of FITC (neurons) and CY3 (astrocytes, oligodendrocytes and microglia) without primary antibodies. The micrographs were taken at the magnification of 10X.

A.2 - Endogenous control test QRT-PCR

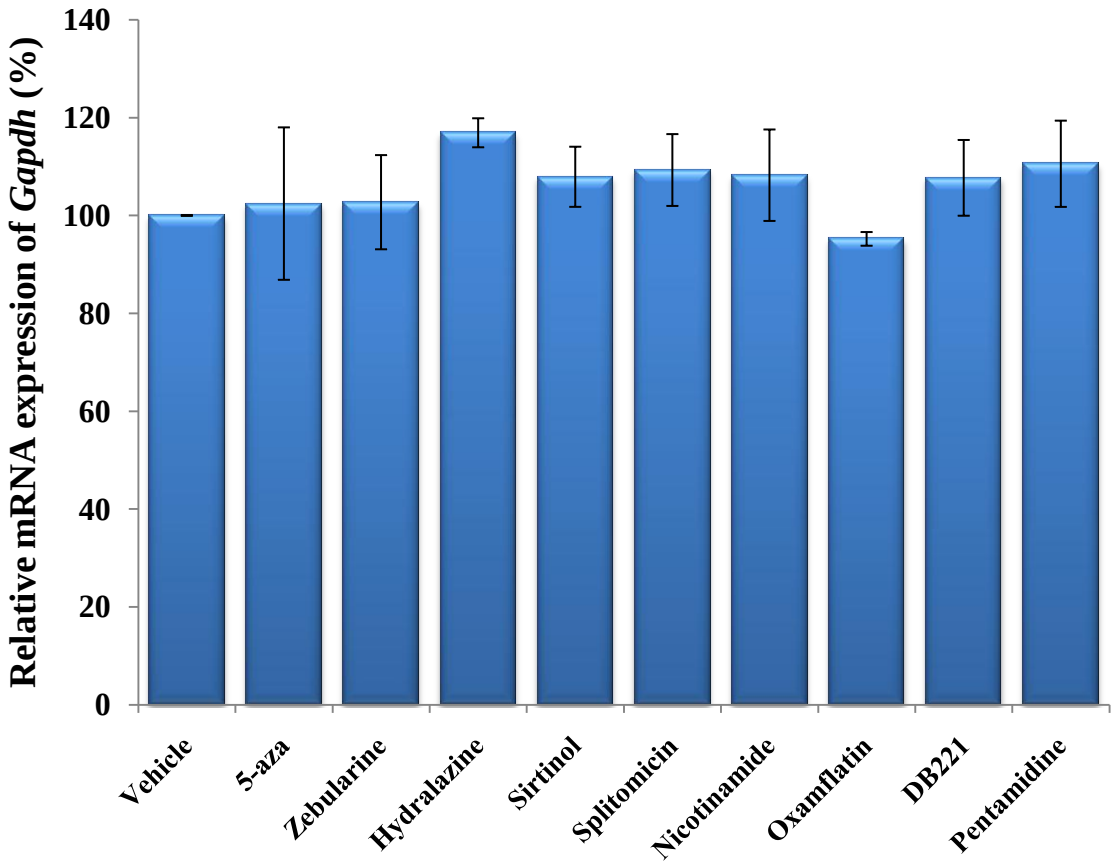

Figure A.2 - *Gapdh* mRNA expression levels. Relative *Gapdh* mRNA expression as determined by QRT-PCR of YG8 rescue mouse primary fibroblasts treated with various compounds, compared with a vehicle-treated control set at 100%. *RER1* used as an endogenous control. Error bars represent s.e.m.

Appendix B - Extra data from *in vivo* studies

B.1 - Previous long-term study functional results of RGFA 136

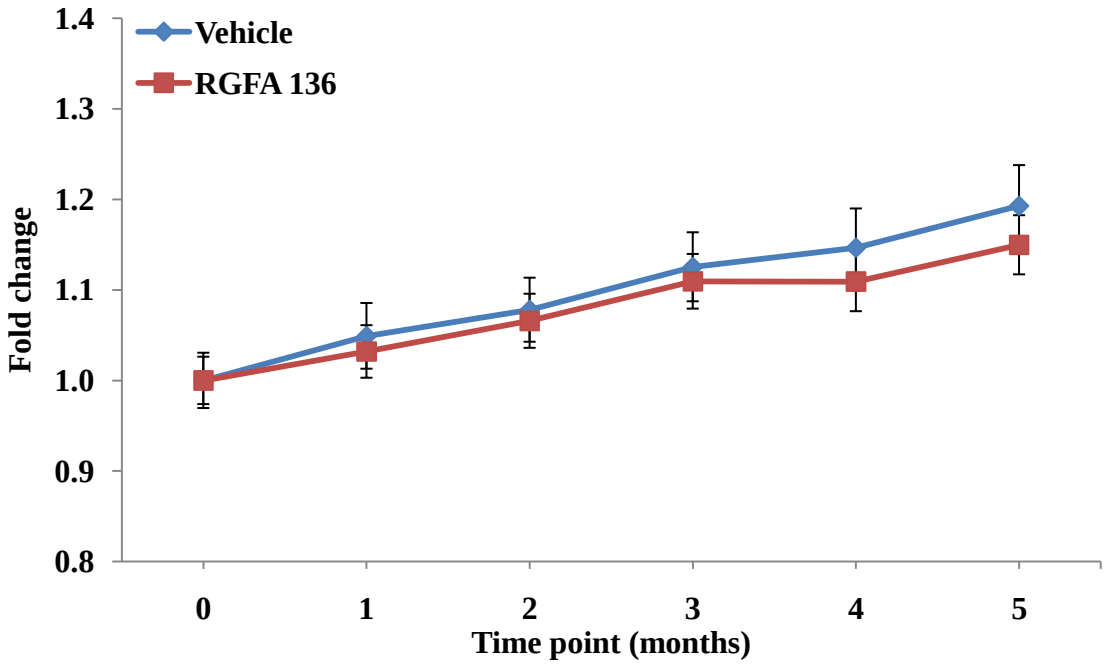

Figure B.1 - Weight analysis during treatment with RGFA 136 in YG8 rescue mice showing vehicle and drug-treated groups (n=20, error bars ± 1 SEM).

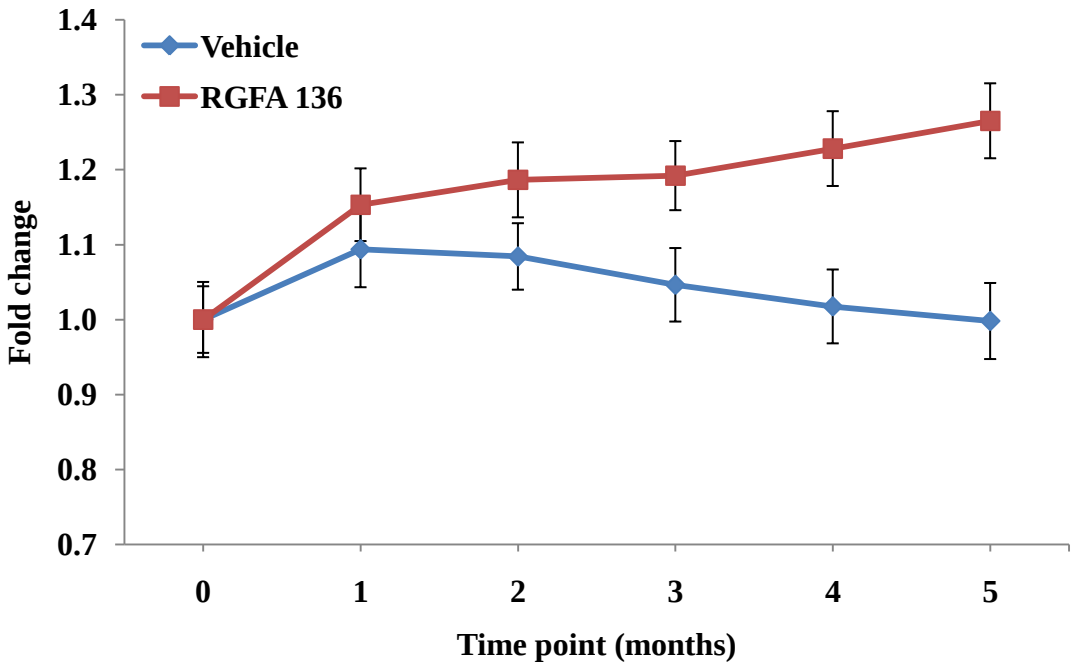

Figure B.2 - Rotarod analysis during treatment with RGFA 136 in YG8 rescue mice showing vehicle and drug-treated groups (n=20, error bars ± 1 SEM).

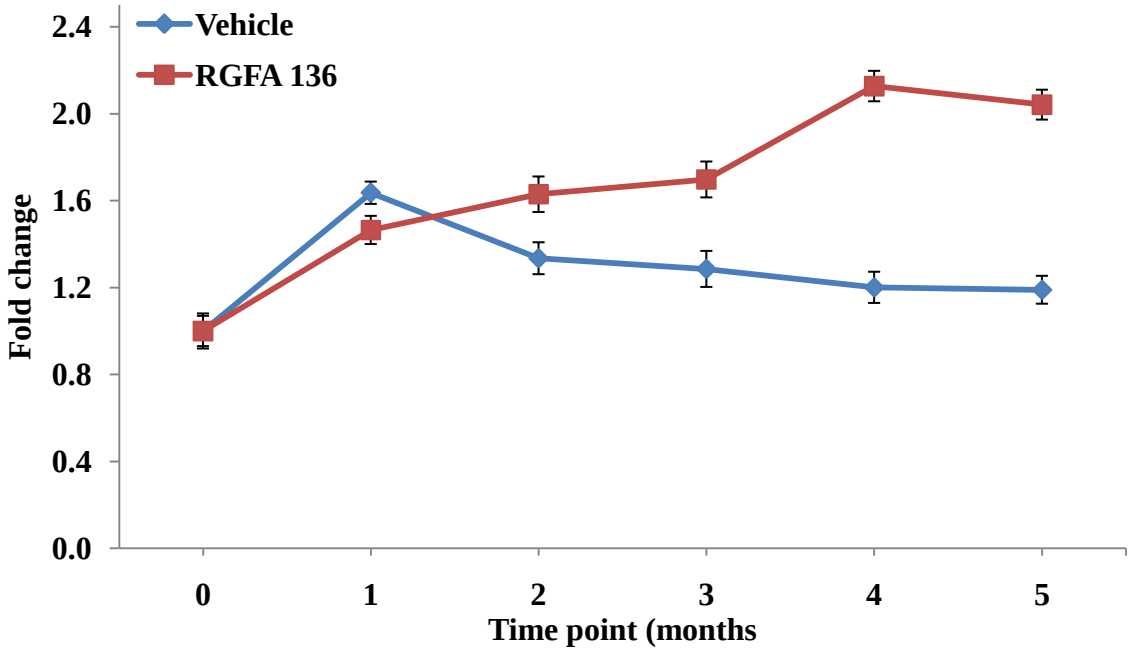

Figure B.3 - Locomotor activity analysis during treatment with RGFA 136 in YG8 rescue mice showing vehicle and drug-treated groups (n=20, error bars ± 1 SEM).

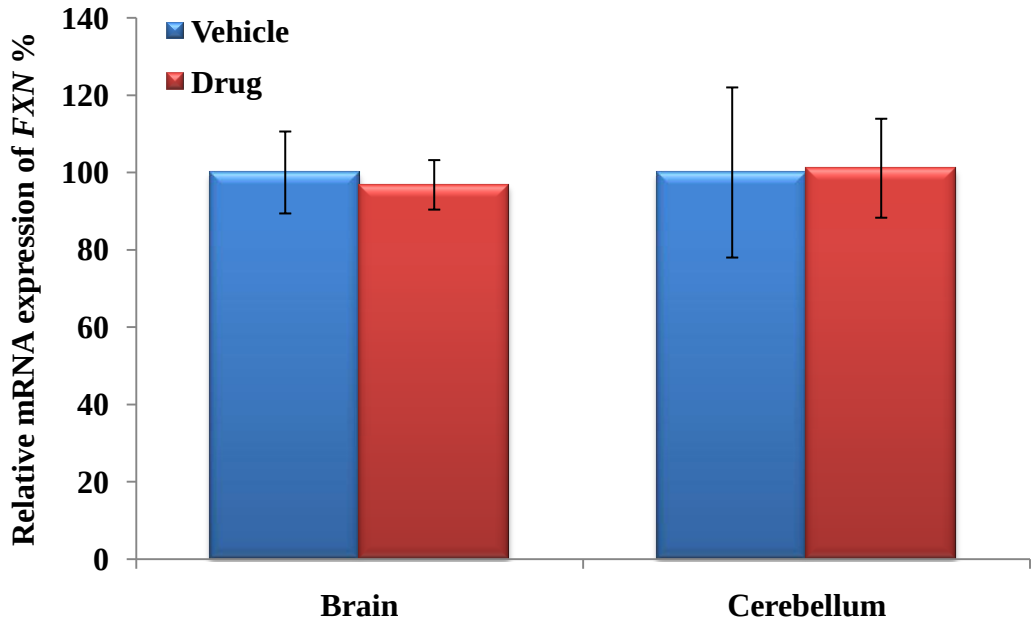

Figure B.4 - Relative mRNA expression in brain and cerebellum tissues following treatment with RGFA 136 in YG8 rescue mice showing vehicle and drug-treated groups (n=4, error bars ± 1 SEM).

B.2 - DB221 in vivo preliminary short-term study

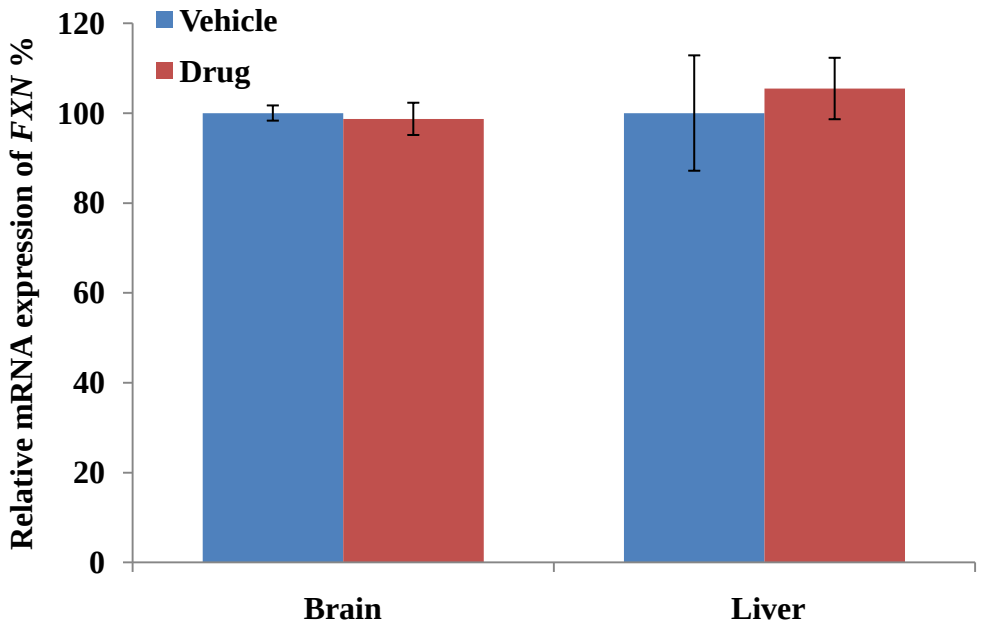

Figure B.5 - Relative mRNA expression of *FXN* following treatment with DB221 in YG8 rescue mice of vehicle and drug-treated mice. The mice were subjected to 3 consecutive daily doses of 10mg/kg DB221 sub-cutaneous injections along with a vehicle control group. *FXN* expression was quantified by QRT-PCR and *Gapdh* was used as an endogenous control (n=5, error bars ± 1 SEM).

B.3 - Endogenous control test QRT-PCR

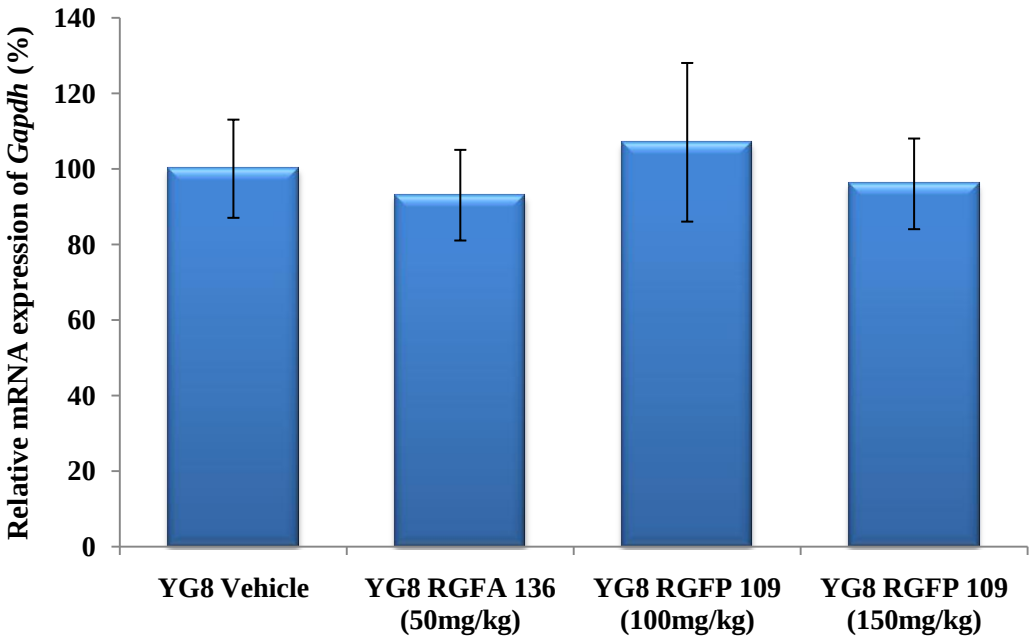

Figure B.6 - *Gapdh* mRNA expression levels. Relative *Gapdh* mRNA expression as determined by QRT-PCR of Vehicle, RGFA 136 (50mg/kg), RGFP 109 (100mg/kg) or RGFP 109 (150mg/kg)-treated YG8 rescue mice. Vehicle-treated control set at 100%. *RER1* used as an endogenous control. Error bars represent s.e.m.

B.4 - ANOVA associated p-values of RGFA 136 treatment

Table B.1 - ANOVA associated p-values of time point and treatment effect on manual functional measurements during RGFA 136 treatment.

RGFA 136 (50mg/kg) 5-months (WT - n=10, YG8 - n=20)					
		F-ratio values		***p*-values**	
Treatment effect on	**Genotype**	**TP**	**TP/TM**	**TP**	**TP/TM**
Weight	WT	6.100	0.062	<0.001	0.803
	YG8	6.316	5.014	<0.001	0.026
Rotarod performance	WT	1.366	45.425	0.235	<0.001
	YG8	0.932	9.096	0.458	0.002
Locomotor activity	YG8	0.237	17.725	0.946	<0.001

Abbreviations: TP-Time point, TM-Treatment

Table B.2 - ANOVA associated *p*-values of time point and genotype effect on manual functional measurements during RGFA 136 treatment.

RGFA 136 (50mg/kg) 5-months (WT - n=10, YG8 - n=20)						
			F-ratio values		***p*-values**	
Treatment effect on	**Genotype**	**TM**	**TP**	**TP/GT**	**TP**	**TP/GT**
Weight	WT vs YG8	Vehicle	17.888	2.974	<0.001	0.086
		RGFA 136	8.189	8.980	<0.001	0.003
Rotarod performance	WT vs YG8	Vehicle	2.105	0.137	0.063	0.711
		RGFA 136	3.618	22.893	0.003	<0.001

Abbreviations: TM-Treatment, TP-Time point, GT-Genotype

Table B.3 - ANOVA associated *p*-values of time point and treatment effect on manual functional measurements of male and female mice during RGFA 136 treatment.

RGFA 136 5-months (WT - n=5, YG8 - n=10)						
			F-ratio values		***p*-values**	
Treatment effect on	**Genotype**	**Sex**	**TP**	**TP/TM**	**TP**	**TP/TM**
Weight	WT	Male	18.443	2.198	<0.001	0.144
		Female	9.574	0.310	<0.001	0.579
	YG8	Male	10.778	9.381	<0.001	0.002
		Female	8.486	3.864	<0.001	0.051
Rotarod performance	WT	Male	0.984	91.187	0.428	<0.001
		Female	1.173	0.002	0.323	0.963

	YG8	Male	3.508	25.937	0.004	<0.001
		Female	2.257	0.110	0.048	0.741
Locomotor activity	YG8	Male	0.324	14.345	0.898	<0.001
		Female	0.289	5.855	0.919	0.016

Abbreviations: TP-Time point, TM-Treatment

Table B.4 - ANOVA associated *p*-values of time point and genotype effect on manual functional measurements of male and female mice during RGFA 136 treatment.

RGFA 136 5-months (n=5)							
Treatment effect on	**Genotype**	**TM**	**Sex**	**F-ratio values**		***p*-values**	
				TP	**TP/GT**	**TP**	**TP/GT**
Weight	WT vs YG8	Vehicle	Male	17.326	3.529	<0.001	0.063
			Female	15.960	2.150	<0.001	0.145
		RGFA 136	Male	31.539	15.895	<0.001	<0.001
			Female	12.106	15.787	<0.001	<0.001
Rotarod performance	WT vs YG8	Vehicle	Male	2.038	15.674	0.072	<0.001
			Female	1.753	35.918	0.121	<0.001
		RGFA 136	Male	15.379	0.160	<0.001	0.689
			Female	0.524	31.567	0.758	<0.001

Abbreviations: TM-Treatment, TP-Time point

Table B.5 - ANOVA associated *p*-values of time point and gender effect on manual functional measurements of male and female mice during RGFA 136 treatment.

RGFA 136 5-months (WT - n=5, YG8 - n=10)							
Treatment effect on	**Sex**	**Genotype**	**TM**	**F-ratio values**		***p*- values**	
				TP	**TP/Sex**	**TP**	**TP/Sex**
Weight	Male vs female	WT	Vehicle	16.710	0.179	<0.001	0.674
			Drug	9.229	1.602	<0.001	0.211
		YG8	Vehicle	8.760	0.023	<0.001	0.879
			Drug	11.328	0.661	<0.001	0.418
Rotarod performance	Male vs female	WT	Vehicle	1.881	32.478	0.098	<0.001
			Drug	2.587	9.304	0.026	0.002
		YG8	Vehicle	1.130	5.824	0.344	0.016
			Drug	3.072	53.978	0.010	<0.001
Locomotor activity	Male vs female	YG8	Vehicle	1.479	0.061	0.195	0.805
			Drug	2.265	1.028	0.047	0.311

Abbreviations: TM-Treatment, TP-Time point

Table B.6 - ANOVA associated *p*-values of time point and treatment effect on beam breaker-based functional measurements during RGFA 136 treatment.

RGFA 136 (50mg/kg) 5-months (WT - n=10, YG8 - n=20)					
		F-ratio values		***p*-values**	
Treatment effect on	**Genotype**	**TP**	**TP/TM**	**TP**	**TP/TM**
Average velocity	WT	0.851	2.003	0.515	0.158
	YG8	2.418	28.905	0.035	<0.001
Ambulatory distance	WT	4.394	0.341	<0.001	0.560
	YG8	13.929	13.581	<0.001	<0.001
Vertical counts	WT	2.672	8.612	0.023	0.004
	YG8	3.494	67.362	0.004	<0.001

Abbreviations: TP-Time point, TM-Treatment

Table B.7 - ANOVA associated *p*-values of time point and genotype effect on different beam breaker-based functional measurements during RGFA 136 treatment.

RGFA 136 (50mg/kg) 5-months (WT - n=10, YG8 - n=10)						
			F-ratio values		***p*-values**	
Treatment effect on	**Genotype**	**TM**	**TP**	**TP/GT**	**TP**	**TP/GT**
Average velocity	WT vs YG8	Vehicle	1.731	0.401	0.126	0.527
		RGFA 136	3.358	9.657	0.005	0.002
Ambulatory distance	WT vs YG8	Vehicle	11.527	6.021	<0.001	0.014
		RGFA 136	10.330	3.193	<0.001	0.074
Vertical counts	WT vs YG8	Vehicle	5.410	24.506	<0.001	<0.001
		RGFA 136	2.924	58.956	0.013	<0.001

Abbreviations: TM-Treatment, TP-Time point

Table B.8 - ANOVA associated *p*-values of time point and treatment effect on beam breaker-based functional measurements of male and female mice during RGFA 136 treatment.

RGFA 136 5-months (WT - n=5, YG8 - n=10)						
			F-ratio values		***p*-values**	
Treatment effect on	**Genotype**	**Sex**	**TP**	**TP/TM**	**TP**	**TP/TM**
Average velocity	WT	Male	0.835	0.264	0.527	0.608
		Female	1.850	2.025	0.109	0.157
	YG8	Male	2.047	15.011	0.073	<0.001
		Female	1.388	12.711	0.229	<0.001
Ambulatory distance	WT	Male	0.780	0.499	0.779	0.499
		Female	9.360	3.446	<0.001	0.066
	YG8	Male	3.674	2.417	0.003	0.121
		Female	12.722	15.295	<0.001	<0.001
Vertical counts	WT	Male	0.591	1.344	0.707	0.248
		Female	9.536	13.572	<0.001	<0.001
	YG8	Male	1.466	22.512	0.202	<0.001
		Female	3.689	50.211	0.003	<0.001

Abbreviations: TP-Time point, TM-Treatment

Table B.9 - ANOVA associated *p*-values of time point and genotype effect on beam breaker-based functional measurements of male and female mice during RGFA 136 treatment.

RGFA 136 5-months (n=5)							
Treatment effect on	**Genotype**	**TM**	**Sex**	**F-ratio values**		***p*-values**	
				TM	**TM/GT**	**TM**	**TM/GT**
Average velocity	WT vs YG8	Vehicle	Male	1.440	6.528	0.211	0.011
			Female	0.940	2.663	0.455	0.104
		RGFA 136	Male	1.393	1.469	0.228	0.227
			Female	2.199	9.851	0.055	0.002
Ambulatory distance	WT vs YG8	Vehicle	Male	2.452	3.576	0.035	0.060
			Female	13.279	1.772	<0.001	0.184
		RGFA 136	Male	2.443	3.741	0.036	0.054
			Female	17.439	31.125	<0.001	<0.001
Vertical counts	WT vs YG8	Vehicle	Male	1.233	12.149	0.295	<0.001
			Female	1.836	15.219	0.106	<0.001
		RGFA 136	Male	1.305	9.481	0.263	0.002
			Female	5.543	78.287	<0.001	<0.001

Abbreviations: GT-Genotype, TP-Time point, TM-Treatment

Table B.10 - ANOVA associated *p*-values of time point and gender effect on beam breaker-based functional measurements of male and female mice during RGFA 136 treatment.

RGFA 136 5-months (WT-n=5, YG8-n=10)							
Treatment effect on	**Sex**	**Genotype**	**TM**	**F-ratio values**		***p*-values**	
				TP	**TP/Sex**	**TP**	**TP/Sex**
Average velocity	Male vs female	WT	Vehicle	0.320	2.604	0.899	0.109
			Drug	0.718	0.463	0.611	0.497
		YG8	Vehicle	1.369	3.411	0.237	0.066
			Drug	2.625	0.784	0.025	0.376
Ambulatory distance	Male vs female	WT	Vehicle	2.106	4.573	0.070	0.034
			Drug	2.983	24.306	0.014	<0.001
		YG8	Vehicle	7.073	3.257	<0.001	0.072
			Drug	6.530	0.386	<0.001	0.535
Vertical counts	Male vs female	WT	Vehicle	0.487	6.403	0.785	0.012
			Drug	8.731	48.239	<0.001	<0.001
		YG8	Vehicle	7.942	6.079	<0.001	0.014
			Drug	1.856	1.962	0.103	0.162

Abbreviations: TP-Time point, TM-Treatment

B.5 - ANOVA associated p-values of RGFP 109 treatment

Table B.11 - ANOVA associated *p*-values of time point and treatment effect on manual functional measurements during RGFP 109 treatment.

RGFP 109 5-months (WT - n=10, YG8 - n=20)					
Treatment effect on	**Genotype**	**F-ratio values**		***p*-values**	
		TP	**TP/TM**	**TP**	**TP/TM**
Weight	WT 109 (100mg/kg)	3.515	3.022	0.006	0.080
	YG8 109 (100mg/kg)	5.229	1.287	<0.001	0.250
	YG8 109 (150mg/kg)	7.475	4.751	<0.001	0.030
Rotarod performance	WT 109 (100mg/kg)	0.635	8.112	0.673	0.004
	YG8 109 (100mg/kg)	0.798	13.465	0.550	<0.001
	YG8 109 (150mg/kg)	2.556	9.869	0.026	0.001

Abbreviations: TP-Time point, TM-Treatment

Table B.12 - ANOVA associated *p*-values of time point and genotype effect on manual functional measurements during RGFP 109 (100mg/kg only) treatment.

RGFP 109 (100mg/kg) 5-months (n=10)						
Treatment effect on	**Genotype**	**TM**	**F-ratio values**		***p*-values**	
			TP	**TP/GT**	**TP**	**TP/GT**
Weight	WT vs YG8	Vehicle	17.888	2.974	<0.001	0.086
		RGFP 109	5.524	0.117	<0.001	0.733
Rotarod performance	WT vs YG8	Vehicle	2.105	0.137	0.063	0.711
		RGFP 109	0.955	0.379	0.445	0.539

Abbreviations: TM-Treatment, TP-Time point, GT-Genotype

Table B.13 - ANOVA associated *p*-values of time point and treatment effect on manual functional measurements of male and female mice during RGFP 109 treatment.

RGFP 109 5-months (WT - n=5, YG8 - n=10)

Treatment effect on	Genotype	Sex	F-ratio values		*p*-values	
			TP	TP/TM	TP	TP/TM
Weight	WT 109 (100mg/kg)	Male	9.976	0.035	<0.001	0.851
		Female	16.038	4.896	<0.001	0.033
	YG8 109 (100mg/kg)	Male	5.289	3.364	<0.001	0.070
		Female	5.776	0.001	<0.001	0.973
	YG8 109 (150mg/kg)	Male	10.820	6.899	<0.001	0.010
		Female	8.663	3.379	<0.001	0.069
Rotarod performance	WT 109 (100mg/kg)	Male	1.727	2.386	0.130	0.124
		Female	2.341	3.344	0.043	0.069
	YG8 109 (100mg/kg)	Male	0.923	0.651	0.466	0.048
		Female	0.652	20.082	0.660	<0.001
	YG8 109 (150mg/kg)	Male	0.744	2.517	0.591	0.113
		Female	2.751	8.662	0.018	<0.001

Abbreviations: TP-Time point, TM-Treatment

Table B.14 - ANOVA associated *p*-values of time point and genotype effect on manual functional measurements of male and female mice during RGFP 109 treatment.

RGFP 109 5-months (n=5)

Treatment effect on	Genotype	TM	Sex	F-ratio values		*p*-values	
				TP	TP/GT	TP	TP/GT
Weight	WT vs YG8	Vehicle	Male	11.215	4.336	<0.001	0.063
			Female	7.294	2.168	<0.001	0.145
		RGFP 109	Male	7.633	2.457	<0.001	0.120
			Female	11.281	0.432	<0.001	0.513
Rotarod performance	WT vs YG8	Vehicle	Male	2.038	15.674	0.072	<0.001
			Female	1.753	35.918	0.121	<0.001
		RGFP 109	Male	1.582	6.468	0.164	0.011
			Female	1.436	2.572	0.210	0.110

Abbreviations: TM-Treatment, TP-Time point, GT-Genotype

Table B.15 - ANOVA associated *p*-values of time point and gender effect on manual functional measurements of male and female mice during RGFP 109 treatment.

RGFP 109 5-months (WT - n=5, YG8 - n=10)

Treatment effect on	Sex	GT	TM	F-ratio values		*p*-values	
				TP	TP/Sex	TP	TP/Sex
Weight	Male vs female	WT	Placebo	16.710	0.179	<0.001	0.674
			109 (100mg/kg)	2.101	0.807	<0.001	0.374
		YG8	Placebo	8.760	0.023	<0.001	0.879
			109 (100mg/kg)	4.865	9.535	<0.001	0.150
			109 (150mg/kg)	13.084	0.081	<0.001	0.770
Rotarod performance	Male vs female	WT	Placebo	1.881	32.478	0.098	<0.001
			109 (100mg/kg)	0.246	56.432	0.941	<0.001
		YG8	Placebo	1.130	5.824	0.344	0.016
			109 (100mg/kg)	0.891	45.918	0.487	<0.001
			109 (150mg/kg)	2.355	0.033	0.040	0.856

Abbreviations: GT-Genotype, TM-Treatment, TP-Time point

Table B.16 - ANOVA associated *p*-values of time point and treatment effect on beam breaker-based functional measurements during RGFP 109 treatment.

RGFP 109 5-months (WT - n=10, YG8 - n=20)

Treatment effect on	Genotype	F-ratio values		*p*-values	
		TP	TP/TM	TP	TP/TM
Average velocity	WT 109 (100mg/kg)	0.943	0.376	0.454	0.541
	YG8 109 (100mg/kg)	1.111	1.464	0.354	0.227
	YG8 109 (150mg/kg)	1.934	4.149	0.087	0.042
Ambulatory distance	WT 109 (100mg/kg)	2.650	1.924	0.024	0.167
	YG8 109 (100mg/kg)	6.719	22.272	<0.001	<0.001
	YG8 109 (150mg/kg)	12.243	19.801	<0.001	<0.001
Vertical counts	WT 109 (100mg/kg)	1.994	2.098	0.082	0.149
	YG8 109 (100mg/kg)	17.99	1.713	<0.001	0.191
	YG8 109 (150mg/kg)	17.186	2.573	<0.001	0.109

Abbreviations: TP-Time point, TM-Treatment

Table B.17 - ANOVA associated *p*-values of time point and genotype effect on different beam breaker-based functional measurements during RGFP 109 treatment.

RGFP 109 (100mg/kg only) 5-months (n=10)						
Treatment effect on	**Genotype**	**TM**	**F-ratio values**		***p*-values**	
			TP	**TP/GT**	**TP**	**TP/GT**
Average velocity	WT vs YG8	Vehicle	1.731	0.401	0.126	0.527
		RGFP 109	1.852	2.047	0.102	0.153
Ambulatory distance	WT vs YG8	Vehicle	11.527	6.021	<0.001	0.014
		RGFP 109	3.393	0.685	0.005	0.408
Vertical counts	WT vs YG8	Vehicle	5.410	24.506	<0.001	<0.001
		RGFP 109	12.218	2.943	<0.001	0.087

Abbreviations: TM-Treatment, TP-Time point, GT-Genotype

Table B.18 - ANOVA associated *p*-values of time point and treatment effect on beam breaker-based functional measurements of male and female mice during RGFP 109 treatment.

RGFP 109 5-months (WT - n=5, YG8 - n=10)						
Treatment effect on	**Genotype**	**Sex**	**F-ratio values**		***p*-values**	
			TP	**TP/TM**	**TP**	**TP/TM**
Average velocity	WT 109 (100mg/kg)	Male	0.747	1.528	0.590	0.219
		Female	0.696	0.065	0.627	0.800
	YG8 109 (100mg/kg)	Male	1.332	0.876	0.252	0.350
		Female	0.370	1.807	0.868	0.180
	YG8 109 (150mg/kg)	Male	1.949	0.657	0.087	0.418
		Female	0.340	5.332	0.888	0.021
Ambulatory distance	WT 109 (100mg/kg)	Male	0.865	0.141	0.507	0.708
		Female	1.993	3.827	0.087	0.050
	YG8 109 (100mg/kg)	Male	1.813	6.306	0.112	0.012
		Female	5.137	9.308	<0.001	0.002
	YG8 109 (150mg/kg)	Male	5.803	0.485	<0.001	0.487
		Female	6.081	26.316	<0.001	<0.001
Vertical counts	WT 109 (100mg/kg)	Male	1.136	6.030	0.348	0.016
		Female	2.478	0.106	0.038	0.746
	YG8 109 (100mg/kg)	Male	3.066	0.486	0.011	0.486
		Female	14.360	0.825	<0.001	0.365
	YG8 109 (150mg/kg)	Male	5.574	0.479	<0.001	0.489
		Female	14.082	9.195	<0.001	0.002

Abbreviations: TP-Time point, TM-Treatment

Table B.19 - ANOVA associated *p*-values of time point and genotype effect on beam breaker-based functional measurements of male and female mice during RGFP 109 treatment.

RGFP 109 5-months (n=5)							
Treatment effect on	**Genotype**	**TM**	**Sex**	**F-ratio values**		***p*-values**	
				TP	**TP/GT**	**TP**	**TP/GT**
Average velocity	WT vs YG8	Vehicle	Male	1.440	6.528	0.211	0.011
			Female	0.940	2.663	0.455	0.104
		RGFP 109	Male	1.750	0.002	0.125	0.962
			Female	1.708	1.140	0.135	0.287
Ambulatory distance	WT vs YG8	Vehicle	Male	2.452	3.576	0.035	0.060
			Female	13.279	1.772	<0.001	0.184
		RGFP 109	Male	1.157	1.686	0.332	0.196
			Female	2.891	0.007	0.015	0.935
Vertical counts	WT vs YG8	Vehicle	Male	1.233	12.149	0.295	<0.001
			Female	1.836	15.219	0.106	<0.001
		RGFP 109	Male	5.859	0.395	<0.001	0.530
			Female	7.161	3.252	<0.001	0.073

Abbreviations: TM-Treatment, TP-Time point, GT-Genotype

Table B.20 - ANOVA associated *p*-values of time point and gender effect on beam breaker-based functional measurements of male and female mice during RGFP 109 treatment.

RGFP 109 5-months (WT - n=5, YG8 - n=10)							
Treatment effect on	**Sex**	**GT**	**TM**	**F-ratio values**		***p*-values**	
				TP	**TP/Sex**	**TP**	**TP/Sex**
Average velocity	Male vs female	WT	Placebo	0.320	2.604	0.899	0.109
			109 (100mg/kg)	0.726	0.065	0.605	0.799
		YG8	Placebo	1.369	3.411	0.237	0.066
			109 (100mg/kg)	1.951	0.355	0.088	0.551
			109 (150mg/kg)	2.028	0.172	0.076	0.678
Ambulatory distance	Male vs female	WT	Placebo	2.106	4.573	0.070	0.034
			109 (100mg/kg)	1.058	0.752	0.389	0.388
		YG8	Placebo	7.073	3.257	<0.001	0.072
			109 (100mg/kg)	3.402	0.146	0.005	0.703
			109 (150mg/kg)	7.734	3.742	<0.001	0.050
Vertical counts	Male vs female	WT	Placebo	0.487	6.403	0.785	0.012
			109 (100mg/kg)	2.801	0.627	0.021	0.430
		YG8	Placebo	7.942	6.079	<0.001	0.014
			109 (100mg/kg)	7.706	0.009	<0.001	0.923
			109 (150mg/kg)	9.132	0.143	<0.001	0.705

Abbreviations: GT-Genotype, TM-Treatment, TP-Time point

Notes